Deformation and flow driven by osmotic processes in porous materials

PhD Thesis
Department of Geotechnical Engineering and Geo-science (ETCG)
Technical University of Catalunya, UPC

Nadia Mokni

February 2011

Supervisor: Dr. Sebastià Olivella

To my mother Alia,

Acknowledgement

Abstract

Coupled transport phenomena in geological and industrial porous media have been a subject of great interest in many engineering disciplines. For deep storage of high-level nuclear waste osmotic flows can be significant and so require a careful analysis. In Belgium, The bituminized nuclear waste (BW) named Eurobitum contained in metallic drums will be placed inside a tunnel or a shaft excavated in the Boom Clay, which is 100 m thick marine clay presenting favourable properties to limit and delay the migration of the leached radionuclides over extended periods of time. In Geological disposal conditions, contact of the bituminized radioactive waste which contains high amounts highly soluble $NaNO_3$ with groundwater will result in water uptake and swelling of the waste and in subsequent diffusion of the dissolved salt through the host clay formation. Basically, two types of disturbance can be distinguished: A geo-mechanical perturbation, caused by the swelling of the waste and the increase of the pressure in and around the waste and a physico-chemical perturbation by the release of large amounts of $NaNO_3$ and other soluble salts.

In this context the aim of this thesis is: (i) to improve the understanding of the processes controlling the water uptake and the subsequent swelling of bituminized waste containing soluble salts ($NaNO_3$), and (ii) to investigate of the possible effects of the increase of pore fluid concentration on swelling, compressibility and shear behaviour of the clay host rock.

A formulation has been proposed for the analysis of deformation induced by dissolution of salts in porous media in contact with water. The equations include the effect of coupled transport phenomena and the formulation has been included as an extension in the coupled THM program CODE_BRIGHT.

A theoretical and experimental work aiming at understanding the mechanical behaviour of the Bituminized Waste has been presented. This material is considered for this purpose as a mixture of bitumen and crystals of sodium nitrate. For BW, both bitumen and crystals contribute to the creep deformations. An elasto-viscoplastic model has been

developed that describes the creep behaviour of BW considering the constituents' creep behaviour. An experimental program has been set up by SCK•CEN to get insight in the material response. The elasto-viscoplastic constitutive model has been implemented into a finite element program. The modelling results have been compared with the experimental data from SCK•CEN program.

The impact of osmotic forces on the swelling of the material has been investigated by simulating water uptake swelling tests under confined conditions and comparing the predictions with experimental results from tests carried out at SCK•CEN. The numerical analysis has proven to be able to furnish a satisfactory representation of the main observed patterns of the behaviour. A sensitivity analysis has also been carried out to examine the effect of various key parameters.

In regard to the second objective of this thesis, a formulation has been proposed for the analysis of deformations induced by osmotic processes in double structure porous media. The formulation is based on the distinction within the material of a microstructural and a macrostructural levels with chemical changes having a significant effect on the microstructure. A macroscopic description of the system is provided. Then the basic equations describing coupled flows of water and solutes and the transport of its components through macropores and mass balance equations for water and solute in macro and micro pores have been obtained. The proposed formulation has been particularly applied to analyze qualitatively the effect of osmotic suction on swelling of clayey soils. Transient and long term effects have been analyzed.

The influence of pore fluid concentration on the geotechnical properties and behavior of Boom Clay under partially saturated conditions has been investigated. A systematic experimental research program involving osmotic suction and matric suction controlled experiments has been carried out at UPC to investigate the effect of the increase of pore fluid concentration on shear strength and on the volume change behaviour under odometer stress state conditions. It has been observed that under partially saturated conditions a change in salinity causes a decrease in compressibility and shear strength.

Resumen

Los procesos acoplados de transporte de solutos en medios geológicos e industriales son tema de interés en varias disciplinas de la ingeniería. En el caso del almacenamiento de los residuos radioactivos los flujos osmóticos pueden ser relevantes y requieren un análisis en detalle. El residuo nuclear bituminizado (BW: bituminized waste) llamado Eurobitum será almacenado mediante contenedores en cavidades excavadas en la Boom Clay, que es una arcilla marina que presenta propiedades favorables para limitar y retrasar la migración de los contaminantes radioactivos. La interacción entre los dos materiales es un proceso acoplado químico-hidro-mecánico y depende de la respuesta hidromecánica de la Boom Clay y del propio bitumen. En condiciones de almacenamiento, el contacto del BW, que contienen cantidades importantes de $NaNO_3$, con el agua subterránea induce la hidratación por gradientes osmóticos y el consiguiente hinchamiento, además de la difusión de la sal disuelta hacia la roca encajante. Básicamente se pueden distinguir dos tipos de afecciones: la perturbación geomecánica causada por el hinchamiento de los residuos y el aumento de presión en el residuo y cambio de las distribución de tensiones en la roca, y la perturbación físico química por la migración de grandes cantidades de sales.

El objetivo de esta tesis es: (i) Mejorar la comprensión de los procesos que controlan la absorción de agua y el consecuente hinchamiento de residuos con bitumen que contengan sales solubles ($NaNO_3$), y (ii) Investigar los posibles efectos de la concentración de fluidos de los poros sobre el hinchamiento, la compresibilidad y comportamiento de corte de la roca arcillosa.

En primer lugar, se ha desarrollado una formulación para el análisis de la deformación inducida por la disolución de sales en medio poroso con contacto con agua. Las ecuaciones planteadas incluyen los flujos acoplados de agua y soluto (fuera de la diagonal en el diagrama Onsager).

El comportamiento mecánico del BW requiere elasticidad no lineal y fluencia. Para este propósito se presenta también un trabajo teórico y experimental que ayuda a la

comprensión del comportamiento mecánico del BW. Se considera este material como una mezcla de bitumen y cristales de nitrato de sodio Se ha desarrollado un modelo elasto-viscoplástico que describe el comportamiento de fluencia del BW considerando el comportamiento de fluencia de sus constituyentes. Se ha establecido un programa experimental en el SCK•CEN con el fin de tener una visión de la respuesta del material. El modelo constitutivo elasto-viscoplástico ha sido implementado en un programa de elementos finitos. Los resultados se han comparado con observaciones experimentales.

Se ha estudiado el comportamiento a largo plazo del BW en contacto con agua al simular ensayos de hinchamiento por absorción de agua bajo condiciones confinadas realizados en SCK•CEN. El análisis numérico ha demostrado ser capaz de proporcionar una representación satisfactoria de los principales patrones observados en su comportamiento. Así mismo, se ha llevado a cabo un análisis de sensibilidad para examinar el efecto de algunos parámetros clave.

En lo que respecta al segundo objetivo de la tesis, se ha propuesto una formulación para el análisis de las deformaciones inducidas por procesos osmóticos en un medio poroso de doble estructura. Esta formulación distingue dentro del material un nivel micro-estructural y otro macro-estructural con cambios químicos que tienen un efecto significativo en la micro-estructura. Se han obtenido las ecuaciones básicas que describen los flujos acoplados de agua y solutos y el transporte de sus componentes a través de los macroporos así como las ecuaciones de balance de masa para agua y soluto en los macroporos y microporos. La formulación propuesta ha sido aplicada particularmente para analizar cualitativamente el efecto de la succión osmótica sobre el hinchamiento de los suelos arcillosos. Se han analizado los efectos a corto y largo plazo.

Se ha investigado también la influencia del aumento de la concentración del fluido en los poros sobre las propiedades geotécnicas y el comportamiento de la Boom Clay no saturada. Se ha llevado a cabo un programa sistemático de investigación experimental en la UPC, con control de succión osmótica y matricial, con el fin de investigar el efecto del incremento de la concentración del fluido de poros sobre la resistencia de corte y el cambio volumétrico bajo condiciones edométricas. Se ha observado, que bajo condiciones parcialmente saturadas, un cambio en la salinidad provoca una disminución en la compresibilidad y en la resistencia de corte del material.

Table of contents

Chapter 1

Introduction

1.1 Background and motivation of the research project

During the last few decades, coupled transport phenomena and their potential effect on fluid and solute transport have raised the interest of the conceptual designers of repositories for radioactive waste disposal in deep geological media (e.g. Garavito et *al.,* 2005; Soler et *al.* 2001). Coupled flow of water and solute may be associated with several types of gradients such as chemical, thermal and/or electrical gradients. Fluid flow caused by driving forces different than hydraulic gradients is referred to as osmosis.

In media with semi-permeable membrane properties, osmosis drives fluid flow from regions of low salt concentration to regions of high salt concentration, inducing the increase of fluid pressure in the region with a high salt concentration. Some porous materials displaying semi permeable membrane properties and containing salts may undergo swelling by water uptake induced by osmotic flows. This is the case for Eurobitum intermediate-level Bituminised radioactive Waste (BW) which contains between 20 and 30 % in weight of sodium nitrate ($NaNO_3$) (Valcke et *al.*, 2009). The bitumen that surrounds the salt crystals has a very low porosity. This property gives to the material the ability to restrict the transport of dissolved ions, that is, bitumen behaves as a highly efficient semi-permeable membrane. Salt crystals are also present in natural environments, which are usually geological materials formed by evaporation of saline waters, like crusts formed in arid and semiarid zones following evaporation of saline waters in the unsaturated zone (Mokni et *al.*, 2010a). The underlying process of the swelling in porous materials containing salt crystals is that the salts attract water as a consequence of osmotic flux. In fact, the brine formed in contact with the salt is associated with a low water activity.

It has been widely demonstrated that clays give rise to chemical osmosis and ultrafiltration (Fritz and Marine, 1983; Fritz, 1986, Keijzer, 2000; Neuzil, 2000, Garavito, 2005). The ability of clay soils to restrict the passage of solutes has been widely investigated (Marine and Fritz, 1981; Fritz and Marine, 1983; Fritz, 1986; Keijzer 2000). The membrane behaviour of clays has been attributed to electrical restriction induced by the existence of an ionic double layer at the clay platelets surface. Concerns exist about possibly negative effects of a salt (NaNO$_3$) plume on the barrier properties of the clay host rock. Two effects that are suspected to be of importance are chemical osmosis and related pore water pressure increase, and the change of hydro-mechanical properties of the clay host rock (e.g. Rao and Shivananda, 2005; Di Maio, 1996; Barbour and Yang, 1993; Barbour and Fredlund, 1989). Although already studied by many researchers, further investigation was deemed necessary to improve the quantitative insights regarding these processes.

One long-term management option of the Belgian Agency for the Management of Radioactive Waste and Fissile Materials (ONDRAF/NIRAS) is the direct underground disposal of Eurobitum Bituminised radioactive Waste (BW) in a geologically stable clay formation (ONDRAF/NIRAS, 2009). The Boom Clay, which is a 30 to 35 million years old and ~100 m thick marine sediment, is presently being studied as a reference host formation because of its favourable properties to limit and delay the migration of the leached radionuclides over extended periods of time (De Craen *et al.*, 2004). The current disposal concept foresees that several Eurobitum 220 litre drums would be grouped in thick-walled cement-based 'secondary' containers, which in turn would be placed in concrete-lined disposal galleries that are excavated about 200 to 300 m below surface, at mid-depth in the clay layer. The remaining voids between the containers would be backfilled with a cement-based material. To better predict the long term behaviour of Eurobitum under geological disposal conditions, a large research program has been launched by ONDRAF/NIRAS. At the Belgian Nuclear Research Centre (SCK•CEN), water uptake experiments in constant stress and constant volume conditions are preformed and the influence of several parameters like NaNO$_3$ content and ageing degree is investigated (Valcke et *al.*, 2010, Mariën et *al.*, 2008, 2009)

The motivation of the present work is the swelling observed in Eurobitum. Indeed, in geological disposal conditions the main factor that affects the long term behaviour of

the material is water uptake, which is expected to take place at an extremely low rate given the low permeability of the waste and the surrounding multi-barrier isolation systems. In contact with water, the hygroscopic soluble salts incorporated in the BW (i.e. $NaNO_3$) will take up ground water resulting in dissolution and subsequent leaching of these salts and in an osmosis-induced swelling of the waste (e.g. Sneyers and Van Iseghem, 1998; Brödersen *et al*., 1998; Mokni et *al.*, 2008; Mokni et *al*., 2011; Valcke *et al*., 2010). If (further) swelling is hindered, the swelling Eurobitum will exert a high osmosis-induced stress on its surroundings (Brödersen *et al*., 1998; Lefebvre *et al*., 2006; Mariën *et al*., 2008; Mariën *et al*., 2009). High swelling-induced deformation and stresses could lead to a mechanical disturbance and possibly damage of the surrounding host formation (Li *et al*., 2006), of which the consequences in terms of barrier performance have to be assessed.

A primary objective of this thesis is to develop a fully coupled chemo-hydro-mechanical constitutive model for Eurobitum. Moreover, the interaction between the swelling bitumen and the host rock involves a set of strongly coupled chemo-hydro-mechanical process and depends not only on the chemo-hydro-mechanical behaviour of BW, but also on that of the Boom Clay itself. Hence, a secondary objective of this thesis is a contribution to the assessment of the impact that may have the large amount of leached salt on the mechanical behaviour of the clay host rock.

1.2 Thesis layout

The thesis is organized in seven chapters, and the content of each chapter is summarized as follows:

- Chapter 1 introduces the general background of the research followed by the motivation and objectives of this thesis.

- Chapter 2 describes the development of a general formulation for osmotically driven transport of water and salts in deformable porous media. This formulation is proposed for the analysis of deformation induced by the dissolution of the salts in porous media in contact with water.

- Chapter 3 presents a mechanical model that describes the creep behavior of the BW considered as a mixture of two viscoplastic constituents, i.e. the bitumen and the salt crystals.

- Chapter 4 presents the calibration and the validation of the developed chemo-hydro-mechanical model with a particular application to Eurobitum.

- Chapter 5 describes the development of a formulation for osmotic processes in double structure deformable media and its particular application for the simulation of the swelling of clayey soils.

- Chapter 6 presents experimental results on the effect of changes of pore fluid concentration on compressibility and shear strength of Boom Clay.

- Chapter 7 presents summary and conclusions on specific achievements and some suggestions for future research topics.

Fundamental contributions of this thesis have been published in the following journal papers:

N. Mokni, S. Olivella, X. Li, S. Smets, E. Valcke, (2008), "Deformation induced by dissolution of salts in porous media". Physics and Chemistry of the Earth, 33, 436-443.

N. Mokni, S. Olivella, E.E. Alonso, (2010), "Swelling in clayey soils induced by the presence of salt crystals". App Clay Sci, 47,105–112.

N. Mokni, S Olivella, X Li, S Smets, E Valcke, A Mariën, (2010), Deformation of bitumen based porous material: experimental and numerical analysis. J Nuc Mat, Vol. 404 (2), 144-153. <doi: 10.1016/j.jnucmat.2010.07.019>.

N. Mokni, S. Olivella, E. Valcke, A. Mariën, S. Smets, X. Li, (2011), "Deformation and Flow Driven by Osmotic Processes in Porous Materials: Application to Bituminized Waste Materials". Transport Porous Med, Vol 86(2), 665-692. DOI 10.1007/s11242-010-9644-2.

1.3 References

Barbour, S., and Fredlund, D.: Mechanisms of osmotic flow and volume change in clay soils. Can Geothec J., 26, 551-562, (1989).

Barbour, S.L., and Yang, N.: A review of the influence of clay-brine interactions on the geothecnical properties of Ca-montmorillonitic clayey soils from western Canada. Can. Geotech. J., 30, 920-934, (1993).

Brödersen, K. Brunel, G. Gens, R. Lambert, F. Nominé, J.C. Sneyers, A. and Van Iseghem, P.: Characteristics of bituminized radioactive waste, Final report for contract no. FI2W-CT-91-0025, EUR 18228 EN, Luxembourg, (1998).

De Craen, M., Wang, L., Van Geet, M., and Moors, H.: Geochemistry of Boom Clay pore water at the Mol site', Scientific report SCK•CEN-BLG-990, SCK•CEN, Mol, Belgium (www.sckcen.be), (2004).

Di Maio, C.: Exposure of bentonite to salt solution: osmotic and mechanical effects. Géotechnique., 46(4), 695-707, (1996).

Fritz, S.J., and Marine, I.W.: Experimental support for a predictive osmotic model of clay membranes", Geochim et Cosmochim Ac., 47, 1515-1522, (1983).

Fritz, S.J.: Ideality of clay membranes in osmotic processes: a review", Clay Clay Miner., 43 (2): 214-223, (1986).

Garavito, A.M.: Chemical osmosis in clayey sediments", PhD thesis, University of Utrecht, the Netherlands, (2005).

Keijzer, T.: Chemical osmosis in natural clayey material. Ph.D. thesis, Universiteit Utrecht, The Netherlands, (2000).

Lefebvre, X., Sercombe, J., Ledieu, A., Gwinner, B., and Adenot, F.: Bituminized waste leaching in restricted and free swelling conditions: mechanisms and analytical modeling. Mat. Res. Soc. Symp. Proc. 932, 681-688, (2006).

Li, X., Bernier, F., and Valcke, E.: Interaction swelling bitumen – host rock: scoping calculations. Mat. Res. Soc. Symp. Proc. 932, 751-758, (2006).

Marine, I.W., and Fritz, S. J.: Osmotic model to explain anomalous hydraulic heads. Water Resour Res., 17 (1), 73-82, (1981).

Mariën, A., Smets, S., Li, X., and Valcke, E.: Processes Related to the Water Uptake by EUROBITUM Bituminized Radioactive Waste: Theoretical Considerations and First Experimental Results, Mat.Res.Soc. Symp. Proc.,Vol.1107,151-159, (2008).

Mariën, A., Smets, S., and Valcke, E.:Study of the Processes Related to the Water Uptake of Eurobitum Bituminized Radioactive Waste: Effect of Salt Concentration. Mater. Res. Soc. Symp. Proc., Vol. 1193, 513-520, (2009).

Mokni N., Olivella, S., Jamei, M., Li X. and Valcke, E.: Deformation in porous media containing salts. Proc 2nd Int Conf on Advances in Geomaterials and Structures, AGS'08, Hamamet, Tunisia, Vol.4,695-703, (2008).

Mokni, N., Olivella, S., Alonso, E.E.: Swelling in clayey soils induced by the presence of salt crystals, 2010, App.Clay. Sci., 47, 105–112, (2010a).

Mokni, N., Olivella, S., Valcke, E., Mariën, A., Smets, S. Li, X.: Deformation and Flow Driven by Osmotic Processes in Porous Materials: Application to Bituminized Waste Materials, Transport Porous Med, Transport Porous Med, Vol 86(2), 665-692. DOI10.1007/s11242-010-9644-2, (2011).

Neuzil, C.: Osmotic generation of"anomalous" fluid pressures in geological environments. Nature., 403, 182–184,(2000).

ONDRAF/NIRAS: The Long-term Safety Assessment Methodology for the Geological Disposal of Radioactive Waste', ONDRAF/NIRAS report NIROND TR-2009-14 E (www.nirond.be), (2009).

Rao, M. and Shivananda, P.: Role of osmotic suction in swelling of salt amended clays. Can. Geotech.J., 42, 307-315, (2005).

Soler, J.M.: The effect of coupled transport phenomena in the Opalinus Clay and implications for radionuclide transport", J Contam Hydrol., 53, 63-8, (2001).

Sneyers, A., and Van Iseghem, P.: The leaching behavior of bituminized radioactive waste in the geologic disposal conditions of the Boom Clay formation. Mat. Res. Soc. Symp. Proc. 506, 565-572, (1998).

Simondi-Teisseire, B., Camaro, S., Vistoli, P.P., Blanc, V., and Romero, M.A.: Long-term behavior of bituminized waste in presence of water. Proc. of Safe waste Conf., October 1-5, 2000, Montpellier, France, Vol. 2 p. 574-581, (2000).

Valcke, E., Mariën, A., and Van Geet, M.: The methodology followed in Belgium for the study of the compatibility of Eurobitum with the geological disposal environment. Mat. Symp. Soc. Symp. Proc. 1193, 105-116, (2009).

Valcke, E., Mariën, A., Smets, S., Li, X., Mokni, N., Olivella, S., and Sillen, X.: Osmosis induced swelling of Eurobitum bituminized radioactive waste in constant total stress conditions. J.Nuc.Mater., 406, 304-316, (2010).

Chapter 2

Formulation for osmotically driven transport of water and salts in deformable porous media

2.1 Background on coupled processes in porous materials

Coupled flow phenomena have gained interest in a variety of problems ranging from pollution studies and waste-containment (e.g. Garavito et *al.,* 2005, Malisius et *al.*, 2003, Soler et *al.* 2001). These phenomena arise from interactions among the flows of fluid, chemicals, heat and electricity in response to gradients of hydraulic, chemical, thermal and electric potentials. The coupled flows are given in Table 2.1 on the non diagonal elements. On the diagonal the well known direct flows appear, i.e. those corresponding to fluxes of quantities driven by gradients of a variable that gives the amount of the same quantity.

Table 2.1: Direct and coupled flow phenomena. The direct flows with their flow laws are given in the shaded cells. (Yeung and Mitchel, 1993; Keijzer 2000; Garavito, 2005; Bader and Kooi, 2005)

Flow	Gradients			
	Hydraulic	Thermal	Electrical	Chemical
Fluid	Hydraulic flow (Darcy's law)	Thermo osmosis	Electro osmosis	Chemical osmosis
Heat	Convective heat flow	Thermal conduction (Fourier law)	Peltier effect	Dufour effect
Electric current	Streaming potential	Seebeck effect	Electrical conduction (Ohm's law)	Diffusion and membrane potentials
solute	Ultrafiltration	Soret effect	Electro-phoresis	Diffusion (Fick's law)

Yeung and Mitchell (1993) stated that coupled flows occur when a flow of one type is induced by a driving force of another type, according to:

$$\mathbf{J}_i = \sum_{j=1}^{n} L_{ij} \mathbf{X}_j \qquad (2.1)$$

where $\mathbf{J}_i$ is the flux of type i, driven by n different driving force of type j and L_{ij} are called the coupling coefficients for $i \neq j$. For $i=j$ the expressions of direct flows are recovered. So that, when written for solute flux induced by chemical gradient (i.e. Diffusion), Equation 2.1 becomes

$$\mathbf{J}_c = D\mathbf{X}_c \qquad (2.2)$$

and is known as Fick's law in which $\mathbf{J}_c$ is the flux of solute in [ms^{-1}], D is the diffusion coefficient in [m^{2}s^{-1}] and $\mathbf{X}_c$ is the chemical gradient. For fluid flux induced by hydraulic gradient, Darcy's law is recovered.

Fluid flow caused by driving forces other than hydraulic gradients is referred to as osmosis. In this study only coupled phenomena induced by hydraulic or chemical gradient under isothermal conditions are considered. Chemical osmosis is the process behind, the flow of a solvent across a semi permeable membrane separating two solutions of different solvent activity (i.e different solute concentration) or within a porous material acting as a semi permeable membrane and in contact with a solution at different concentration compared to the material pore water concentration.

A semi permeable membrane is a membrane that allows the passage of solvent and partially restricts the passage of solutes due to, for example, the small size of the connected pores, i.e. smaller than the solute molecules but larger than the solvent molecules. For clay membranes, solute rejection is generated by electrical restrictions induced by the existence of an ionic double layer in the clay platelets surfaces. Low permeability clayey materials have pore size generally large enough to allow the passage of the largest hydrated radii of ions commonly found in ground water. Thus membrane behaviour for clays is mainly due to the electrical properties of the minerals that constitute the geological material (Marine and Fritz, 1981; Fritz, 1986; Garavito, 2005). For other porous media like biological membranes or porous ceramic nanofiltration membranes (Palmeri et *al.*, 1999), porosity plays an important role in solute restriction as only a part of total porosity allows solute migration

For the case where a semi permeable membrane separates two reservoirs containing solutions with different concentrations, chemical osmosis causes a rise in pressure in the reservoir containing the solution at higher concentration (i.e. osmotically-induced pressure) and a reduction in the other reservoir. For the case of an ideal semi permeable membrane, the passage of salts is totally restricted and only water is transported through the membrane. The induced osmotic pressure ($\Delta\pi$) persists indefinitely. For a non ideal semi permeable membrane the hydraulic pressure generated by osmosis (ΔP) is less than $\Delta\pi$.

The membrane behaviour is quantified by the osmotic efficiency coefficient σ, which is defined as the observed osmotic pressure (ΔP) divided by the theoretical osmotic pressure ($\Delta\pi$) as calculated from solution properties only (Marine and Fritz, 1981),

$$\sigma = \left(\frac{\Delta P}{\Delta\pi}\right)_{J=0} \tag{2.3}$$

where J is the flux of solution across the membrane.

The osmotic efficiency coefficient is then a parameter that describes the non-ideality of a membrane. It ranges from 1 for an ideal membrane to 0 for porous media having no membrane properties. This parameter has been widely characterized for clay materials (e.g. Bresler 1973; Fritz and Marine 1983; Barbour and Fredlund, 1989; Mitchell, 1993; Malusis et *al.*, 2001; Malusis et *al.*, 2003).

Another coupled flow is ultrafiltration commonly referred to as hyperfiltration (Fritz and Marine, 1983, Manassero and Dominijanni, 2003; Keijzer, 2000) which is a process by which a solution is hydraulically forced through a semi permeable membrane, that is, the solute molecules are partially or totally filtered (depending of the value of osmotic efficiency coefficient) causing a build-up of solute on the high pressure side of the membrane and a dilution of solute on the low pressure side. Therefore, the solute concentration is greatest at the membrane/ solution interface (Fritz and Marine, 1983). To quantify coupled flow phenomena two main approaches were followed: empirical methods and non-equilibrium thermodynamics (e.g. Katchalsky and Curran, 1965; Greenberg et *al.* 1973; Yeung and Mitchell, 1993; Olsen *et al.*, 2000; Soler, 2001; Malusis and Shakelford 2002a, b; Manassero and Dominijanni, 2003; Brader and Kooi,

2005). Non-equilibrium thermodynamics delivers a general framework for the macroscopic formulation of irreversible transport processes. It describes systems out of thermodynamic equilibrium such as soil-water systems subjected to one or more gradients. The theory assumes the validity of laws of classical thermodynamics in addition to the following assumptions (Yeung and Mitchell, 1993)

- Local equilibrium.
- Linear phenomenological equations (Equation 2.1).
- Validity of Onsager reciprocal relations ($L_{ij} = L_{ji}$).

One of the fundaments of the irreversible thermodynamic is the definition of the dissipation function Φ which is the energy dissipated by irreversible processes. The dissipation function is defined as the sum of the products of fluxes and driving forces (Yeung and Mitchell, 1993)

$$\Phi = \sum_{i=1}^{n} \mathbf{J}_i \mathbf{X}_i \tag{2.4}$$

Several models of osmotic processes, based on the theory of irreversible (non equilibrium) thermodynamics, have been developed. Katchalsky and Curran (1965) (after Olsen et *al.*, 2000) developed theories for non charged and electrolyte solute. In this model the membrane is considered as an interface between two reservoirs at different solute concentration. This theory was motivated primarily by interest in the transport of matter through biological membranes. The theory by Greenberg et *al.* (1973) for non charged solutes was developed to analyse the transient migration of water and salt effect in fine grained soils. Yeung and Mitchell (1993) presented a coupled flow theory to describe the transport of fluid, electricity and chemical species induced respectively by the influences of hydraulic, electrical and chemical gradients in soil membranes under isothermal conditions. A laboratory testing programme was developed by theses researchers to measure the migration of cations and anions in compacted silty clay of moderate plasticity under the influences of hydraulic electrical and chemical gradients imposed simultaneously. A sodium chloride solution was used to simulate the contaminant. The authors observed a good agreement between the measured and the computed profiles.

All these theories have been derived starting from a dissipation function and then following the formalism of non equilibrium thermodynamics which consist of (Yeung and Mitchel, 1993):

- Defining the conjugated fluxes J_i and driving forces X_i
- Formulation of the phenomenological equations in the form of Equation (2.1)
- Applying the Onsager reciprocal relations
- Relating the phenomenological coefficient to measurable quantities

More recently Soler (2001) used a one-dimensional model to study the role of coupled transport processes, including thermal osmosis, in radionuclide transport from a repository of high level nuclear waste in the Opalinus Clay in Switzerland. The model was reduced, however, to a conventional diffusion-advection equation with a constant advection velocity, thereby neglecting temporal and spatial changes in the concentration gradients on osmotic transport. Malusis and Shakelford (2002a, b) presented a continuum formulation to model reactive solute transport across clay membrane barriers in which the salt cations undergo ion exchange at the clay particle surface during transient transport and are replaced in solution by exchangeable cation species. Their model was based on the theory presented by Yeung and Mitchell (1993) for the special case in which no electrical current exists across the soil. However, they only presented model simulations in which membrane effects were set to zero. Manassero and Dominijanni (2003) proposed a theoretical model of osmotic effect on solute transport within clayey soils under solute concentration and pressure gradients. The case of dilute solution allowing the validity of relationship for ideal solution has been assumed. The authors followed the same methodology as Katchalsky and Curran (1965) and identified the coupling coefficients by analogy to the classical constitutive laws (Darcy's law and Fick's law). The model was validated by simulating experimental tests on geo-synthetic clay liners.

Garavito (2005), Kooi et *al.* (2003) and Brader and Kooi (2005) presented a model of chemically and hydraulically coupled flow phenomena in clay soils, which incorporates the strong dependence of the efficiency of the membrane on pore water chemistry. Bader and Kooi (2005) have shown that the model reproduces correctly the results of an

ultrafiltration test conducted by Keitjzer (1999), as well as the results of an in situ chemical osmotic experiment on the Pierre Shale of South Dakota (USA) conducted by Neuzil (2000). Garavito (2005) used the same model to analyse to influence of osmosis on ground water flow and transport of dissolved particles in various situations and for various clay soils. This model is presented briefly below and is used as a basis of the formulation proposed in this Chapter.

Bader and Kooi (2005) derived the flux equations in terms of hydraulic pressure p and chemical potential of the solute μ_s,

$$\mathbf{J}_l = L_{11}\nabla(-p) + L_{12}\nabla(-\mu_s)$$
$$\mathbf{J}_l^s = L_{21}\nabla(-p) + L_{22}\nabla(-\mu_s)$$

(2.5)

where $\mathbf{J}_l$ is the solution flux and J_l^s denotes the diffusive flux of solute relative to the solution.

The solute flux relative to the porous medium is defined as $\mathbf{J}_s = \mathbf{J}_l^s + \dfrac{\rho_l w_l^s}{M_s}\mathbf{J}_l$

where ρ_l [kg/m^3] is the liquid density, w_l^s [-] is the solute mass fraction and M_s [kg/mol] the solute molar mass.

The chemical potential of the solute is defined as:

$$\mu_s = \mu_s^0 + \upsilon RT \ln a_s$$

(2.6)

where μ_s^0 is the constant chemical potential for the pure solvent, ν is the dissociation coefficient (a solute dissociate into ν ions), R [J/mol.K] is the gas constant , T [K] in temperature and a_s [-] is the solute activity.

Considering the definition of the osmotic efficiency coefficient (Equation (2.3)) the following relation is obtained

$$\sigma = \left(\frac{\Delta P}{\Delta \pi}\right)_{J=0} = -\frac{M_s L_{12}}{\rho_l w_l^s L_{11}}$$

(2.7)

Then employing the analogy with Darcy's law and using Equation (2.7) the coupling coefficients L_{11} and L_{12} are obtained as

$$L_{11} = \frac{k}{\mu} \quad \text{and} \quad L_{12} = -\frac{\sigma k \rho_s}{\mu M_s} \tag{2.8}$$

where k is the intrinsic permeability of the porous medium [m^2] and μ is the dynamic viscosity of the fluid. Applying Onsager reciprocal relations the following relation is obtained:

$$L_{21} = L_{12} = -\frac{\sigma k \rho_s}{\mu M_s} \tag{2.9}$$

To determine the coupling coefficient L_{22}, Bader and Kooi (2005) defined the solute permeability coefficient (θ) and related it to the effective diffusion coefficient (D) as

$$\theta = L_{22} \frac{M_s}{\rho_s} - \frac{\sigma^2 k w_l^s \rho_f}{\mu M_s} \tag{2.10}$$
$$D = \nu R T \theta$$

Finally, substituting Equations (2.8), (2.10) into (2.5) gives the expressions for the liquid and solute fluxes as

$$\mathbf{J}_l = -\frac{k}{\mu} \nabla p + \sigma \lambda \nabla w_l^s = -\frac{k}{\mu} \left(\nabla p - \sigma \nabla \pi \right) \ ; \ \lambda = \frac{k \rho_l \nu R T}{\mu M_s} \tag{2.11}$$
$$\mathbf{J}_l^s = -\sigma \rho_l w_l^s \mathbf{J}_l - D \rho_l \nabla w_l^s$$
or in term of gradients $\mathbf{J}_l^s = \sigma \rho_l w_l^s \frac{k}{\mu} \nabla p - \sigma^2 \rho_l w_l^s \lambda \nabla w_l^s - D \rho_l \nabla w_l^s$

Bader and Kooi (2005) completed their model by writing the balance equations for the fluid and the solute assuming no mass exchange between the fluid and the porous medium and no chemical reactions. In addition the authors defined the equations of state assuming that the fluid density is only a function of pressure, i.e. neglecting the effect of temperature and solute mass fraction on liquid density.

2.2 Problem formulation

As mentioned above, several coupled flow formulations to model the osmotic processes in clays have been proposed in the literature (Katchalsky and Curran, 1965; Greenberg et *al.* 1973; Yeung and Mitchell, 1993; Soler, 2001; Malusis and Shakelford, 2002a,b: Garavito 2005; Manassero and Dominijanni, 2003; Kooi et *al.,* 2003; and Brader and Kooi, 2005). These theories were mostly used to model aspects such as osmotically induced consolidation, salt water intrusion and investigations on clay barriers for ensuring the long term safety of a disposal system. However, few studies have been concerned with osmotically induced swelling. Swelling has been observed in some waste materials containing salt crystals. This is the case of the Bituminized Waste (BW) in which swelling is induced by the presence of soluble salt crystals of sodium nitrate (Sercombe et *al.,* 2006; Gwinner et *al.*, 2006; Mokni et *al.,* 2008; Mokni et *al.,* 2011; Mariën et *al.,* 2008,2009; Valcke et *al.,* 2010). For this kind of materials, the brine formed in contact with the salt is associated with a low water activity. Water flows by osmotic flux from zones of high water activity to zones of low water activity. If the material behaves as a semi permeable membrane, chemical osmosis causes a rise in pressure within the material's pores inducing swelling deformations.

In what follows a formulation is proposed aiming at studying the effect of osmotic processes on the swelling of porous material containing salt crystals.

The following assumptions are made:

- The medium is constituted of a single soluble salt plus an inert solid phase.
- Multiphase flow including phase change is considered (dissolution/precipitation of the salt crystals).
- Only chemical and hydraulic gradients are considered.
- The medium is supposed not to be saturated with water.
- Binary diffusion of salt and water at high concentration is assumed.
- Permeability, diffusion and osmotic efficiency coefficients are considered variable with porosity.

The porous medium under study is composed of three phases:

- Solid phase: solid matrix and salt crystals;
- Liquid phase (*l*): dissolved salt in water, dissolved air;
- Gas phase (*g*): mixture of dry air and water vapor.

And four species:

- Solid matrix (*m*): matrix embedding the crystals;
- Salts: as crystal (*c*) and as dissolved salt (*s*) resulting of the dissolution of the crystals;
- Water (*w*): as liquid or evaporated in the gas phase;
- Air (*a*): dry air as gas or dissolved in the liquid phase.

An example of a schematic representation of the porous medium is displayed in Figure 2.1.
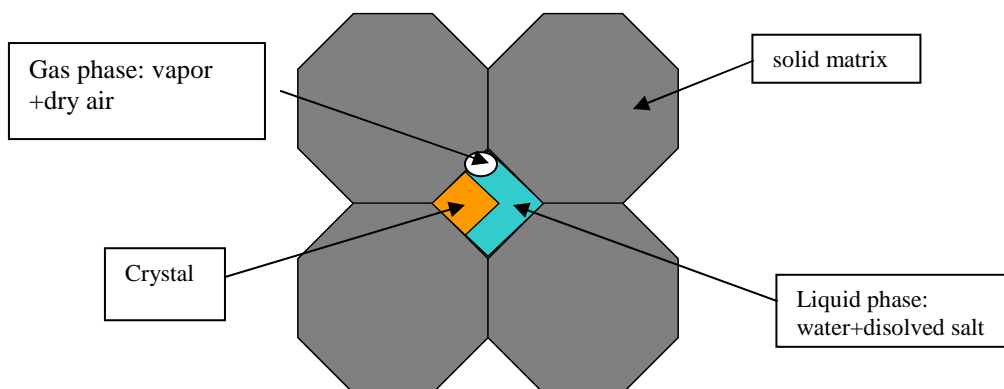
Figure 2.1: Schematic representation of the medium

The total volume of the medium can be decomposed into the volume occupied by the crystals, the fluids (liquid or gas) and the solid matrix, i.e. $V_t = V_c + V_f + V_m$. These volumes permit to define the porosity occupied by the fluids (ϕ_f) and the volume fraction of the crystals (ϕ_c).

These variables are defined as:

$$\phi_c = \frac{V_c}{V_t}; \qquad \phi_f = \frac{V_f}{V_t}; \qquad \phi_m = \frac{V_m}{V_t} \tag{2.13}$$

$$V_t = V_c + V_f + V_m; \qquad 1 = \phi_c + \phi_f + \phi_m = \phi_{c+f} + \phi_m$$

$$\phi_{c+f} = \phi_c + \phi_f$$

where V_c, V_f and V_m are respectively, volume of crystals, fluid and solid matrix. The sum of the porosity (ϕ_f) plus the volume fraction of the crystals (ϕ_c) is defined as a volume fraction ϕ_{c+f} (i.e. $\phi_{c+f} = \phi_c + \phi_f$). In this way, $1 - \phi_{c+f} = \phi_m$ is the volumetric fraction occupied by the solid matrix.

An initial porosity ϕ_{f0} is assumed. In fact $NaNO_3$ is a very hygroscopic, it will strongly absorb large amounts of water or water vapour from the environment it is exposed to, resulting in the formation of an aqueous solution (*i.e.* deliquescence) (Caroll et *al.*, 2005) . As a consequence of the dissolution of the crystals the pore volume available for the fluids (ϕ_f) will increase resulting in a deformation of the sample (swelling). Without loss of generality, the void ratio can be calculated as $e = \phi_f / (1 - \phi_f)$.

2.3 Constitutive theory

Considering the case where the fluid phase is composed of two components (i.e. water (w) and solute (s)), each components has a mass density ρ_i ; $i=w,s$ (mass of an i component per unit volume of the phase, with $\sum \rho_i = \rho$) and an average velocity v^i at any point within the phase. Several kinds of velocities with respect to a fixed frame may be defined for the phase as a whole at any point expressed as weighted averages of the components velocities v^i. The more commonly used velocities are the mass weighted velocity and the volume weighted velocity defined as (Bear, 1990),

- Mass weighted velocity

$$\mathbf{V}^m = \frac{(\omega_l^s \rho_l)\mathbf{v}^s + (\omega_l^w \rho_l)\mathbf{v}^w}{(\omega_l^s \rho_l) + (\omega_l^w \rho_l)} \tag{2.14}$$

where ω_l^i ; $i = w, s$ is the mass fraction of the i-component in the liquid phase, with $\omega_l^s + \omega_l^w = 1$.

- Volume weighted velocity

$$\mathbf{V}^v = \frac{\rho_l^w v_l^w \mathbf{v}^w + \rho_l^s v_l^s \mathbf{v}^s}{\rho_l^w v_l^w + \rho_l^s v_l^s} \tag{2.15}$$

where $\rho_l^i = \rho_l \omega_l^i$; $i = w, s$ and $\dfrac{1}{v_l^i} = \dfrac{m_i}{v_i}$

with $\rho_l^w v_l^w + \rho_l^s v_l^s = 1$

The velocity of a fluid phase is decomposed into two terms: motion with respect to the solid phase and motion of the solid phase with respect to a fixed reference. The term expressing the solid motion is obtained multiplying the solid velocities by the mass amount of the specie i per unit volume of the medium (Olivella et *al.,* 1994).

The total mass flux of specie i in a phase α, with respect to a fixed reference system is defined as,

$$\mathbf{j}_\alpha^i = \mathbf{J}_\alpha^i + w_\alpha^i \rho_\alpha \mathbf{J}_\alpha + w_\alpha^i \rho_\alpha \phi_f S_\alpha d\mathbf{u}/dt \tag{2.16}$$

where $\mathbf{J}_\alpha^i$ is the nonadvective flux and $\mathbf{J}_\alpha$ is the advective flux with respect to the solid phase and $d\mathbf{u}/dt$ is the velocity of the solid phase with respect to a fixed reference system.

We assume that the advective flux with respect to a fixed reference system is carried by the volume weighted velocity of the phase, that is

$$\mathbf{V}^v = \frac{\mathbf{J}_\alpha}{\phi_f S_\alpha} + d\mathbf{u}/dt \tag{2.17}$$

The non advective flux is then expressed with respect to the volume average velocity as

$$\mathbf{J}_l^i = \rho_\alpha^i \phi_f S_\alpha \left(v^i - V^v \right) \tag{2.18}$$

The constitutive equations that relate the mass- average flow of fluid and the mass flow of solute to chemical and pressure gradients are as follows (Bader and Kooi, 2005),

$$\mathbf{J}_l = -\frac{\mathbf{k} k_{rl}}{\mu}\left(\nabla p + \rho_l \mathbf{g} \nabla z\right) + \frac{\alpha_s}{\mu}\mathbf{k}\sigma\nabla(w_l^s); \quad \alpha_s = \frac{k_{rl} R T \rho_l}{M_s} \tag{2.19}$$

This is the flux of liquid phase induced by both pressure and concentration gradients. It is an advective flux in the sense that it drags both the solute and the water.

The non-advective flux of solute is then written as:

$$\mathbf{J}_l^s = -\sigma \rho_l^s \mathbf{J}_l - D \nabla \rho_l^s \qquad (2.20)$$

Further derivation of Equation (2.20) yields

$$\mathbf{J}_l^s = -\sigma w_l^s \rho_l \mathbf{J}_l - D^* \rho_l (1 + \gamma w_l^s) \nabla w_l^s \; ;$$

$$\gamma = \frac{1}{\rho_l} \frac{\partial \rho_l}{\partial w_l^s} \qquad (2.21a)$$

Or in term of gradients

$$\mathbf{J}_l^s = \sigma w_l^s \rho_l \frac{\mathbf{k} k_{rl}}{\mu} (\nabla p + \rho_l \mathbf{g} \nabla z) - \sigma^2 w_l^s \rho_l \frac{\alpha_s}{\mu} \mathbf{k} \nabla(w_l^s) - D^* \rho_l (1 + \gamma w_l^s) \nabla w_l^s \qquad (2.21b)$$

$$\alpha_s = \frac{k_{rl} R T \rho_l}{M_s}$$

where $\mathbf{k}$ [m^2] denotes the intrinsic permeability tensor, k_{rl} [-] denotes the relative permeability of the liquid, $\mathbf{g}$ is the gravity vector, μ [MPa.s] is the dynamic viscosity, p [MPa] is the hydraulic pressure, w_l^s is the mass fraction of solute in the liquid phase, R [J/(mol.K)] is the gas constant , T [K] is temperature, ρ_l [kg/m^3] is liquid density, M_s [kg/mol] the solute molar mass and σ osmotic efficiency coefficient. The dissociation coefficient (ν) considered by Brader and Kooi (2005) (Equation (2.11)) is here neglected.

In addition to the explicit coupling effect of chemical osmosis and ultrafiltration an additional coupling effect, characterized by a decrease in the diffusion coefficient with an increase in the efficiency coefficient, has also been considered. The diffusion coefficient D^* [m^2/s] must be dependent on σ and it should comply the flowing limiting behavior: for media presenting ideal membrane properties the diffusion of the solute is completely prohibited. It should also represent the conventional meaning of diffusivity for media without membrane properties. Manassero and Dominijanni (2003) and Bader and Kooi, (2005), proposed a simple relationship that is consistent with these requirements as $D^* = (1 - \sigma) \tau \phi_f D_0$ where τ is the tortuosity and D_0 is a Fickian diffusion coefficient for a solute in free water.

When $\nabla w_l^s = 0$ and neglecting the gravity effect, the solute mass flux reduces to $\mathbf{J}_l^s = \sigma w_l^s \rho_l \dfrac{\mathbf{k} k_{rl}}{\mu} \nabla p$. This term represents ultrafiltration. The second term in Equation (2.21) arises because the concentration gradient drives fluid flow by osmosis. In the case of non membrane properties (σ=0) Equations (2.19) and (2.20) fall into Darcy's and Fick's law respectively.

It is interesting to observe that the third term in Equation (2.21b) is different from the one proposed by Bader and Kooi (2005), which did not include the term into the brackets. The formulation presented in this work deals with high concentrations of salts. In order to prevent volume variations induced by binary diffusive gradients, diffusive fluxes are defined for each of the components with respect to the volume weighted velocity. This can be considered equivalent to including the gradient of liquid density (γ in Equation (2.21)).

In this situation the non-advective flux satisfies the following condition:

$$\frac{\mathbf{J}_l^w}{\overline{\rho}_l^w} + \frac{\mathbf{J}_l^s}{\overline{\rho}_l^s} = \mathbf{0} \ ; \overline{\rho}_l^i = \frac{1}{v_l^i} = \frac{m_i}{v_i} \ ; \ i = w, s \tag{2.22}$$

where v_i and m_i are the volume and mass of the i component. Consequently, the non-advective flux of water including ultrafiltration is written as:

$$\mathbf{J}_l^w = \frac{\beta}{\alpha} \sigma w_l^s \rho_l \mathbf{J}_l - D^* \rho_l (1 - \gamma w_l^w) \nabla w_l^w \tag{2.23}$$

$$\alpha = 1 + \frac{1}{\rho_l} \frac{\partial \rho_l}{\partial w_l^s} w_l^s = 1 + \gamma w_l^s \qquad \beta = 1 + \frac{1}{\rho_l} \frac{\partial \rho_l}{\partial w_l^w} w_l^w = 1 - \gamma w_l^w$$

The details of theoretical development of Equations (2.22) and (2.23) are presented in Appendix A.

It is now possible to define the effective diffusivity for semi permeable membrane in case of high salt concentration gradients of water and solute respectively as

$$D_w = D^* (1 - \gamma w_l^w) \tag{2.24a}$$

$$D_s = D^* (1 + \gamma w_l^s) \tag{2.24b}$$

Equations (2.24) show that this approach leads to different diffusion coefficients for water and solute. As noted above, if the nonadvective flux was expressed with respect to the mass weighted velocity, Equation (2.22) reduces to the binary flux condition (i.e. $\mathbf{J}_l^w + \mathbf{J}_l^s = \mathbf{0}$) and the additional terms α, β, γ would not appear in Equations (2.21), (2.23) and (2.24) which is useful for sufficiently diluted solution where the gradient of liquid density is negligible. Therefore the case of dilute solutions can be viewed as a limiting case of the more general approach adopted in this work.

In the following section the mass balance of different species are derived. Balance of momentum of the medium as a whole is reduced to the equation of stress equilibrium.

2.4. Mass balance equations

2.4.1 Balance equations of solid phases

As noted above, the porous medium under study is viewed as an inert or inactive matrix, (in comparison to clay platelets which may experience a chemical change when exposed to a given saline solution. For instance, by changing the adsorbed cations) embedding salt crystals. Chemical processes i.e. dissolution/precipitation are taken into account. Therefore, salt is considered as specie forming solid phase and it is also dissolved at high concentrations in the liquid phase. The compositional approach (Olivella *et al.,* 1994) is followed to establish the mass balance equations. This approach consists of balancing the species rather than the phases. In case of writing the phase balance equations, non-advective fluxes of species inside the phase would cancel.

a) Crystal mass balance

The mass balance of the crystals is expressed as:

$$\frac{\partial}{\partial t}(\rho_c \phi_c) + \nabla.(\rho_c \phi_c \frac{d\mathbf{u}}{dt}) = -\frac{dm}{dt}$$

(2.25)

where ρ_c is the density of the crystal, and $\mathbf{u}$ is the displacement vector of the solid phase. This equation provides the evolution of the amount of salt crystal in the material. The time derivative $\frac{dm}{dt}$ is the dissolution/precipitation term.

The form of the function for kinetically controlled dissolution/precipitation is typically written as:

$$\frac{dm}{dt} = r = \phi_c \sigma_c k \xi (\Omega^\theta - 1)^\eta = \phi_c \sigma_c k \xi \left(\left(\frac{c}{c_{sat}(T,p)} \right)^\theta - 1 \right)^\eta ; \quad \xi = \frac{c_{sat} - c}{|c_{sat} - c|}$$

(2.26)

where σ_c is the specific surface [m²/m³], which may depend on the number of crystals and their radius, k is the rate constant [kg/s/m³] that can depend on temperature (Arrhenius type), ξ is the sign of the rate (positive for precipitation and negative for dissolution), θ and η are experimental parameters, and c_{sat} is the concentration at equilibrium.

One can note that equation (2.26) vanishes when the crystals are consumed, i.e. $\phi_c=0$. The material derivative with respect to solid velocity field will be very useful to obtain the final expressions for the balance equations, it is defined as

$$\frac{D(\bullet)}{Dt} = \frac{\partial(\bullet)}{\partial t} + \frac{du}{dt} \nabla(\bullet)$$

(2.27)

Using (2.27) in Equation (2.25) leads to:

$$\frac{D\phi_c}{Dt} = -\frac{1}{\rho_c} \frac{dm}{dt} - \frac{\phi_c}{\rho_c} \frac{D\rho_c}{Dt} - \phi_c \nabla.(\frac{d\mathbf{u}}{dt})$$

(2.28)

This equation expresses the variation of the crystal volume fraction caused by dissolution, density variations and volumetric deformations.

b) Solid matrix mass balance

The mass balance of the solid matrix is expressed as:

$$\frac{\partial}{\partial t}(\rho_m(1-\phi_{c+f})) + \nabla.(\rho_m(1-\phi_{c+f})\frac{d\mathbf{u}}{dt}) = 0$$

(2.29)

where ρ_m is the density of the solid matrix and $\dfrac{d\mathbf{u}}{dt}$ is the velocity of the solid phase due to the deformation of the material. This equation provides the evolution of volumetric fraction ϕ_{c+f} induced by deformations. The fact that the volume fraction of the salt crystals is included in the volume fraction $\phi_{c+f}\left(=\phi_c + \phi_f\right)$ implies that under compressive deformations the reduction of ϕ_{c+f} is limited by the presence of the crystals.

The variation of ϕ_{c+f} is obtained as:

$$\frac{D\phi_{c+f}}{Dt} = \frac{(1-\phi_{c+f})}{\rho_m}\frac{D\rho_m}{Dt} + (1-\phi_{c+f})\nabla.\frac{d\mathbf{u}}{dt}$$

(2.30)

Since porosity will be used for the calculation of several parameters, it is convenient to transform Equation (2.30) into its variation. This is achieved by substitution of Equation (2.28) in (2.30):

$$\frac{D\phi_f}{Dt} = \frac{1}{\rho_c}\frac{dm}{dt} + \frac{\phi_c}{\rho_c}\frac{D\rho_c}{Dt} + \frac{(1-\phi_f-\phi_c)}{\rho_m}\frac{D\rho_m}{Dt} + (1-\phi_f)\nabla.\frac{d\mathbf{u}}{dt}$$

(2.31)

For constant densities, Equation (2.31) reduces to:

$$\frac{D\phi_f}{Dt} = \frac{1}{\rho_c}\frac{dm}{dt} + (1-\phi_f)\nabla.\frac{d\mathbf{u}}{dt}$$

(2.32)

At constant volume (i.e. with no volumetric deformation), the porosity will increase as dissolution takes place.

2.4.2. Balance equations of water and solute

As described above, salt is present in the medium as crystal and as dissolved salt at high concentration resulting of the dissolution of the crystals. Water in the main specie in the liquid phase, it can also be present in the gaseous phase as vapor. Dry air is considered a single species, it is the main component of the gaseous phase and it is also dissolved in the liquid phase. In what follows, the balance equation of each specie is written. Phase equation can be obtained by adding the equations of balance of all species contained in each phase.

a) Solute mass balance

The total solute mass balance is expressed as:

$$\frac{\partial}{\partial t}(w_l^s\rho_l S_l\phi_f) + \nabla.(\mathbf{j}_l^s) = \frac{dm}{dt}$$

(2.33)

The total flux of solute is obtained as the sum of diffusion plus advection:

$$\mathbf{j}_l^s = \mathbf{J}_l^s + w_l^s\rho_l\mathbf{J}_l + w_l^s\rho_l S_l\phi_f d\mathbf{u}/dt = \mathbf{j}_l'^s + w_l^s\rho_l S_l\phi_f d\mathbf{u}/dt$$

(2.34)

where $\mathbf{j}_l'^s$ is the flux of solute relative to the solid phase.

The use of material derivative and the introduction of equation (2.31) lead to:

$$\phi_f \frac{D(w_l^s \rho_l S_l)}{Dt} + w_l^s \rho_l S_l \left(\frac{(1 - \phi_{c+f})}{\rho_m} \frac{D\rho_m}{Dt} + \frac{\phi_c}{\rho_c} \frac{D\rho_c}{Dt} + \frac{1}{\rho_c} \frac{dm}{dt} \right) + \nabla \cdot (\mathbf{j}_l^{'s}) \qquad (2.35)$$

$$+ w_l^s \rho_l S_l \nabla \cdot (\frac{d\mathbf{u}}{dt}) - \frac{dm}{dt} = 0$$

It has to be noted that the material derivative can be approximated as Eulerian if a small strain rate is assumed while the volumetric deformation is not neglected.

b) Water mass balance

Water is present in two phases. The total mass of water per unit volume of the porous medium under unsaturated conditions is $w_l^w \rho_l S_l \phi_f + w_g^w \rho_g S_g \phi_f$, where ρ_g is the gas phase density and w_l^w and w_g^w are respectively the mass fraction of water in the liquid phase and gas phase. S_l and S_g are respectively the volumetric fraction of liquid and gas in the pores. As we are dealing with a multiphase flow problem the vapour diffusion may be important when the material is dry and the crystals attract the water with a high osmotic suction.

The total water mass balance is expressed as:

$$\frac{\partial}{\partial t} (w_l^w \rho_l S_l \phi_f + w_g^w \rho_g S_g \phi_f) + \nabla \cdot (\mathbf{j}_l^w + \mathbf{j}_g^w) = 0 \qquad (2.36)$$

where $\mathbf{j}_l^w$ and $\mathbf{j}_g^w$ are respectively the total fluxes of liquid water and water vapour with respect to a fixed reference system. Therefore these expressions contain a term that refers to the velocity of the solid phase (d$\mathbf{u}$/dt):

$$\mathbf{j}_g^w = \mathbf{i}_g^w + w_g^w \rho_g \left(-\frac{\mathbf{k}k_{rg}}{\mu_g} (\nabla p_g + \rho_g \mathbf{g} \nabla z) \right) + w_g^w \rho_g S_g \phi_f \frac{d\mathbf{u}}{dt} \qquad (2.37)$$

$\mathbf{i}_g^w$ is the diffusive flux of water vapour and is equal to:

$$\mathbf{i}_g^w = -D^{vap} \nabla w_g^w \qquad (2.38)$$

where D^{vap} is the molecular diffusion coefficient of vapour in the medium.

The total flux of water is decomposed into an advective flux caused by fluid and solid motion and a non-advective flux, and it is written as:

$$\mathbf{j}_l^w = \mathbf{J}_l^w + w_l^w \rho_l \mathbf{J}_l + w_l^w \rho_l \phi_f S_l d\mathbf{u}/dt = \mathbf{j}_l'^w + w_l^w \rho_l \phi_f S_l d\mathbf{u}/dt \tag{2.39}$$

$\mathbf{j}_l'^w$ is the total flux of water relative to the solid phase.

We note that for $\sigma =1$, *i.e.* when the solute migration is completely restricted ($\mathbf{j}_l'^s = 0$), the total flux of water relative to the solid phase is $\mathbf{j}_l'^w = \rho_l \mathbf{J}_l (w_l^w + \frac{\beta}{\alpha} w_l^s)$. For dilute solutions the total flux satisfies the general condition $\rho_l \mathbf{J}_l = \mathbf{j}_l'^w + \mathbf{j}_l'^s$. When the membrane properties are totally absent ($\sigma =0$), $\mathbf{j}_l'^w$ reduces to the classical Fick's law plus Darcy's law.

The use of material derivative on the water balance leads to:

$$\phi_f \frac{D(w_l^w \rho_l S_l + w_g^w \rho_g S_g)}{Dt} + (w_l^w \rho_l S_l + w_g^w \rho_g S_g)\frac{D\phi_f}{Dt} +$$
$$+ \nabla \cdot (\mathbf{j}_l'^w + \mathbf{j}_g'^w) + \left(w_l^w \rho_l \phi_f S_l + w_g^w \rho_g \phi_f S_g \right) \nabla \cdot (\frac{d\mathbf{u}}{dt}) = 0 \tag{2.40}$$

The porosity appears in this equation not only as a coefficient, but also in a term involving its variation caused by different processes. The way of expressing the derivative term as a function of the state variables is via Equation (2.31).

$$\phi_f \frac{D(w_l^w \rho_l S_l + w_g^w \rho_g S_g)}{Dt} + (w_l^w \rho_l S_l + w_g^w \rho_g S_g)\left(\frac{(1-\phi_{c+f})}{\rho_m}\frac{D\rho_m}{Dt} + \frac{\phi_c}{\rho_c}\frac{D\rho_c}{Dt} + \frac{1}{\rho_c}\frac{dm}{dt} \right) +$$
$$+ \nabla \cdot (\mathbf{j}_l'^w + \mathbf{j}_g'^w) + \left(w_l^w \rho_l S_l + w_g^w \rho_g S_g \right) \nabla \cdot (\frac{d\mathbf{u}}{dt}) = 0 \tag{2.41}$$

2.4.3. Stress equilibrium equation

The balance of momentum for the porous medium reduces to the equilibrium equation for the macroscopic total stresses if inertial terms are neglected (Olivella et *al.*, 1994).

$$\nabla \cdot \boldsymbol{\sigma} + \mathbf{b} = 0 \tag{2.42}$$

where $\boldsymbol{\sigma}$ is the stress tensor and $\mathbf{b}$ is the vector of body forces.

2.5. Equations of state

Equations of mass balance and motion have to be completed by equations establishing the link between the sate variables (unknowns) and the dependent variables.

It is assumed that liquid density is a function of pressure, and temperature. The Effect of temperature on liquid density is disregarded. The equation of state is given by

$$\rho_l = \rho_{l0} \exp\left(\gamma w_l^s + \beta(p_l - p_0)\right) \tag{2.43}$$

where ρ_{l0} is the mass density of pure water at the reference pressure p_0, and γ [−] and β [MPa^{-1}] are temperature dependent parameters taken equal to (Handbook of chemistry and physics, 1982),

$$\gamma = 0.6923; \quad \beta = 4.510^{-4} \, \text{MPa}^{-1} \tag{2.44}$$

Crystal density is assumed to be function of temperature. The following expression is used:

$$\rho_c = \rho_{c0} \exp\left(\xi(T - T_0)\right) \tag{2.45}$$

where ρ_{c0} is the density of the crystal defined at T_0.

Dependence of dynamic viscosity of salt mass fraction at a constant temperature is described by (Lever and Jackson, 1985, after Hassanizadeh, 1988)

$$\mu = \mu_0 \left(1 + 1.85 w_l^s - 4.1\left(w_l^s\right)^2 + 44.5\left(w_l^s\right)^3\right) \tag{2.46}$$

where μ_{0i} (MPa s) is viscosity for pure water.

For the retention curve the classical expression proposed by Van Genuchten (1980) is used

$$\left(S_e\right)_M = \left(\frac{S_l - S_{rl}}{S_{ls} - S_{rl}}\right)_M = \left(1 + \left(\frac{p_g - p_l}{P}\right)^{\frac{1}{1-\lambda}}\right)^{-\lambda}; P = P_o \frac{\sigma}{\sigma_o} \tag{2.47}$$

where λ, P, σ_0, P_0 are material parameters and σ is surface tension parameter.

2.6 Numerical implementation in a THM Code

The described formulation was implemented in the Finite element code CODE_BRIGHT. The final objective is to find the unknowns (u, P_l, w_l^s) from the governing equations (assuming isothermal conditions). The dependent variables have to be related to the unknowns. For example, degree of saturation will be computed using retention curve. In addition, dependent variables such as the salt crystal volume fraction are solved locally, once the unknowns are solved globally.

The resulting system of partial differential equations is solved numerically. The finite element method is used for the spatial discretization while the finite difference is used for the temporal discretization. Since the problem is non linear, the Newton-Raphson method is adopted to find an iterative scheme. A detailed description of the numerical resolution is given by Olivella *et al.* (1996).

After the spatial and temporal discretization of the partial differential equations, the residuals that are obtained are written as (Olivella *et al.,* 1996)

$$\mathbf{r}\left(\mathbf{X}^{k+1}\right) = \frac{\mathbf{d}^{k+1} - \mathbf{d}^k}{\Delta t^k} + \mathbf{A}\left(\mathbf{X}^{k+\varepsilon}\right)\mathbf{X}^{k+\theta} + \mathbf{b}\left(\mathbf{X}^{k+\varepsilon}, \mathbf{X}^{k+\theta}\right) = \mathbf{0} \qquad (2.48)$$

where $\mathbf{r}$ are the residuals, k is the time step index, $t^{k+\theta}$ and $t^{k+\varepsilon}$ are intermediate time between the initial t^k and final t^{k+1} times, $\mathbf{d}$ are the storage or accumulation terms $\mathbf{X} = \left(\left(u_x, u_y, u_z, P_l, P_g, T, w_l^s\right)_1, ..., \left(u_x, u_y, u_z, P_l, P_g, T, w_l^s\right)_n\right)$ is the vector of unknowns for the (*n*) nodes, and $\mathbf{A}$ represents the conductance matrix and $\mathbf{b}$ are the sink/source terms and boundary conditions, and for the case which includes all the equations.

The first contributions implemented in the code have been the implementation of subroutines for calculation of

- Activity and osmotic pressure (π) (Chapter 4, Equation (4.3)), variation of relative humidity by the presence of solutes.

- Osmotic efficiency coefficient as a function of porosity (Chapter 4, Equation (4.1)). Since porosity is integrated explicitly, the osmotic efficiency coefficient is evaluated at time t^k.
- Density for the crystals.
- Rate equation for dissolution and precipitation (Equation (2.26)). This is a source/sink term in the mass balance equations of water and solute. Incorporation of this term implies modification of the residual terms (Equation (2.48))

It has been mentioned that the sum of the porosity (ϕ_f) plus the volume fraction of the crystals (ϕ_c) is defined as a volume fraction ϕ_{c+f} (i.e. $\phi_{c+f} = \phi_c + \phi_f$). The crystal volume fraction is defined as an internal variable and computed in every element. Equation (2.28) is used for the computation of crystal volume fraction changes. Variation of porosity is given by Equation (2.30). Variation of ϕ_f is mainly caused by dissolution and volumetric deformation. Accordingly, once ϕ_c is calculated it is used to calculate porosity variation.

One of the main updates of the Finite Element Code is the introduction of the coupled fluxes in mass balance of water and solute. These fluxes comprise osmotic induced flux of water and ultrafiltration for solute. Introduction of these coupled fluxes implies modification of advective and diffusive terms of the water and solute mass balance equations.

In the water balance equation of node i, the following advective term is found after application of the weighed residual method and of Green's theorem,

$$-\int_v \nabla^t N_i \left(w_l^w \rho_l + \frac{\beta}{\alpha} \sigma w_l^s \rho_l \right) \mathbf{J}_l \, dv = \left(\int_v \nabla^t N_i \left(\rho_l w_l^w + \frac{\beta}{\alpha} \sigma w_l^s \rho_l \right) \frac{\mathbf{k} k_{rl}}{\mu} \nabla N_j \, dv \right) (p_l)_j -$$

$$\left(\int_v \nabla^t N_i \left(\rho_l w_l^w + \frac{\beta}{\alpha} \sigma w_l^s \rho_l \right) \frac{\alpha_s}{\mu} \mathbf{k} \sigma \nabla N_j \, dv \right) (w_l^s)_j + \left(\int_v \nabla^t N_i \left(\rho_l w_l^w + \frac{\beta}{\alpha} \sigma w_l^s \rho_l \right) \frac{\mathbf{k} k_{rl}}{\mu} \rho_l \mathbf{g} \, dv \right)$$

(2.49)

$$\mathbf{J}_l = -\frac{\mathbf{k} k_{rl}}{\mu} (\nabla p + \rho_l \mathbf{g} \nabla z) + \frac{\alpha_s}{\mu} \mathbf{k} \sigma \nabla(w_l^s); \quad \alpha_s = \frac{k_{rl} R T \rho_l}{M_s}$$

$$\alpha = 1 + \frac{1}{\rho_l} \frac{\partial \rho_l}{\partial w_l^s} w_l^s = 1 + \gamma w_l^s \qquad \beta = 1 + \frac{1}{\rho_l} \frac{\partial \rho_l}{\partial w_l^w} w_l^w = 1 - \gamma w_l^w$$

Where the subscript j indicates summation over elements nodes, and N_i is the shape function for node i.

The two first terms in Equation (2.49), expressed at node i are approximated as;

$$\left(\int_{e_m} \nabla^t N_i \left(\rho_l w_l^w + \frac{\beta}{\alpha} \sigma w_l^s \rho_l \right) \frac{\mathbf{k} k_{rl}}{\mu} \nabla N_j dv \right) (p_l)_j$$ (2.50)

$$-\left(\int_{e_m} \nabla^t N_i \left(\rho_l w_l^w + \frac{\beta}{\alpha} \sigma w_l^s \rho_l \right) \frac{\alpha_s}{\mu} \mathbf{k} \sigma \nabla N_j dv \right) (w_l^s)_j$$

$$\approx \left((\rho_l w_l^w)_{e_m}^{k+\varepsilon} + \sigma^k \frac{\beta}{\alpha} (w_l^s \rho_l)_{e_m}^{k+\varepsilon} \right) \left(\frac{k_{rl}}{\mu} \right)_{e_m}^{k+\varepsilon} \left(\int_{e_m} \nabla^t N_i (\mathbf{k})_{e_m}^k \nabla N_j dv \right) \left((p_l)_j^{k+\theta} - \sigma^k \pi^{k+\theta} \right)$$

where e_m is an element is volume v. intrinsic permeability is evaluated at time k because it is function of porosity.

In the water balance equation of node i, the following diffusive term is found after application of the weighed residual method and of Green's theorem,

$$\left(\int_{e_m} \nabla^t D^* \rho_l (1 - \gamma w_l^w) \mathbf{I} \nabla N_j dv \right) (w_l^w)_j \approx (1 - \sigma^k) (\phi_f \tau)_{e_m}^k (D_0 \rho_l (1 - \gamma w_l^w))_{e_m}^{k+\varepsilon} \left(\int_{e_m} \nabla \mathbf{I} \nabla N_j dv \right) (w_l^w)_j^{k+\theta}$$ (2.51)

$$D^* = (1 - \sigma) \tau \phi_f D_0$$

A similar approach is used to derive the advective and the non advective terms of solute mass balance of node i.

2.7. Summary

In this chapter, a formulation has been proposed for the analysis of deformation induced by the dissolution of the salts in porous media in contact with fresh water. The balance equations for water, dissolved salts, crystals and solid phase are written including the coupled flows, namely osmotic flow and ultrafiltration, and the dissolution/precipitation of salts. The balance equations are coupled to the equilibrium of stresses. The formulation has been implemented in the finite element program CODE_BRIGHT.

2.8. References

Bader, S. and Kooi, H.: Modelling of solute and water transport in semi-permeable clay membranes: comparison with experiments. Adv.Water.Res. 28,203–214, (2005).

Barbour, S., Fredlund, D.: Mechanisms of osmotic flow and volume change in clay soils. Can Geotech.J. 26, 551-562, (1989).

Bear, J., and Bachmat, Y.: Introduction to modeling of transport phenomena in porous media. Kluwer Acad. Publ., New York, (1990).

Bresler, E.: Anion Exclusion and coupling effects in nonsteady transport through unsaturated soils. Soil Sci. Soc. Am.Proc., 37, 663-669, (1973).

Carroll, S., Craig, L., Wolery, T.: Deliquescence of $NaCl-NaNO_3$, KNO_3-NaNO_3, and $NaCl-KNO_3$ salt mixtures from 90 to 120°C. Geochem Trans., 6,19-30, (2005).

Fritz, S.J., and Marine, I.W.: Experimental support for a predictive osmotic model of clay membranes, Geoch et Cosochim Ac., 47,1515-1522, (1983).

Fritz, S.J.: Ideality of clay membranes in osmotic processes: a review", Clay Clay Miner., 43 (2): 214-223, (1986).

Garavito, A.M.:Chemical osmosis in clayey sediments. PhD thesis, University of Utrecht, the Netherlands, (2005).

Greenberg, J.A., Mitchell, J.K., and Witherspoon, P.A.: Coupled salt and water flows in a ground water basin. J Geophys Res., 78(227), 6341-6353, (1973).

Gwinner, B., Sercombe, J., Tiffreau, C., Simondi-Teisseire, B., Felines, I., and Adenot, F.: Modelling of bituminized radioactive waste leaching. Part II. Constitutive equations. J.Nucl. Mat., 349, 96-106, (2006).

Handbook of chemistry and physics, 63rd edn., edited by R.C. Weast, CRC Press, Cleveland, Ohio, p. D261, (1982).

Hassanizadeh, S.M: Modelling species transport by concentrated brine in aggregated porous media. Transport Porous Med ., 3: 299-318, (1988).

Katchalsky, A., and Curran, P.F.: Non equilibrium thermodynamics in biophysics. Harvard University Press, Camridge, Mass, (1965).

Keijzer, T., Kleingeld, P.J. and Loch, J.P.G.: Chemical osmosis in compacted clayey material and the prediction of water transport. Eng. Geo. 53,151-159, (1999).

Keijzer, T.: Chemical osmosis in natural clayey material", Ph.D. thesis, Universiteit Utrecht, The Netherlands, (2000).

Kooi, H., Garavito, A.M., and Bader, S.: Numerical modelling of chemical osmois ans ultrafiltration across clay formations. J Geochem Explor 78-79, (2003).

Lever, D.A. and Jackson, C. P.: On the equation for flow of concentrated salt solution through a porous medium, U.K. DOE Report No. DOE/RW/85.100, (1985).

Malusis M.A, Shackelford C.D, Olsen H.W.: A laboratory apparatus to measure chemico-osmotic efficency coefficents for clay soils", Geotech Test J, ASTM 24 (3), 229-242, (2001).

Malusis M.A, Shackelford C.D.: Theory for reactive solute transport through clay membrane barriers. J Contam Hydrol, 59, 291– 316, (2002a).

Malusis M.A, Shackelford C.D.: Coupling effects during steady state solute diffusion through a semipermeable clay membrane. Environ. Sci. Technol., 36, 1312-1319, (2002b).

Malusis M.A, Shackelford C.D, Olsen H.W.: Flow and transport through clay membrane barriers", Eng Geol., 70, 235-248, (2003).

Manassero M. and Dominijanni A.: Modelling the osmosis effect on solute migrationthrough porous media", Geotechnique 53, (5):481-492, (2003).

Mariën, A., Smets, S., Li, X., and Valcke, E.: Processes Related to the Water Uptake by Eurobitum Bituminised Radioactive Waste: Theoretical Considerations and First Experimental Results", Mat. Res. Soc. Symp. Proc.1107, 151-159, (2008).

Mariën, A., Smets, S., and Valcke, E.:Study of the Processes Related to the Water Uptake of Eurobitum Bituminized Radioactive Waste: Effect of Salt Concentration. Mater. Res. Soc. Symp. Proc., Vol. 1193, 513-520, (2009).

Marine, I.W., and Fritz, S. J.: Osmotic model to explain anomalous hydraulic heads. Water Resour Res., 17 (1), 73-82, (1981).

Mitchell J.K.: Fundamentals of soil behavior, 2nd Edition. John Wiley and Sons. New York. (1993).

Mokni, N., Olivella, S., Li, X., Smets, S., and Valcke, E.: Deformation induced by dissolution of salts in porous media. J. Phys. Chem. Earth., 33, 436-443, (2008).

Mokni, N. Olivella, S. Valcke, E. Mariën A., Smets S., Li X.: Deformation and Flow Driven by Osmotic Processes in Porous Materials: Application to Bituminised Waste Materials, Transport Porous Med, Vol. 86(2), 665-692. "DOI 10.1007/s11242-010-9644-2". (2011).

Neuzil, C.: Osmotic generation of"anomalous. fluid pressures in geological environments. Nature., 403, 182–184,(2000).

Olivella, S., Carrera, J., Gens, A., and Alonso, E.E.: Non isothermal multiphase flow of brine and gas through saline media. Transport Porous Med., 15, 271-293, (1994).

Olivella, S., Gens, A., Carrera, J., and Alonso, E.E: Numerical formulation for a simulator (CODE_BRIGHT) for the coupled analysis of saline media. Eng. Comp. 13, 87-112, (1996).

Olsen, H.W., Gui, S. and Lu, N.: Critical review of coupled flow theories for clay barriers.Trans.resour.res., 57-64, (2000).

Palmeri, J. Blanc, P., Larbot, A., David P.: Theory of pressure-driven transport of neutral solutes and ions in porous ceramic nanofiltration membranes. J Membrane Sci., 160, 141-170,(1999).

Sercombe, J., Gwinner, B., Tiffreau, C., Simondi-Teisseire, B., and Adenot, F.: Modelling of bituminized radioactive waste leaching. Part I. Constitutive equations. J. Nucl. Mat. 349, 96-106, (2006).

Soler, J.M.,:The effect of coupled transport phenomena in the Opalinus Clay and implications for radionuclide transport. J Contam Hydrol., 53, 63-8, (2001).

Valcke, E., Mariën, A., Smets, S., Li, X., Mokni, N., Olivella, S., and Sillen, X.: Osmosis induced swelling of Eurobotum bituminized radioactive waste in constant total stress conditions. J.Nuc.Mater., 406, 304-316, (2010).

Van Genuchten, M.T.: A closed form equation for prediction the hydraulic conductivity of unsaturated soils. Soil. Sci.Soc.Am., 44, 379-392, (1980).

Yeung, A.T., and Mitchell, J.K.: Coupled fluid, electrical and chemical flows in soil", Géothechnique 43(1), 121-134, (1993)Yang, N., and Barbour, S.L.: The impact of soil structure and confining stress on the hydraulic conductivity of clays in brine environments. Can.Geotech.J., 29, 730-739, (1992).

Chapter 3

Deformation of bitumen based porous material. Experimental and numerical analysis

3.1. Introduction

Since the late 1960's, bitumen has been applied by the nuclear industry as a matrix for the immobilisation of low and intermediate level radioactive wastes, amongst others because of its good binding capacity, its low solubility and low permeability to water, and its good chemical and biological inertia. Depending upon the nature of the confined waste and in consequence to the chemical pre-treatment process, the bituminised waste contains important quantities of soluble salts.

The intermediate-level Bituminised radioactive Waste (BW) called Eurobitum has been produced at the EUROCHEMIC/BELGOPROCESS reprocessing facility (Mol-Dessel, Belgium), to immobilise precipitation sludge and evaporator concentrates originating from the chemical reprocessing of spent nuclear fuel and cleaning of high-level waste storage tanks. Eurobitum typically contains between 20 and 30 % in weight of sodium nitrate ($NaNO_3$) and about 60 % in weight of hard bitumen Mexphalt R85/40. The remainder of the BW consists of sparingly soluble salts such as $CaSO_4$, CaF_2, and $Ca_3(PO_4)_2$, and oxides and hydroxides of Al, Fe, and Zr. Radionuclides are estimated to be present but for some 0.2 wt% at most (Valcke et *al.*, 2009).

The current reference solution of the Belgian Agency for the Management of Radioactive Waste and Fissile Materials (ONDRAF/NIRAS) envisages the direct underground disposal of this waste in a geologically stable clay formation. In Belgium, the Boom Clay is studied as a potential host formation because of its favorable properties to limit and delay the migration of the leached radionuclides to the biosphere over extended periods of time.

Under geological disposal conditions the main factor that affects the long term behaviour of the material is water uptake, which is expected to take place at an extremely low rate given the low permeability of the waste and the surrounding multibarrier isolation systems. At the long term conditions, when the water reaches the waste, the hygroscopic soluble salts incorporated in the BW (i.e. $NaNO_3$) will take up ground water resulting in dissolution and subsequent leaching of these salts. The material progressively becomes porous and permeable, but the rate of this process is controlled by the mobility of the water and solute. Moreover, it is well known that porous materials containing salts may undergo swelling by water uptake induced by osmotic flows (Mokni et *al.*, 2008). As mechanical effects are expected, it is necessary to investigate the deformation properties of this waste and its possible interaction with the multibarrier system, especially with the host rock.

For bitumen, creep deformations are expected and these depend in a nonlinear way on stresses and temperature (Cheung and Cebon, 1996 and 1997). In addition, several factors like chemical composition and structure of the bitumen, time, temperature, radiation and exposure to oxygen might induce a change of the rheological properties of bitumen with time (a phenomenon called ageing). As bitumen ages, it becomes harder and increasingly brittle (Valcke et *al.*, 2009). When other viscoplastic constituents are introduced into it, the creep behaviour of the resulting multi-component material (mixture) may be influenced, as is the case of the BW.

Another characteristic of the BW is the presence of pores inside the bitumen matrix, which affect the creep behavior, and which requires a specific numerical treatment when building the constitutive law. A good understanding of the mechanical behavior of the BW is thus an absolute prerequisite for understanding the overall behavior of such a complex mixture material. The objective here is to develop a model capable of predicting the overall creep strain of a mixture of bitumen and salt crystals.

3.2 Experimental aspects

To investigate the mechanical behaviour of the BW, two types of tests have been performed: (1) unconfined compression tests and (2) confined compression tests (oedometer tests).

3.2.1 Unconfined compression creep tests

The experiments are focused on the creep behaviour of the studied materials. Several bitumen/salt mixtures were tested (DENG et *al*., 2009). Tests were also conducted on pure bitumen samples, for reference. The description of the samples is shown in Table 3.1.

Table 3.1: Description of tested samples

No.	Reference	Descriptions
1	Mexphalt R85/40	Pure bitumen without salts
2		
3	BW 0-2//CR15/16//08	Reference Eurobitum with 28 wt% $NaNO_3$
4	BW 0-4//CR15/15//09	Reference Eurobitum with 28 wt% $NaNO_3$
5	BW 0-3//CR15/9//08/18	Eurobitum with 18 wt% $NaNO_3$
6	Mexphalt R85/40	Pure bitumen without salts
7		

The experimental set-up is shown in Figure 3.1. The diameter of the sample was smaller than that of the cell, thus allowing lateral deformation (unconfined condition). The cell itself was put in the oedometer frame for application of the vertical stress. An oedometer frame is an apparatus to apply stress, by means of weights and a lever, on a cell that usually contains a confined porous sample. Different constant loading steps were applied on the samples. Each loading step was applied instantaneously and maintained for about 30 minutes. The vertical displacement for each loading step was recorded as a function of time. Meanwhile, the temperature inside and outside the cell

was carefully monitored in order to check its possible influence on the measurement. The results allow interpreting the creep behaviour of the bitumen and the mixtures (bitumen/salt) at various stress levels.
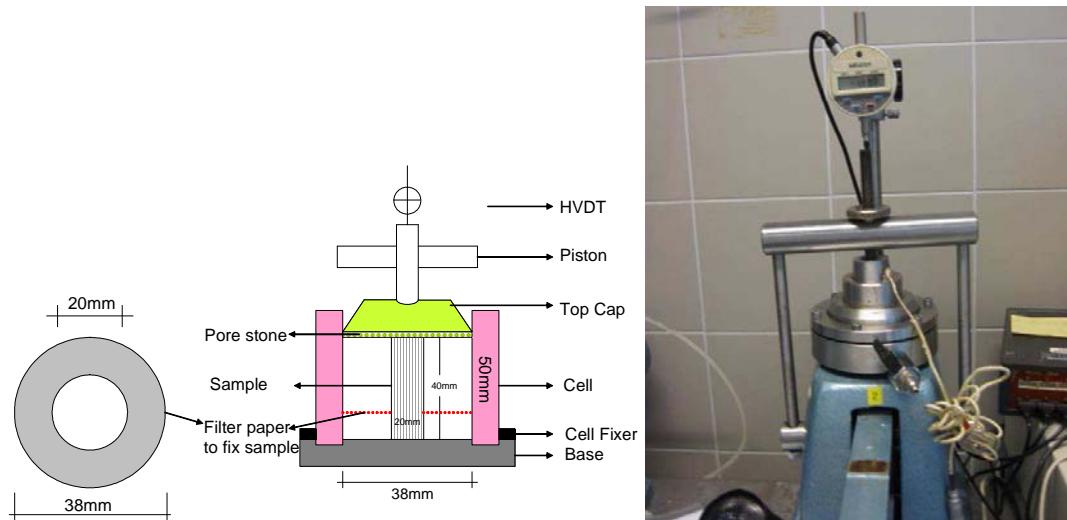
Figure 3.1: Device for the unconfined compression test

The result of the constant stress creep test is displayed in Figure 3.2.a. Here the steady state strain rate is plotted against the stress for six specimens. For reference, Figure 3.2.b shows the results obtained by Cheung and Cebon (1996), which indicate that the creep of pure bitumen is well represented by a power law equation relating strain rates with the power of the stress. Although the results show some scattering, it can be seen that the behaviour of the pure bitumen and the BW can be represented by a creep power law, in a similar way as reported in the literature (Cheung and Cebon, 1996 and 1997) for other bitumens. The incorporation of salt crystals decreases strain rates. This is expected as the crystals deform at slower rates as compared with bitumen material.

3.2.2 Confined compression tests

A confined compression test consists of a series of steps of uniaxial deformation under confined conditions, i.e. with lateral deformations not permitted. This test, often referred to as oedometer test, is quite standard in mechanics of porous materials, and it was originally developed in the field of soil mechanics. An oedometer test produces vertical deformations which imply volumetric deformations ($\varepsilon_{volumetric} = \varepsilon_{vertical}$) and deviatoric deformations ($\varepsilon_{deviatoric} = (2/3)\varepsilon_{vertical}$).
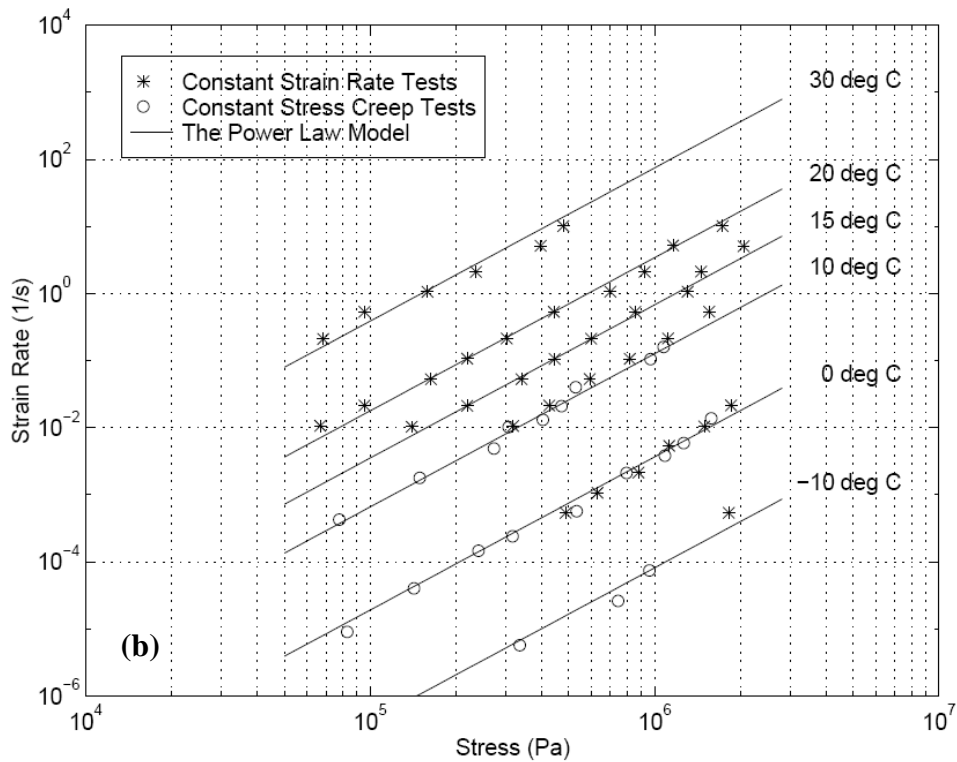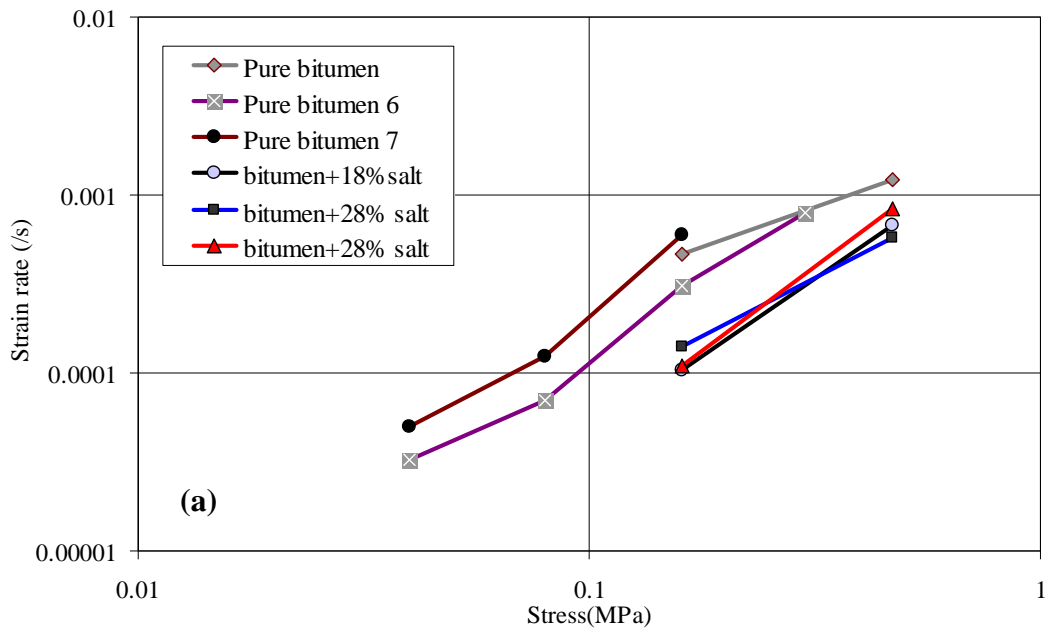
Figure 3.2: (a) Steady state creep behaviour in compression for Eurobittum. (b) Steady state creep behaviour of a different bitumen (Cheung and Cebon, 1996)

A series of confined compression tests was performed on non-radioactive samples taken from drums of Eurobitum produced about 25 years ago, during the inactive start-up phase of the bituminisation plant. The production method and composition of this non-radioactive reference BW are entirely similar to that of the radioactive BW, except for

the presence of radionuclides. The samples had a diameter of 38 mm and were 10 mm in height, and were artificially aged before the tests (by gamma irradiation in the absence of oxygen) (Valcke et *al.*, 2009).

The tests were performed using a conventional oedometer cell, with sintered metal filters above and below the samples, so that the material could be hydrated in a later phase (water-uptake test) (Figure 3.3). It is assumed that the samples were dry before the compression tests. However some condensed water could have reached the pores.
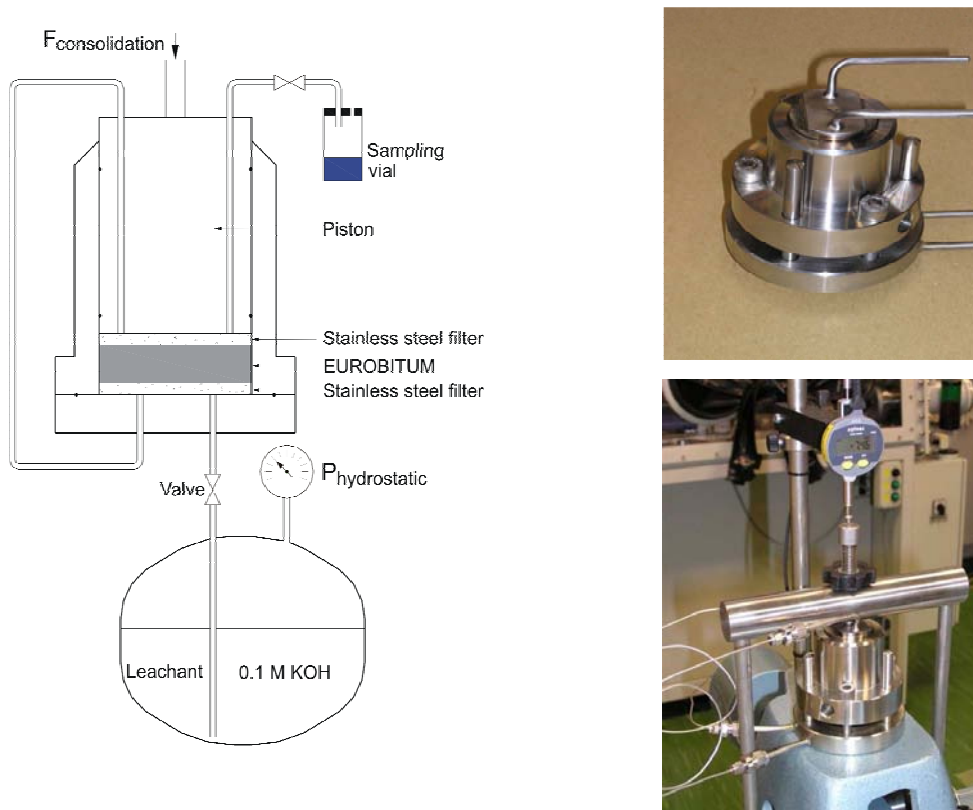
Figure 3.3: Confined compression test set-up (combined with water uptake test)

A series of seven experiments was performed on non-radioactive BW in a laboratory with controlled temperature (about 22 °C). The oedometric tests were performed under dry conditions. The tests mainly consist in the loading and unloading events which finally lead to a material which was practically incompressible (Figure 3.4). Because the compression is irreversible, it is deduced that initial porosity is at least of the order of these irreversible deformations. In absence of porosity, the incompressibility of the material would not permit irreversible deformation under oedometric conditions. The soft nature of the bitumen permits to assume that porosity reduces during compression.

It has to be kept into consideration that this series of tests were performed in order to obtain mechanical properties of the studied materials. The stress level applied is close to the expected in situ stress conditions.
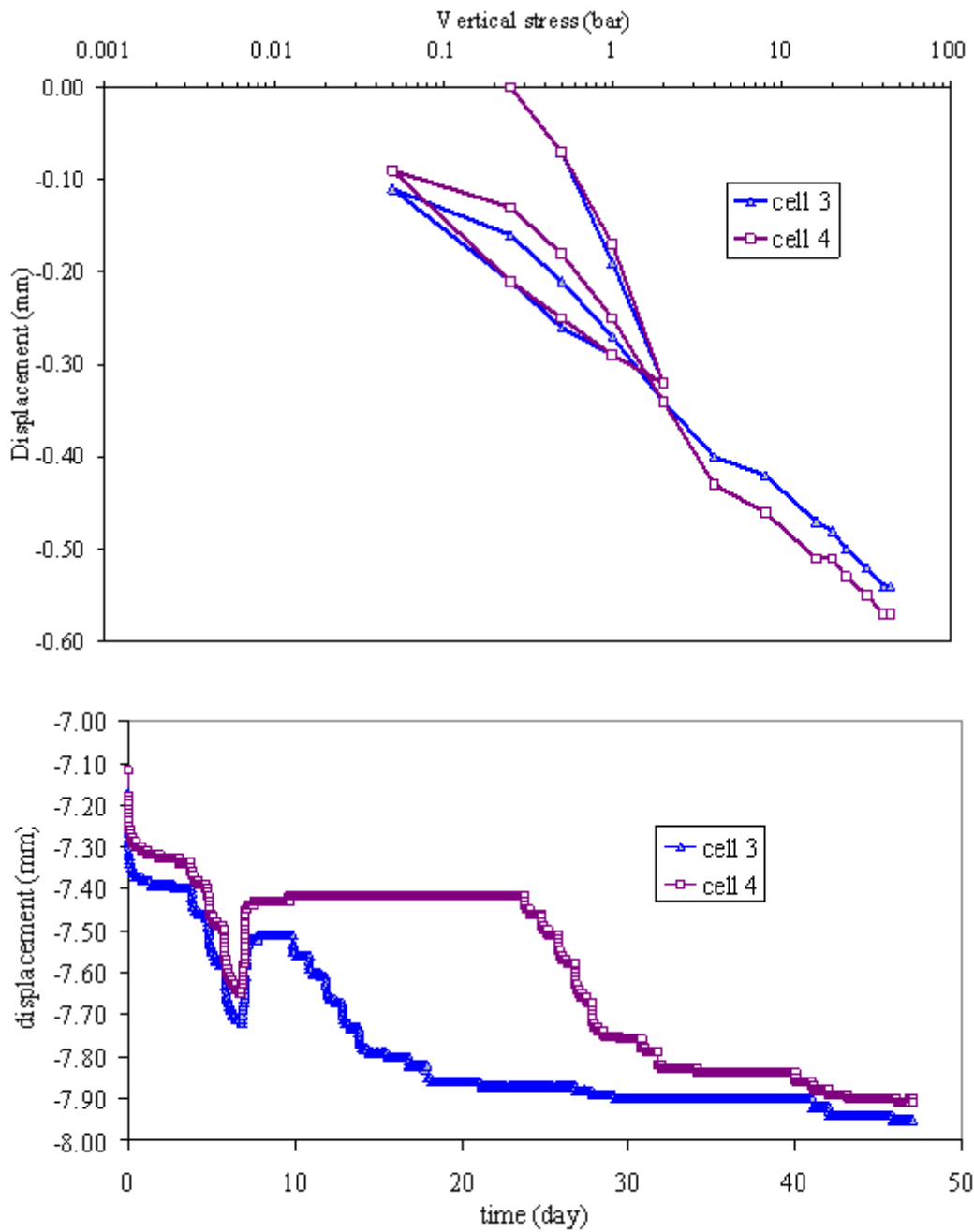
Figure 3.4: Representative odometer test results (cell 3 and cell 4).

3.3 Mechanical constitutive model

The bituminized waste is considered as a homogeneous suspension of soluble $NaNO_3$ salt crystals in bitumen (Figure 3.5). As mentioned above, the hygroscopic soluble salts incorporated in the BW will take up water from the surrounding host formation resulting in dissolution, but this is expected to occur at a very low rate in geological disposal conditions. Therefore, the bitumen matrix progressively becomes porous and permeable (Figure 4.1.b, Chapter 4).
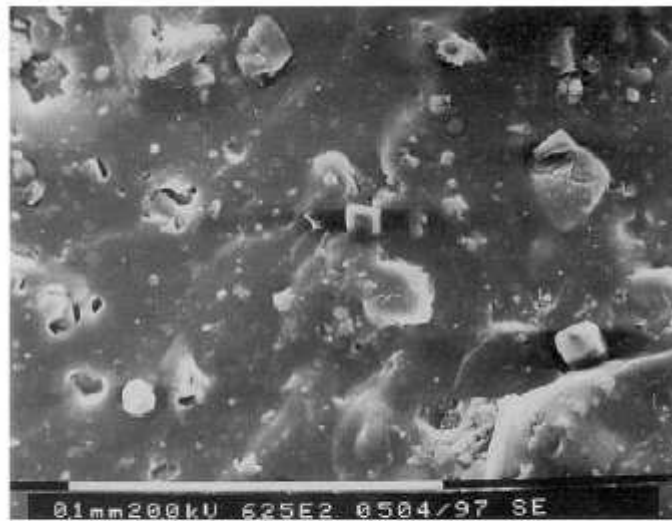
Figure 3.5: ESEM observation of a dry sample of BW (Mokni et *al.*, 2008)

From a mechanical point of view, both bitumen and salt crystals show significant creep deformation that may control the response of the mixture. The complex mechanical behaviour of such a material requires an adequate mechanical constitutive model to describe its elastic and viscoplastic behaviour.

For a material presenting elastic-viscoplastic behaviour, the total strain tensor can be described by:

$$\varepsilon_{ij} = \varepsilon_{ij}^{e} + \varepsilon_{ij}^{vp} \tag{3.1}$$

where $\varepsilon_{ij}^{e}, \varepsilon_{ij}^{vp}$ denote the elastic and viscoplastic strain components, respectively.

3.3.1 Constitutive model for creep deformation

In general the BW can be envisaged as composed of a porous bituminized matrix embedding crystals (Figure 3.6).

The total volume of the medium (V_t) can be decomposed into the volume occupied by the crystals (V_c), the pores (voids: V_v) and the bitumen (V_b), i.e. $V_t = V_c + V_v + V_b$. The volume of the pores varies as the consequence of dissolution of the crystals and may be occupied by water or air.
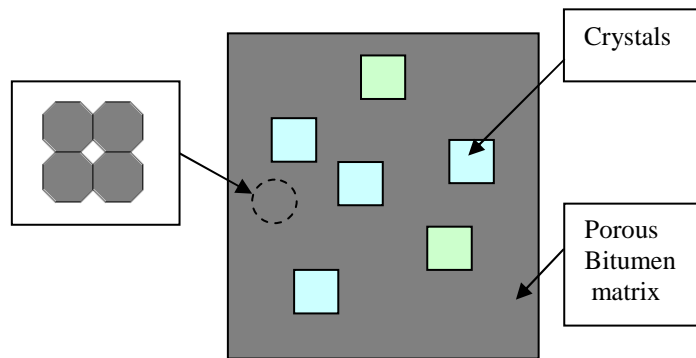
Figure 3.6: Schematic representation of the medium

These volumes permit to define the volume fraction of the different components (ϕ_c and ϕ_b) and the volume fraction of pores, i.e. the porosity (ϕ). These variables are defined as:

$$\phi_c = \frac{V_c}{V_t}; \qquad \phi = \frac{V_v}{V_t}; \qquad \phi_b = \frac{V_b}{V_t} \tag{3.2}$$

$$V_t = V_c + V_v + V_b; \qquad 1 = \phi_c + \phi + \phi_b = \phi_c + \phi_m$$

$$\phi_m = \phi + \phi_b$$

The sum of the porosity (ϕ) plus the volume fraction of the bitumen (ϕ_b) is defined as the volume fraction of the porous bitumen matrix ϕ_m, i.e. $\phi_m = \phi + \phi_b$. In this way, $1 - \phi_m = \phi_c$ is the volumetric fraction occupied by the crystals.

Creep of crystalline materials is modeled with the so-called creep power law (Perzyna, 1966), which relates deviatoric strain rates and deviatoric stresses, in a linear or

nonlinear way. In addition, temperature effects and hardening or softening responses can be incorporated. Creep deformation of solids and viscous response of fluids are expressed with the same mathematical equation. In case of fluids it leads to Newtonian or non-Newtonian behavior, respectively, for linear or nonlinear response. For Newtonian materials, the shear strain rate is proportional to the shear stress. The constant of proportionality is known as the viscosity. For non-Newtonian materials the linearity is lost and the strain rate is usually written as proportional to a nonlinear function of the shear stress.

Crushed rocks, metal powders and other porous materials like the porous bituminized matrix, made of viscous components, require constitutive equations with significant volumetric contribution as compared to crystals which are practically incompressible. Olivella and Gens (2002) have developed a model for porous crushed salt that combines the power law and a simple geometric representation of grains and pores. The model has been applied to simulate an in situ test in the Asse salt mine performed during more than 10 years (Olivella et *al*., 2003). The crushed salt model converges to the model of rock salt as porosity vanishes. The fundamentals of the model developed by Olivella and Gens (2002) are included in Appendix B. This model is used as the basis for the development of a model for the mixture of bitumen and crystals, both materials assumed to deform with elastic and creep contributions.

In the model presented here, the strain rates of a mixture can be obtained from the properties of the components under shear conditions assuming a weighted geometric average. This represents a combination of mechanisms in series and/or in parallel. Series would imply that the more deformable material dominates while parallel would imply that the stiffer material dominates. In contrast, the arithmetic average seems more appropriate for volumetric deformations, which represents more a combination of mechanisms in series in this case. Actually the crystals are more or less floating in the bitumen matrix.

Under these assumptions, the viscoplastic strain of the mixture (BW) would be defined as follows:

$$\frac{d\varepsilon_d^{vp}}{dt} = \left(\frac{d\varepsilon_d^m}{dt}\right)^{\phi_m} \left(\frac{d\varepsilon_d^c}{dt}\right)^{\phi_c}$$

$$\frac{d\varepsilon_v^{vp}}{dt} = \phi_m \left(\frac{d\varepsilon_v^m}{dt}\right) + \phi_c \left(\frac{d\varepsilon_v^c}{dt}\right)$$

(3.3)

where ε^m and ε^c denote respectively the viscoplastic strain of the bitumen matrix and of the crystal, and the subscript "d" stands for deviatoric (shear) while the subscript "v" corresponds to volumetric. These assumptions imply that the crystals have more effect on deviatoric deformation than on volumetric. Other possibilities could be investigated. As will be shown below, assuming these combinations permits to obtain the form of the equivalent parameters for power and viscosity in a relatively simple way.

As explained above, the creep of crystalline materials is governed by a power law, so the following equation is considered for the crystals:

$$\frac{d\varepsilon_{ij}^c}{dt} = A_c q^{n_c} \frac{\partial q}{\partial \sigma_{ij}}$$

(3.4)

where $A_c (T)$ is a temperature dependent parameter, n_c the power of the deviatoric stress of the creep law of the crystal, and q the deviatoric stress. It is important to notice that this law does not allow volumetric creep deformation.

The description of the mechanical behavior of the porous bitumen matrix requires constitutive equations with significant volumetric creep contribution. As indicated above, Olivella and Gens (2002) developed a model to represent the creep behaviour of porous salt aggregates. Creep for this kind of materials is explained with the theory of dislocations (Dislocation Creep deformation), which refers to intracrystalline mechanisms, and is characterized by a power law. In contrast, the bitumen used for the bituminized waste is an amorphous polymer material (Cheung and Cebon, 1996) but its creep can also be described with a power law in the range of stresses and temperatures considered in this research. So the common point is the creep power law, which is referred to also as a non-newtonian fluid equation. While crystalline rocks are solid materials, bitumen has a behavior that is closer to that of fluids.

The mechanical model was based on an idealized geometry (polyhedrons representing the particles) that was used as a basis for calculating strain rates and to obtain macroscopic laws (see Appendix B). It should be noticed that all geometrical variables were only a function of porosity (actually: void ratio). In that model, it was assumed that volumetric deformation was produced by the deviatoric deformation of the solid phase (example: a packing of incompressible spheres may reduce its porosity if the spheres change their shape).

Considering the adopted geometry and making further assumptions of stress distributions in the solid mass, the model was expressed in the following generalized form (see Appendix B):

$$\frac{d\varepsilon_{ij}^{vp}}{dt} = \frac{1}{\eta}\Phi(F)\frac{\partial G}{\partial \sigma_{ij}^{'}}$$

(3.5)

where G is the viscoplastic potential to describe the flow rule, F is a stress function, Φ is a scalar function and η is a viscosity parameter. The application of the model to the bitumen matrix requires only the use of the appropriate material parameters A_m and n_m (see below).

Therefore, it is possible to write:

$$F = G = \sqrt{q^2 + \left(\frac{p}{\alpha_p}\right)^2} \qquad \Phi(F) = F^{n_m}$$

(3.6)

where α_p was a function of viscosities, i.e.

$$\eta = \eta^d, \qquad \alpha_p = \left(\frac{\eta^v}{\eta^d}\right)^{1/(n_m+1)}$$

(3.7)

where η^v and η^d are respectively viscosities for volumetric and deviatoric creep, defined as:

$$\frac{1}{\eta^v} = A_m g^v(\phi); \qquad \frac{1}{\eta^d} = A_m g^d(\phi)$$

(3.8)

where $A_m(T)$ is a temperature dependent parameter and n_m is the power of the deviatoric stress of the creep law of the bitumen matrix. The definition of g^v and g^d is given in the appendix. Both equations (3.4) and (3.5) are Perzyna type equations (Perzyna, 1966), respectively for pure deviatoric deformation (3.4) and for coupled deviatoric-volumetric

deformation (3.6). A main assumption here is that a material obeying a creep power law and containing pores can be modelled with a similar approach, irrespective of its micro structure (crystalline or amorphous).

In order to extend this model to a mixture and to incorporate the contribution of the salt crystals, the equivalent parameters are defined in the following way:

$$\frac{1}{\eta_{eq}^d(\phi)} = A_{eq}^d(\phi) = \left(A_m g^d(\phi)\right)^{\phi_m} \left(A_c g^d(0)\right)^{\phi_c} = \left(A_m g^d(\phi)\right)^{\phi_m} \left(A_c\right)^{\phi_c} \tag{3.9}$$

$$\frac{1}{\eta_{eq}^v(\phi)} = A_{eq}^v(\phi) = \phi_m A_m g^v(\phi) + \phi_c A_c g^v(0) = \phi_m A_m g^v(\phi)$$

$$n_{eq}(\phi) = n_m \phi_m + n_c \phi_c$$

The form comes from the proposed assumption given above (Equation 3.3) and provides some conditions that are described later. Without loss of generality other assumptions could be considered, but the ones chosen (arithmetic mean for volumetric and for the power, and geometric mean for deviatoric) are a conjecture.

In this model extension, it is assumed that the crystals do not have pores; this is why the functions corresponding to crystals have been written for zero porosity. Actually this is equivalent to: $g^v(0) = 0$ and $g^d(0) = 1$ (apply zero porosity or void ratio to equations in Appendix B). Therefore, the volumetric contribution is due solely to the bitumen matrix deformation.

Finally, the viscoplastic potential and the stress function are written as:

$$\tag{3.10}$$

$$G = \sqrt{q^2 + \left(\frac{p}{\alpha_p}\right)^2} \quad \text{and} \quad F = \sqrt{q^2 + \left(\frac{p^{\frac{n_m}{n_{eq}}}}{\alpha_p}\right)^2} \quad \text{and} \quad \Phi(F) = F^{n_{eq}}$$

$$\tag{3.11}$$

$$\alpha_p = \left(\frac{\eta_{eq}^v(\phi)}{\eta_{eq}^d(\phi)}\right)^{\frac{1}{1+n_{eq}}} \qquad \frac{1}{\eta_{eq}^v(\phi)} = A_{eq}^v(\phi) = \phi_m A_m g^v(\phi)$$

$$\eta = \eta_{eq}^d(\phi) \qquad \frac{1}{\eta_{eq}^d(\phi)} = A_{eq}^d(\phi) = \left(A_m g^d(\phi)\right)^{\phi_m} \left(A_c\right)^{\phi_c}$$

No threshold stress is defined, which implies that strain rates develop at any stress level (this is also the case for salt rock).

The new model was developed to accomplish the following conditions described below.

When the stress state is isotropic ($(\sigma_1) = (\sigma_2) = (\sigma_3)$; the subscripts 1, 2, 3 indicate the principal stress directions) only the properties of the bitumen matrix play a role:

$$\frac{d\varepsilon_v^{vp}}{dt} = \phi_m A_m g^v(\phi) p^{n_m} = \frac{1}{\eta_{eq}^v(\phi)} p^{n_m} \tag{3.12}$$

When pure shear conditions are reached ($(\sigma_3) = -(\sigma_1)$ and $(\sigma_2) = 0$) the equivalent parameters (power and viscosity) are recovered for the calculation of strains:

$$\frac{d\varepsilon_1^{vp}}{dt} = \frac{3}{2} A_{eq}^d (\sigma_1)^{n_{eq}} = \frac{3}{2} \frac{1}{\eta_{eq}^d(\phi)} (\sigma_1)^{n_{eq}} \tag{3.13}$$

Both viscosities η^v and η^d depend on the porosity (see Appendix B). The shape of these functions is crucial to describe adequately the porosity influence on the creep deformations of the mixture. The chosen functions for viscosities have been represented in Figure 3.7, considering the case of a porous bitumen matrix ($\phi_c=0$) and of a bituminised waste ($\phi_c=0.16$), and using $n_{eq}=2$. It shows that η^v tends to infinity as porosity vanishes. Therefore, at low porosity the original power law (Equation 3.4) is recovered by Equation (3.6). The limiting values can also be easily verified from Equations (3.10): f tends to zero when the pore volume disappears (it tends to zero) and consequently g tends to 1. The effect of porosity on the volumetric creep is much larger than on the deviatoric creep, except for high porosities (close to 0.40). Figure 3.7 also shows that changing the crystal volume fraction from 0 to 0.16 increases significantly the viscosity for deviatoric creep.
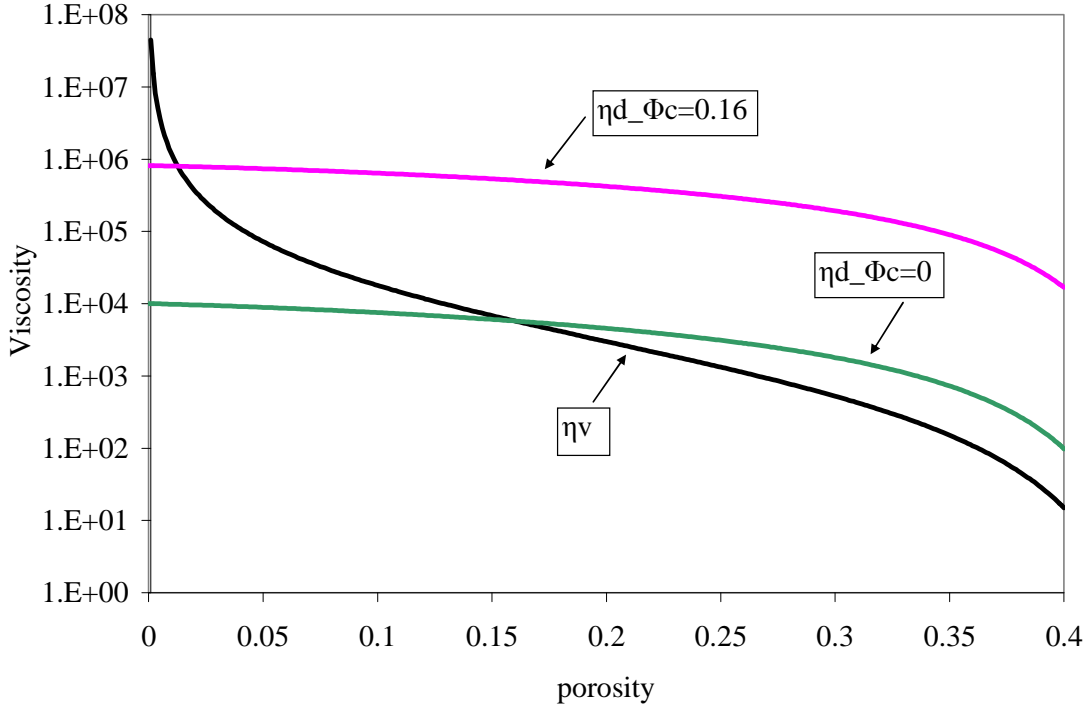
Figure 3.7: Viscosities (in MPa^{2}s) for volumetric and deviatoric creep as a function of porosity using $n_{eq}=2$.

3.3.2 Elastic behaviour

Elastic volumetric deformations of the BW are described by an appropriate nonlinear law which is a logarithmic relationship often found in constitutive models for soils.

$$d\varepsilon_v^e = \frac{k}{1+e}\frac{dp'}{p'} = \frac{dp'}{K}; \quad K = \frac{p'(1+e)}{k} \tag{3.14}$$

where p' (MPa) is the mean effective stress (defined as $p' = (\sigma_1 + \sigma_2 + \sigma_3)/3$), e and k are respectively the void ratio and the slope of the unload/reload curve in the (e - $\ln p'$) diagram. $K(p')$ is the nonlinear bulk modulus. For a given initial stress, paths for which $dp'>0$ lead to compression and paths for which $dp'<0$ lead to expansion. Since the above defined logarithmic law does not allow tension, an additional condition is considered as follows

$$K = \max\left(\frac{p'(1+e)}{k}; K_{\min}\right) \tag{3.15}$$

In this equation, K_{min} is a lower bound of the stiffness modulus, which may be small but positive. It is used for low stress confinement and also for tension conditions.

3.3.3 General formulation for elasticity plus elasto-viscoplastic creep

In summary, a general formulation for elasticity plus creep (elasto-viscoplastic) law for the studied BW can be written in the following way:

$$\frac{d\varepsilon_{ij}}{dt} = \frac{d\varepsilon_{ij}^{elastic}}{dt} + \frac{d\varepsilon_{ij}^{vp}}{dt} = \frac{d\varepsilon_{ij}^{elastic}(\sigma_{ij})}{dt} + \frac{d\varepsilon_{ij}^{vp}(\sigma_{ij},T,\phi)}{dt}$$

(3.16)

which has a particular form for the isotropic case:

$$\frac{d\varepsilon_v}{dt} = a_1 \frac{1}{p'}\frac{dp'}{dt} + \frac{1}{\eta^v(T,\phi)}p'^{n_m}$$

(3.17)

where a_1 is a parameter for the nonlinear elastic contribution defined as:

$$a_1 = \frac{k}{1+e}$$

(3.18)

Although the isotropic part is used here for the description of the model equations, the model is used for a general stress state, including a Poisson ratio for the elastic part and the full viscoplastic formulation for the creep part as given above.

As it has been written above, the model does not allow extension behavior. In that case, when the material is subjected to tension stresses, Equation (3.17) becomes:

$$\frac{d\varepsilon_v}{dt} = \frac{1}{K_{\min}}\frac{dp'}{dt} + \frac{1}{\eta^v(T,\phi)}|p'|^{(n_m-1)}p'$$

(3.19)

The described model includes thus nonlinear elasticity plus nonlinear creep. For elasticity the nonlinearity comes from the mean effective stress dependence of stiffness (Equation 3.14). The non-elastic part of the model is a power function of stress. As shown in Equation (3.11) viscosity functions also depend in a nonlinear way of porosity.

3.4 Modelling of mechanical behaviour of BW

The model described above has been implemented in the Finite Element code CODE_BRIGHT. Several numerical simulations were performed in order to explore the model ability to reproduce the influence of the presence of the crystals on the creep behaviour of the BW. A numerical exercise is first shown, which permits to consider assumptions to simplify the problem.

The numerical example concerns a simulation of a creep test under oedometric conditions (vertical stress=0.2 MPa). The model parameters are summarized in Table 3.2. Figure 3.8 displays the evolution of creep deformation with time for three cases: (1) porous bitumen matrix, (2) mixture of bitumen and 16% in volume of $NaNO_3$ (ϕ_c = 0.16), and (3) mixture of bitumen and 20% in volume of $NaNO_3$ (ϕ_c = 0.20). The plot shows that creep deformations decrease significantly when ϕ_c increases, at this stress level. This is a consequence of the increase of the viscosity for deviatoric creep.

Table 3.2: Material parameters for the numerical example

Parameters	Symbols	Values
Elastic model	υ	0.3
	a_1	0.0078
Creep model	n_m	2.1
	n_c	5
Initial porosity	ϕ_0	0.06
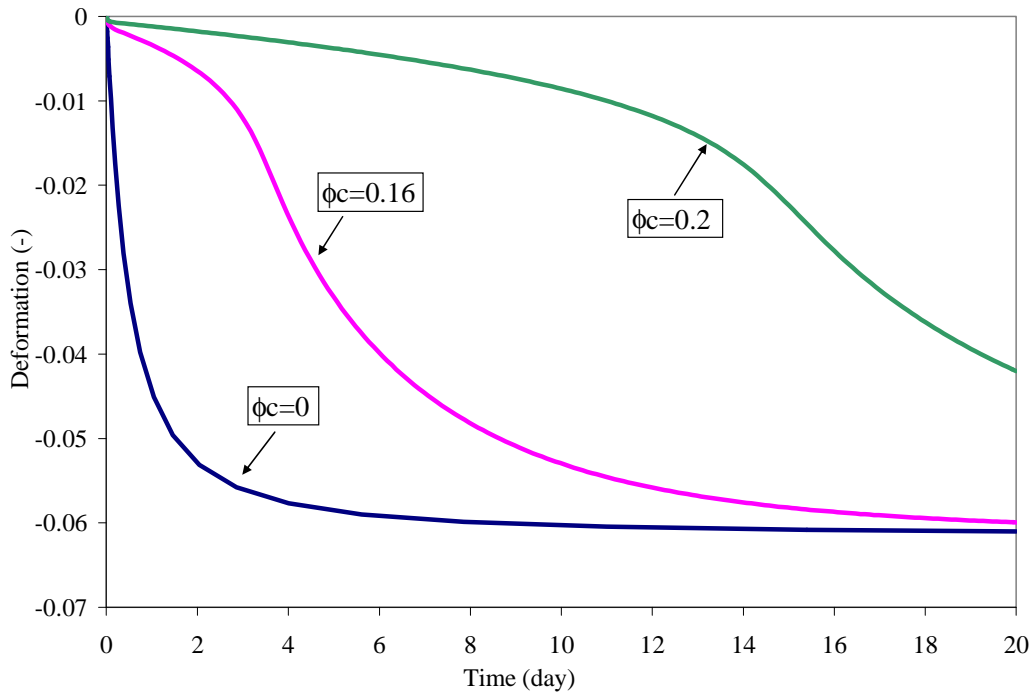
Figure 3.8: Effect of crystal volume fraction on creep deformation for an oedometric test under constant vertical stress of 0.2 MPa.

3.4.1 Modelling of compression tests under confined conditions

As explained previously (Section 3.2.1), a series of conventional oedometric tests with cylindrical inactive gamma irradiated Eurobitum samples containing 28% in weight of $NaNO_3$ were performed in the laboratory of SCK•CEN. From the experimental results it is clear that the material shows a nonlinear elastic behavior (deformation varies rather linearly with the logarithmic vertical stress). These results permit to determine the parameters for the mechanical constitutive model described above.

An initial porosity of these samples for the oedometric tests was estimated to have the value $\phi_0 = 0.06$ according to the deformation of the samples (a precise measurement would be envisaged). The parameters have been calibrated to simulate the experiment performed with cell 3 and cell 4 (Table 3.3), which are representative of the series of tests and show little scatter of the test results. The power of the creep power law for porous bitumen matrix has been deduced on the basis of the results of pure bitumen given in Figure 3.2.

Table 3.3: Material parameters for modelling of compressions tests

Parameters	Symbols	Values
Elastic model	υ	0.3
	a_1	0.0078
Creep model	n_m	2.1
	n_c	5
Initial porosity	ϕ_0	0.06
Crystal volume fraction	ϕ_c	0.16

For the model prediction we have used the following values of the temperature dependent parameter of the bitumen matrix and the crystals:

$$A_m(T) = 8 \exp\left(-\frac{22900}{RT}\right)$$

$$A_c(T) = 5 \times 10^{-6} \exp\left(-\frac{59650}{RT}\right)$$

(3.20)

It should be recalled that these viscosity parameters are not comparable as they correspond to power law creep equations with different power.

For the bitumen matrix, the constant inside the exponential has been taken from Cheung and Cebon (1996), while the pre-exponential constant has been determined to obtain a good prediction of the experimental test represented in Figure 3.9. For the crystals, the adopted values correspond to typical values for rock salt deviatoric deformation Olivella and Gens (2002). Evolution of the deformation versus time for the oedometric cells together with the model results are shown in Figure 3.9. The modeled results show many similarities with the experimental data (taking into account that the viscosity has been calibrated with these tests). They are characterized, for each loading step, by instantaneous deformations followed by creep. Beyond a certain time, for high stress levels volumetric creep deformations disappear because the volume of pores becomes negligible and the material shows only a volumetric elastic response. It must be noticed that η^v tends to infinity as porosity vanishes, which guarantees that the volumetric creep part disappears progressively.

Some discrepancies are observed, however, between the experimental and model results. The model does not predict very well the large instantaneous deformations that occur immediately after the first loading. These discrepancies could be attributed to uncertainties that occurred during the experiment. In fact, it is unlikely that the piston was totally in contact with the sample after first loading (25 kPa), since the upper surface of the material was rough. Therefore the first loading step produces a large deformation increment in the test which, as mentioned before, can be attributed to accommodation of the piston on the material surface. In contrast the model predicts the deformation increment corresponding to the first loading step (from 0 to 25 kPa).

3.4.2 Simulation of other experiments under different conditions

In the previous section, the model was applied to 2 experiments and the viscosity constant and elastic compressibility were calibrated. The power of the creep law was maintained equal to the value determined from unconfined compression. In this section, other experiments are modeled. Figure 3.10 shows the simulation of a multistep test under different conditions of crystal content and the comparison with experimental results. The sample in this case is assumed to have a low porosity (2.5%), as it was pre-compressed to guarantee good contact at the initial loading step. No variation of the model parameters has been carried out in this case. In addition, Figure 3.11 shows the

simulation of another multistep test for a radioactive sample. The radioactive BW was of different nature as the material tested in experiments in Figure 3.2: it was a less deformable material, and the viscosity constant (*A*) had to be reduced by a factor 1000 to simulate the test results (two series showing good repeatability). Further experiments will be modeled in the future and special attention should be paid to the initial conditions of the material before application of the stress levels.
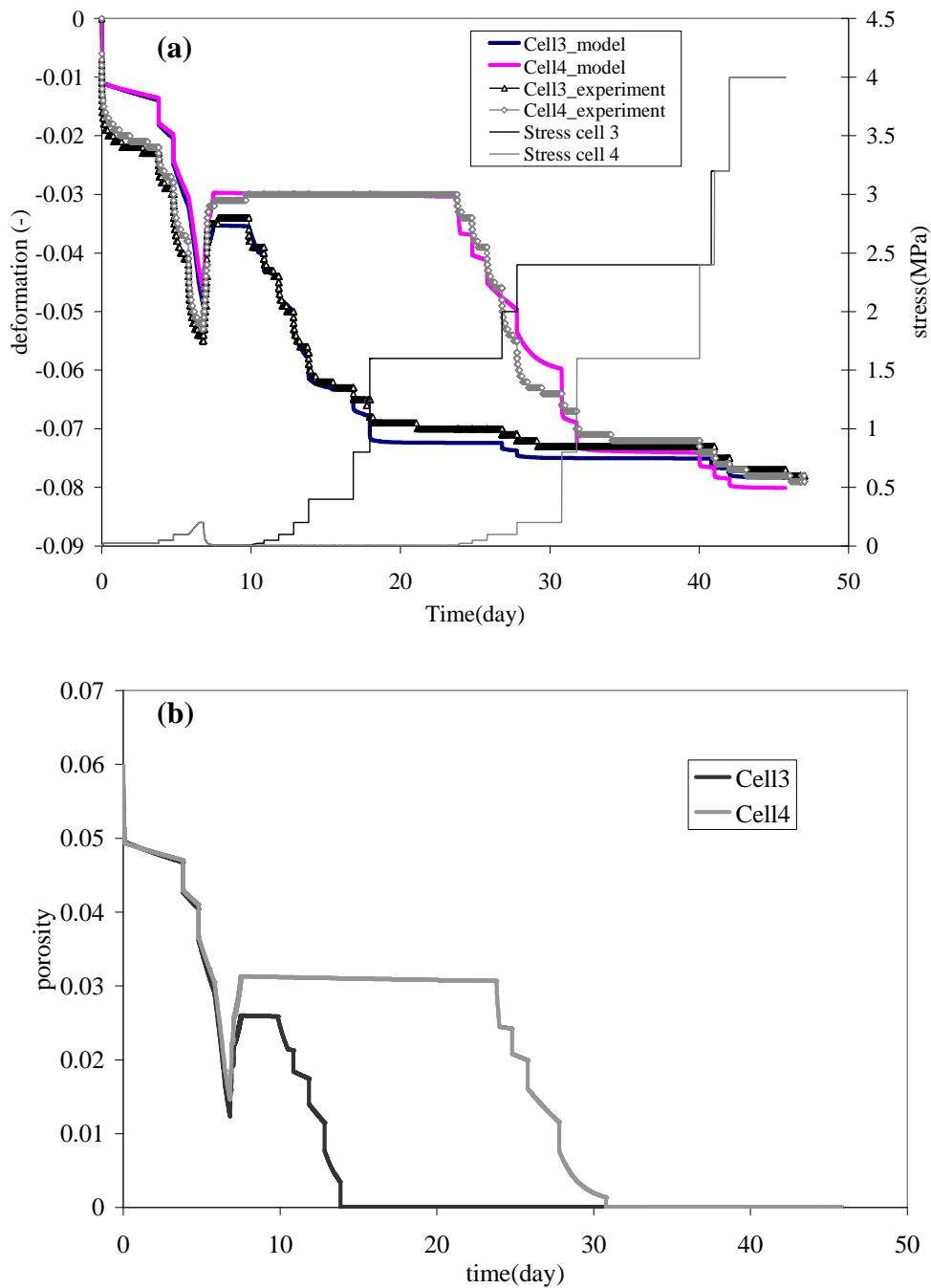
Figure 3.9: Vertical deformations and porosity profile as a function of time for cell 3 and cell 4. Experimental results and model calculations. (a) Measured and calculated deformations and (b) Porosity evolution during compression.
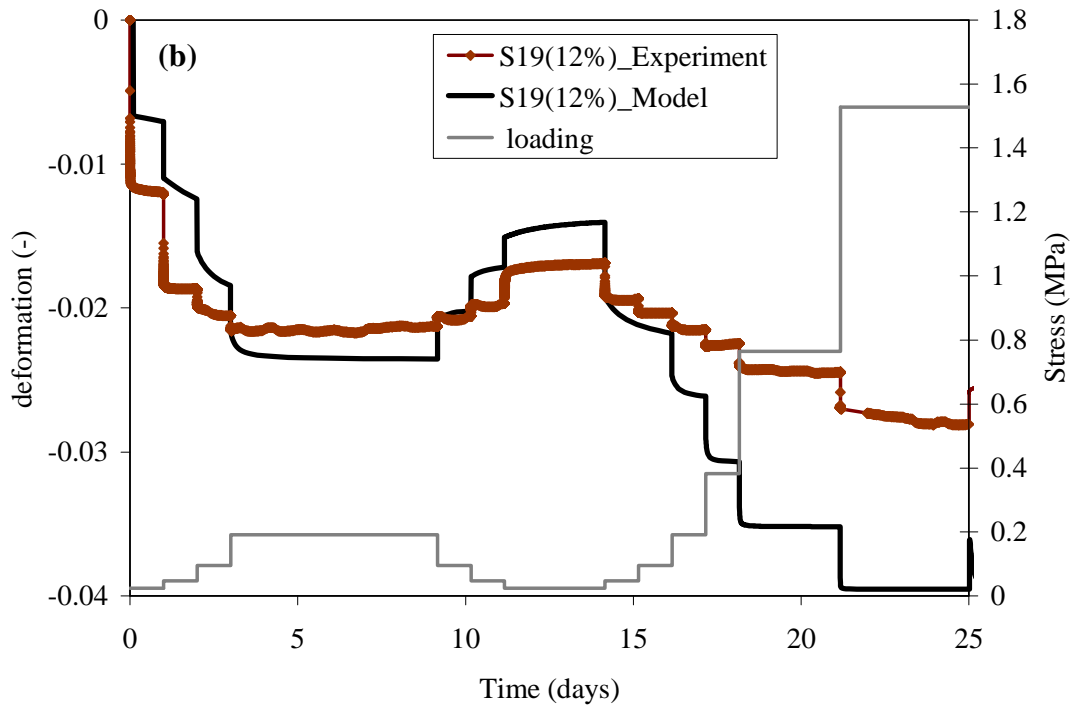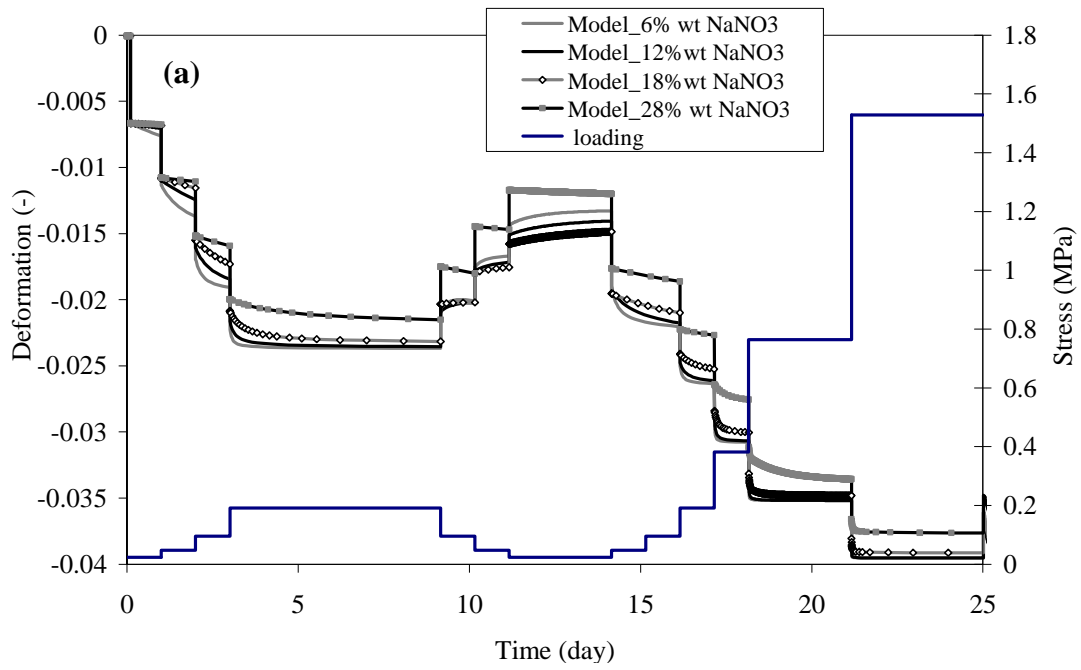
Figure 3.10: Effect of crystal content in a multistep test (initial porosity 2.5%). (a) Model results for different crystal contents (weight percent) and (b) Comparison of model with experimental results for a test with 12% of salt content.
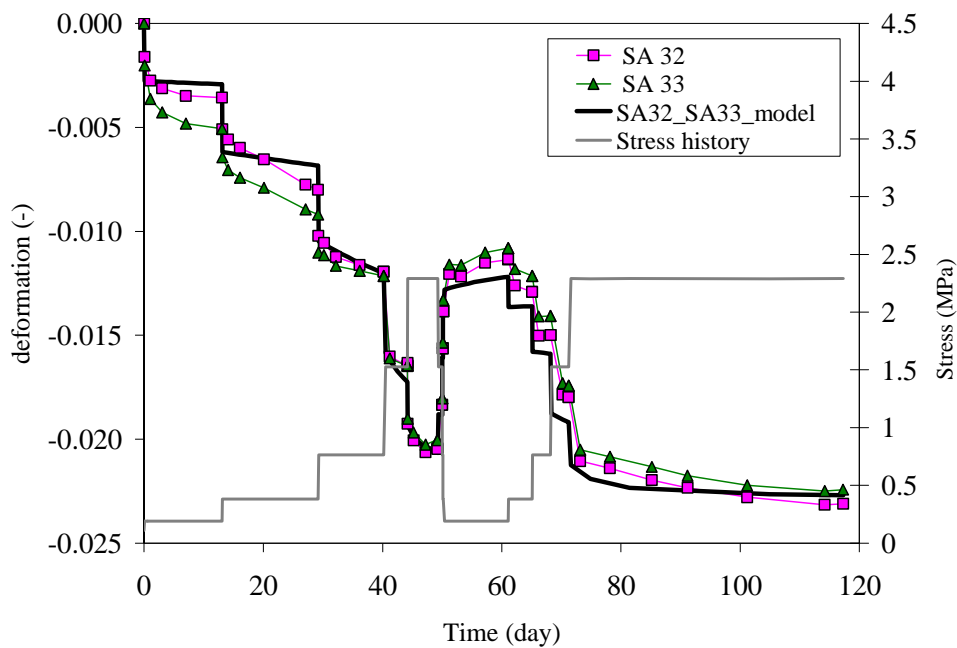
Figure 3.11: Simulation of a test on a radioactive sample (initial porosity 2.5%, viscosity reduced by a factor of 1000).

3.5 Summary

One long-term management option of the Belgian Agency for the Management of Radioactive Waste and Fissile Materials is the direct underground disposal of Eurobitum in a geologically stable clay formation. The presence of the radioactive waste should not disturb the favorable properties of the host formation. The interaction of a BW and the host formation is complex due to the presence of hygroscopic salts. To better understand the interaction between the swelling Eurobitum and the host formation, coupled hydro-chemical-mechanical constitutive laws have to be developed. An essential part of the modelling approach is its mechanical response which should be interpreted with a constitutive equation.

This Chapter presents the laboratory and numerical research on the mechanical behavior of a BW. The material is considered as a porous medium, i.e. a mixture of a porous bitumen matrix and salt crystals. A model that predicts the overall creep behavior of the BW, whose both constituents are viscoplastic, has been presented. The model has been included in a finite element program. The influence of the crystals on deviatoric creep deformation has been investigated. The results of the numerical test offer a preliminary evidence of the effect of the crystals on the creep deformation. It has been observed that

there is a significant decrease of creep deformation when the crystal volume fraction increases. The creep model has been compared with the experimental data. It has been observed that by volumetric deformation the bituminized waste evolves from porous conditions to an uncompressible material.

3.6. References

Cheung, C.Y. and Cebon, D.: Experimental study of pure bitumen in tension compression, and shear, J. Rheol., 41, 45-73, (1996).

Cheung, C.Y. and Cebon, D.: Deformation mechanisms of pure bitumen, ASCE J. Mater.Civil.Eng., 117–129, (1997).

Mokni, N., Olivella, S., Li, X., Smets, S., and Valcke, E.: Deformation induced by dissolution of salts in porous media. J. Phys. Chem. Earth., 33, 436-443, (2008).

Olivella, S., and Gens, A.: A constitutive model for crushed salt, Int. J. Num. Anal. Mat. Geom., 26, 719-746, (2002).

Olivella, S., Luna, M., and Gens, A.: Thermo-Mechanical Analyses of A Large Scale Heating Test In Salt Rock, VII International Conference on Computational Plasticity, COMPLAS VII, E. Oñate and D. R. J. Owen (Eds). CIMNE, Barcelona, (2003).

Perzyna, P.: Fundamental problems in viscoplasticity, Adv. Appl. Mech., 9,346-377 (1966).

Sercombe, J., Gwinner, B., Tiffreau, C., Simondi-Teisseire, B., and Adenot, F.: Modelling of bituminized radioactive waste leaching. Part I. Constitutive equations, J.Nuc.Mat., 349, 96-106, (2006).

Valcke, E., Mariën, A., and Van Geet, M.: The methodology followed in Belgium to investigate the compatibility with geological disposal of Eurobitum bituminized intermediate-level radioactive waste', Mater. Soc. Symp. Proc. Vol. 1193, 105-116, (2009).

Valcke, E., Rorif, F., and Smets, S.: Ageing of EUROBITUM Bituminised Radioactive Waste: an ATR-FTIR spectroscopy study, J. Nuc. Mat, 393, 175-185, (2009)

Deng, Y.F., Tang, A.M., Cui, Y.J.: A study on the creep behavior of bitumen using unconfined compression test, Final test report, U.R. Navier/CERMES, Ecole des Ponts – ParisTech, (2009).

Chapter 4

Deformation and flow driven by osmotic processes in porous materials: application to bituminized waste materials

4.1 Background

Porous materials containing salts may undergo swelling by fresh water uptake induced by osmotic flows. Depending on the mechanical and hydraulic properties of the medium, the response may be quite different in magnitude and time evolution. In fact, swelling may change all these properties (for instance stiffness, intrinsic permeability, osmotic parameters) thus leading to non-linear responses.

As mentioned in Chapter 3, the Belgian Bituminized Waste (BW) named Eurobitum consists of ~60 weight% (wt%) of 'hard' (also called 'blown' or 'oxidized') bitumen (Mexphalt R85/40) and between 20 and 30 % in weight of sodium nitrate ($NaNO_3$), which is a soluble and hygroscopic salt. The waste further contains 4–6 wt% of $CaSO_4$ in addition to CaF_2, $Ca_3(PO_4)_2$, $Ni_2[(Fe,Mn)(CN)_6]$, and oxides and hydroxides of Fe, Zr, and Al (4–10 wt%). Radionuclides are estimated to be present but for some 0.2 wt% at most (Valcke et $al.$, 2010). All these are dispersed in a matrix of bitumen (Figure 4.1.a).

The current reference solution of the Belgian Agency for the Management of Radioactive Waste and Fissile Materials (ONDRAF/NIRAS) envisages underground disposal of this waste in a geologically stable clay formation. In Belgium, the Boom Clay, which is a 30 to 35 million years old and ~100 m thick marine sediment is being studied as a potential host formation because of its favorable properties to limit and delay the migration of the leached radionuclides to the biosphere over extended periods of time (De Craen et $al.$, 2004). The current disposal concept foresees that several drums (220 litres) of Eurobitum would be grouped in thick-walled cement-based secondary containers, which in turn would be placed in concrete-lined disposal galleries

that are excavated at mid-depth in the clay layer. The remaining voids between the containers would be backfilled with a cement-based material (Figure 4.2).
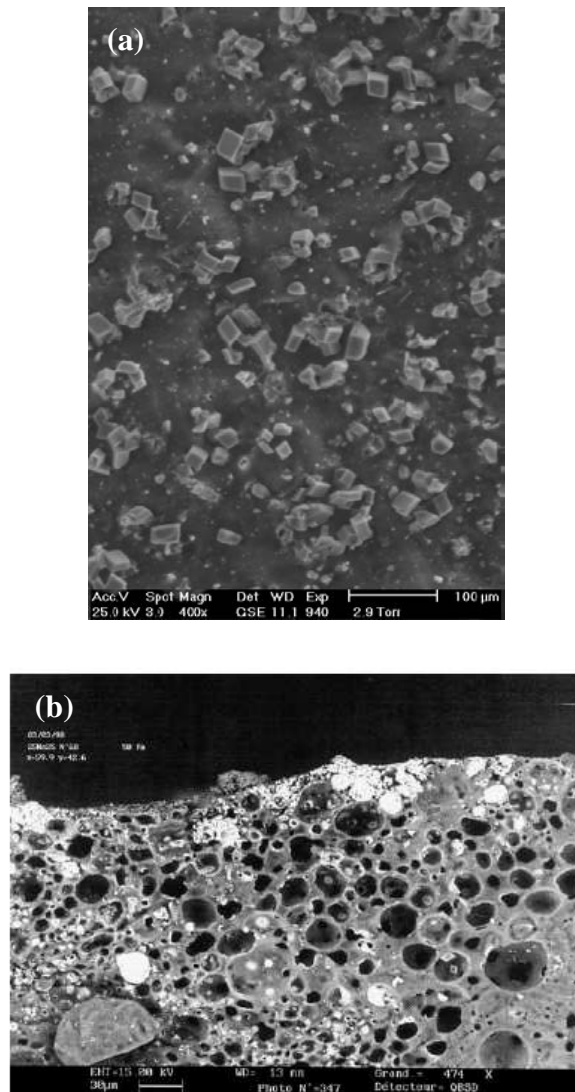
Figure 4.1: ESEM observations of BW. a) ESEM photo of non-leached center layer of an Eurobitum sample (sample S4), after 872 days of contact with 0.1 M KOH in constant stress conditions. b) Observation of a leached synthetic BW showing the typical aspect of the material when it starts to swell in free swelling conditions (bubbles filled with a saline solution)(Sercombe et *al.*, 2006).

Under geological disposal conditions the main factor that affects the long term behaviour of the BW is water uptake. In fact, the interaction of the bituminized waste with clay pore water is of great importance. The hygroscopic soluble salts incorporated in Eurobitum ($NaNO_3$) will absorb large amounts of groundwater or water vapour resulting in dissolution and subsequent leaching of these salts.
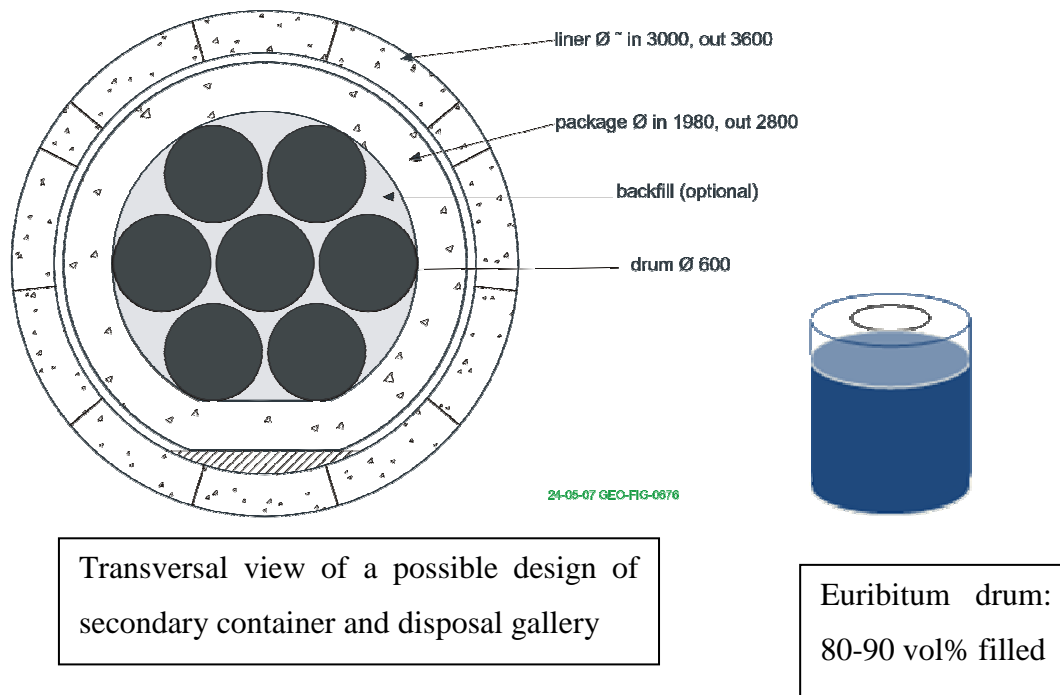
Figure 4.2: Schematic lay out of the disposal gallery.
(Valcke *et al.*, 2009)

Various studies have already been devoted to this subject. One approach consists of considering the water uptake and salt leaching as a diffusive mechanism. Sercombe et *al.* (2006), Gwinner et *al.* (2006), and Gwinner et *al.* (2007) presented theoretical and experimental studies of the behaviour of the BW material under free swelling conditions. The authors presented a complete explanation of the phenomenology of water uptake and swelling of this material under free swelling conditions. They considered BW as constituted of a single soluble salt ($NaNO_3$) embedded in a bitumen matrix. Water is considered to be transported only by diffusion. The authors reported that the diffusion coefficient of water through the bitumen matrix is in the order of $5x10^{-15}$ m^2/s (very low value as compared with the diffusion coefficient of solutes in free water). As diffusion is a slow process, water will diffuse slowly through the bitumen matrix and start to dissolve the $NaNO_3$ crystals situated in the outer most layers of the BW. This result in formation of pores filled with partially dissolved $NaNO_3$ crystals in contact with a saturated $NaNO_3$ solution. As the volume of the $NaNO_3$ solution is larger than that of crystals of $NaNO_3$, this layer of the BW swells. Total dissolution of the crystals leads to the formation a porous layer referred to as permeable layer (Figure 4.3).

Diffusion of water in this layer, estimated to $3x10^{-13}$ m^2/s (Sercombe et *al.*, 2006), occurs at much greater rate than in pure bitumen. Once the crystals in this layer have dissolved and the salt solution stars to dilute, water diffuses deeper in the material. A continuously growing permeable layer consisting of connected pores is then created (Figure 4.1.b). The authors demonstrated that the pore structure evolution of the material is at the origin of salts release in BW. To model these processes they proposed a constitutive model consisting of a system of coupled diffusion-dissolution-swelling equations without mechanical constrain.
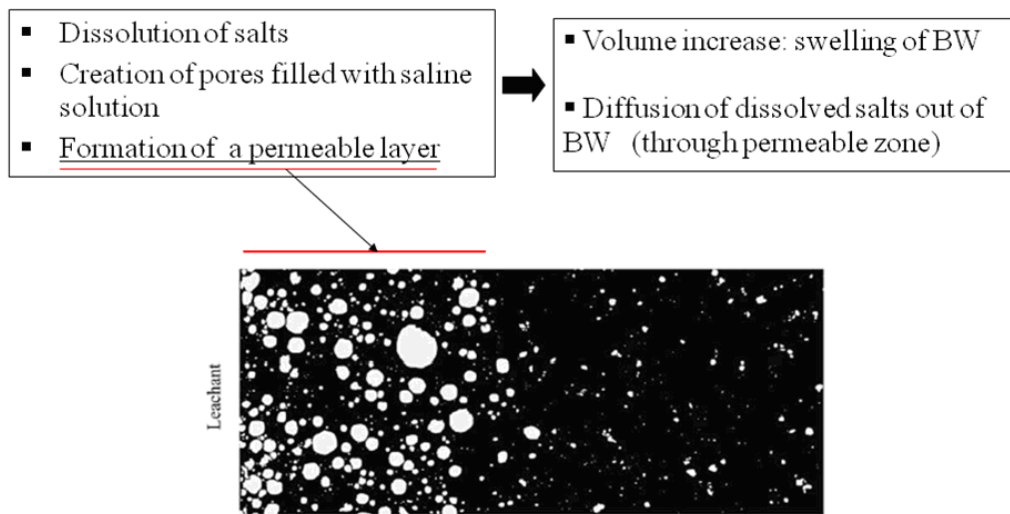
Figure 4.3: Binary image of a BW sample leached during 11 months under free swelling conditions. (Gwinner et *al.,* 2006)

For Eurobitum, in geological disposal conditions, free swelling will only be possible during a first phase, until the free volume in 220 litre drums is filled with swollen material. In a next phase, further water uptake will induce an increasing stress on the concrete secondary container and on the surrounding Boom Clay. This makes important the investigation of swelling under mechanical constraint. Another important observation is the importance that coupled fluxes may play in the transport of water for a material like BW experiencing such a pore structure evolution (Brodersen, 1983). Considering the hygroscopic character of the embedded soluble salts in the BW, there may be water flowing towards the salts and, at a lower rate, dissolved salts migrating towards the less concentrated water of the host formation. The bitumen that surrounds the salt crystals has a very low porosity. This property gives to the material the ability to restrict the movement of dissolved ions that is, to behave as a highly efficient semi-permeable membrane. This property gives rise to chemical osmosis (*i.e.* a fluid flow in

response to a chemical gradient over a semi-permeable membrane). As a consequence, contact of the bituminized waste with water will result in an osmosis-induced swelling of the waste (Sneyers et *al.,* 1998; Mariën et *al*., 2008, and 2009; Valcke et *al.*, 2010).

The interaction between the swelling bitumen and the host rock is a very complicated chemo-hydro-mechanical process and depends not only on the hydro-mechanical behaviour of the Boom Clay itself, but also on the chemo-hydro-mechanical behaviour of the bituminised waste. The salts contained in the BW are important because they can induce mechanical disturbance of the Boom Clay through an osmosis-induced pressure caused by osmotic uptake of water by the waste (Li et *al.*, 2006; Valcke et *al.,* 2009). When water comes into contact with the BW the salt will dissolve and diffuse away. Inducing change of the pore fluid chemistry which may affect the hydro-mechanical properties of the clay host rock (e.g. Yang and Barbour, 1992; Barbour and Yang, 1993).

To study these processes, and to enable the prediction of the long-term behaviour of Eurobitum in underground disposal conditions, an experimental program is in progress at the Belgian Nuclear Research Centre SCK•CEN. Water uptake experiments in constant volume and constant stress conditions are performed, and the influence of several parameters is investigated (e.g. $NaNO_3$ content in the BW and in the leachant) (Mariën et *al*., 2008, and 2009; Valcke et *al.,* 2010).

This Chapter shows from a theoretical point of view the importance of osmotically induced swelling and leaching of the BW. The constitutive model including creep is adopted in order to describe the mechanical behavior of the material .The theoretical trends given by the model are compared with the experimental results. The swelling may be controlled by several processes including the mechanical behavior of the material.

4.2 Simulations of swelling tests carried out at SCK•CEN

In Chapter 2, a formulation has been presented for osmotically driven transport of water and solutes in deformable porous media. The balance equations for water, dissolved salts, crystals and solid phase have been written including the coupled flows, namely osmotic flow and ultrafiltration, and the dissolution/precipitation of salts. The Eulerian

form of the equations is transformed into a Lagrangian form based on the solid velocity field. This formulation is used here to analyze the swelling induced by dissolution of NaNO$_3$ crystals embedded in a bitumen matrix, when the BW is in contact with fresh water. For this material, deformations take place and several aspects related to porosity changes have to be taken into account.

The variations of the osmotic efficiency coefficient σ and of the intrinsic permeability k with porosity are considered in the formulation. For this case, it is postulated that the osmotic efficiency coefficient is a nonlinear function of the porosity ϕ_f:

$$\sigma = \sigma_0 \frac{\phi_{f0}}{\phi_f} \tag{4.1}$$

where ϕ_{f0} and σ_0 are reference values. This simple equation may be improved in the future if is deemed necessary.

A constitutive law that describes the variation of the permeability as a function of porosity can be written as (as proposed in Olivella *et al.*, 1994 as a first approximation):

$$\mathbf{k} = \mathbf{k}_o \frac{\phi_f{}^3}{(1-\phi_f)^2} \frac{(1-\phi_{fo})^2}{\phi_{fo}{}^3} \tag{4.2}$$

As we are dealing with high concentrated solutions, the osmotic pressure is calculated using the following equation, (Beyers 1965):

$$\pi = \frac{RT}{v_{H2O}} \ln\left(\frac{P^0_{H2O}}{P_{H2O}}\right) = -\frac{RT\rho_l}{M_w} \ln a_w \tag{4.3}$$

where R [J/(mol.K)] is the gas constant, T [K] is the temperature, M_w [kg/mol] is the molar mass of water and a_w is the water activity which is calculated using an empirical equation for sodium nitrate:

$$a_w = \left(\frac{P^0_{H2O}}{P_{H2O}}\right)^{-1} = 1 - \left(w_l^s\right)^2 \tag{4.4}$$

where w_l^s is the mass fraction of solute (NaNO$_3$) in the liquid phase. The evolution of the calculated osmotic pressure with the mass fraction of the solute in the liquid phase is displayed in Figure 4.4. The plot also includes some experimental points determined

using the WP4 *dewpointmeter* (Decagon Devices, Inc) to measure the osmotic suction of several NaNO$_3$ solutions.
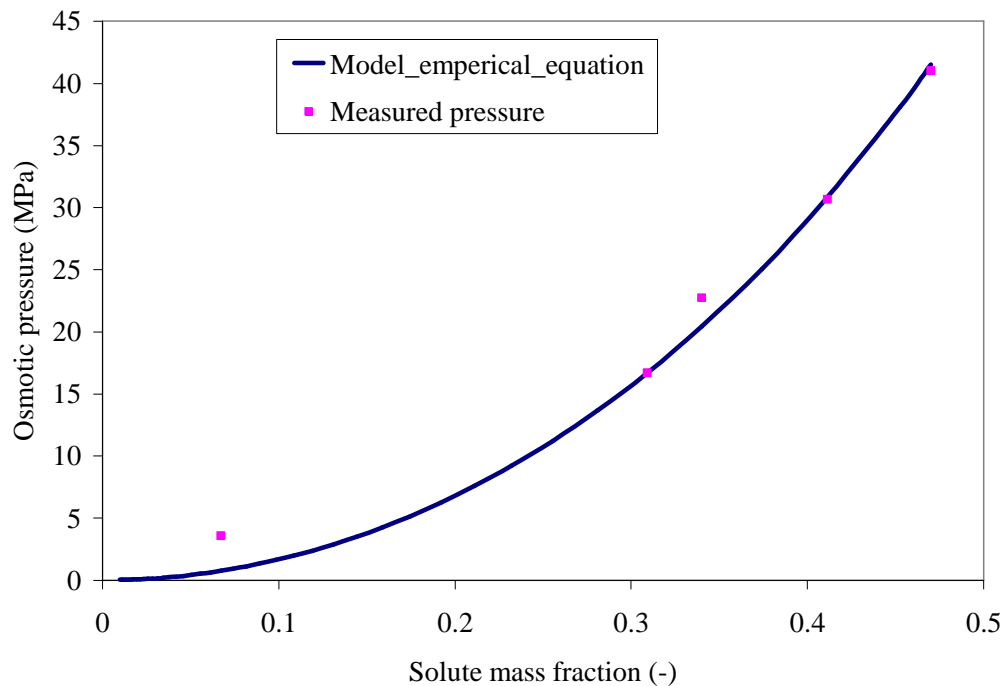
Figure 4.4: Evolution of the osmotic pressure with solute mass fraction for NaNO$_3$

The coupled migration of dissolved salt and water is controlled by the following variables:

- Intrinsic permeability: It controls the flow of water due to hydraulic pressure gradients, but also the flow of water due to osmotic pressure gradients. It controls the flow of solutes by advection.
- Osmotic efficiency: It controls the flow of water and solutes due to osmotic effects.
- Diffusivity of solutes and water: It controls the diffusion of dissolved salt and water. It is affected by the osmotic efficiency.
- Diffusivity of vapour. It controls the diffusion of vapour. It vanishes as the material becomes fully saturated.

4.2.1 Calibration and validation of the model

A first series of water uptake tests under constant stress and nearly constant volume have been performed in the laboratory of SCK•CEN. The samples are constituted of small inactive Eurobitum with 28 weight% NaNO$_3$ (diameter 38 mm, height 10 mm).

The experimental aspects of the water uptake tests are briefly summarized here. A more detailed description is given in Valcke *et al.* (2010). The samples have been cored from inactive drums that have been produced by the EUROCHEMIC reprocessing facility during some cold-runs in the start-up phase of the bituminization plant. Their composition is similar to the composition of radioactive Eurobitum, except for the presence of the radionuclides. In the water uptake tests, the samples are hydrated in so-called water uptake cells with a 0.1 M KOH leachant solution (Figure 4.5), which is chosen to represent young cement water. In fact, after penetration through the large amounts of concrete in the disposal gallery, the composition of the Boom Clay pore water will be that of young cement water (Berner, 1992). The leachant solution is supplied through two filters at both sides of the samples. In constant stress water uptake tests, the piston on top of the upper filter is allowed to move under a constant stress. The experimental results of a first series of constant stress tests are reported by Valcke et *al.* (2010). In the nearly constant volume tests, the pistons are present in a fixed frame to prevent a displacement, and hence a swelling of the samples. The pressure exerted by the hydrating Eurobitum samples is measured by means of load cell. Due to the very high osmosis-induced pressures, the strain gauges in the load cells have deformed slightly, thus allowing some swelling of the samples (~ 2 volume% after 3 years) (Figure 4.20). Therefore, these tests are referred here as "nearly constant volume tests".
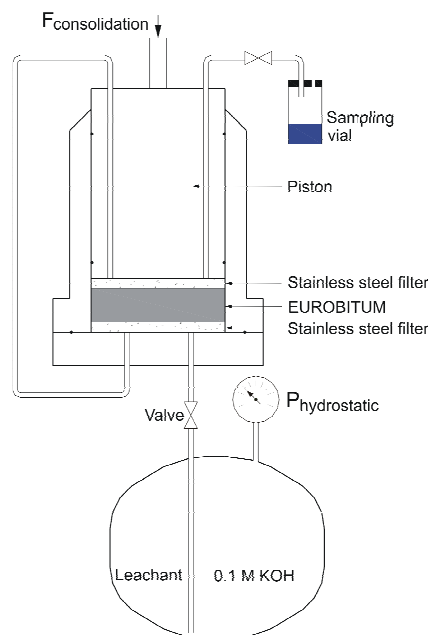

Figure 4.5: Schematic visualisation of the experimental set-up for water uptake tests with Eurobitum samples (diameter 38 mm, height 10 mm), contacted at both sides with 0.1 M KOH. (Valcke et *al.,* 2010).

In order to explore the model ability to reproduce swelling of the leached BW, the water uptake tests under 'semi-confined' (constant stress) and confined conditions (constant volume) are modelled. The model is first fitted to the constant stress test's data. The results of the constant volume tests are used to validate the model. It is important to mention that prior to contact with water, the samples in the water uptake cells were submitted to repeated compression-decompression steps ('compressibility test'). The simulation of the results of these compression tests in oedometric conditions, and hence the validation of the mechanical constitutive law, are presented in Chapter 3. Additional results can be found in Mokni et *al.* (2008).

4.2.1.1 Modeling of swelling under semi-confined (constant stress) conditions

In order to analyze in a systematic way the results of the modeling work and the influence of the parameters on the results, a base case is first considered for which the results are presented in detail. The alternative cases are defined by changing only one feature at a time to identify its influence and show its sensitivity.

Base Case

The model domain consists of two regions (Figure 4.6). One corresponds to a reservoir representing a filter saturated with water and a low $NaNO_3$ concentration. The initial solute mass fraction for the reservoir is $w_l^s = 0.001 \, kg/kg$. Within the reservoir, the permeability is set to a high value ($k = 10^{-16} \, m^2$). The central region corresponds to the BW material containing sodium nitrate crystals occupying 16 % of the total volume of the BW (corresponding to 28 % in weight). Pure water inflow, brine outflow, and salt diffusion through the reservoir are allowed at the upper and lower side of the sample. The medium is considered to be saturated with $NaNO_3$ brine (initial solute mass fraction: $w_l^s = 0.47 \, kg/kg$). The test was simulated under a constant vertical stress (2.2 MPa), which is the lower counter pressure in the tests reported in Mariën et *al.* (2008) and Valcke et *al.* (2010). Along the vertical boundaries of the domain, horizontal displacements are restricted to represent the oedometric conditions.
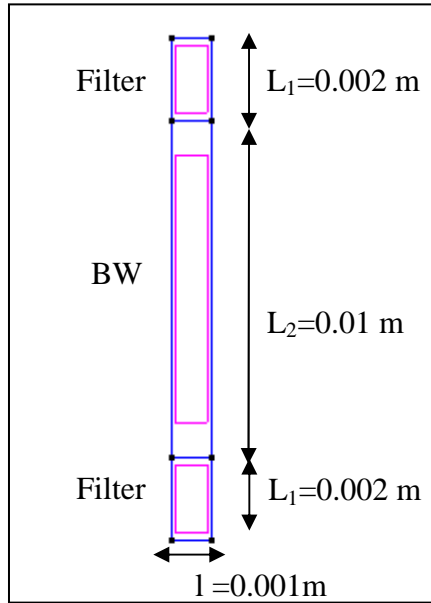
Figure 4.6: Schematic representation of the model domain

Table 4.1. Material properties (Base Case)

Parameters (Initial values)	Symbols	Values	
Crystal volume fraction	ϕ_{c_0}	0.16	
Porosity	ϕ_{f_0}	0.01	
Intrinsic permeability	k_0 (m^2)	BW	3×10^{-26}
		Porous stone	10^{-16}
Efficiency coefficient	σ_0	BW	0.95
Diffusion coefficient	D* (m^2/s)	1.6×10^{-16}	
Dissolution Rate	κ	10^{-5}	
Solute mass fraction	w_l^s	BW	0.47
		Filter	0.001
Mechanical constitutive model			
Elastic model	Poisson ratio	0.3	
	a_1	0.007	
Creep model	n	2.3	
	$A\left(\text{s}^{-1}\text{MPa}^{-2.3}\right)$	0.00041	
Applied vertical stress	(MPa)	2.2	
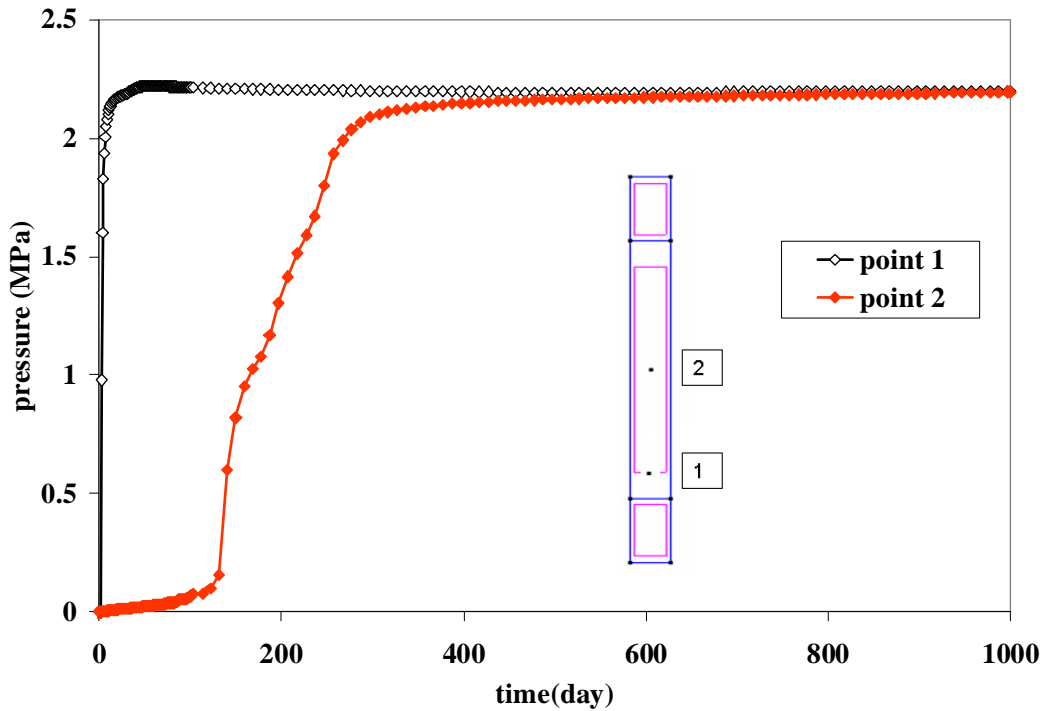
Figure 4.7: Fluid pressure evolution

Figure 4.7 shows the time evolution of water pressure within the simulated sample. Two representative points have been selected. One can see that there is a significant rise in pressure which corresponds to the dominance of osmotically driven flow towards the sample. This plot shows that, for the properties considered, the water pressure increases and tends to the value of the applied vertical stress (2.2 MPa). A small decrease of the pore pressure in point 1 is observed after almost 60 days. At the center of the sample (point 2), pore pressure increases after a delay of more than 100 days.

The volumetric deformation evolution (*i.e.* swelling) is displayed in Figure 4.8. The plot shows comparisons between the experimental data and the numerical simulations including the cases where the vertical applied stress is equal to 3.3 MPa and 4.4 MPa. For this range of stresses, the effect is moderate according to the model but the scattering of the experimental data is significant which does not permit a more refined calibration. The effect of stress level on swelling is discussed later in regard to the maximum osmosis-induced pressure achievable taking into account the high osmotic pressure associated to the sodium nitrate. The scattering of the experimental data may be caused by several factor including differences in salt content of the studied BW samples or others indicating that it is very important to know the test conditions very precisely (Valcke et *al.,* 2010).

A higher swelling rate in Figure 4.8 was observed for a sample for which the cumulative amount of leached $NaNO_3$ was also higher (See Figure 4.16), therefore indicating that the $NaNO_3$ content of the samples, sampled from an industrially produced batch of non-radioactive Eurobitum, were probably not the same. According to the model, the excess of pressure developed within the sample due to osmosis results in the swelling of the material. In fact, the developed pressure induces a volumetric expansion which contributes to a porosity increase. One should notice that after 1000 days the sample is still swelling.
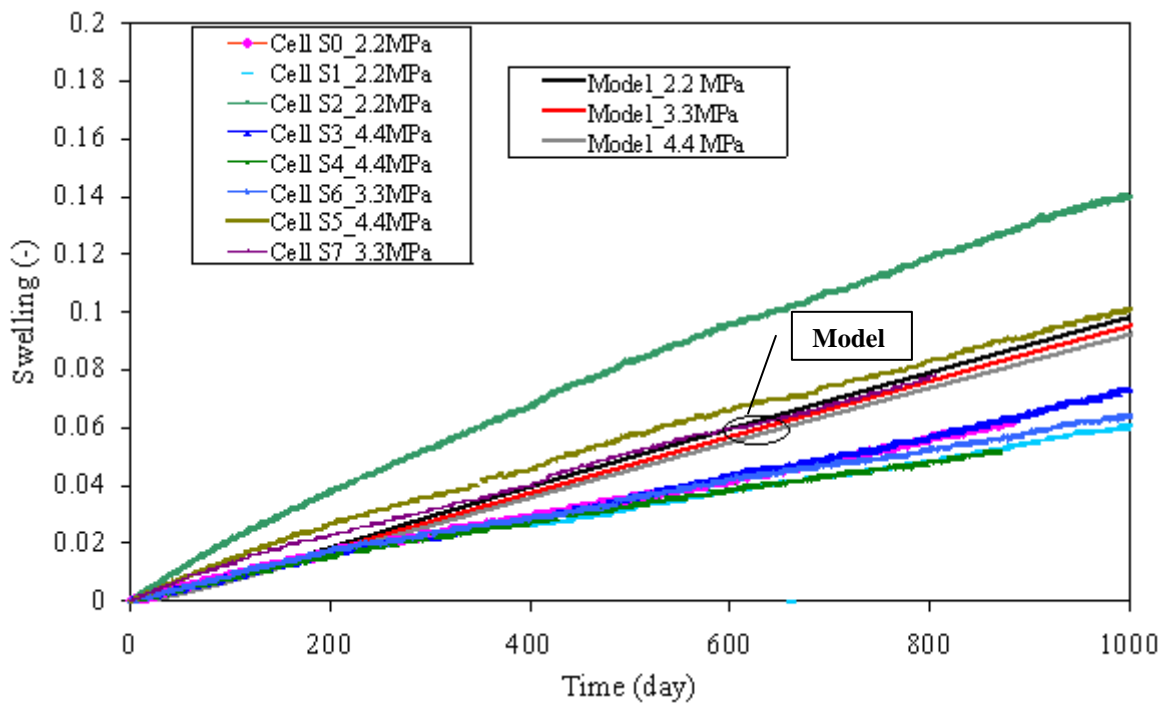
Figure 4.8: Volumetric deformation versus time. Experimental and modelling results

The excess of pressure produces a decrease of the mean effective stress (see the path in Figure 4.9) (mean effective stress is the average of the vertical and the lateral effective stresses, the vertical stress is imposed while the lateral is calculated by the model). The material shows some swelling (2%) during the unloading phase (effective stress decrease). Near the leached surface (point 1), a large swelling deformation (12%) develops because the mean effective stress reaches a value of zero and passes to tension. Swelling takes place due to the elastic response produced by decrease of effective stress and due to creep, simultaneously. In the centre of the sample (point 2), the pore pressure remains below the applied vertical stress and for this reason there is only a small swelling in this zone.
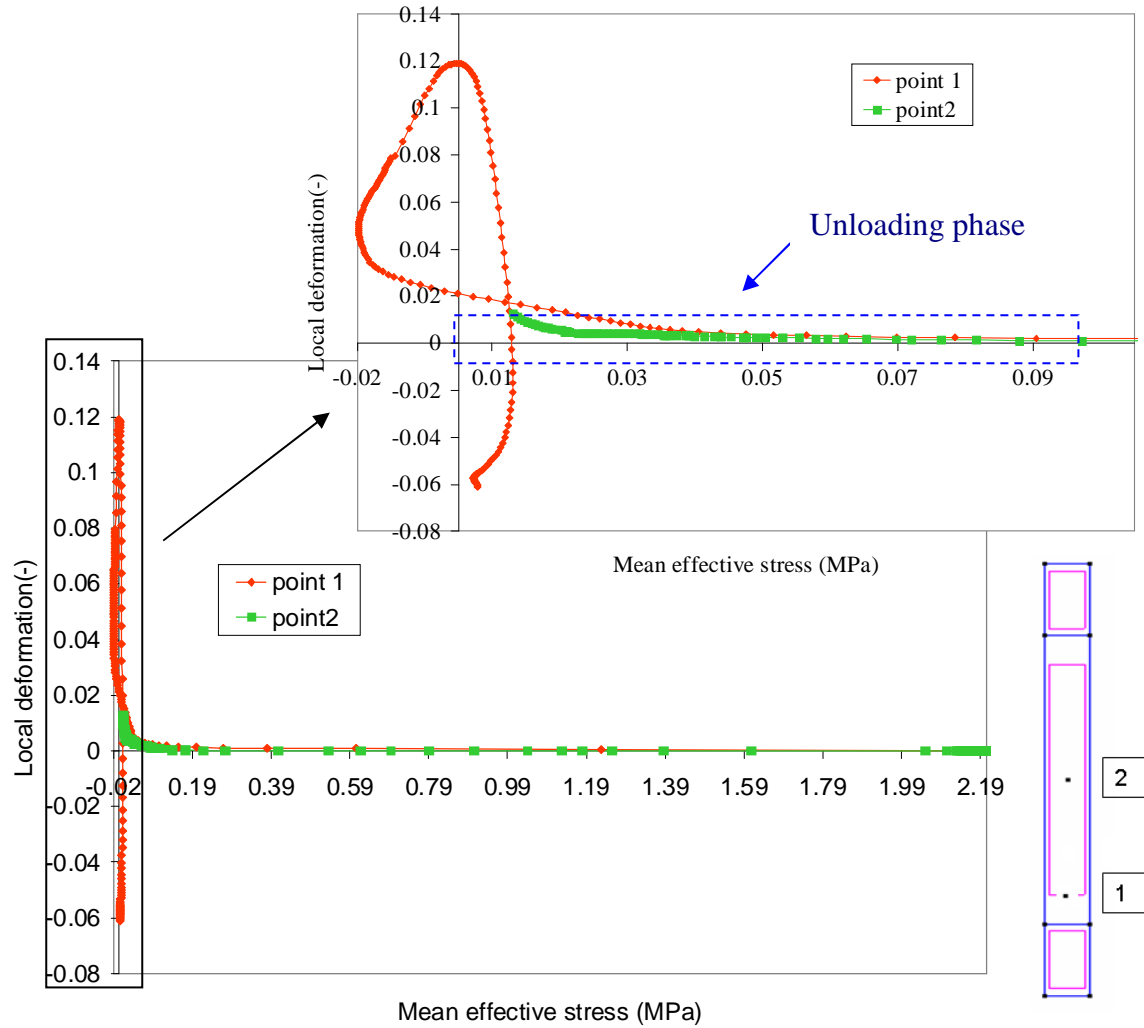
Figure 4.9: Deformation versus mean effective stress

Figure 4.10.a shows the time evolution of the crystal volume fraction at two selected points. Near the leached surface (point 1) ϕ_c decreases and tends to zero after 1000 days. A continuous flow of water towards the material is favoured by the dissolution of the crystals, and as a result the porosity increases by swelling plus dissolution (Figure 4.10.b). Permeability tends to increase and drainage is favoured. Hence, as the crystal volume fraction starts vanishing, and because of the boundary condition (a lower water pressure in the contact solution) the pore pressure decreases, resulting in an increase of the effective stress (Figure 4.9). As a consequence, there is a compression of the layer near the leached surface (Figure 4.9 and 4.10.b) and as result porosity decreased, *i.e.* a local consolidation occurred.
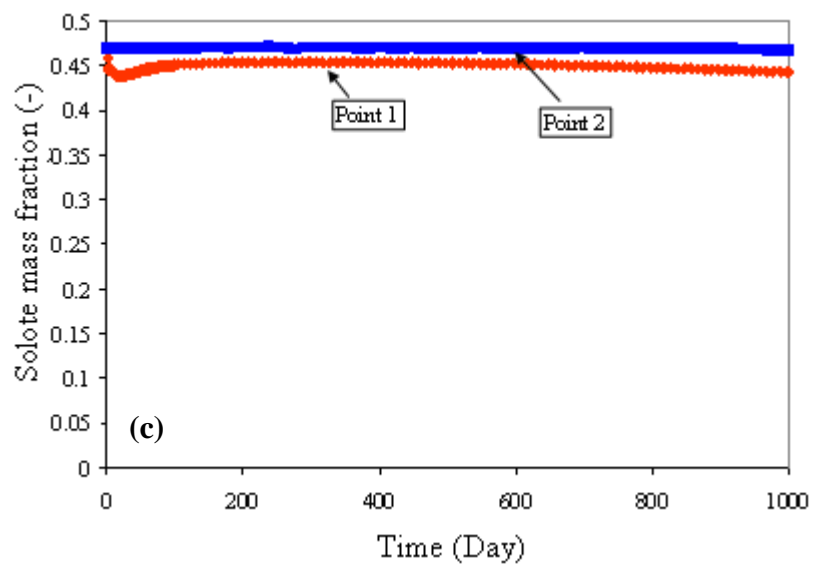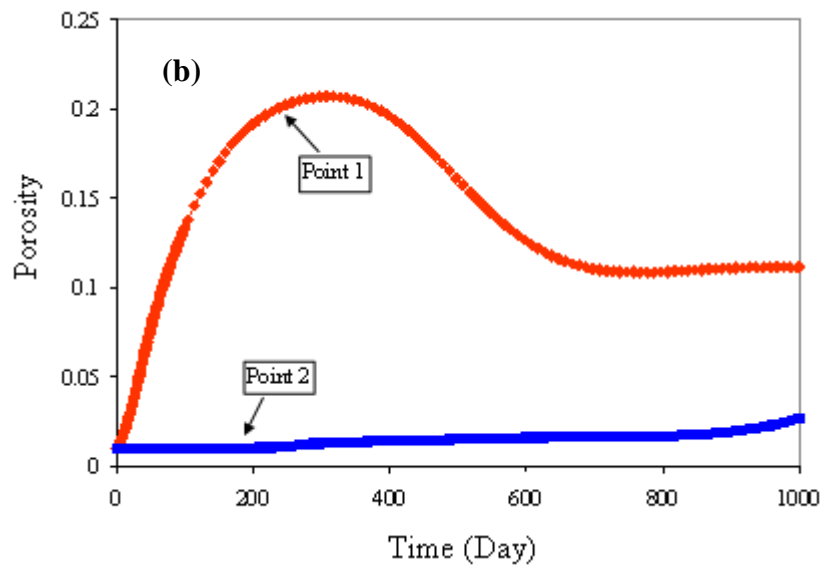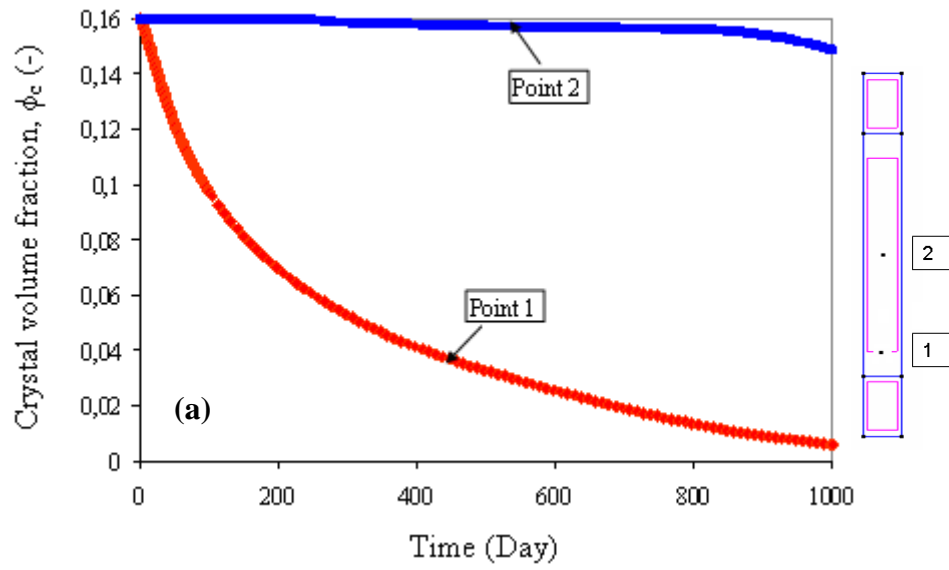
Figure 4.10: (a) Evolution of crystal volume fraction with time. (b) Evolution of porosity versus time. (c) Concentration versus time

Valcke et *al.* (2010) presented ESEM image of some Eurobitum samples tested under semi confined conditions after 887 days of hydration. Figure 4.11 shows the ESEM image of sample S0 obtained at the outer layers and at the middle of the sample respectively. The authors reported the existence of a very thin layer with a very low porosity. This observation supports the modeling result about the existence of a low permeability layer formed by the compression of the outermost leached layer of the sample.
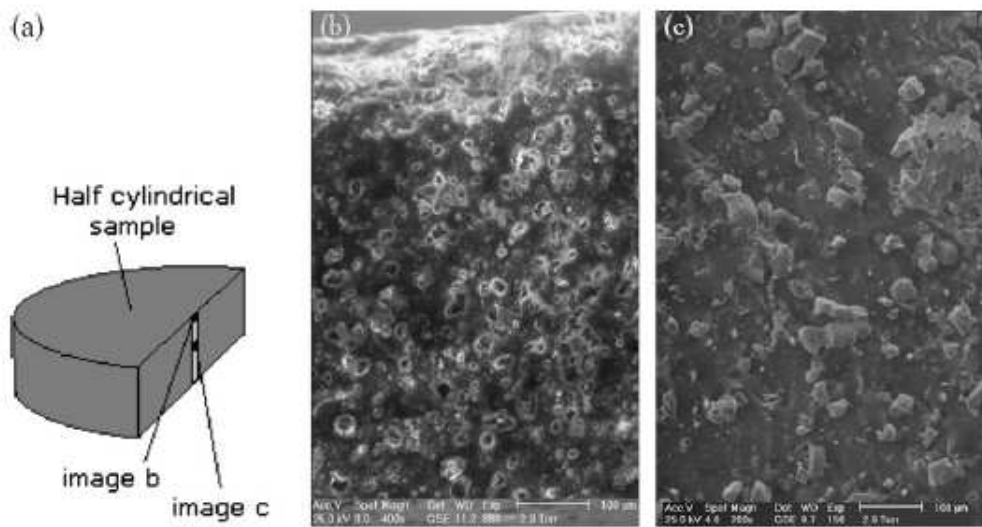
Figure 4.11: ESEM images of the fracture surface of Eurobitum sample S0, after 887 days of hydration. (a) Visualization of the positions where the ESEM images were recorded. (b)ESEM images of a small area near the sample surface that has been in contact wit the leachant solution. (c) ESEM images of a small area in the middle of the sample, (Valcke et *al.,* 2010).

Figure 4.10.b shows that according to the modelling results, no significant changes in porosity are observed at the centre of the sample (point 2) because the process progresses very slowly. Figure 4.10.c shows that the concentration of the $NaNO_3$ solution inside the sample is more or less constant over the total length of the leached part and constant in time.

Valcke et *al.* (2010) characterised some of leached samples with micro focus X-ray Computer Tomography (μCT), this technique permitted to visualise the hydrated area of the leached sample. Figure 4.12 shows the μCT image of samples S0 and S4 after 887 days and 872 days of hydration respectively. The red parts represent the stainless steel filters. The thin green-yellow layers near the filters represented in red are the hydrated

layers. The central part in red-yellow corresponds to the dry Eurobitum. For both samples, only a thin layer has been hydrated (green-yellow layer near the filters represented in red). The central part of the samples appears to be no hydrated which suggests that it will take several years before the hydration front has reached the center of the samples, and it will require even more time before all NaNO$_3$ has dissolved. During this time, the sample is likely to continue to swell.
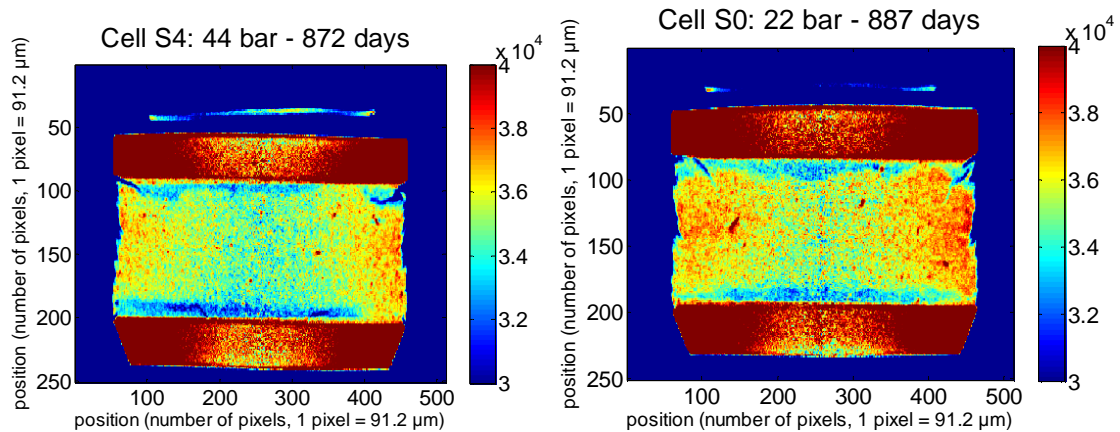
Figure 4.12: µCT images of two Eurobitum samples. (Valcke et al., 2010)

More information from the modelling analyses of the porosity evolution is given in Figure 4.13.a in terms of contours. It indicates that there is a formation of a porosity front that progresses slowly towards the centre of the sample. This is consistent with the results obtained by Sercombe et *al.* (2006) (Figure 4.13.b); it has to be noted that the results of Sercombe et *al.* (2006) were obtained for the leaching of a BW in free swelling conditions, which explains why there is no formation of a compressed layer, as discussed above. For comparison, an ESEM photo of the leached layer of the tested material (sample S0) after 887 days of contact with 0.1 M KOH solution in constant stress condition is shown Figure 4.13.c.

(a) Porosity distributions at 30 days, 100 days, 400 days, and 1000 days with associated porosity scales. Compressed layers are indicated at 1000 days.

Porosity (30 days)
0.12004
0.10781
0.095584
0.083357
0.071131
0.058905
0.046679
0.034452
0.022226
0.01

Porosity (100 days)
0.15231
0.1365
0.12069
0.10487
0.089061
0.073249
0.057437
0.041624
0.025812
0.01

Porosity (400 days)
0.27859
0.24874
0.2189
0.18906
0.15922
0.12937
0.099529
0.069686
0.039843
0.01

Porosity (1000 days)
0.496
0.442
0.388
0.334
0.28
0.226
0.172
0.118
0.064001
0.010001

Compressed layers

30 days   100 days   400 days   1000 days

(b) 2 months   6 months   12 months   25 months   37 months

1 mm

(c) 887 days

Figure 4.13: (a) Porosity distribution for the simulated case. (b) Binary images based on ESEM observations performed on BW leached by pure water (Sercombe et al., 2006). (c) ESEM photo of the leached layer of an Eurobitum sample (sample S0) after 887 of contact with 0.1 M KOH in constant stress conditions (Valcke et *al.,* 2010)

73

The porosity profiles obtained after 30, 100, 300, 600 and 1000 days are displayed in Figure 4.14. The maximum porosity is obtained near the leached surface. The maximum peak is followed by a continuous and pronounced decrease of the porosity when progressing in the depth of the sample. After 600 days the central part of the material has not experienced a significant change in porosity which is in agreement with the ESEM and µCT results (Figures 4.11 and 4.12).
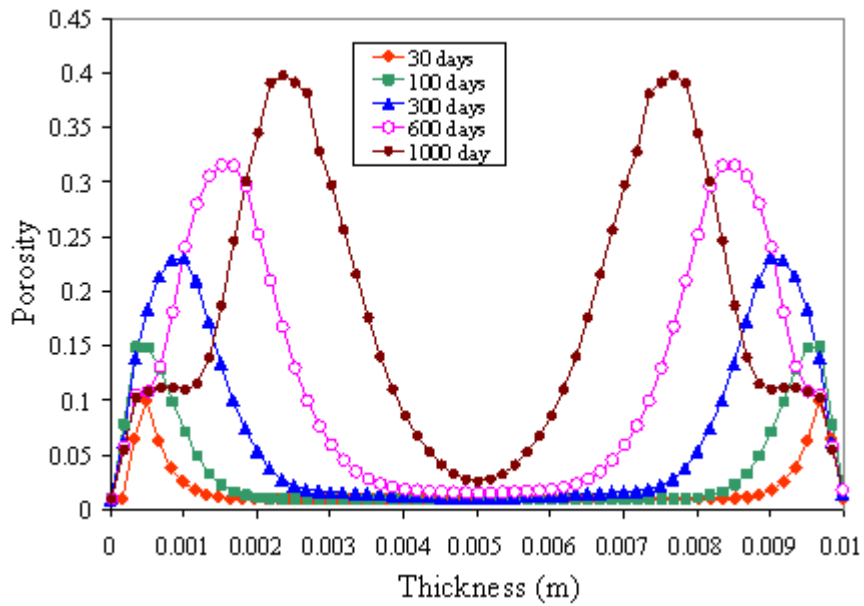
Figure 4.14: Profiles of porosity

The permeability k, the diffusion coefficient D, and the efficiency coefficient σ have been considered as a function of porosity. Profiles of k, D and σ are presented in Figure 4.15. Near the leached surface the permeability increases and reaches a maximum. After 1000 days, porosity varies between 0.01 and 0.44 near the leached surface and decreases deeper in the sample. For the same period, the permeability varies between 1×10^{-20} m² and $\sim 1 \times 10^{-24}$ m² when progressing deeper in the sample (Figure 4.15.a).

The osmotic efficiency profile also reflects the presence of a porosity front. Osmotic efficiency remains near the initial value (0.95) in the central part of the sample but sharply drops to ~ 0.05 near the leached surface (Figure 4.15.b). The diffusion coefficient profile shows the same shape as porosity and permeability, with lower and higher values of $\sim 1 \times 10^{-16}$ m²/s and $\sim 10^{-13}$ m²/s, respectively (Figure 4.15.c).

74
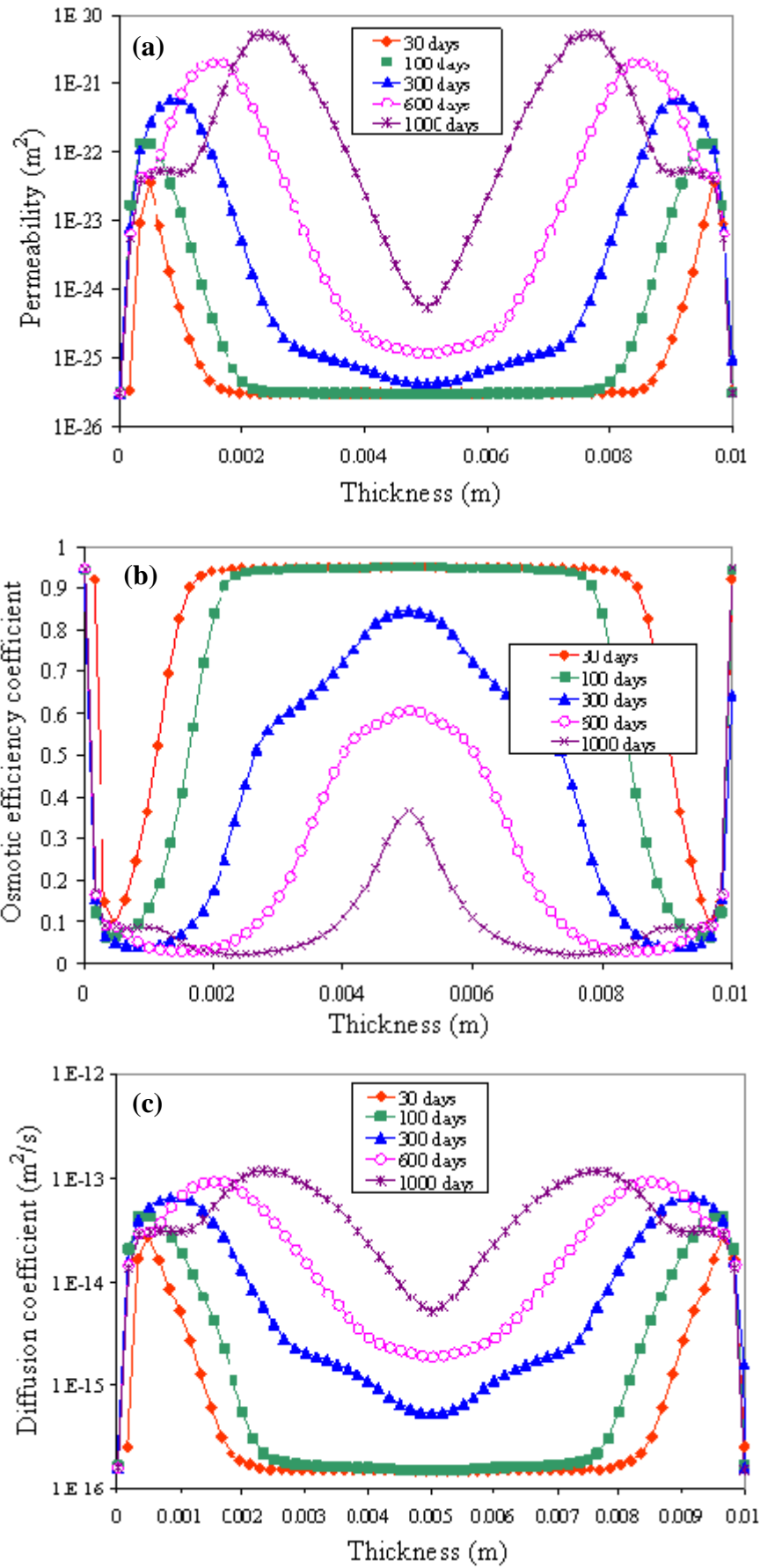
Figure 4.15: Profiles of (a) the permeability coefficient, (b) the osmotic efficiency coefficient, and (c) diffusion coefficient (D*).

The bitumen surrounding the soluble salt crystals and the pores with salt solution is not an ideal semi-permeable membrane, and hence $NaNO_3$ can leach from the swelling BW. Experimental and numerical results concerning the sodium nitrate release are shown in Figure 4.16. The plot also includes the case with a vertical stress (σ_v) equal to 4.4 and 3.3 MPa. The experimental results show some scattering for the case with σ_v=2.2MPa which may indicate that the $NaNO_3$ content of the samples was not the same. The model calculations for the case where σ_v=3.3-4.4 MPa are in the range of the experimental results. After almost 3 years of hydration about 0.4 to 1.2 g of $NaNO_3$ has been released by the samples which represents 10 to 19% of the initial $NaNO_3$ crystals content. The higher leached amount corresponds to a sample for which a higher swelling rate was observed (Figure 4.8) therefore indicating that the $NaNO_3$ content of the samples, were probably not the same. The low leached amount a $NaNO_3$ indicates that it will take several years to completely leach these small samples (diameter 38 mm, height 10 mm).
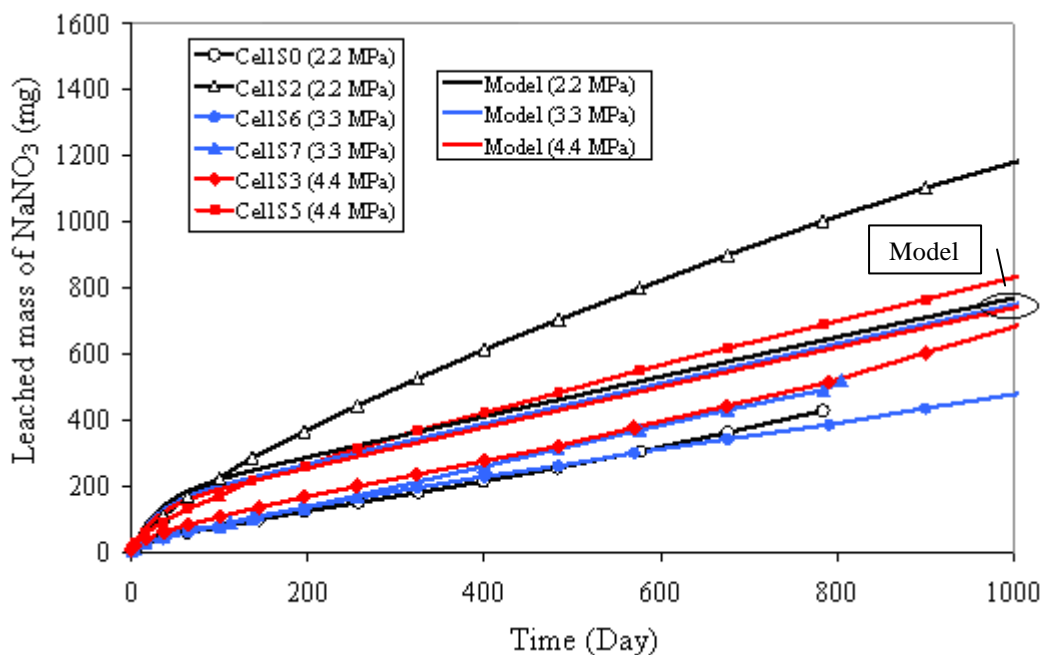
Figure 4.16: Leached mass of sodium nitrate.

The model response at long term is shown in Figure 4.17. The plot shows the non linear behaviour of swelling versus time. The stationary state is reached after 8 years when all salts in the material are dissolved (Figure 4.18). The maximum swelling deformation is of the order of 22%. As the crystals have completely dissolved, the average concentration in the BW start to decrease (Figure 4.19) and consequently the related

osmotic pressure will decrease. Therefore, full re-compression of the leached material is expected.
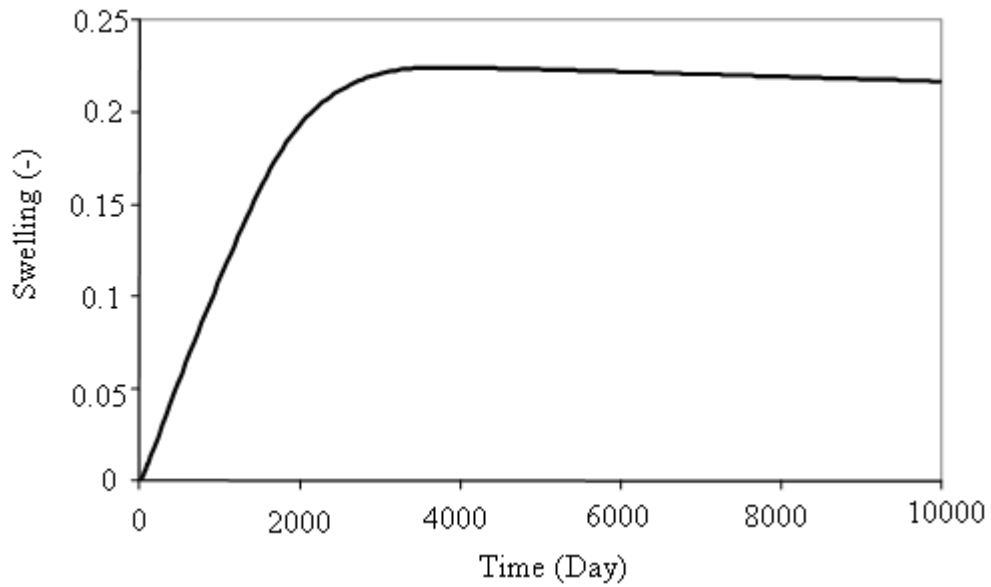
Figure 4.17: Volumetric deformation versus time. Long term response
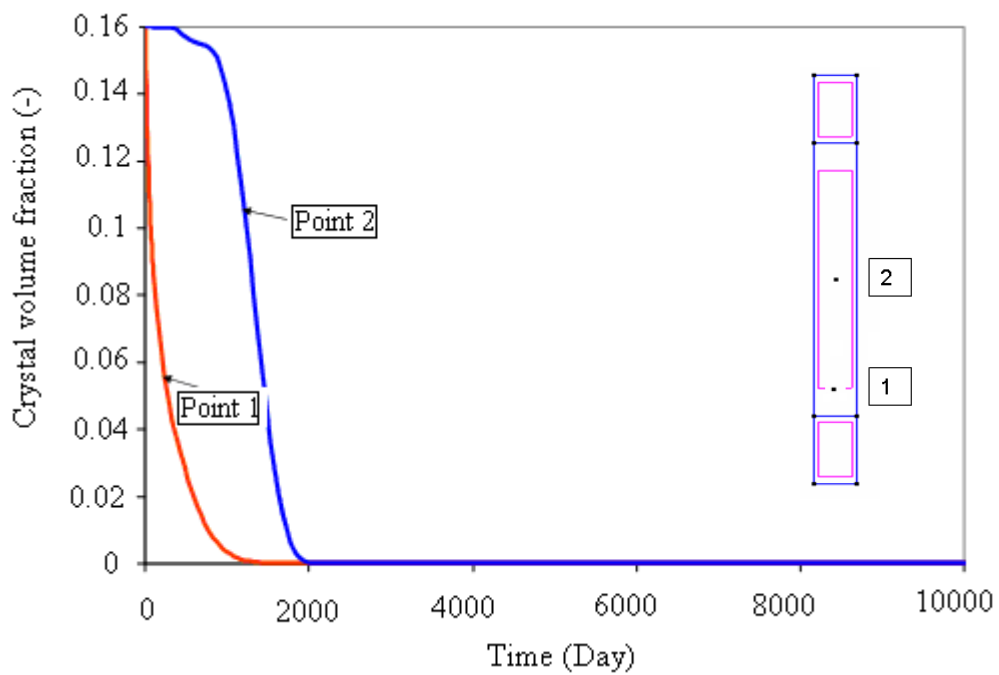
Figure 4.18: Evolution of crystal volume fraction with time at long term
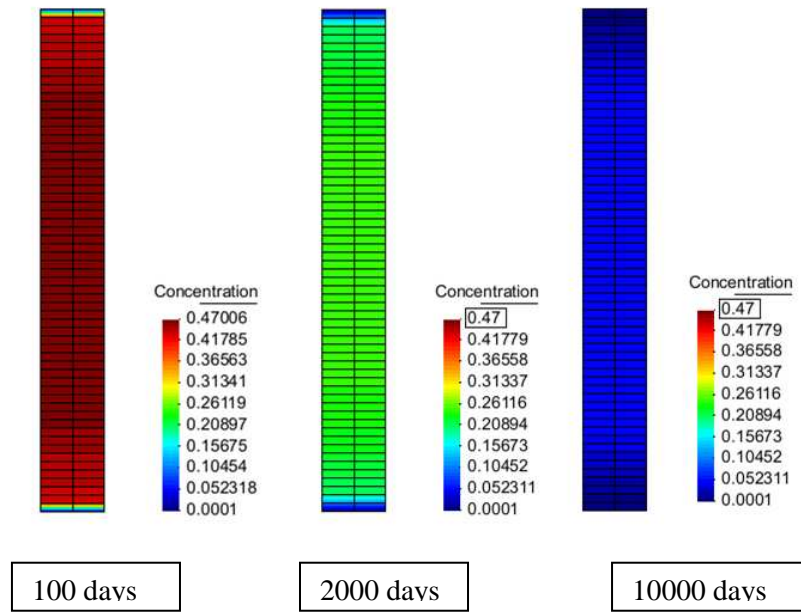
Figure 4.19: contours of solute mass fraction after 100, 2000 and 10000 days.

4.2.1.2 Modeling swelling test under constant volume conditions

In this section numerical simulations of swelling tests under (nearly) constant volume condition using the developed model are presented. These tests were performed on the same type of material used for the semi confined swelling tests. In this case, swelling was possible due to the stretching of the frame of the water uptake cells under the high osmotically induced pressures (~16 MPa after 1000 days of hydration, Mariën et *al.*, 2010).

The same model domain (Figure 4.6) and material parameters (Table 4.1) as in the previous section were used to calculate the osmosis-induced pressure exerted by the leaching BW. Along all the boundaries of the domain, horizontal displacements are restricted. To take into account the deformation of the load cell, vertical displacement along the upper boundary of the sample were not totally restricted. Figure 4.20 compares the modelled swelling of a sample that is hydrated under the conditions of the (nearly) constant volume test with the measured displacement of the piston in test S12.
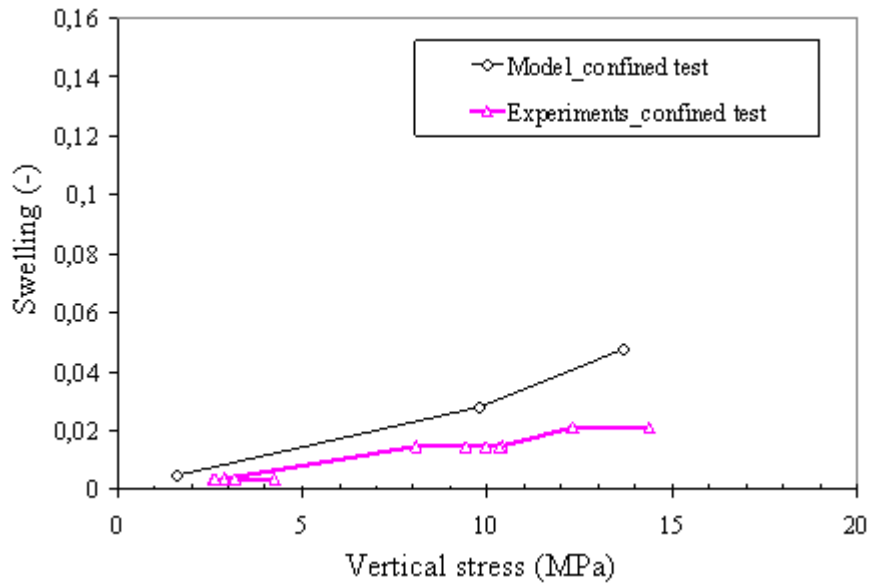
Figure 4.20: Swelling in the constant volume tests due to the deformation of the load cells under the high osmosis-induced pressures.(Experiments from Mariën et *al.*, 2010)

Figure 4.21 displays comparisons between the numerical simulations and experimental data. The proposed model is able to describe the main features observed in the experiments. The modelling and the experimental results both show that the water pressure is still rising after almost 3 years of contact with water and reaches a value about 18 MPa. The model can reproduce rather well the pressure increase and swelling of the samples in the constant volume tests.

Figure 4.21: Osmosis induced pressure versus time. Experimental results (Mariën et *al.*, 2010) and model predictions.

Mariën et *al.* (2010), presented µCT image of some Eurobitum samples tested under nearly constant volume conditions. Figure 4.22 shows the image of samples S9 and S12 hydrated after 1036 and 1555 days respectively. As for the samples tested under constant stress, only a thin layer has been hydrated (green-yellow layer near the filters represented in red). Mariën et *al.*, (2010) reported that for sample S12 hydrated during more than 4 years, the hydrated zone extend over a length of 2 mm (the initial height of the sample being 10 mm).
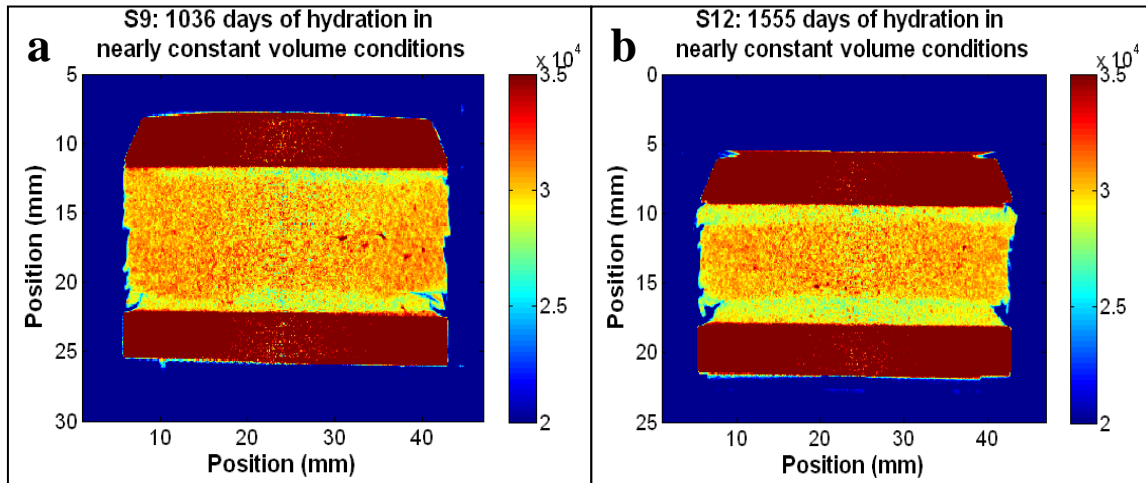
Figure 4.22: µCT images: visualization of the hydration front in Eurobitum samples with 28 weight% NaNO$_3$ after (a) 1036 and (b) 1555 days of hydration in nearly constant volume conditions. (Mariën et *al.*, 2010)

Figures 4.23.a and 4.23.b show respectively contours of NaNO$_3$ concentration and the profiles of NaNO$_3$ concentration over the total thickness of the sample and after 1555, and 10000 days. After almost 3 years of hydration, except of the outer most layers, concentration is still high inside the sample. This support the µCT results (Mariën et *al.*, 2010), which shows that only a thin layer of 2 mm width has been hydrated. After almost 30 years, NaNO$_3$ concentration inside the sample reaches a value of about 0.15 which demonstrate that more than 30 years are necessary for the salt to be completely leached out of the 10 mm height samples.
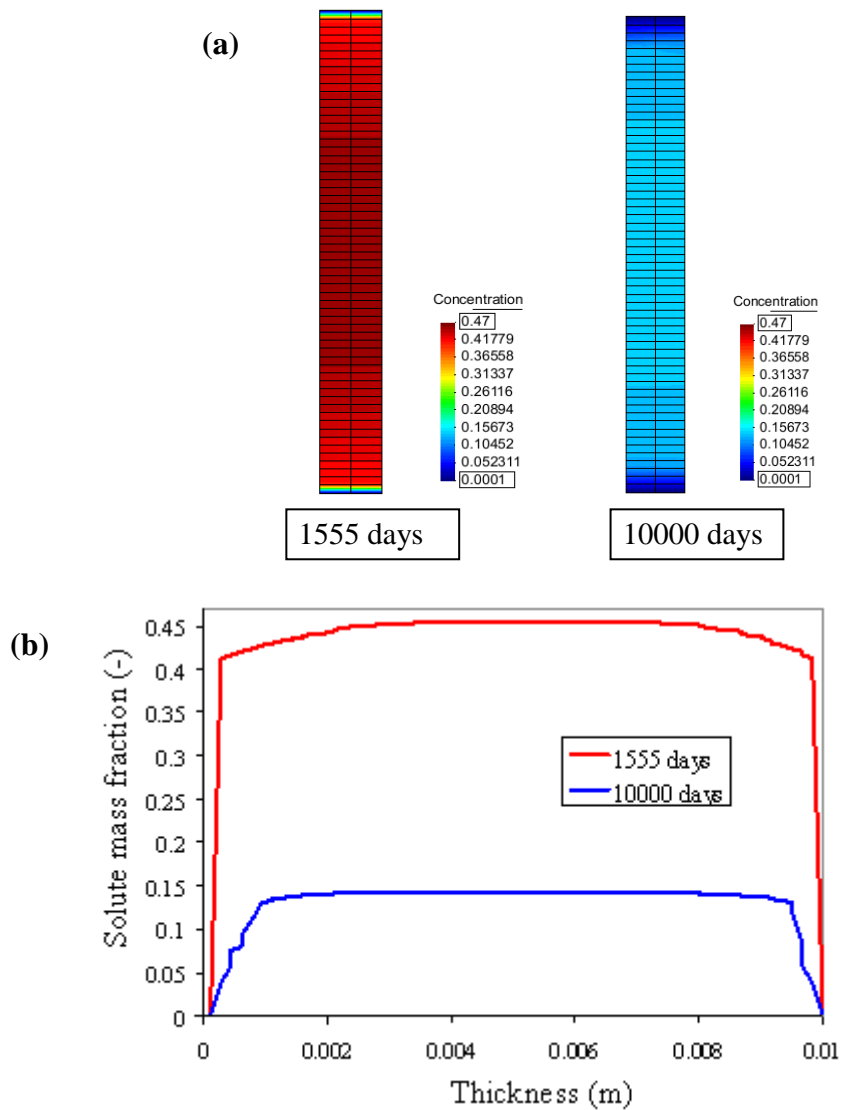
Figure 4.23: Profile of concentration (a) and profile of concentration (b) after 1555 days and 10000 days

Figure 4.24.c shows the time evolution of the crystal volume fraction at two selected points. Near the leached surface (point 1), ϕ_c decreases and tends to zero after almost 1200 days. A continuous flow of water towards the material is favoured by the dissolution of the crystals. The sample swells slightly because deformation is allowed at some degree in order to reproduce the deformation of the load cells. As a result porosity increases by swelling plus dissolution (Figure 24.b). Permeability tends to increase and drainage is favoured. As for the case of swelling test under constant stress, there is a compression of the layer near the leached surface (Figures 24.a and b). However, the induced volume reduction affects locally the sample because it is counteracted by the water uptake which provokes the increase of pressure in the deeper layers.
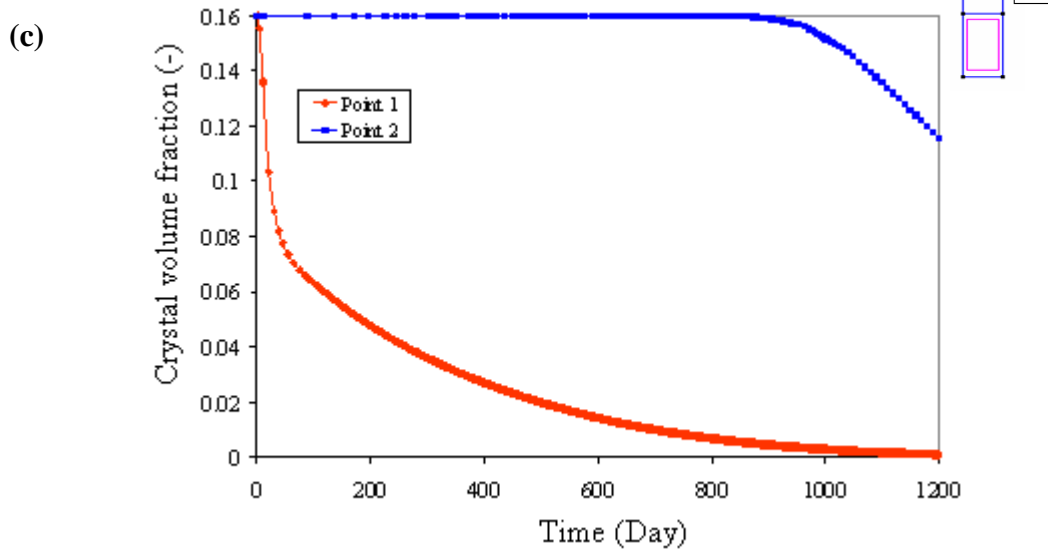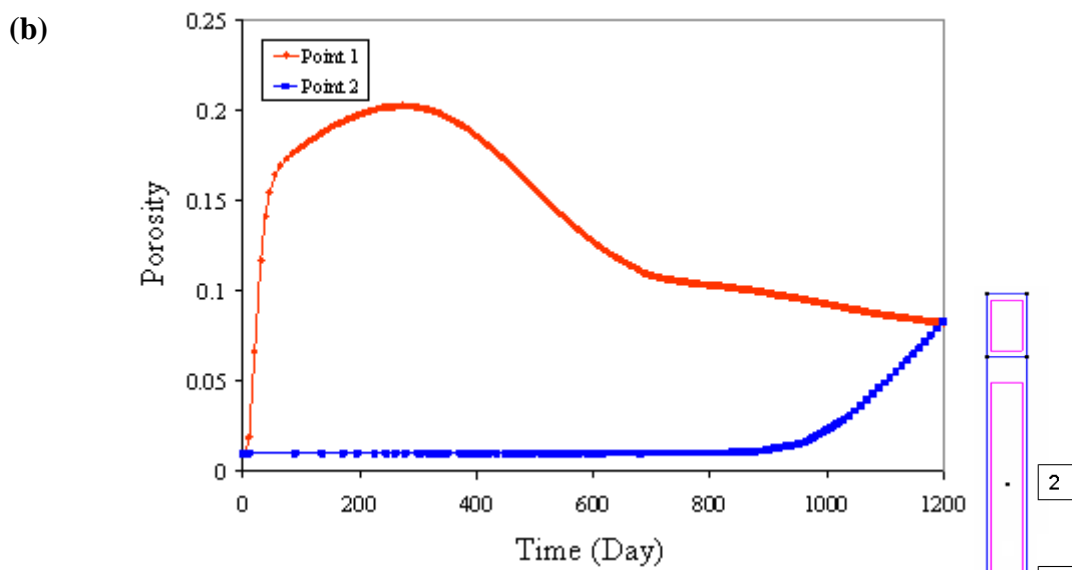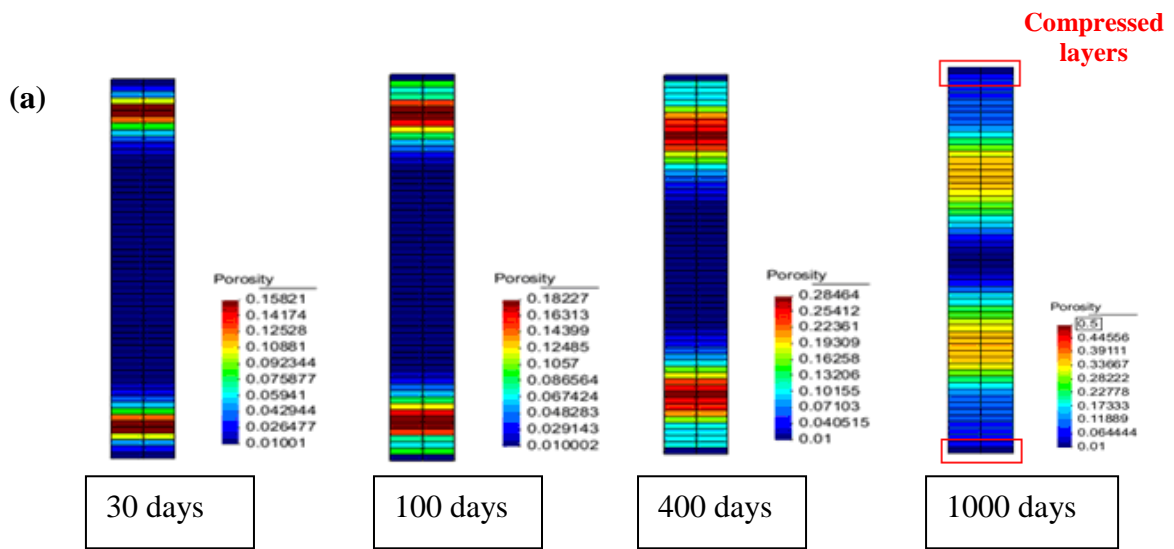
Figure 4.24: Constant volume test. (a) Porosity contours after 30, 100, 400 and 1000 days. (b) Porosity evolution. (c) Crystal volume fraction evolution

Compression of the outer most layers is considered here, as a limiting or controlling process for water uptake and of the release of $NaNO_3$. The profiles of concentration within the sample (Figure 4.23) which suggest that the mean concentration within the sample after 4 years is still high support this observation. In fact, reduction of the outer pores induces the decrease of permeability and of the diffusion coefficient and the increase of the osmotic efficiency in these compressed layers while deeper in the sample they are increasing. Therefore, the outer layers act as highly efficient semi permeable membrane surrounding the less efficient swollen material. This maintains very slow the inflow of water toward the sample and the out flow of the solute over a long time period.

The model response at long term is shown in Figure 4.25. The plot shows that pressure reaches a maximum of 20 MPa after 2000 days (~5.5 years). After this period the pressure starts to decrease. In fact, at long term, when all the crystal within the sample have dissolved that is, after 2000 days (Figure 4.26) there is also compression of the pores deeper in the sample favoured by drainage due to the high prevailing hydraulic gradient (pore pressure reaches a value of 20 MPa while at the boundary it is almost zero) . Although water is still driven into the sample because of the gradient of concentration existing between the sample and the external reservoirs, it is believed that this is a slow process as a consequence of the existence of the outer low porosity layers. As a result there is a global compression of the sample which in turn induces the decrease of the swelling pressure.
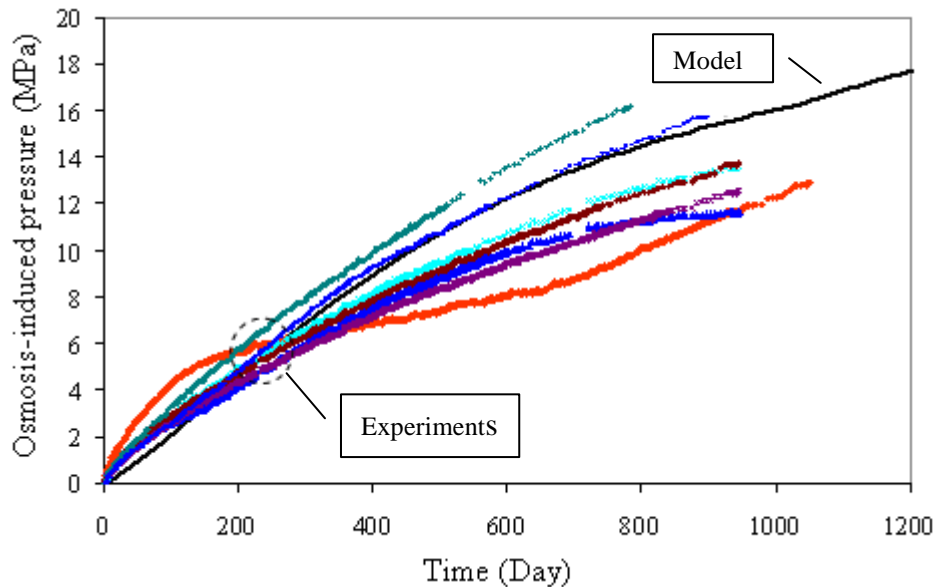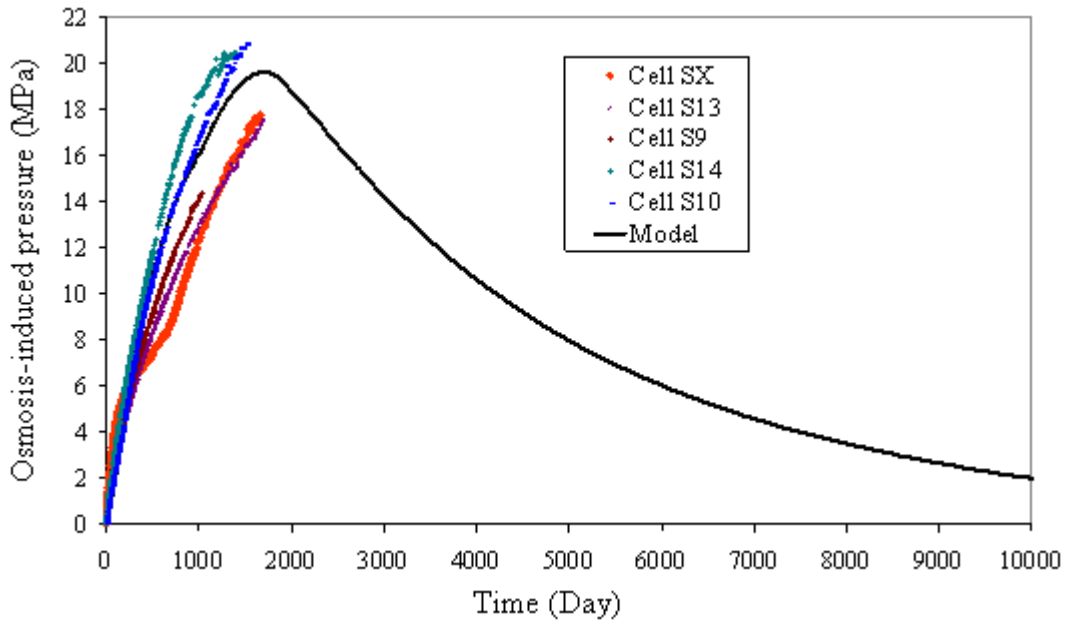
Figure 4.25: Osmosis-induced pressure versus time. Experimental results (Mariën et *al.*, 2010) and model prediction, long term response.
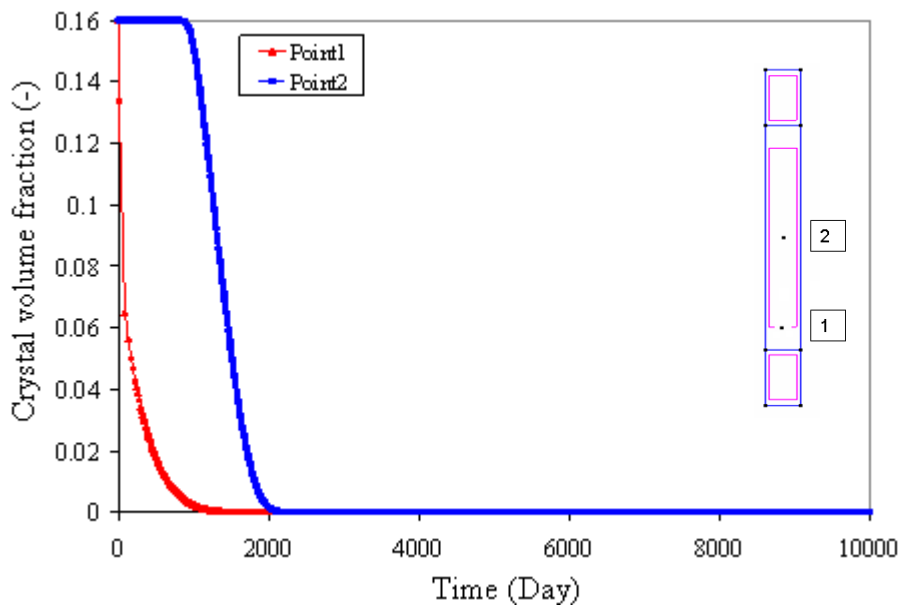
Figure 4.26: Evolution of crystal volume fraction at long term

To demonstrate that osmosis is the key process of the pressure increase, the contact solution was replaced by a saturated $NaNO_3$ solution after 1037 days of hydration (i.e. prescribed solute mass fraction at the outer boundaries was set to 0.47). As a result, no more water was taken up and the pressure started to decrease (Figure 4.27). This pressure decrease is induced by drainage due to the high prevailing hydraulic gradient (~16 MPa).
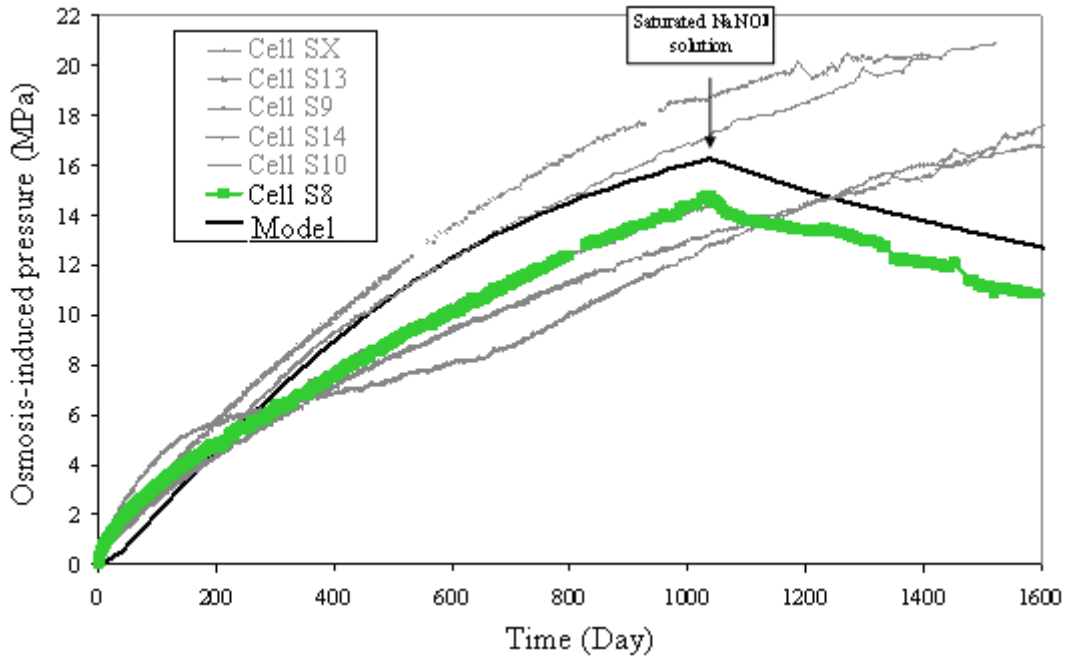
Figure 4.27: Evolution of osmosis-induced pressure with time. Effect of change leachant solution activity on the osmosis- induced pressure. Experimental and modelling results.

4.2.2. Effect of permeability, diffusion, and efficiency coefficients on the magnitude and duration of swelling (constant stress conditions)

The coupled solute water transport equations (Equations 2.19 and 2.21) indicate that two major processes control the transport of water: diffusion and advection. For low values of the intrinsic permeability the advection term is negligible and water is transported only by diffusion. As the permeability increases the advection term is added to the diffusive term and water is transported by both advection and diffusion. Therefore the variation of the intrinsic permeability and diffusion coefficient is bound to have a profound effect on the material behavior.

In the base case the material was considered with an extremely low initial permeability and diffusion coefficient and high efficiency coefficient (Table 4.1). As it was shown in Figure 4.15, these three parameters depend on the porosity and are coupled. It was demonstrated in the previous section that a material having a higher value of the permeability and diffusion has a lower value of the efficiency coefficient. Figure 4.28 shows the results of two numerical simulations of the swelling in constant stress conditions where the values of k and D^* have been varied in one case by one order of

85

magnitude and in the other case by two orders of magnitude. The corresponding value of σ is deduced on the basis of the result given in Figure 4.15.

Cases	K (m^2)	D^* (m^2/s)	σ(−)
Base case	3×10^{-26}	1×10^{-16}	0.95
Case 1	1×10^{-25}	1×10^{-15}	0.46
Case2	1×10^{-24}	1×10^{-14}	0.16
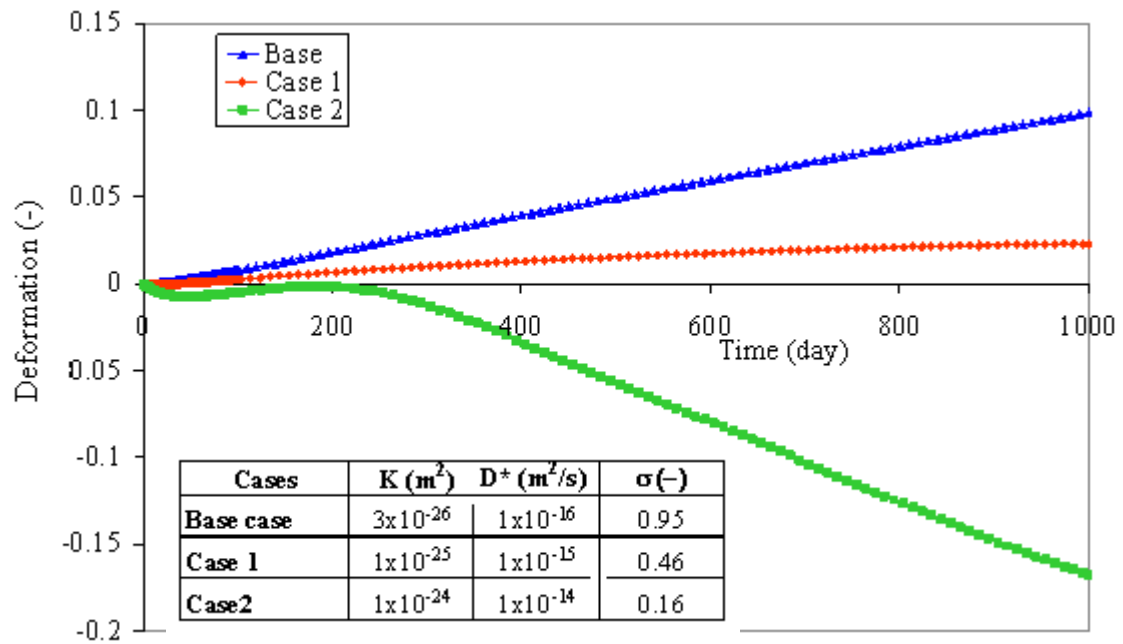
Figure 4.28: Evolution of deformation for various initial values of permeability, diffusion coefficient and efficiency coefficient

In the first case, although the initial values of the intrinsic permeability and the diffusion coefficient are higher, the rate and the magnitude of the swelling are reduced. This is a direct consequence of the lower initial value of the efficiency coefficient (σ_0=0.45). In the second case, it is shown that a further increase of k and D^* results in a compression of the material. In fact, the corresponding value of the efficiency coefficient is too low to induce osmotic effects (σ_0=0.16). As in this case D^* is larger, all the salt is removed and the salt concentration tends to zero quite early (Figures 4.29.a and b).
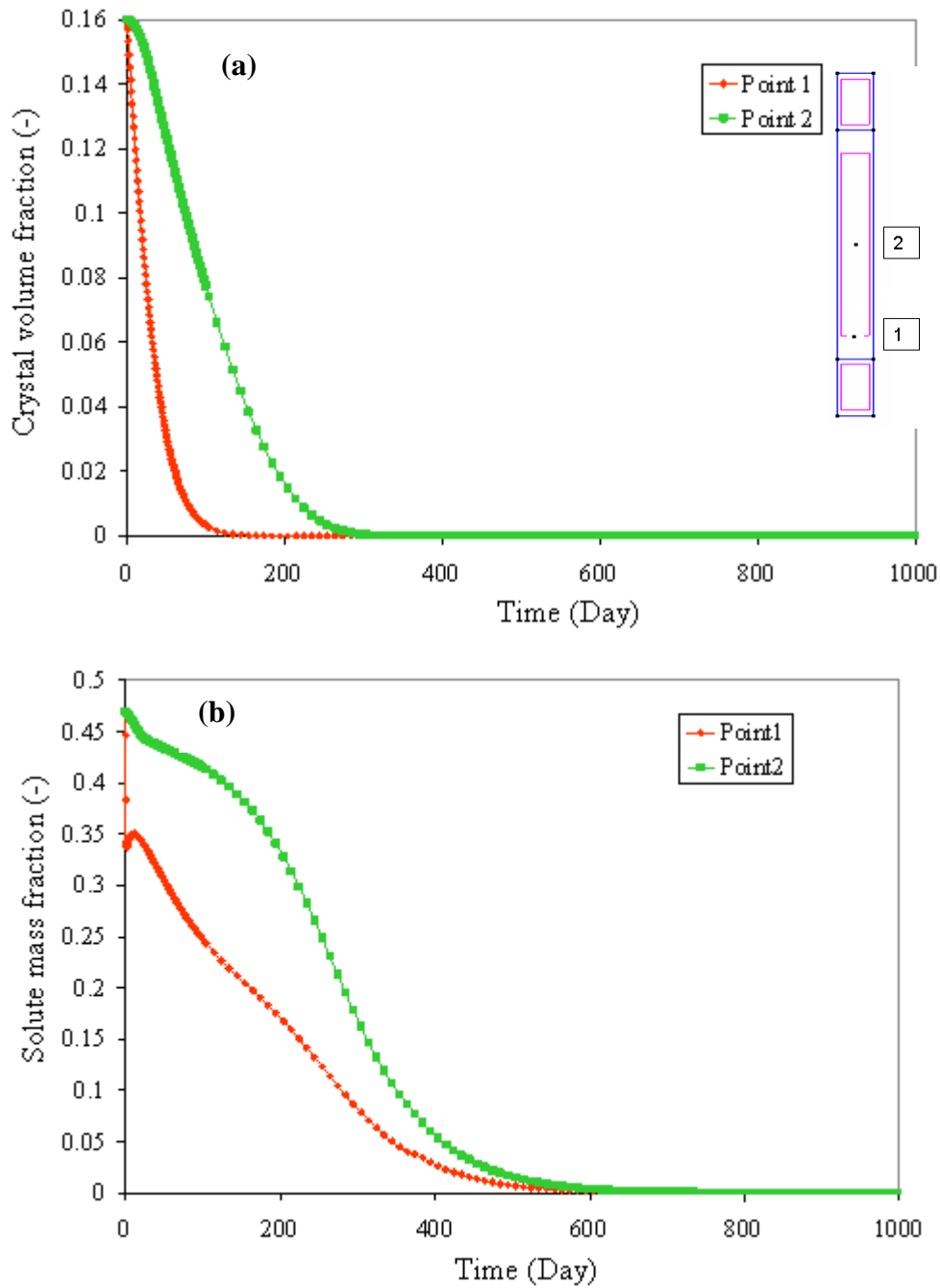
Figure 4.29: evolution of (a) crystal volume fraction and (b) solute mass fraction. Case 2

Characteristic times for the different transient processes (diffusion, advection and dissolution) are important to predict which of the processes controls the overall response.

Assuming one-dimensional conditions, the characteristic times for the diffusion, dissolution and advection processes can be determined from the preceding parameters (Base case):

$$t_{diffusion} = \frac{L^2}{D_0(1-\sigma)} \approx 2.76 \times 10^8 \text{s} \qquad\qquad t_{dissolution} = \frac{\phi_l \rho_l}{\phi_c \sigma_c k} \approx 4.22 \times 10^4 \text{s} \qquad (4.5)$$

$$t_{advection} = \frac{L\phi_l}{J_l} \approx 1.44 \times 10^7 \text{s}$$

where L is the length of the studied sample and D_0 is the coefficient of molecular diffusion, σ_c is the specific surface [m²/m^3], which may depend on the number of crystals and their radius; k is the rate constant [kg/s/m²] that depends on temperature.

For the particular case of this simulation (Base case) the characteristic times for the dissolution is in the order of 10 hours and it is 0.5 years for advection. While for diffusion it falls in the range of 10 years. Here advection appears to be the dominant process. Diffusion is very slow and this is attributed to the low diffusion coefficient and the high osmotic efficiency of the BW.

In this section, the effect of the key parameters for the transport coefficients has been analysed. Further work is required to obtain appropriate evolutive functions that permit to better calibrate the experimental response.

4.2.3. Modelling of additional experiments

In this section, other water uptake experiments are modeled. Again, the same material parameters, are used to reproduce the deformation of the leached BW (Table 4.1)

Semi confined swelling tests have been performed under different vertical stress. The experimental results have shown that increasing σ_v till 4.4 MPa does not significantly affect the response of the material (Mariën et *al.*, 2008; Valcke et *al.*, 2010). Further numerical analyses have been performed using values of σ_v ranging from 2.2 MPa to 55 MPa. Figure 4.30.a shows that the swelling deformation decreases significantly when the value of σ_v approaches the value of osmotic pressure of a saturated NaNO$_3$ solution (~ 42 MPa). This is immediately apparent in the calculated results shown in Figure

4.30.b for high value of σ_v: the water uptake process and therefore the salts' dissolution process slow down significantly.
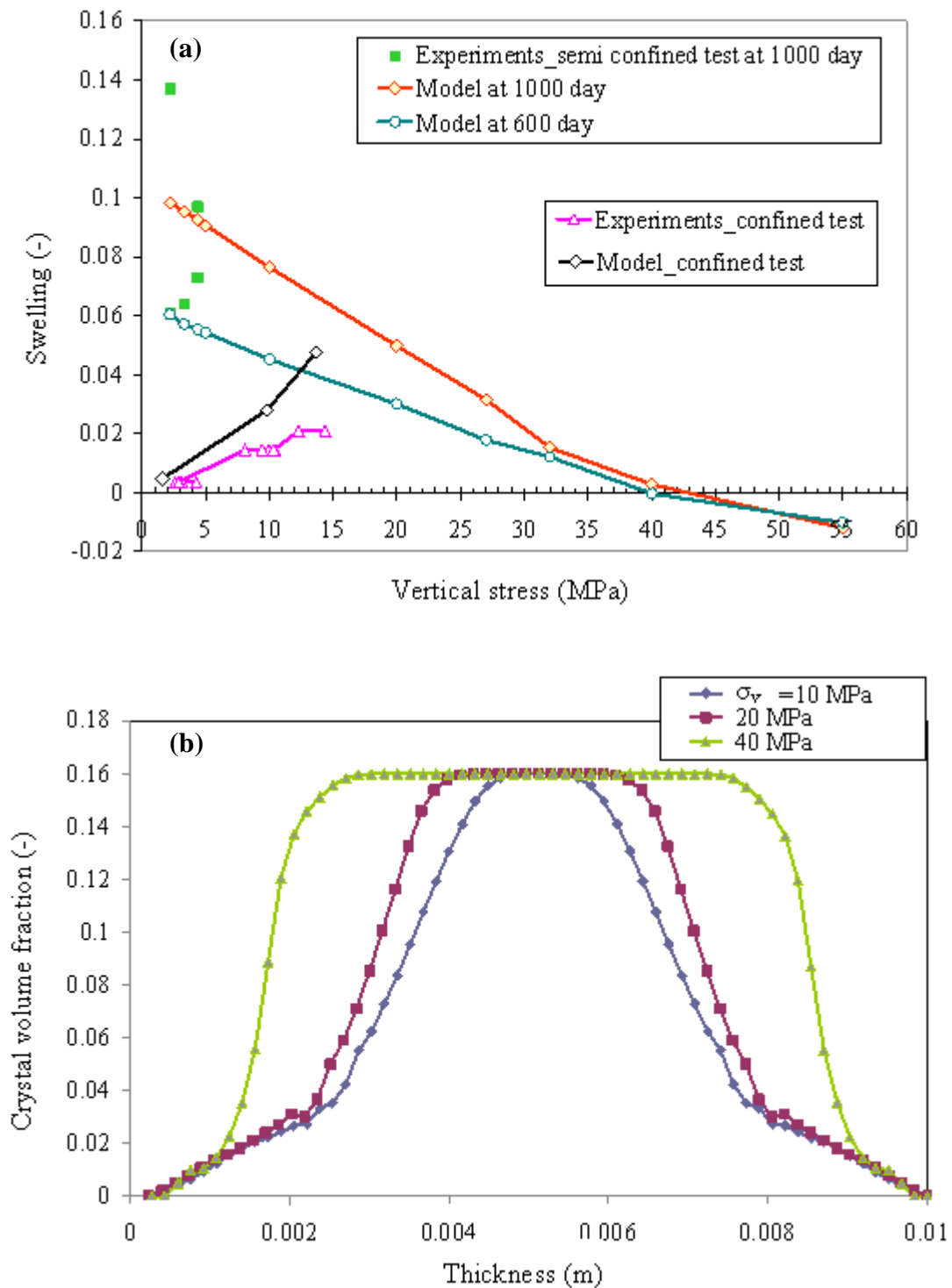
Figure 4.30: (a) Evolution of swelling deformation with the external vertical stress at 600 and 1000 days for the confined and semi confined tests. (b) Profile of evolution of crystal volume fraction after 1000 days for the semi confined test.

Figure 4.30 also shows the osmotic-induced swelling pressure in the nearly constant stress test at different times. According to the modeling results the maximum osmosis-induced swelling pressure is about 20 MPa. The theoretical maximal osmosis-induced pressure can be calculated by considering the bitumen matrix in Eurobitum as a perfect semi-permeable membrane. The dissolution of all $NaNO_3$ crystals will result in a saturated $NaNO_3$ solution when Eurobitum is hydrated in real constant volume conditions, where no swelling is possible. Hence, an osmosis-induced water uptake would result in a maximal pressure corresponding to the osmotic pressure of a saturated $NaNO_3$ solution, being 42 MPa (Equation 4.3). These high pressures are not attained in the nearly constant volume tests, since (1) bitumen is not a perfect semi-permeable membrane, hence allowing a slow release of $NaNO_3$ and since (2) the Eurobitum samples can swell slightly due to the deformation of the load cells.

These tests offer an interesting evidence of osmotic effects on swelling of BW under restricted mechanical conditions. On the basis of the ideas discussed previously, the type of phenomena developing inside the BW samples may be discussed with the help of Figure 4.31.

Two cases may be distinguished:

- Case1: porous medium, initially saturated with water with a given concentration C, crystals are not present

When the external applied pressure (P_{ext}) is lower than the osmotic pressure (π), water is driven into the pores of the medium because of the gradient of concentration existing between the reservoir and the water filling initially the pores. Pore water concentration will decrease until it reaches the value corresponding to an osmotic pressure equal to the external applied stress (Figure 4.31.a). In contrast, when P_{ext} is higher than π (Figure 4.31.b), Water is driven out of the medium, pore water concentration increases until it reaches the value corresponding to an osmotic pressure equal to the external applied stress.
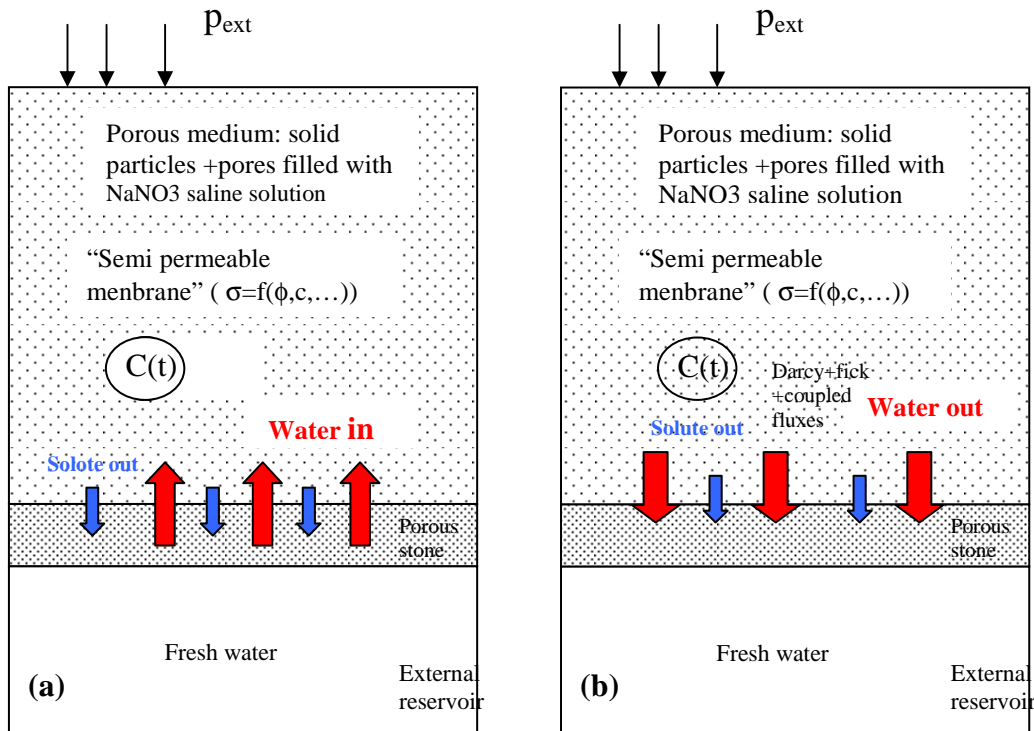
Figure 4.31 Interpretation of transport processes in water uptake tests

- Case 2: Porous medium, composed of a solid matrix embedding salt crystals: case of BW

Independently of the material being or not ideal semi permeable membrane, a major characteristic of the medium, which plays an important role in the process of water uptake, is the presence of salt crystals. Crystals provide a source term of solutes that prevent the decrease of concentration. The same scenarios as in case 1 applies, except that in this case the crystals ensure, for long time, high concentration inside the material which has a great influence on the time duration of the process (long term swelling). The constant volume experiment demonstrates that pressure can grow continuously as crystals still dissolve (Figure 4.21).

To check on the influence of the initial amount of the crystals on swelling, additional semi confined water uptake tests have been performed on samples of BW having different initial amounts of $NaNO_3$. Figure 4.32 shows the evolution of swelling deformation after a given time with the initial crystal volume fraction. Further calculations have been performed using values of ϕ_{c0} varying between 0.034 and 0.185 (Figure 32.b). As the calculated results show, a higher initial crystal content induces an

increase of swelling. In fact for low values of ϕ_{c0} the crystal is consumed rapidly, the concentration inside the sample decreases and the osmotic pressure vanishes.

The influence of the initial amount of the crystal on the osmosis-induced pressure has been also investigated. Water uptake tests under nearly constant volume condition have been performed on BW samples having ϕ_{c0} varying between 0.034 and 0.23. Figure 4.33.a shows the evolution of the measured osmosis-induced pressure in Eurobitum samples with ϕ_{c0} equal to 0.034, 0.067, 0.1, 0.16, and 0.185. The plot shows that for the samples with low crystal content (ϕ_{c0} equal to 0.034, 0.067 and 0.12) and in the samples with ϕ_{c0} equal to 0.185, the pressure increases at a slower rate than in the samples with ϕ_{c0} equal to 0.16. Figure 4.33.b shows the modeled evolution of the osmosis-induced pressure after 1000 days with the initial amount of crystal volume fraction. One can observe that a higher initial crystal content induces an increase of the osmosis-induced pressure. However, for values of ϕ_{c0} higher than 0.14, a drop of the osmosis-induced pressure is observed. A possible explanation of these results is that higher salt content means that there is less bitumen matrix surrounding the crystal. In other words, high crystal content may affect the ability of the BW to behave as a semi permeable membrane. Moreover, for higher crystal content porosity development by dissolution can develop further thus leading to faster reduction of the efficiency of the material.

The table embedded in figure (b):

Cases	Point 1 after 1000 days		
Φ_{co}	Φ_l	Φ_c	wsl(*)
0.034	0.105	0	0.211
0.067	0.097	1x10-5	0.366
0.1	0.103	3x10-4	0.42
0.185	0.114	0.01	0.448
0.45	0.267	0.16	0.464
(*) solute mass fraction			
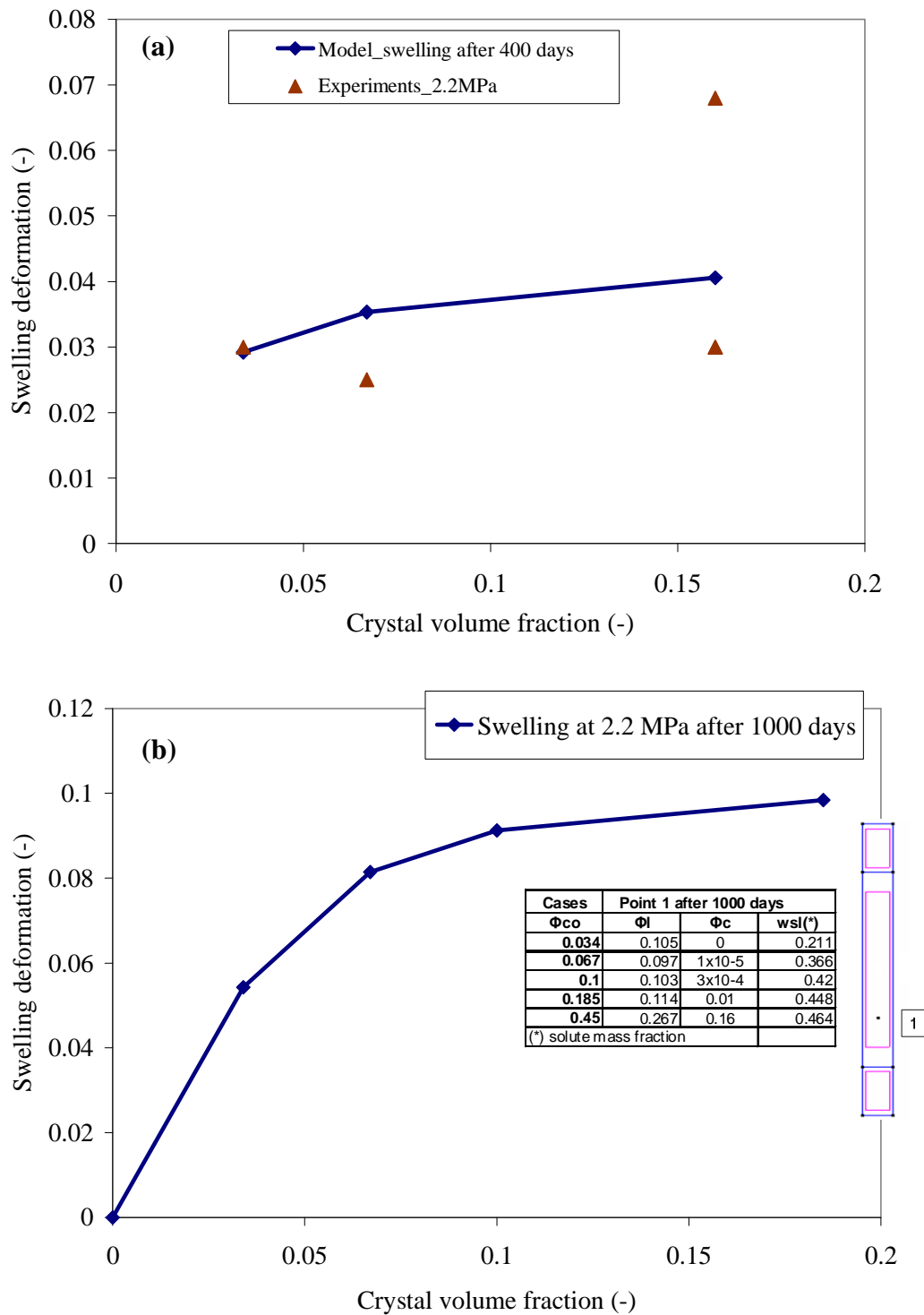
Figure 4.32: Variation of swelling deformation with the initial amount of the crystals. (a) Experimental and modelling results after 400 days. (b) Model prediction after 1000 days. Note that the legend shows the crystal volume fraction (ϕ_c), the liquid porosity (ϕ_l) and the dissolved NaNO$_3$ concentration (w_l^s), after 1000 days of hydration, in a point that is situated close to the sample surface
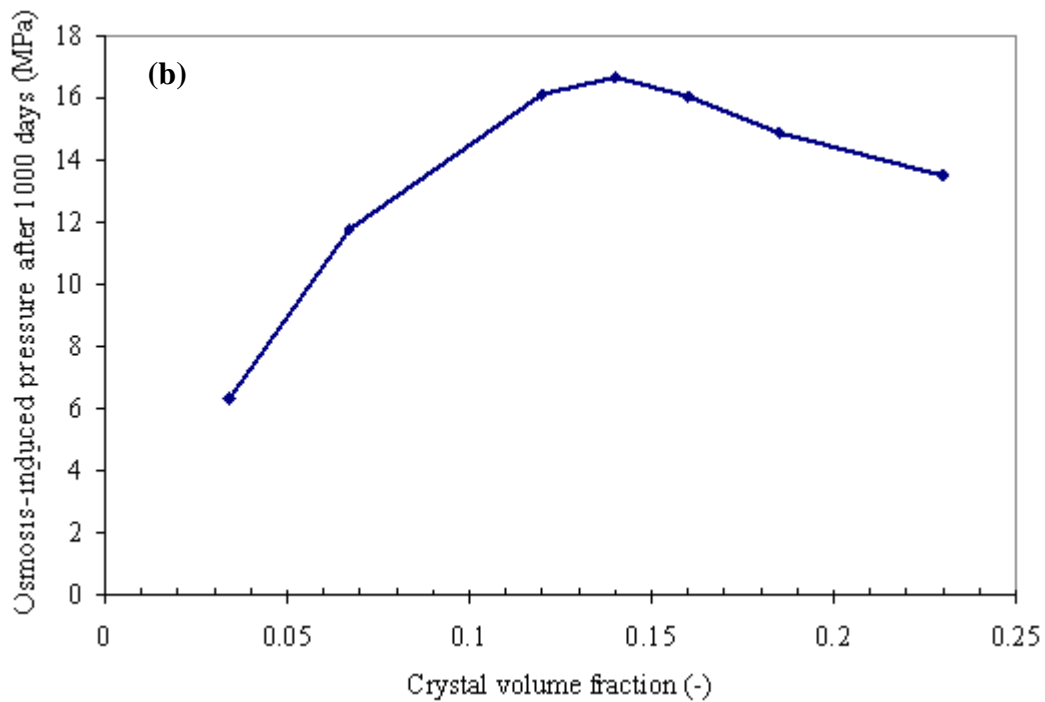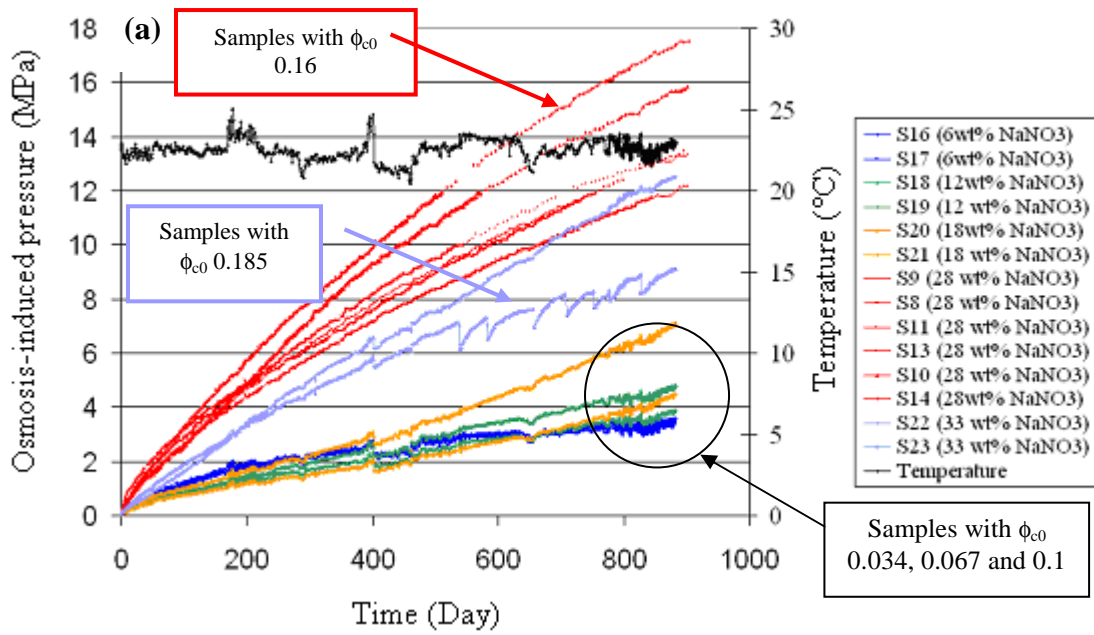
Figure 4.33: Variation of osmosis induced pressure with the initial amount of the crystals. (a) Experimental results (Mariën et *al.*, 2010). (b) Model prediction showing osmosis-induced pressure after 1000 days

94

4.3 Possibilities of application to large scale scheme: preliminary hydro-chemical analysis

As described above, the Belgian disposal concept foresees that several Eurobitum 220 litre drums would be grouped in a thick-walled cement-based 'secondary' container, which in turn would be placed in concrete-lined disposal galleries that are excavated at mid-depth in Boom Clay. Only 80-90 % of the total volume of the drum is filled with Eurobitum. The remaining voids between the containers would be backfilled with a cement-based material. A schematic view of the design for in situ disposal of Eurobitum is shown in Figure 4.2.

In the frame of the study of the possibility to dispose Eurobitum bituminized radioactive waste in the Boom Clay formation, a preliminary hydro-chemical analysis is presented here. The objective is to get first insights on the kinetics of water uptake, dissolution, solute leaching, and maximum generated pressure under disposal conditions.

Figure 4.34 shows the model domain. The analysis has assumed axis-symmetric conditions. The drums of Eurobitum, the concrete container, the concrete liner, the backfill, and the host rock have been represented. The outer boundary is placed at a distance of 14 m from the symmetry axis. It is assumed that 80% of the volume of the drum is filled with BW. The remaining void is modelled using a high porosity and highly deformable artificial material. It is assumed that the steel constituting the drums has been corroded so that it was not represented in the model. The backfill, the concrete container, the concrete liner and the Boom Clay are considered to be partially saturated with water with low $NaNO_3$ concentration (initial mass fraction is $w = 0.001$ kg/kg). The BW filling the drums contains $NaNO_3$ crystals occupying 16% of the total volume of the BW (corresponding to 28 % in weight) and is considered to be partially saturated with $NaNO_3$ brine (initial mass fraction: $w = 0.47$ kg/kg). The same initial values for permeability, osmotic efficiency and diffusion coefficient for BW as in Section 4.2 are used for this analysis. Detailed materials parameters are summarized in Table 4.2.

Section AA

Drums of BW (80% vol filled)

Backfill

Concrete container and Liner

Boom clay

Artificial material

0.88m

12.5 m
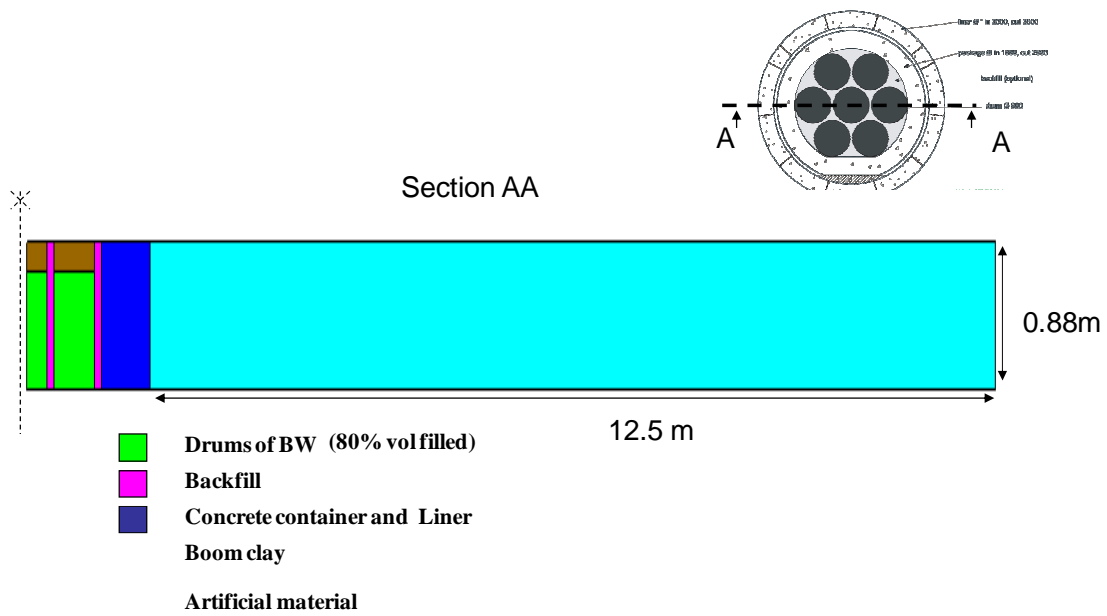
Figure 4.34: Model domain

Table 4.2. Material properties used for large scale hydro-chemical analysis

Parameters (Initial values)		Symbols	Values
BW	Crystal volume fraction	ϕ_{c0}	0.16
	Porosity	ϕf_0	0.01
	Intrinsic permeability	k_0 (m^2)	3×10^{-26}
	Efficiency coefficient	σ_0	0.95
	Diffusion coefficient	D (m^2/s)	1.6×10^{-16}
	Dissolution Rate	κ	10^{-5}
	Solute mass fraction	w_l^s	0.47
Boom Clay	Intrinsic permeability	K (m^2)	10^{-19}
	Solute mass fraction	w_l^s	0.001
Concrete container +liner	Intrinsic permeability	K (m^2)	10^{-18}
	Solute mass fraction	w_l^s	0.001
Backfill	Intrinsic permeability	K (m^2)	10^{-16}
	Solute mass fraction	w_l^s	0.001

Figure 4.35 shows the contour field of crystal volume fraction after, 0.01 days, 5 and 100 years together with contours of porosity. After 5 years, ϕ_c decreases and tends to zero at the outer boundary of the drums while, no change of ϕ_c is observed in the middle of the drum after 100 years. This suggests that it will take several hundred of years before the hydration front has reached the center of the drums. Indeed, at early times, due to the high concentration gradient, water is attracted from the backfill to the BW. Consequently there is dissolution of the crystals at the outer vertical boundary of the drums. The kinetics of water supply will basically be controlled by the permeability of the host clay formation. The degree of saturation and water pressure will increase in the disposal system including the artificial material ensuring a continuous flow of water towards the BW. Therefore, water pressure increases in the BW. After 5 years the maximum value is attained at the outer boundary of the drums and is about 6 MPa (Figure 4.36.b). This pressure front progresses slowly toward the middle of the drum (Figure 4.36.a). However, a low decrease of the maximum value of pressure is observed after 100 year. In fact, dissolution of the crystals at this zone induces the increase of porosity (Figure 4.35.b) and eventually an increase of permeability and diffusion coefficient and a decrease of efficiency of the membrane. Drainage and solute diffusion out of the BW are favoured, resulting in a decrease of the pore pressure (Figure 6.36.b).
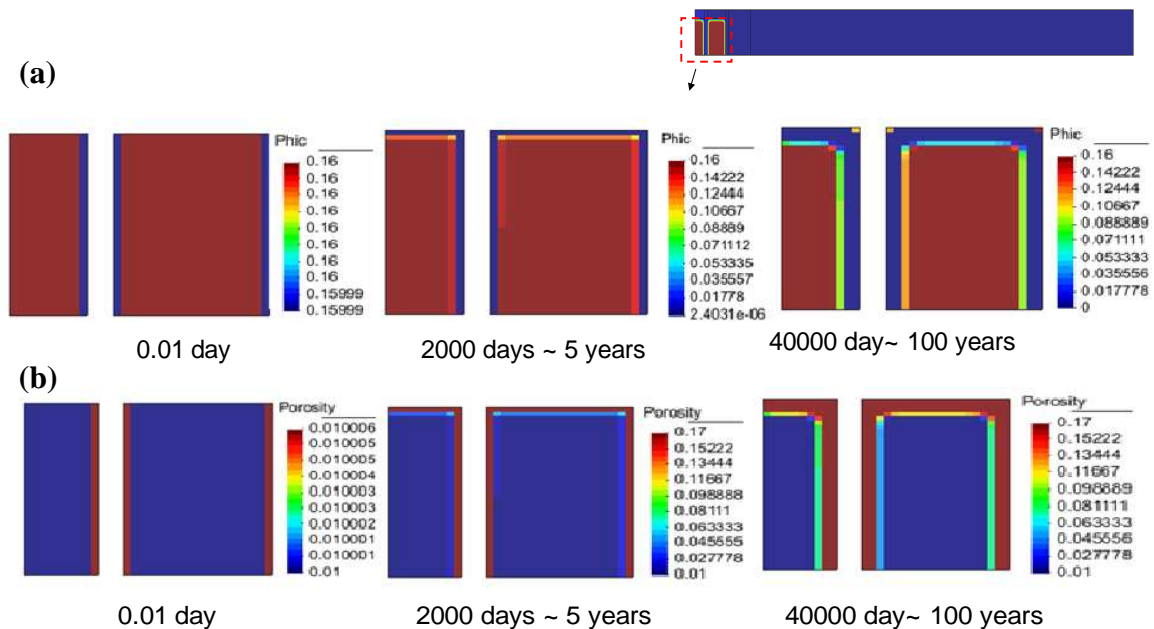
Figure 4.35: contours of crystal volume fraction (a) and porosity (b) after 0.01 days, 5 and 100 years

Figure 4.37 shows the concentration profile and contours field of concentration after 0.01 days, 5 years and 100 years. Except of the outer boundary where the crystals have vanished, the concentration of the NaNO$_3$ solution inside the BW drums remains constant and equal to that of a saturated NaNO$_3$ solution after 100 years. In fact, the crystals provide a source term of solutes that prevent the decrease of the concentration.

The concentration profile through the Boom Clay after 100 years is shown in Figure 4.38. Because the BW is not a perfect semi permeable membrane, the solute is allowed to diffuse out of BW. Concentration increases at the outer boundary of the gallery and reach a maximum value of 0.06 after 100 years. Despite this low value it is expected that this chemical disturbance will probably have some effects on the mechanical and hydraulic properties of the clay formation (experimental results are shown in chapter 6), in the region close to the drift.
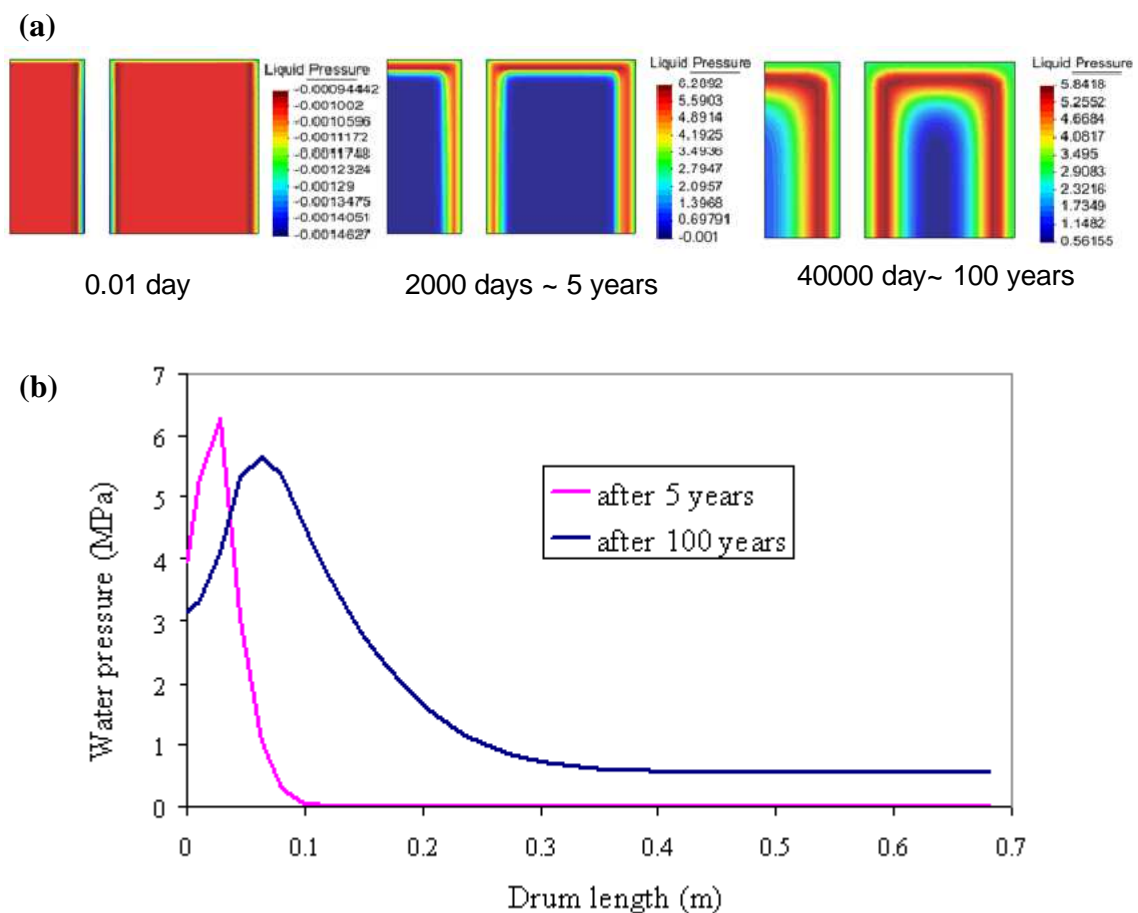
Figure 4.36: (a) Contour field of liquid pressure after 0.01 day, 5 years and 100 years. (b) Profile of liquid pressure in a BW drum after 5 years and 100 years

(a) 0.01 day   2000 days ~ 5 years   40000 day~ 100 years

(b)
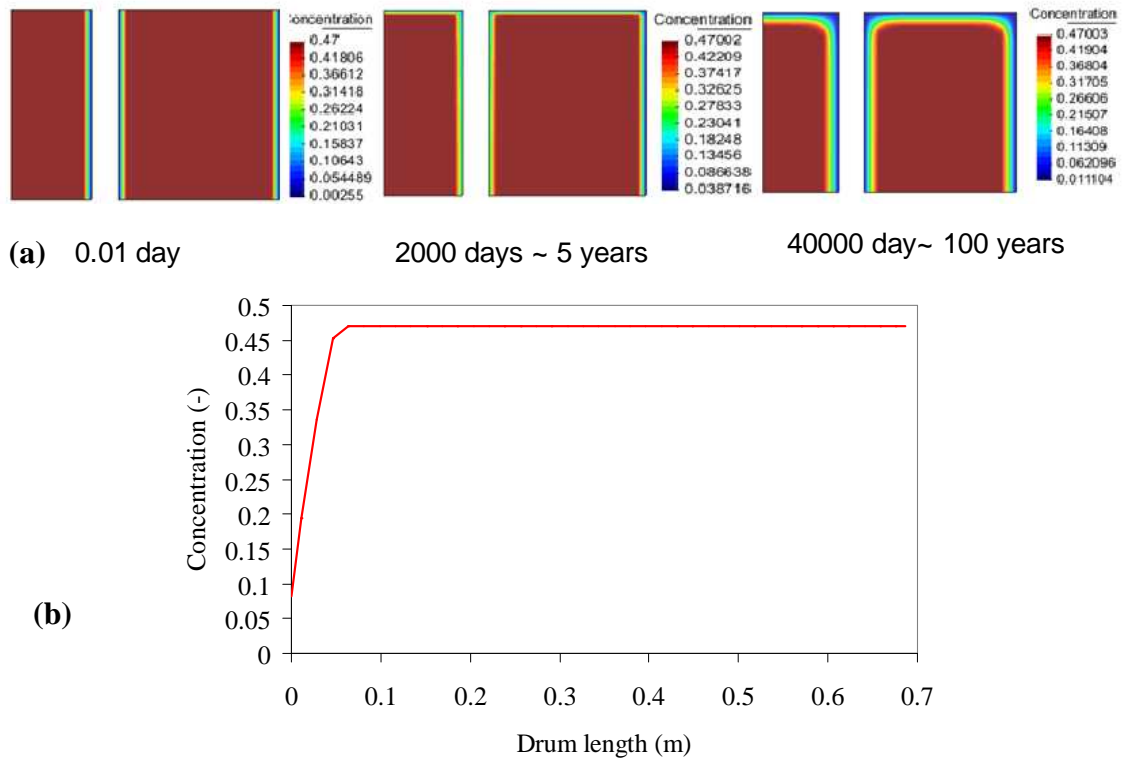
Figure 4.37 (a) Contours of concentration in BW drums after 0.01 days, 5 years and 100 years. (b) Profile of concentration through a BW drum after 100 years.

(a)

40000 day~ 100 years

(b)
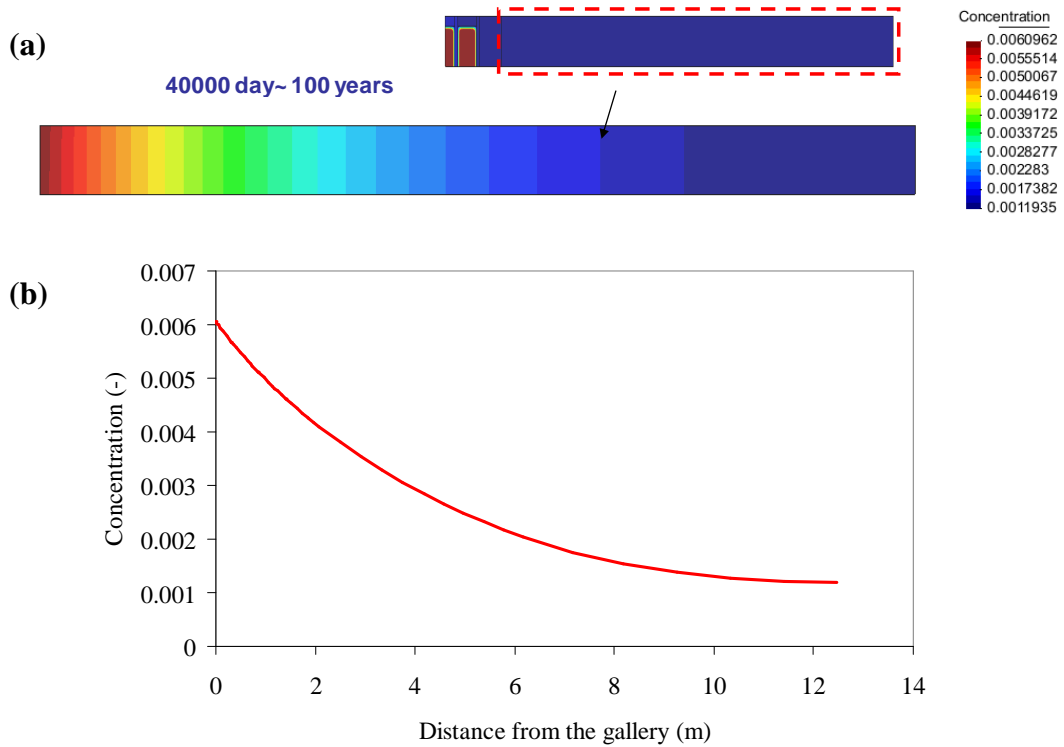
Figure 4.38 (a) Contour of concentration in Boom Clay after 100 years. (b) Profile of concentration trough the Boom Clay after 100 years

4.5. Summary

In this chapter, the behaviour of bituminized waste materials in contact with water has been studied in restricted swelling conditions (semi confined (or constant stress) and confined (or "nearly"constant volume) water uptake tests). The contribution of osmosis on the swelling of the material is investigated. A formulation has been proposed (Chapter 2) for the analysis of deformation induced by the dissolution of the salts in porous media in contact with fresh water.

The combination of an adequate elasto-viscoplastic constitutive model with the proposed formulation provides a powerful tool to model the volumetric deformations induced by the uptake of water by the crystals in the bituminized radioactive waste. In this Chapter, it is shown that the swelling depends on the mechanical behavior of the material, and is moreover strongly coupled with the fluid fluxes. From a mechanical point of view, it has been observed that expansion is caused not only by reduction of the effective stress but also because values in tension have been reached. If this latter takes place, the expansive volumetric strain will be much larger than during unloading. The results obtained from the model are consistent in all aspects with those obtained from the water uptake experiments. Indeed, reasonably good estimates of the evolution of the deformation for swelling test have been obtained as well as of the evolution of the osmosis induced pressure in the confined (constant volume) tests. In addition it was demonstrated that permeability, diffusivity and efficiency coefficient affect the magnitude and the duration of the overall process.

4.6. References

Barbour, S.L. and Yang, N.: A review of the influence of clay-brine interactions on the geothecnical properties of Ca-montmorillonitic clayey soils from western Canada. Can. Geotech. J. 30, 920-934, (1993).

Berner, U.: Evolution of pore water chemistry during degradation of cement in radioactive waste repository environment.Waste Manage., 12, 201-219, (1992)

Brodersen, K.: The influence of water uptake on the long term stability condition waste. Radioactive waste management (proc. CEC Sem. Geel, Belgium, Vol 13, Commission of the European Communities, Luxemburg and Brussels, 147-162. (1983).

Beyers, H.R.: in 'Elements of Cloud Physics', University of Chicago Press, p. 24,(1965).

De Craen, M., Wang, L., Van Geet M., and Moors, H.: Geochemistry of the Boom clay pore water at Mol site, Scientific Report SVK.CEN-BLG-990, SCK.CEN, Mol, Belgium, (2004).

Gwinner, B., Sercombe, J., Tiffreau, C., Simondi-Teisseire, B., Felines, I., and Adenot, F.: Modelling of bituminized radioactive waste leaching. Part II. Constitutive equations. J.Nucl. Mat., 349, 96-106, (2006).

Gwinner, B., Sercombe, J., Tiffreau, C., Simondi-Teisseire, B., Adenot, F, Felines, I., and Favre, E.: Experimental and theoretical study of the pore structure and diffusion properties of an evolving heterogeneous material: Application to radioactive bituminized waste. Chem. Eng. Commun, 194:2, 234 – 247, (2007).

Li, X., Bernier, F., and Valcke, E.: Interaction swelling bitumen – host rock: scoping calculations. Mat. Res. Soc. Symp. Proc. 932, 751-758, (2006).

Mariën, A., Smets, S., Li, X., and Valcke, E.: Processes Related to the Water Uptake by Eurobitum Bituminised Radioactive Waste: Theoretical Considerations and First Experimental Results", Mat. Res. Soc. Symp. Proc.1107, 151-159 (2008).

Mariën, A., Smets, S., and Valcke, E.: Study of the Processes Related to the Water Uptake of Eurobitum Bituminized Radioactive Waste: Effect of Salt Concentration. Mater. Res. Soc. Symp. Proc., Vol. 1193, 513-520, (2009).

Mariën, A., Mokni, N., Valcke, E., Olivella, S., Smets, S., Li, X.: Osmosis-induced pressure by Eurobitum bituminized radioactive waste hydrated in constant volume conditions. (In preparation), (2010).

Mokni, N., Olivella, S., Li, X., Smets, S., and Valcke, E.: Deformation induced by dissolution of salts in porous media" J. Phys. Chem. Earth. 33 Supplement, 436-443, (2008).

Olivella, S., Carrera, J., Gens, A., and Alonso, E.E.: Non isothermal multiphase flow of brine and gas through saline media. Transport Porous. Med., 15, 271-293, (1994).

Petterson, M., Elert, M.: Characterisation of bituminised waste in SFR1", SKB Rapport R-01-26, (2001).

Sercombe, J., Gwinner, B., Tiffreau, C., Simondi-Teisseire, B., and Adenot, F.: Modelling of bituminized radioactive waste leaching. Part I. Constitutive equations. J. Nucl. Mat. 349, 96-106, (2006).

Sneyers, A., Van Iseghem, P.: The leaching behaviour of bituminized radioactive waste in the geologic disposal conditions of the Boom Clay Formation. Mater, Res. Soc.Symp. Proc. 506, 565-572, (1998).

Valcke, E., Mariën, A., and Van Geet, M.: The methodology followed in Belgium to investigate the compatibility with geological disposal of Eurobitum bituminized intermediate-level radioactive waste, Mat. Res. Soc. Symp. Proc. Vol. 1193, 105-116, (2009).

Valcke, E., Mariën, A., Smets, S., Li, X., Mokni, N., Olivella, S., and Sillen, X.: Osmosis induced swelling of Eurobotum bituminized radioactive waste in constant total stress conditions. J.Nuc.Mater., 406, 304-316, (2010).

Yang, N., and Barbour, S.L.: The impact of soil structure and confining stress on the hydraulic conductivity of clays in brine environments. Can.Geotech.J. 29, 730-739, (1992).

Chapter 5

Formulation for osmotic processes in unsaturated double structure deformable media

5.1 Introduction

Clay minerals are widely distributed in the clay crust and play a crucial role in many geotechnical practices. Understanding of coupled solute and water flows in clay-rich formations is essential for many problems ranging from pollution studies to waste containment. For deep nuclear waste disposal, active clay rich deposits are often selected as potential host formation due to their low hydraulic conductivity, plasticity, swelling and adsorptive capacity for contaminants.

Experimental investigations have shown that clays give rise to osmosis and ultrafiltration (Fritz and Marine, 1983; Fritz, 1986; Keijzer, 2000; Garavito, 2005). If the clay host rock acts as a semi permeable membrane (see Chapter 2 for definition), the release of pollutants out of the nuclear waste produces an osmotic driven flow which may affect the host rock through an osmosis-induced pressure. The value of the osmotic efficiency coefficient is affected by several factors, including the state of stress in the soil, the type and amount of clay minerals comprising the soil, and the type and concentrations of the solutes in pore water (Mitchell, 1993; Malusis et *al*., 2001; Malusis et *al.*, 2003).

Fritz and Marine (1983) in their experimental study of Na-Bentonite concluded that porosity has an important effect on the membrane ideality. For Na-Bentonite membrane in NaCl system, the obtained osmotic efficiency coefficient (σ) was 0.87 for 59% of porosity and 0.89 for 41 % of porosity. The efficiency of clay membrane increases as the level of compaction increases. Keijzer et *al*. (1999) reported the same result. They presented the evolution of the osmotic efficiency coefficient as a function of the porosity for montmorillonite, illite and Ankerpoort bentonite which was used in the

Netherlands as a low permeable barrier to prevent the transport of water and contaminants from landfill sites (Figure 5.1).
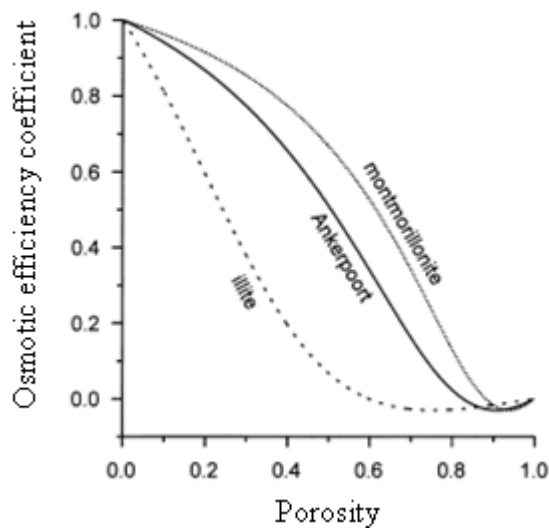
Figure 5.1: Osmotic efficiency coefficient for a typical montmorillonite, illite and bentonite as a function of porosity (Keijzer et *al.*, 1999)

The dependency of the osmotic efficiency coefficient on the average salt concentration across the clay membrane has been well documented in the literature (Fritz and Marine, 1983; Barbour and Fredlund, 1989; Mitchell, 1993; Malusis et *al.*, 2001; Malusis et *al.*, 2003). Figure 5.2 shows values of σ for different types of bentonite specimens. When the salt concentration increases for a given porosity and salt type solution, the efficiency coefficient decreases.
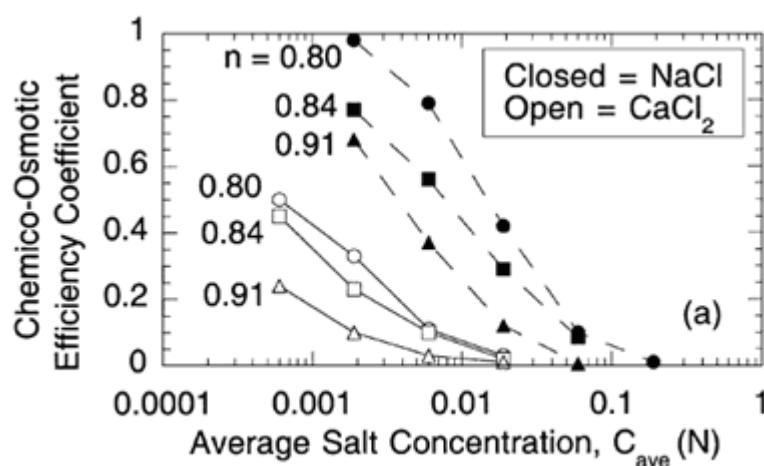
Figure 5.2: Osmotic efficiency coefficient as a function of average salt concentration across a bentonite specimen (Malusis et *al.*, 2003)

Malusis et *al.* (2003) have shown the existence of a threshold average concentration for the initiation of membrane behaviour of a sodium bentonite specimen. They demonstrated that depending on the type of the salt solution this limit value of concentration is sensitive to porosity (Figure 5.3).
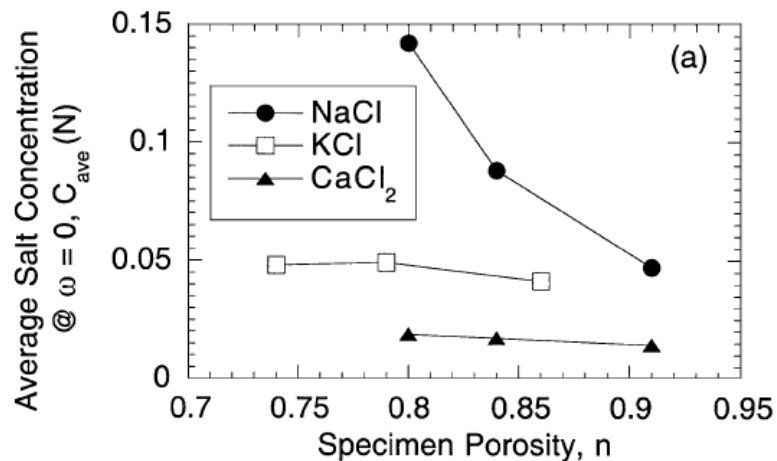
Figure 5.3: Effect of specimen porosity on average salt concentrations required to establish semi permeable membrane (Malusis et *al.*, 2003)

Other factor which has an important effect on the efficiency of a membrane is the Cation Exchange Capacity (CEC). Fritz (1986) observed that the membrane efficiency of high CEC materials like smectite, which posses a high surface charge density, is less affected by pore water salinity. Therefore, for constant value of porosity, the efficiency of montmorillonite to act as a semi permeable membrane is higher than that of illite which support the result obtained by Keijzer et *al.* (1999).

Most of these phenomena have been explained on the basis of the Diffuse Double Layer theory (DDL). In fact, an evident explanation of the effect of porosity on the osmotic efficiency coefficient is that decreasing the porosity by compaction promotes a greater degree of DDL. The DDL is defined by the charged surface platelets and its cation-dominated sorption layer within sufficiently large micropores (Figure 5.4). The DDL theory derived from the Poisson- Boltzman equation has been widely discussed in the literature (e.g. Mitchell, 1993).

The thickness of the diffusive double layer (*d*) can be estimated from the Gouy-Chapman theory in accordance to Equation (5.1) (Mitchell, 1993)

$$d = \sqrt{\frac{\varepsilon_0 DBT}{2n_0 e^2 v^2}}$$

(5.1)

where ε_0 is the permittivity of vacuum [C^2/J.m], D is the dielectric constant of the medium, *B* is the Boltzman constant [$1.38.10^{-23}$ J/K], *T* is the temperature [K], n_0 is the electrolyte concentration, *e* is the electronic charge [1.6×10^{-19} C] and *v* is the cation valence.
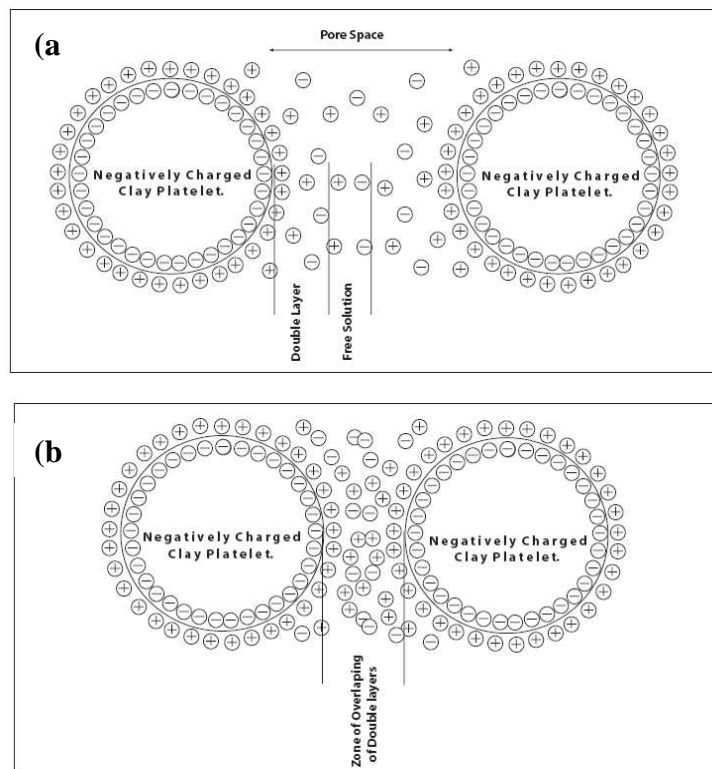
Figure 5.4: Schematic representation of double layer of clay platelets, (a) non-overlapping layer. (b) Overlapping layer. (Garavito, 2005)

Equation (5.1) shows that the thickness of the DDL decreases when the electrolyte concentration increases, or when the cation valence increases or when the dielectric constant decreases.

The hypotheses assumed by the DDL theory are very restrictive. Among these, is the condition of colloidal suspension arrangement. In fact, this theory fails in the description of compacted, high density clay materials like most of natural and engineered barriers (Hueckel, 1992).

When clay layers are exposed to water of different salinities or separate them, osmosis may be given as explanation for anomalous hydraulic heads. Marine and Fritz (1981) reported anomalously high pore water pressures as a result of different pore water compositions separated by a shale. They concluded that the degree of compaction is fundamental to observe high semi-permeable membrane efficiency. Neuzil (2000) reported an in situ chemical osmotic experiment on the Pierre Shale of South Dakota (USA). To conduct the experiment, water of different salinities were added to four boreholes and the water levels monitored. Membrane properties of the Pierre Shale, especially the water film between the clay platelets and the corresponding efficiency coefficient were calculated. The result implies that when sufficiently compacted, shale membrane generate osmotic pressure up to about 20 MPa.

Recently Garavito et al. (2006) reported results of an in situ osmosis experiment in the Boom Clay Formation. Studies on the compatibility of a large amount of nitrate-bearing bituminized radioactive waste with Boom Clay have recently raised a particular interest for osmosis induced effects in this reference formation in Belgium (see Chapter 4). The experiment was performed using existing piezometers in Boom Clay. A solution of 0.14 M $NaHCO_3$ corresponding to 10 times the pore water concentration in the Boom Clay was used as concentrated solution for the osmosis experiment. It was concluded that the semi permeable membrane behavior of the Boom Clay is relevant for the radioactive waste disposal. However, the presently observed osmotically induced pressure was very low (0.02 MPa).

Description of the physical and chemical processes controlling the water and solute transport through low-permeability argillaceous formations is a key step for assessing their suitability as host rocks. Moreover, it is well documented that the behavior of clayey soil is strongly influenced when there is a change on pore fluid chemistry (Yang and Barbour, 1992; Barbour and Yang, 1993; Di Maio, 1996; Gajo and Loret, 2004; Rao et al., 2005, 2006, and 2007; Alonso et al., 1998; Castellanos et al., 2006, 2008; Musso and Romero, 2003, 2005).

It is well known that active clay material presents a double structure arrangement (e.g. Gens and Alonso, 1992; Alonso, 1998; Romero, 1999; Guimarães, 2002; Sanchez et al., 2005; Castellanos et al., 2006, 2008). The two dominant pores size may be associated

with two basic structural levels: The microstructure is composed by the clay platelets arranged into clusters enveloped by external adsorbed water. The interlamellar pores are filled with internal absorbed water. This water has properties, such as density, or viscosity different form those of free water (Hueckel, 1992b). The macrostructure is composed by the global arrangements of clay clusters, with macro pores between them, partially filled with free water. Figure 5.5 shows a schematic representation of the conceptual model.
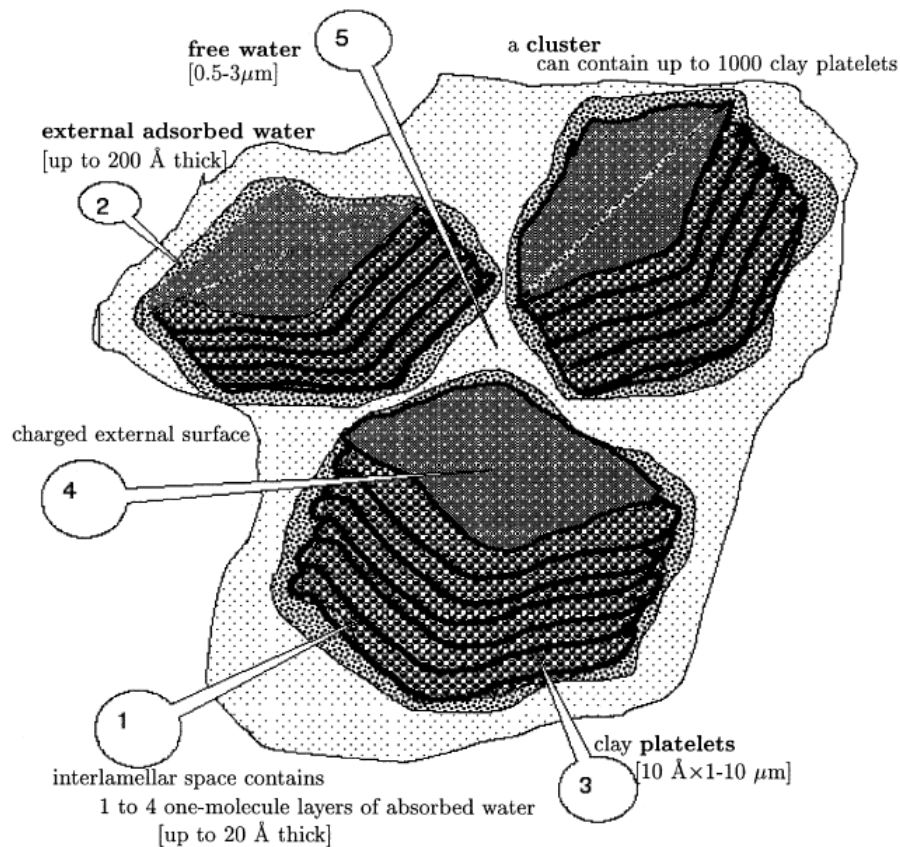
Figure 5.5: Schematic representation of clay microstructure. (Loret et *al.*, 2002)

Change of pore water chemistry can affect clays through a variety of adsorption/desorption, intercalation, and cationic exchange mechanisms. The main resulting deformation mechanisms are volume changes (contraction/expansion) (Di Maio, 1996; Barbour and Fredlund, 1989; Rao et *al.*, 2005, 2006, and 2007; Alonso et *al.*, 1998; Musso et *al.*, 2003, Musso and Romero, 2005; Castellanos et *al.*, 2006, 2008). Hueckel (1992b) and Loret et *al.* (2002), pointed out that, these changes result from changes in volume of a fraction of the external adsorbed and interlamelar water. Change

of pore water concentration has also an effect on shear strength (Di Maio, 1996; Gajo and loret, 2004, Yang and Barbour, 1992).

Barbour and Fredlund, (1989) stated that when clay is exposed to concentrated salt solution two processes take place, chemical consolidation and chemically induced consolidation. Chemical consolidation occurs due to the transfer of mass of water and salt from the pore space into the interlamelar space and/or external surface of cluster and vice versa. Chemically induced consolidation is due to the osmotic flow of water out of the sample that takes place in response to the chemical gradient.

For partially saturated expensive clay rich soils, the swelling potential and swelling rate reduce with increasing solute concentrations of the hydration fluid (e.g. Alwaji, 1999; Yong et *al.* 1992; Rao et *al.*, 2005, 2006, and 2007; Alonso et *al.*, 1998; Castellanos et *al.*, 2006, 2008; Pusch, 2001; Musso et *al.*, 2003, Musso and Romero 2005). These materials show a marked secondary behavior interpreted as a progressive hydration of the expensive microstructure (Figures 5.6 and 5.8). When the material is soaked with a saline solution, water and solute are driven into the macro pores because of the gradient of matric suction. Micropores are progressively hydrated but this is a long term process. Gradient in solute concentration will also generate an osmotic flow of water out of the sample. Solute concentration may also change through the macroporosity as a consequence of the diffusion of the salt from the external reservoir. As a consequence, clay clusters acting as a semi permeable membrane will loose water. In most of the studies where the hydro-mechanical behaviour of clay formation is addressed, local hydraulic equilibrium is assumed (e.g. Gens and Alonso, 1992; Sanchez et *al.,* 2005; Guimarães 2002). In an attempt to study coupled chemo-hydro-mechanical behaviour of clay soils, Ma and Hueckel (1992), Hueckel (1992a,b) and Loret et *al.* (2002) proposed to treat clays exposed to thermal and chemical paths as a two phase mixture, with absorbed water being a part of solid phase, and an interphase transfer to model its absorption and desorption process. Gajo et *al.* (2002), Guimarães (2002) and Gajo and Loret (2004), presented an extended formulation including the presence of several counter ions, by introduction of electrochemical potentials. Murad (1999) have addressed the transfer of water into interlamellar space in clays through a two- or three-spatial scale modeling using homogenization schemes.

In most of these studies the solute is assumed to exist at low concentration such that it does not influence the density and motion of the fluid. At present, little is done on studying the effect of high salt concentration and osmotic processes in double structure deformable porous media. In this work a macroscopic description of the system is provided. Then the basic equations describing coupled flows of water and solutes and the transport of its components through macropores and mass balance equations for water and solute in macro and micro pores are obtained. A relation is developed to describe the exchange of mass between the macropores and micropores. The effect of water and salt mass exchange between micropores and macropores on the deformation of the material is also addressed.

5.2 General framework and hypothesis

In this work, clay is considered as a three phase material. Each phase is composed of several species.

The three phases are:

- Solid phase;
- Liquid phase (l): dissolved salt in water, dissolved air;
- Gas phase (g): mixture of dry air and water vapor.

The four species are:

- Solid matrix : Clays platelets;
- Water (w): as liquid (free water and adsorbed or /and absorbed water) or evaporated in the gas phase;
- Salts (s): as dissolved salt in liquid phase
- Air (a): dry air as gas or dissolved in the liquid phase.

The macro pores are considered to be partially filled with the liquid phase. Here, gas is considered as separate phase. The macroscopic transport of liquid and its components takes places in macropores which are also called flowing pores. The clay clusters are assumed to be saturated under prevailing suctions since the inter-platelets distances are small and typically in the range of 10-100 A (e.g., Alonso, 1998; Romero et *al.* 1999;

Loret et *al.*, 2002). Adsorbed and absorbed water can transfer into free water or conversely depending on the pressure and chemical gradients existing between the micopores and the macropores.

The total volume of the medium can be decomposed into the volume occupied by the macropores, the micropores and the solid matrix, i.e. $V_t = V_{v_M} + V_{v_m} + V_s$. These volumes permit to define the macroporosity (ϕ_M) and the microporosity (ϕ'_m) with respect to the total volume of the medium as follows,

$$\phi_M = \frac{V_{v_M}}{V_t}; \qquad \phi'_m = \frac{V_{v_m}}{V_t} \tag{5.2}$$

where $\phi'_m = (1 - \phi_M)\phi_m;$

and ϕ_m is the volume of the micropores with respect to the volume of the clusters. The volumes V_t, V_{v_M} and V_{v_m} are respectively, the total volume, the volume of the macro voids and the volume of the micro voids.

Therefore, the total porosity is defined as,

$$\phi = \phi_M + \phi'_m \tag{5.3}$$

both with respect to the total volume of the soil.

In addition, the following assumptions are made:

- Temperature of the medium is constant
- The medium is constituted of a single soluble salt.
- Only chemical and hydraulic gradients are considered for the flow of water and solute.
- Binary diffusion of salt and water at high concentration is assumed.

Following Loret et *al.* (2002), it is assumed that the clusters of particles are surrounded by a semi permeable membrane allowing at various degrees the transfer of solutes.

5.3 Equations for Mass Balance

In this section, macroscopic mass balance equations are given for macropores as well as micropores species and the mass exchange between them is treated as source/sink for which and additional relation is provided.

5.3.1 Mass Balance equation of the macroscopic fluid and its components

The compositional approach (Olivella *et al.,* 1994) is followed to establish the mass balance equations. This approach consists of balancing the species rather than the phases. In case of writing the phase balance equations, non-advective fluxes of species inside the phase would cancel. Coupled fluxes induced by hydraulic or chemical gradient under isothermal condition will be considered.

5.3.1.1 Mass balance of water

Water is present in two phases. The total mass of water per unit volume of the porous medium under unsaturated conditions is $w_l^w \rho_l S_l \phi_M + w_g^w \rho_g S_g \phi_M$, where ρ_g and ρ_l are respectively the gas phase and the liquid phase densities and w_l^w and w_g^w are respectively the mass fraction of water in the liquid phase and gas phase. S_l and S_g are respectively the volumetric fraction of liquid and gas in the macro pores.

The mass balance of water is expressed as:

$$\frac{\partial}{\partial t}(w_l^w \rho_l S_l \phi_M + w_g^w \rho_g S_g \phi_M) + \nabla.(\mathbf{j}_l^w + \mathbf{j}_g^w) = -\Gamma^w \tag{5.4}$$

where Γ^w is the rate of local mass transfer of water from the micropores towards the macropores.

In Equation (5.4), $\mathbf{j}_l^{\ w}$ and $\mathbf{j}_g^{\ w}$ are respectively the total fluxes of water and vapour with respect to a fixed reference system.

$$\mathbf{j}_g^w = \mathbf{i}_g^w + w_g^w \rho_g \left(-\frac{\mathbf{k}k_{rg}}{\mu_g}\left(\nabla p_g + \rho_g g \nabla z\right)\right) + w_g^w \rho_g S_g \phi_M \frac{d\mathbf{u}}{dt} \tag{5.5}$$

where $\mathbf{i}_g^w$ is the diffusive flux of water vapour and is equal to:

$$\mathbf{i}_g^w = -D^{vap}\nabla w_g^w \tag{5.6}$$

Where D^{vap} is the molecular diffusion coefficient of vapour in the medium.

The total flux of water is defined as follows

$$\mathbf{j}_l^w = \mathbf{J}_l^w + w_l^w \rho_l \mathbf{J}_l + w_l^w \rho_l \phi_M S_l d\mathbf{u}/dt \tag{5.7}$$

where $\mathbf{J}_l$ and $\mathbf{J}_l^w$, the mass average flow of the fluid and the mass flow of water related to pressure and chemical gradients, are given by Equations (2.19) and (2.23).

The use of material derivative leads to

$$\left(w_l^w \rho_l S_l + w_g^w \rho_g S_g \right) \frac{D\phi_M}{Dt} + \phi_M \left(\frac{Dw_l^w \rho_l S_l}{Dt} + \frac{Dw_g^w \rho_g S_g}{Dt} \right) + \tag{5.8}$$
$$\left(w_l^w \rho_l S_l + w_g^w \rho_g S_g \right) \nabla.\left(d\mathbf{u}/dt \right) + \nabla.\left(\mathbf{j}_l^{'w} + \mathbf{j}_l^{'w} \right) = -\Gamma^w$$

5.3.1.2 Mass balance of solute

The solute mass balance is expressed as:

$$\frac{\partial}{\partial t}(w_l^s \rho_l S_l \phi_M) + \nabla.(\mathbf{j}_l^s) = -\Gamma^s \tag{5.9}$$

where Γ^s is the rate of local mass transfer of solute from the micropores towards the macropores.

The total flux of solute is expressed as:

$$\mathbf{j}_l^s = \mathbf{J}_l^s + w_l^s \rho_l \mathbf{J}_l + w_l^s \rho_l S_l \phi_M d\mathbf{u}/dt \tag{5.10}$$

where $\mathbf{J}_l^s$, the mass flow of solute related to pressure and chemical gradient, is given by equations (2.21.a, b).

The use of material derivative leads to

$$w_l^s \rho_l S_l \frac{D\phi_M}{Dt} + \phi_M \frac{Dw_l^s \rho_l S_l}{Dt} + w_l^s \rho_l S_l \phi_M \nabla.\left(d\mathbf{u}/dt \right) + \nabla.\left(\mathbf{j}_l^{'s} \right) = -\Gamma^s \tag{5.11}$$

5.3.1.3 Mass balance of solid matrix

The mass balance of the solid matrix is expressed as:

$$\frac{D\phi_M}{Dt} + \frac{D\phi_m^{'}}{Dt} = \left(1 - \phi\right) \nabla.(\frac{d\mathbf{u}}{dt}) + \frac{1}{\rho_s} \frac{D\rho_s}{Dt} \tag{5.12}$$

Where ρ_s is the density of the solid matrix and $d\mathbf{u}/dt$ is the velocity of the solid phase due to the deformation of the material.

We assume that the evolution of micro porosity (calculated with respect to the total volume of the medium) is defined as

$$\frac{D\phi'_m}{Dt} = \left(1 - \phi'_m\right)\frac{d\varepsilon_v^m}{dt}$$

(5.13)

where ε_v^m denotes the microstructural volumetric deformations.

Since macro porosity will be used for the calculation of several parameters, it is convenient to transform Equation (5.12) into its variation

$$\frac{D\phi_M}{Dt} = \left(1 - \phi_M\right)\nabla.(\frac{d\mathbf{u}}{dt}) + \frac{1}{\rho_s}\frac{D\rho_s}{Dt} - (\phi'_m\nabla.(\frac{d\mathbf{u}}{dt}) + \frac{D\phi'_m}{Dt})$$

(5.14)

This equation provides the evolution of the macro porosity induced by volumetric deformations caused either by mechanical, hydraulic or chemical changes. Obviously, contraction or expansion of the micropores induces decrease or increase of the macropores.

5.3.2 Mass balance equation of the fluid in the micropores and its components

Under geological repository condition, diffusion of contaminants through the clay host rock (dissolved salts) is expected. Accordingly, the concentration of salts associated with the macro pores and the micro pores are no longer in equilibrium. This difference implies the local transfer of water from the microstructure to the macrostructure. If the semi permeable membrane surrounding the clusters is not perfect or ideal (See definition in Chapter 2) transport of salt from the macrostructure to the microstructure will also be allowed. If the material is partially saturated, upon hydration a long term flow of water from the macrostructure to microstructure will occur. Therefore, transport of adsorbed and/or absorbed water and salt is idealized as mass transfer from the microstructure to the macrostructure and vice versa. Therefore Equations similar to (5.4) and (5.9) without advective and non advective terms, will be obtained.

For water it is expressed as:

$$\frac{\partial}{\partial t}(w_l^w \rho_l (1-\phi_M)\phi_m) = \Gamma^w \tag{5.15}$$

$$\frac{\partial}{\partial t}\left(w_l^w \rho_l \phi_m'\right) = \Gamma^w \qquad \Gamma^w = A_w \Delta w_l^s + B_w \Delta p$$

$$\Delta w_l^s = \left(w_l^s\right)^M - \left(w_l^s\right)^m \qquad \Delta p = p_M - p_m$$

And for the solute it is expressed as:

$$\frac{\partial}{\partial t}(w_l^s \rho_l (1-\phi_M)\phi_m) = \Gamma^s \qquad \Gamma^s = A_s \Delta w_l^s + B_s \Delta p \tag{5.16}$$

$$\Delta w_l^s = \left(w_l^s\right)^M - \left(w_l^s\right)^m \qquad \Delta p = p_M - p_m$$

The term $\Gamma^\alpha, \alpha = w, s$ in Equations (5.4), (5.9), (5.15) and (5.16) is the rate of exchange of mass between the flowing fluid in the macropores and the fluid in the micropores within an averaging volume. It includes the effect of diffusion of salt into the micropores, as well as transfer of water in response to a chemical or/and hydraulic gradients from the micropores to the macropores and vice versa.

The rate of transfer of adsorbed or/and interlamelar water or of solute per unit volume of porous medium and per unit time is defined through the following relation (Bear, 1991; Hassanizadeh, 1986a, 1988):

$$\Gamma^\alpha = \frac{1}{\partial V}\int_S \mathbf{j}_l'^\alpha . \mathbf{n} \, ds \, ; \, \alpha = w, s \tag{5.17}$$

where ∂V is a the averaging volume, S designates the union of interfacial areas between the micropores and the macropores which lie inside ∂V , $\mathbf{n}$ a vector normal to the interface pointing out of the micropores, ds in the infinitesimal element of area and $\mathbf{j}_l'^\alpha$ is the total flux of the component α in the liquid phase relative to the solid phase defined in terms of the microscopic quantities.

For water it is expressed as:

$$\mathbf{j}_l^{\prime w} = -\left[(\rho_l)_m \left(\frac{\beta}{\alpha} \sigma_m (w_l^s)_m + (w_l^w)_m \right) \frac{\alpha_s}{\mu_m} k_m \sigma_m + D_m (\rho_l)_m (1-\sigma_m)(1-\gamma)(w_l^w)_m \right] \nabla w_l^s +$$

$$-\left[-(\rho_l)_m \left(\frac{\beta}{\alpha} \sigma_m (w_l^s)_m + (w_l^w)_m \right) \frac{k_m}{\mu_m} \right] \nabla p = A_w \nabla w_l^s + B_w \nabla p; \qquad \alpha_s = \frac{RT(\rho_l)_m}{M_s} \qquad (5.18)$$

For solute it is expressed as:

$$(5.19)$$

$$\mathbf{j}_l^{\prime s} = -\left[-D_m (\rho_l)_m (1-\sigma_m)(1+\gamma(w_l^s)_m) + (1-\sigma_m)(w_l^s)_m (\rho_l)_m \frac{\alpha_s}{\mu_m} k_m \sigma_m \right] \nabla w_l^s +$$

$$-\left[-(1-\sigma_m)(\rho_l)_m (w_l^s)_m \frac{k_m}{\mu_m} \right] \nabla p = A_s \nabla w_l^s + B_s \nabla p; \quad \alpha_s = \frac{RT(\rho_l)_m}{M_s}$$

In these equations, the subscript m refers to microstructure, and

$$\gamma = \frac{1}{\rho_l} \frac{\partial \rho_l}{\partial w_l^s}, \quad \alpha = 1 + \frac{1}{\rho_l} \frac{\partial \rho_l}{\partial w_l^s} w_l^s = 1 + \gamma w_l^s, \quad \text{and} \quad \beta = 1 + \frac{1}{\rho_l} \frac{\partial \rho_l}{\partial w_l^w} w_l^w = 1 - \gamma w_l^w$$

Finally, σ_m is the osmotic efficiency coefficient for the microstructure, μ_m liquid viscosity in the microstructure and k_m and D_m are permeability and diffusion coefficient for the microstructure. The parameter D_m is dependent on the porosity of the microstructure.

Using Equations (5.18) and (5.19), Equation (5.17) becomes

$$\Gamma^w = \frac{1}{\partial V} \int_S A_w \nabla w_l^s . \mathbf{n} \ ds + \frac{1}{\partial V} \int_S B_w \nabla p . \mathbf{n} ds \qquad (5.20)$$

Within an averaging volume A_w and B_w are assumed constant and then the following equation is obtained:

$$\Gamma^w = A_w \frac{1}{\partial V} \int_S \frac{\partial w_l^s}{\partial n} \ ds + B_w \frac{1}{\partial V} \int_S \frac{\partial p}{\partial n} \ ds \qquad (5.21)$$

where $\partial / \partial n$ denotes the derivative in the direction normal to the micropore-macropore interface (pointing out of the micropores).

The integral on this Equation may be represented by the following relation

$$\int_S \frac{\partial w_l^s}{\partial n} = \frac{S}{l}\left[\left(w_l^s\right)_M - \left(w_l^s\right)_m\right]$$

(5.22)

$$\int_S \frac{\partial p}{\partial n} = \frac{S}{l}\left[p_M - p_m\right]$$

where l is a microscopic characteristic length over which changes in microposcopic solute concentration occur, $\left(w_l^s\right)_M$ and $\left(w_l^s\right)_m$ are respectively the solute mass fraction in the liquid phase occupying the macropores and the micropores. Therefore, Equation (5.21) becomes

$$\Gamma^w = A_w \frac{1}{\partial V}\frac{S}{l}\left[\left(w_l^s\right)_M - \left(w_l^s\right)_m\right] + B_w \frac{1}{\partial V}\frac{S}{l}\left[p_M - p_m\right]$$

(5.23)

The ratio $\dfrac{S}{l\partial V} = \xi$ is a geometrical parameter that may depend on several variables, among them the specific surface of the micropores and the size and geometry of the micro and macropores. This geometrical parameter is kept separated from the permeability, diffusivity coefficients so the physical meaning and range and units of these parameters are maintained.

The rate of transfer of adsorbed or/and interlamelar water becomes

$$\Gamma^w = A'_w\left[\left(w_l^s\right)_M - \left(w_l^s\right)_m\right] + B'_w\left[p_M - p_m\right]$$

(5.24)

$$A'_w = \xi A_w \quad \text{and } B'_w = \xi B_w$$

Following the same methodology, the rate of local mass transfer of solute is expressed as follows:

$$\Gamma^w = A'_s\left[\left(w_l^s\right)_M - \left(w_l^s\right)_m\right] + B'_s\left[p_M - p_m\right]$$

(5.25)

$$A'_s = \xi A_s \quad \text{and } B'_s = \xi B_s$$

As described above, we consider that both solute and water in the microstructure can be transported by hydraulic and chemical gradients. This general case can be simplified assuming local hydraulic equilibrium. This means that capillary suction associated with the macrostructure and the microstructure are in equilibrium. The local mass transfer in this case is only induced by a chemical gradient.

In summary the rate of local mass transfer of water and solute are written as follows

$$\Gamma^w = -\xi\left[\rho_l\left(\frac{\beta}{\alpha}\sigma_m\left(w_l^s\right)_m + \left(w_l^w\right)_m\right)\frac{\alpha_s}{\mu_m}k_m\sigma_m + D_m\rho_l\left(1-\sigma_m\right)\left(1-\gamma\right)\left(w_l^w\right)_m\right]\Delta w_l^s + \tag{5.26}$$

$$-\xi\left[-\rho_l\left(\frac{\beta}{\alpha}\sigma_m\left(w_l^s\right)_m + \left(w_l^w\right)_m\right)\frac{k_m}{\mu_m}\right]\Delta p = A'_w\,\Delta w_l^s + B'_w\,\Delta p$$

$$\Gamma^s = -\xi\left[-D_m\rho_l(1-\sigma_m)(1+\gamma\left(w_l^s\right)_m) + (1-\sigma_m)\left(w_l^s\right)_m\rho_l\frac{\alpha}{\mu_m}k_m\sigma_m\right]\Delta w_l^s + \tag{5.27}$$

$$-\xi\left[-(1-\sigma_m)\rho_l\left(w_l^s\right)_m\frac{k_m}{\mu_m}\right]\Delta p = A'_s\,\Delta w_l^s + B'_s\,\Delta p$$

The transfer coefficients A'_w, B'_w, A'_s and B'_s depend on a number of parameters among these are microstructural osmotic efficiency coefficient σ_m, diffusion coefficient D_m in the micropores, and permeability of the microstructure k_m.

It is interesting to note here, that for this formulation two distinct osmotic efficiency coefficients are considered, one for the microstructure and another one for the macrostructure. As mentioned in Section 1, the osmotic efficiency coefficient is dependent on several parameters, among these are, porosity, solute concentration and the type of clay. In fact, if we make the hypothesis that osmotic efficiency is only dependent on porosity, obviously the solutes penetrate into the macropores easier than into the micropores. In this case, the osmotic efficiency coefficient for the macrostructure should be lower than osmotic efficiency for the microstructure. Therefore considering different osmotic efficiency for the microstructure and the macrostructure is a reasonable assumption given the different characteristics of the two structural levels.

5.3.3 Equations of state

Equations of mass balance and motion have to be completed by equations establishing the link between the sate variables (unknowns) and the dependent variables. It is assumed that liquid density is a function of pressure, and temperature. The Effect of temperature on liquid density is disregarded.

The equation of state is given by

$$\rho_l = \rho_{l0} \exp\left(\gamma w_l^s + \beta(p_l - p_0)\right) \tag{5.28}$$

where ρ_{l0} is the mass density of pure water at the reference pressure p_0, and γ [−] and β [MPa^{-1}] are temperature dependent parameters taken equal to (Handbook of chemistry and physics, 1982):

$$\gamma = 0.6923; \quad \beta = 4.5 10^{-4} \, \text{MPa}^{-1} \tag{5.29}$$

Dependence of dynamic viscosity of salt mass fraction at a constant temperature is described by (Lever and Jackson, 1985 ,After Hassanizadeh,1988)

$$\mu = \mu_0 \left(1 + 1.85 w_l^s - 4.1 \left(w_l^s\right)^2 + 44.5 \left(w_l^s\right)^3\right) \tag{5.30}$$

where μ_0 (MPa.s) is viscosity for pure water.

The retention curve adopted for the Macrostructure is the classical expression proposed by Van Genuchten (1980)

$$\left(S_e\right)_M = \left(\frac{S_l - S_{rl}}{S_{ls} - S_{rl}}\right)_M = \left(1 + \left(\frac{s_M}{P}\right)^{\frac{1}{1-\lambda}}\right)^{-\lambda} \; ; \; P = P_o \frac{\sigma}{\sigma_o} \tag{5.31}$$

where λ, P, σ_0, P_0 are material parameters and σ is surface tension parameter.

For the microstructure a simple exponential law is adopted

$$\left(S_e\right)_m = \exp\left(\frac{s_m^\beta}{p_a}\right) \tag{5.32}$$

where β and p_a are material parameters.

5.4 Numerical implementation in a THM Code

The formulation described above contains several processes which have to be implemented in the program CODE_BRIGHT which is a simulator for COupled, DEformation, BRIne, Gas and Heat Transport problems. The first contributions implemented in the code have been the implementation of the Balance equation including osmotically driven transport of water and salt in deformable porous media detailed in Chapter 2.

The upgrades included the following:

- Activity and osmotic pressure, variation of relative humidity by the presence of solutes
- Osmotic fluxes, both for water and solute, including binary diffusion as the concentrations are expected to be high
- Ultrafiltration term, this is the symmetric term for osmosis within the Onsager matrix
- Osmotic efficiency as a function of porosity, this is a function that is qualitative at this level of development
- Rate equation for dissolution and precipitation
- Balance of crystal equation which permits to track the amount of crystals at any point.

For the formulation presented in this Chapter the main upgrades are, the implementation of the mass transfer terms of water and solute and update of porosity equation.

For the water and solute transfer terms, liquid pressure p_m and solute mass fraction $\left(w_l^s\right)_m$ for the microstructure were defined for each finite elements as history variables. $\left(w_l^s\right)_m$ and p_m, are integrated implicitly at an intermediate time ($t^{k+\varepsilon}$) between t^k and t^{k+1} times. The transfer coefficients A'_w, B'_w, A'_s and B'_s were then calculated at time $t^{k+\varepsilon}$.

Spatial and temporal discretization of Equations (5.15) and (5.16) gives the following:

$$r_w\left(\left(w_l^s\right)_m^{k+1}, p_m^{k+1}\right) = \frac{d_w^{k+1} - d_w^k}{\Delta t^k} - A'^{k+\varepsilon}_w\left[\left(w_l^s\right)_M^{k+1} - \left(w_l^s\right)_m^{k+1}\right] + B'^{k+\varepsilon}_w\left[p_M^{k+1} - p_m^{k+1}\right] \qquad (5.33)$$

$$r_s\left(\left(w_l^s\right)_m^{k+1}, p_m^{k+1}\right) = \frac{d_s^{k+1} - d_s^k}{\Delta t^k} - A'^{k+\varepsilon}_s\left[\left(w_l^s\right)_M^{k+1} - \left(w_l^s\right)_m^{k+1}\right] + B'^{k+\varepsilon}_s\left[p_M^{k+1} - p_m^{k+1}\right]$$

where r_α (α= w,s) are the residuals, d_α are the accumulation terms and k is the time step index.

Since the problem presented here is non linear, the Newton-Raphson method has been adopted to find an iterative scheme. For each Newton-Raphson iteration, the

accumulation terms are calculated and used for the calculation of the residual equations and residual derivatives. Finally $\left(w_l^s\right)_m$ and p_m are deduced using corrections, and Γ^w and Γ^s calculated. The balance equations of water and solute are updated in consequence. The residual terms are finally modified to incorporate Γ^w and Γ^s.

For these equations, computation of the micro porosity is integrated explicitly, that is, the values at t^k are used. Micro porosity changes are computed in every element .The variation of micro porosity is deduced from the mechanical model. In fact, it is assumed to be equal to volumetric microstructural deformations as defined in Section 5.5 (Equation 5.36).

5.5 Numerical experiments: Analysis of swelling driven by osmotic effects in double structure clay soils

A great number of experimental studies dealing with the chemical effects on the swelling behaviour of clayey soils are available in the literature. Rao and Shivananda, (2005) studied the influence of salt addition on the swelling potential of expensive clay soils. Two electrolyte solutions (NaCl, CaCl$_2$) were added to the clay soil to prepare specimens with variable initial osmotic suctions. The samples were then inundated with deionised water and allowed to swell. The specimens absorbed water in response to matric suction and because of the osmotic flow in response to the chemical concentration gradient. The authors concluded that only the rate of swelling is affected by the initial pore fluid osmotic suction. The swelling potentials of specimens are independent of the initial pore fluid osmotic suction.

Rao et *al.* (2006) studied the impact of salt diffusion on the swelling behavior of compacted expensive clays. A series of oedometer swelling tests were performed on compacted clay specimens (γ_d=1.42 Mg/m^3, w= 28%). The samples were inundated with distilled water or with sodium chloride solution with different initial salt concentrations. Higher swelling has been observed for samples in contact of distilled water (Figure 5.6). The authors concluded that two competitive processes develop. The samples swell due to the inward flow of salt solution or distilled water in order to dissipate the initial matric suction of the compacted specimens. Initial difference in

osmotic pressure dissipates through outflow of soil water and diffusion of salt molecules, which induces the compression of the clay. The authors observed that the compacted clay samples swell on inundation with NaCl solution which implies that capillary effects dominate the osmotically induced compression.
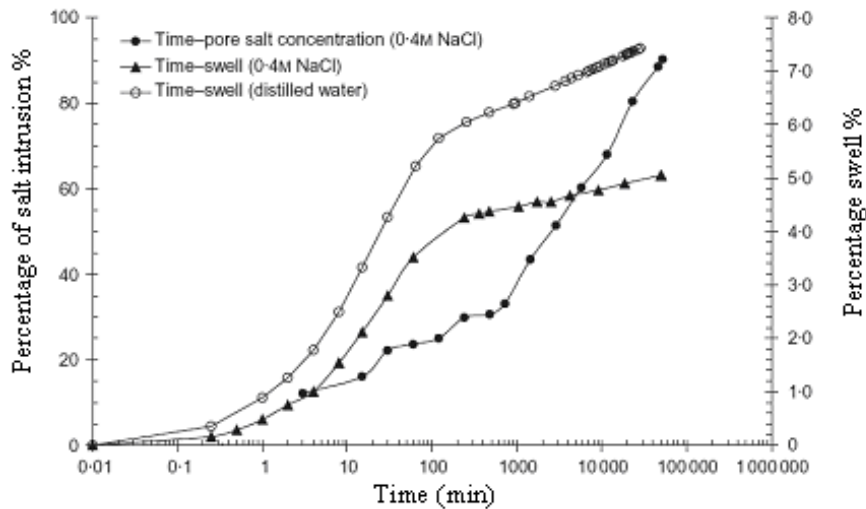
**Figure 5.6: Variation of percentage swelling with time
for specimens inundated with distilled water and 0.4 M NaCl solution
(Rao et *al.*, 2006)**

Alonso (1998) performed oedometer swelling tests on samples of Boom Clay (γ_d =1.4 kg/m^3, w= 15%) using an organic compound (PEG) at various concentration. As for Rao et *al.* (2006), Alonso (1998) concluded that solute concentration definitely controls the rate of swelling (Figure 5.7).
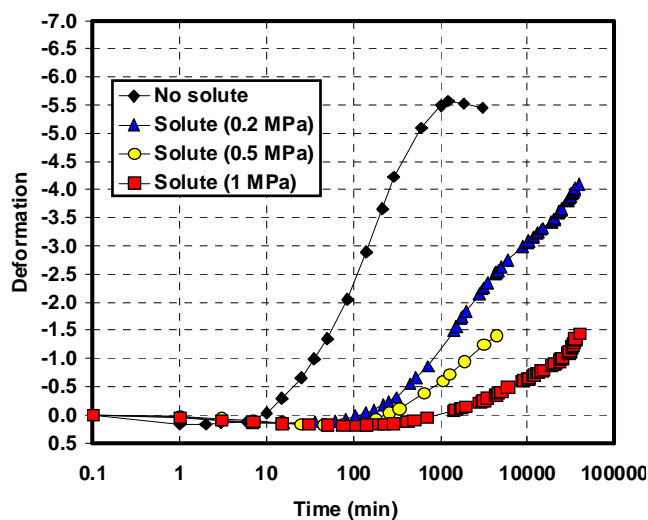
**Figure 5.7: Swelling strains measured in oedometer
tests for different concentrations of PEG20000 solute in the soaking water
(Alonso, 1998)**

Alwaji (1999) has shown that the swelling potential and swelling rate of two types of sand bentonite mixtures prepared with $NaNO_3$ or $Ca(NO_3)$ solution decrease with the increase of chemical concentration. Yong et *al.* (1992) also investigated the effect of salt concentration on swelling pressure of a sodium montomorillonite. They observed that the lower the salt concentration, the higher the measured swelling pressure. Pusch (2001) investigated the influence of different NaCl and $CaCl_2$ concentrations on swelling pressure of highly compacted active clay. The swelling pressure was sensitive to the salt concentration but it was not very different from those measured with distilled water.

Musso et *al.* (2003) and Musso and Romero (2005) studied the effect of chemical paths on the swelling behaviour of bentonite. The researchers showed that in samples prepared starting from slurries, chemical swelling evolves with time in a continuous manner, while swelling in compacted samples is discontinuous (Figure 5.8). The authors attributed these results to the existence of a double structure in the compacted samples, with swelling controlled by a delayed chemical equilibrium in smaller pores.
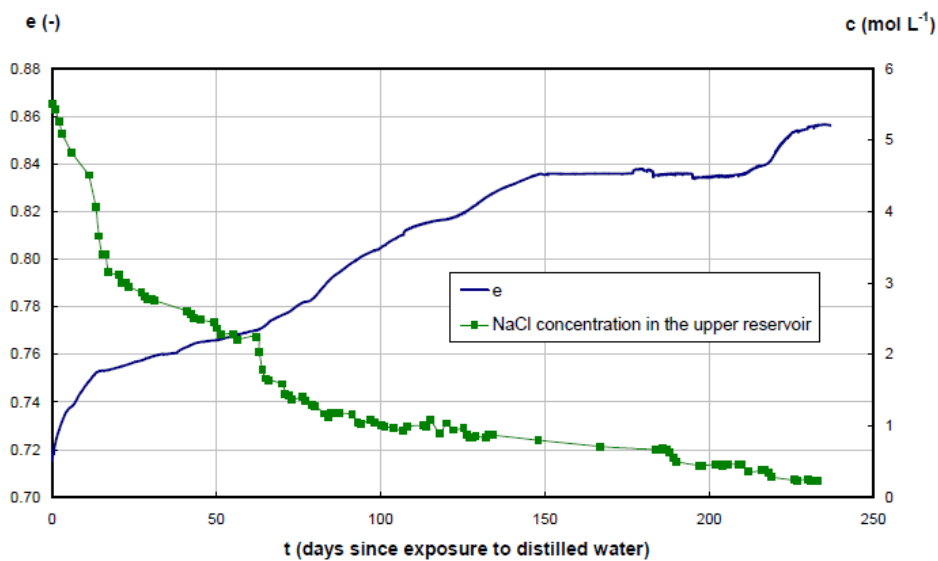

**Figure 5.8: Swelling and NaCl breakthrough during desalination path.
(Musso and Romero 2005)**

The effect of salt solution in the expansion of clay soils have been always attributed to the effect of the DDL. A number of researchers (Barbour and Fredlund, 1989; Mitchell 1993; Barbour and Yang, 1993) have demonstrated that the behavior of clay particles is

strongly influenced by long range stresses $(R - A)$. The long-range attractive stress (A) between clay particles is due to Van der Walls stresses. The long-range repulsive stress (R) between clay particles is due to electrostatic repulsion between the negatively charged clay surfaces. The difference between these two long-range stresses is termed the net long range repulsive stress $(R - A)$. Barbour and Fredlund (1989) have suggested that the influence of $(R - A)$ on the osmotic volume change of the soil could be considered by introducing this value to obtain the true effective stress, σ^*:

$$\sigma^* = \sigma' - (R - A) \tag{5.34}$$

where $\sigma' = \sigma - u_w$ is the effective stress; σ is the total stress and u_w is the pore fluid pressure. The two stress variables are visualized as a single stress variable and changes in $(R - A)$ are considered to be effective as σ' in producing behavioral changes in he soil. However, a problem arises here, related to difficulty to measure directly $(R - A)$.

An increase of the concentration of pore fluid induces the contraction of the double layer and the decrease in the net repulsive stress. This leads to true effective stress increases causing contraction of the aggregates and shrinkage of the sample. When clay soils are mixed with solute solution and then exposed to fresh or dilute salt solution, diffusive double layers develop around each particle resulting in an increase of the physicochemical stresses $(R - A)$ within the soil aggregates. In this case σ^* decrease induces the swelling of the clay soil.

Schmitz et *al.* (2006), Ma and Hueckel (1992), Hueckel (1992a, b) and Guimaraes (2002) discussed the extent at which the DDL theory can describe chemically induced changes in compacted clays. They reported that in the case of highly compacted clays, (as used for radioactive waste repositories), the effect of the DDL is limited because the particles are compacted and are too close together for the DDL to form correctly. Therefore, the influence of the DDL is smaller than at lower stress levels when the soil is more slurry like.

Following Alonso and Gens (1992), the mean effective stress for the microstructure is defined as:

$$p^* = p + \chi s_m \tag{5.35}$$

where p is the net mean stress, s_m is the microstructural matric suction and χ is a constant ($\chi > 0$). For a given initial effective stress paths for with $p^*>0$ leads to microstructural compression and paths for which $p^* < 0$ lead to microstructural expansion. The deformation arising from the microstructure phenomena can be considered elastic and volumetric (Gens and Alonso, 1992, Alonso 1998, Sanchez et *al.*, 2005, Guimaraes 2002).

Assuming independent effect of matric suction and concentration, the increment of microstructural elastic deformation can be expressed as:

$$d\varepsilon_v^{\;m} = \frac{dp}{K_m} + \chi \frac{ds_m}{K_m} + \frac{d\pi}{K_{mc}} \qquad K_m = \frac{(1+e_m)}{\kappa_m} p^* \qquad K_{mc} = \frac{(1+e_m)}{\kappa_{mc}} \pi \tag{5.36}$$
$$p^* = p + \chi s_m$$

where K_m is a microstructural bulk modulus, κ_m a material parameter, K_{mc} is a microstructural modulus for changes in osmotic suction, and κ_{mc} a material parameter. The subscript m refers to the microstructural level; the subscript v refers to volumetric component. The term proportional to osmotic suction has been introduced but it is not necessary to simulate swelling by semi-permeable membrane effects. Actually, when the coupled fluxes are incorporated, the osmotic pressure develops in a medium simply increasing the water pressure and therefore it is not necessary to write it explicitly.

A macrostructural elastic component for unsaturated conditions is also defined, for changes in net stress and matric suction (Alonso et *al.*, 1990, Gens and Alonso, 1992 Sanchez et *al.*, 2005, Guimaraes 2002):

$$d\varepsilon^M = \frac{dp}{K_M} + \frac{ds_M}{K_s}; \quad K_M = \frac{1+e_M}{\kappa} p; \quad K_s = \frac{1+e_M}{\kappa_s} s_M \tag{5.37}$$

K_M is macrostructural bulk modulus for changes in mean net stress (p) and K_s the macrostructural bulk modulus for changes in macrostructural matric suction (s_M). κ and κ_s are material parameters.

Model description

In order to explore the model ability to reproduce swelling in double structure clay soils, a numerical simulation has been carried out. The numerical examples concern a simulation of free swelling tests. The objective here is to reproduce qualitatively the above described results (Figures 5.6, 5.7 and 5.8). The tested material is assumed to have an initial macro porosity ϕ_M= 0.5 and initial microposority ϕ_m=0.25. The Samples are assumed to be initially partially saturated with distilled water (s_M=3 MPa). Initially the conditions of local hydraulic and chemical equilibrium are considered between the macro and the micro structures so that, s_M=s_m=3 MPa and c_M=c_m=0.

Four tests are modelled in which the sample is inundated with distilled water, 0.8 M, 2M, and 4M Sodium Nitrate solution. The tests were simulated under free swelling conditions. Along the vertical boundaries of the domain, horizontal displacement is restricted to represent the oedometric condition. Along the lower boundary of the domain, liquid pressure is kept at p=0 MPa while the concentration of the contact fluid is varied. The above described mechanical elastic model has been used to model the mechanical behaviour of the material. Material properties are summarized in Table 5.1, and correspond to values within the appropriate range for each variable.

Effect of matric suction

Figure 5.9 plots axial deformation with time for the case of a sample inundated with fresh water (c=0M) under oedometric conditions. Therefore, no gradient of osmotic suction exists between the sample and the external reservoir. The plot shows, that the inward flow of water in response to the matric suction promotes swelling of the expensive material. The time-swelling plot falls into three regions: a small initial swelling, followed by a large primary swelling and a small secondary swelling.

Table 5.1. Material properties

Parameters (Initial values)	Symbols	Values
Micro porosity	ϕ'_m	0.25
Macro Porosity	ϕ_M	0.5
Intrinsic permeability for Micro	$k_m \, (\text{m}^2)$	10^{-18}
Intrinsic permeability for Macro	$k_M \, (\text{m}^2)$	10^{-17}
Efficiency coefficient for Micro	$\sigma_m \, (*)$	0.95
Efficiency coefficient for Macro	σ_M	0.2
Retention curve for micro	P_o	10^4
	b	0.7
Retention curve for Macro	$P_o \, (\text{MPa})$	0.5
	λ	0.3
	S_{rl}	0
	S_{ls}	1
Geometrical parameter	$\xi \, (\text{m}^{-2})$	100
Elastic model for Macro	ν	0.3
	$a_1 = -\kappa/(1+e_M)$	-0.02
	$a_2 = -\kappa_s/(1+e_M)$	-0.014
Elastic model for Micro (for capillary and osmotic effects)	$a_m = -\kappa_m/(1+e_m)$	-0.028

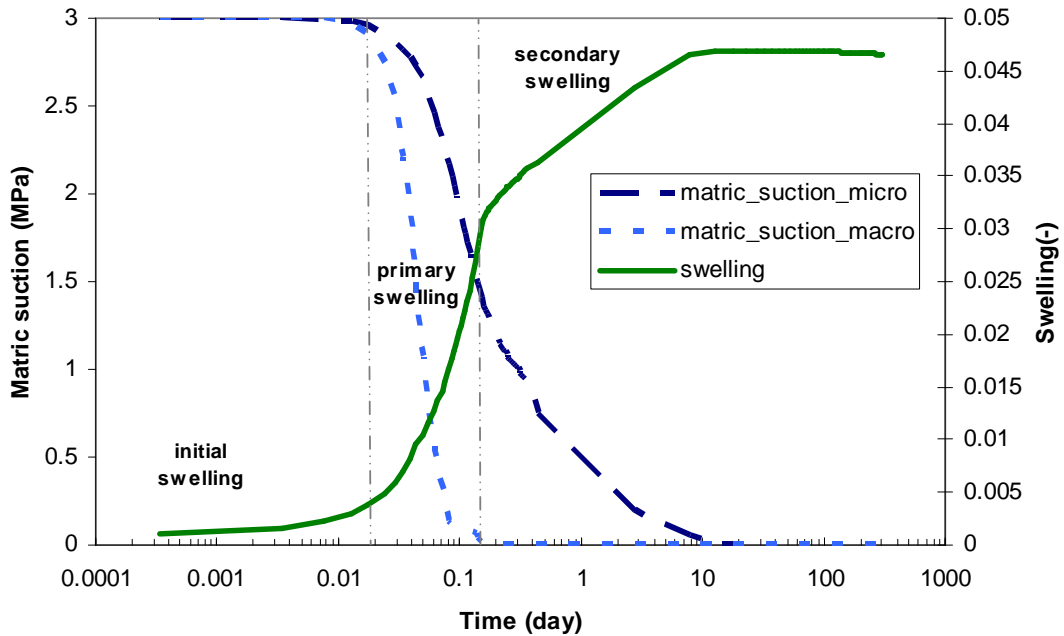(*) for some cases σ_m is equal to 1.

Figure 5.9. Evolution of swelling deformation and matric suction in the macro and micro structures with time for the case of a sample inundated with fresh water (c=0M)

Figure 5.9 also includes the evolution of matric suction in both structural levels. Upon hydration, suction associated with the macrostructure and microstructure, are no longer in equilibrium. This implies the local transfer of water from macrostructure to microstructure. The plots show that the local transfer of water is relatively fast. Visible microstructural deformations develop at an earlier date; local transfer of water is rapid and primary swelling results of an overlapped macrostructural and microstructural swelling deformations. Complete dissipation of matric suction into the macrostructure coincides with the end of primary swelling. Secondary swelling is related to further hydration of the clay microstructure. It attains equilibrium when there is stabilization of matric suction within the microstructure.

For this case, since no solute is present, Equations (5.26) and (5.27) become

$$\Gamma^w = B'_w \Delta p \tag{5.33}$$

$$B'_w = \xi \rho_l \frac{k_m}{\mu_m}$$

$$\Gamma^s = 0$$

The rate of mass transfer of water is dependent on the value of the parameter B'_w which is mainly influenced by the value of the parameter k_m.

Figure 5.10, shows the evolution of swelling deformation when different values of k_m are considered. If k_m is set to zero the microstructure is not activated. Only macrostructural deformations are computed, that is, primary swelling is induced by dissipation of macrostructural matric suction. This case is illustrated in Figure 5.11.a. In a log(t) scale, a typical s-shape curve describes the development of total vertical deformations. If a low value of k_m is set (Figure 5.11.b), a reduced local water transfer is allowed and the primary swelling is controlled by the primary macrostructural mechanisms. However, beyond a certain time, microstructural deformation becomes significant induced by the progressive hydration of the microstructure resulting in a slow secondary swelling (Figure 5.11.b).
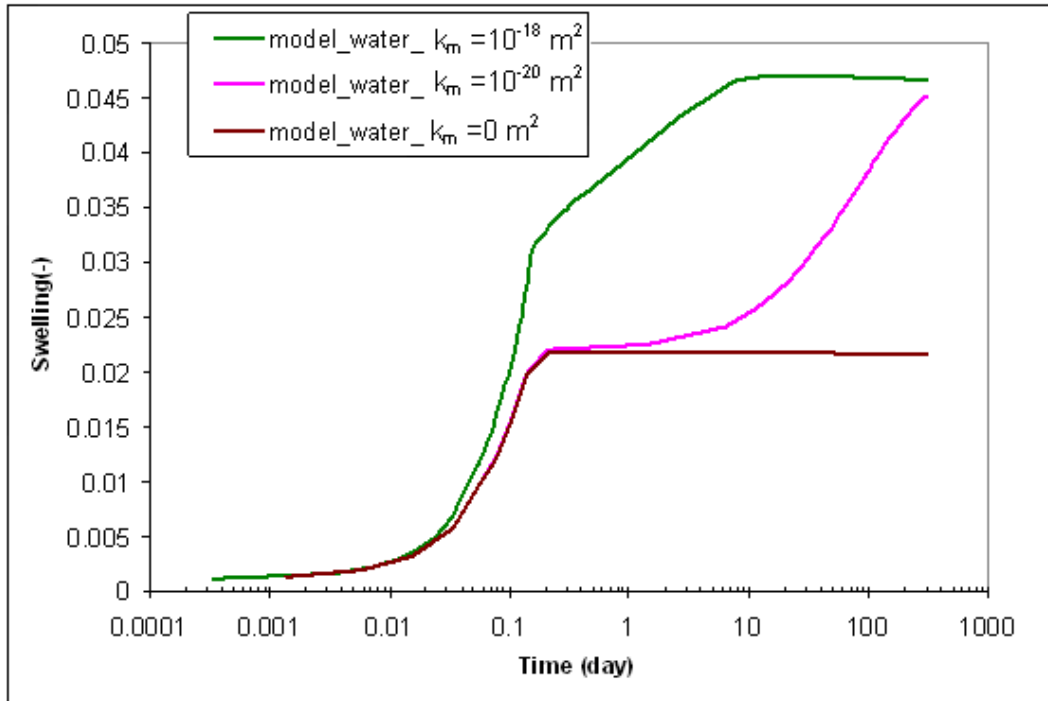
Figure 5.10. Evolution of swelling deformation with time for the case of a sample inundated with fresh water (c=0M). Effect of variation of the value of the parameter k_m

Effect of matric and osmotic suction

The swelling-time plots in Figure 5.12 (a, b) show the effect of solute concentration on swelling of expensive clays. Two cases have been considered. For the fist one an ideal semi permeable membrane is assumed to surround the clay clusters (σ_m=1) (Figure 5.12.b). For the second case it was assumed that a non ideal membrane is surrounding the clay clusters ($0<\sigma_m<1$) (Figure 5.12.a). For both cases the macro efficiency coefficient was kept constant and equal to (σ_M= 0.2). The plots show that pore water solute concentration controls the rate of swelling and swelling potential of the material.

The curves in Figure 5.12 may be compared with the experimental curves in Figures (5.6, 5.7 and 5.8). No attempt is made here to reproduce precisely the different experimental curves by adjusting the relevant parameters but the model is flexible enough to reproduce the observed swelling behaviour in time.
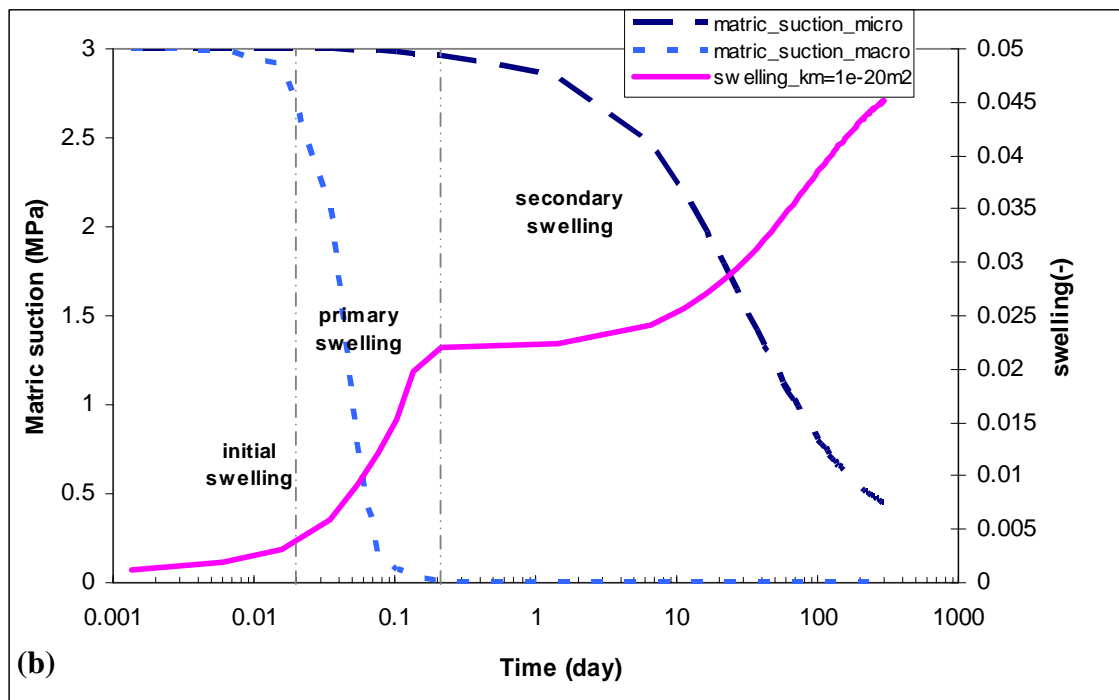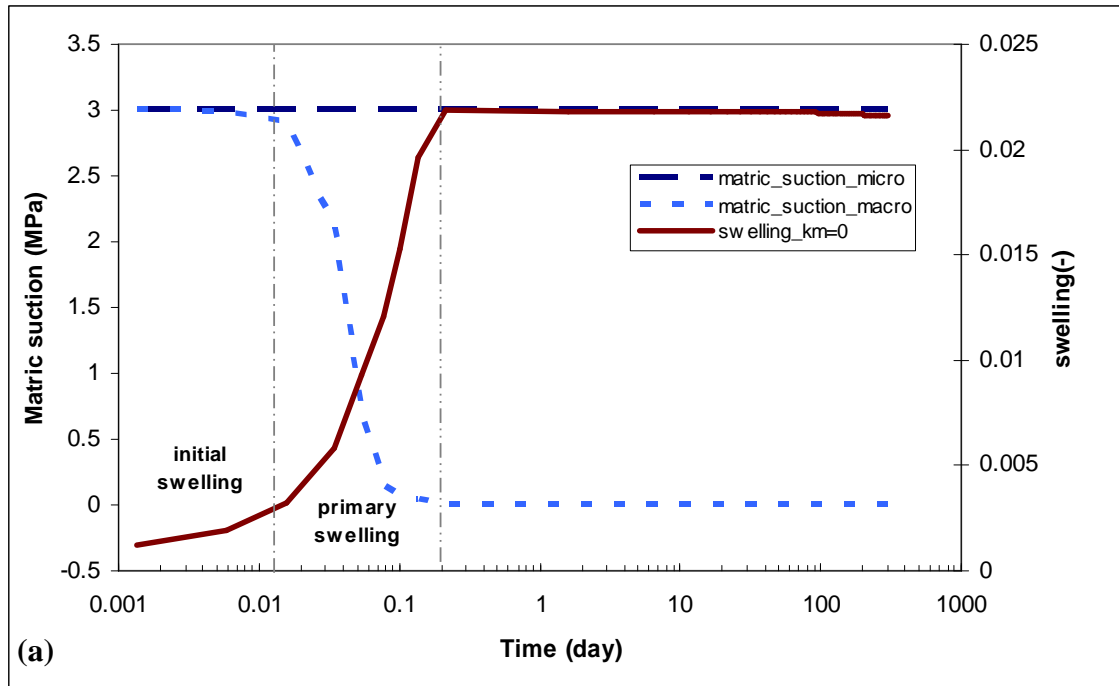
Figure 5.11. Evolution of swelling deformation and matric suction in the macro and micro structures with time for the case of a sample inundated with fresh water (c=0). (a) Case of k_m=0. (b) Case of $k_m=10^{-20}$ m^2

Initially, the dissolved salt concentration in the soil water (c=0M) is much smaller than the concentration of 0.8 M to 4M of the external reservoir. As a result initial osmotic suction differences of 0.4 MPa to 11 MPa are induced between soil water and the reservoir solution on inundation of the expensive clay with these $NaNO_3$ solutions. Water and solute are driven by advection and diffusion into the soil macropores because of the gradient of osmotic and matric suctions existing between the water filling partially the soil macropores and the external reservoir. As a consequence macrostructural matric suction dissipates and pore water concentration increases. Gradient in solute concentration will also generate an osmotic flow of water out of the sample. The outflow of soil water decreases the liquid pressure, increases the effective stress and compresses the clay (Chemically induced consolidation). In contrast the inflow of water and solute promotes the swelling of the material. Figure 5.12.a shows that the time-swell plot falls into three regions: a small initial swelling, followed by a large primary swelling, then a small secondary swelling followed by a small tertiary swelling. These regions are shown in details in Figure 5.13 for the case of c=0.8M. Interestingly there is no tertiary swelling for the case where the osmotic efficiency for the microstructure is equal to 1 (ideal semi permeable membrane surrounding the clay clusters) (Figure 5.12.b). For the case of high concentration, some compression is observed which can be explained by the water in the microstructure attracted by the prevailing macroscopic osmotic suction.

Figure 5.13.a shows the evolution of swelling with time together with the matric suction evolution in the two structure levels for the case of c=0.8M. as for the previous case (c=0M), local transfer of water is instantaneous and primary swelling results of an overlapped macrostructural and microstructural swelling deformation induced by dissipation of matric suction in the two structural levels.
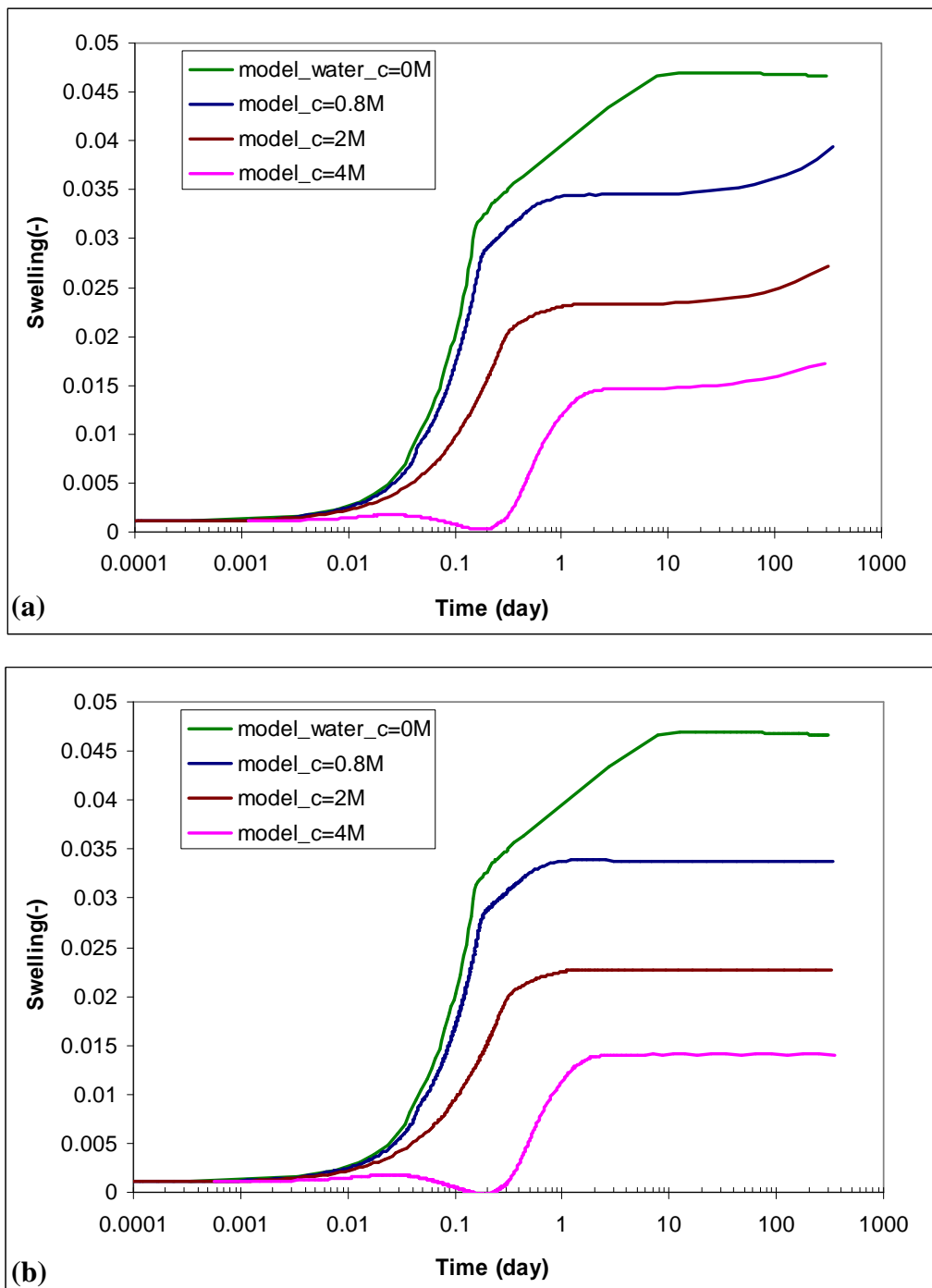
Figure 5.12. Evolution of swelling deformation with time for different concentrations of NaNO₃ solution in the reservoir water.(a) case of σ_m=0.95. (b) case of σ_m =1

Several types of phenomena develop inside the clay sample. Water and solute is driven into the soil macropores because of the gradient of matric suction existing between the water filling partially the soil macropores and the external reservoir. Gradient of osmotic suction will also drive water out of the sample. Solute concentration increases through the macro porosity as the passage of the solute is allowed due to the low value of the macro osmotic efficiency coefficient (σ_M= 0.2) (Figures 5.13.b and 5.13.c).

Figure 5.13. Case of c=0.8M and σ_m =0.95. (a) Swelling and evolution of matric suction in the macro and micro structures. (b) Swelling and evolution of solute mass fraction in macro and microstructures. (c) Evolution of matric suction together with the solute mass fraction in macro and microstructures.
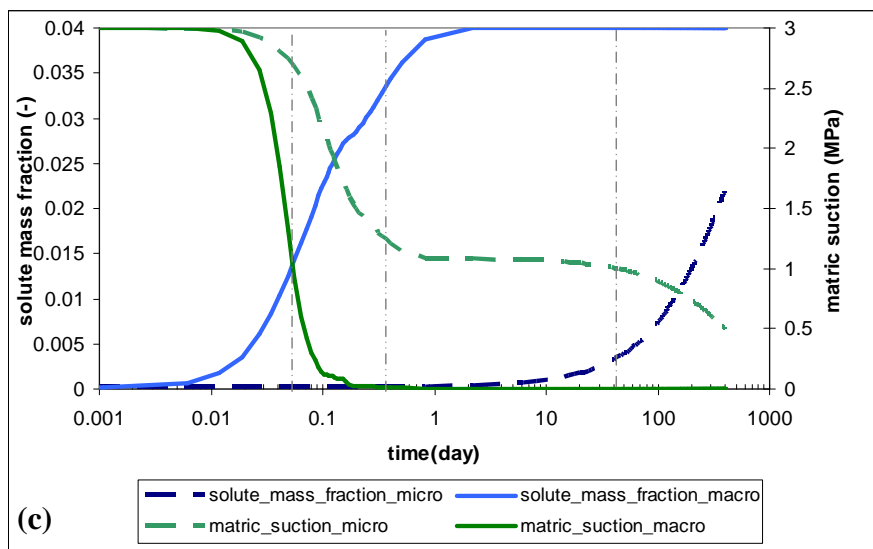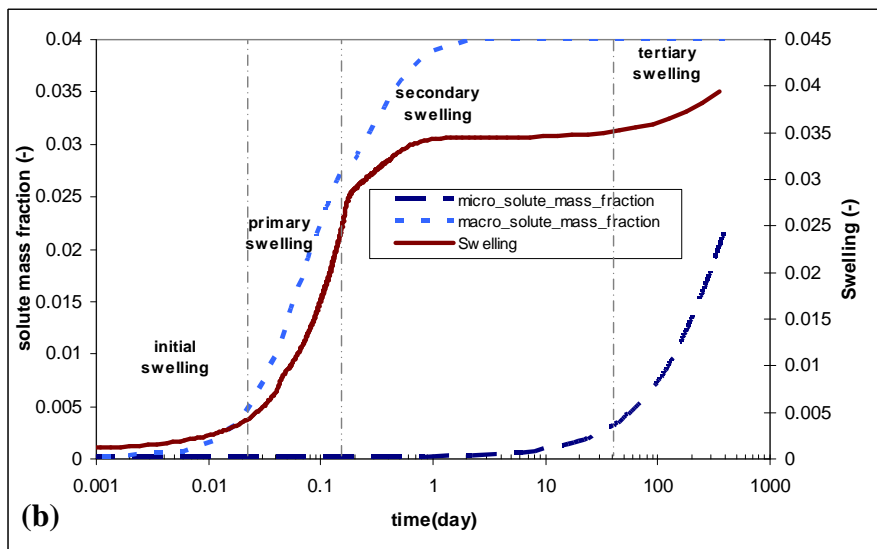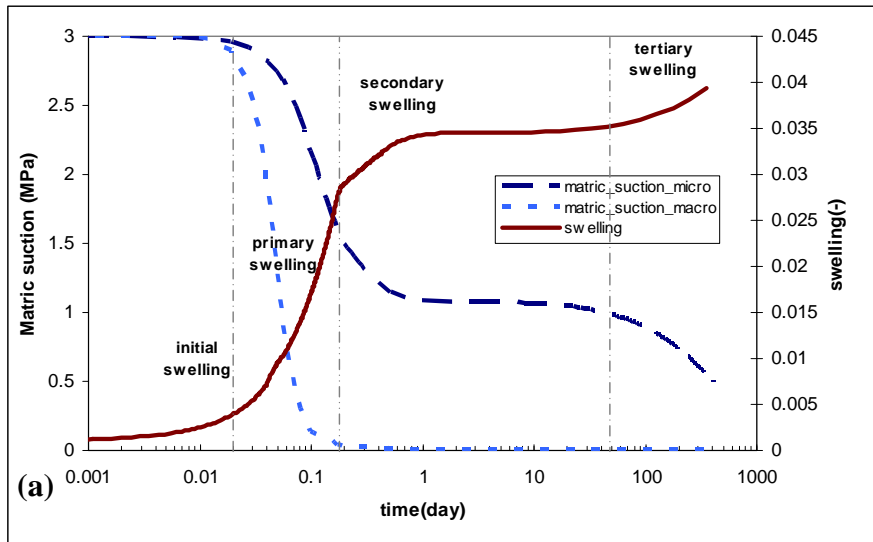
133

Osmotic and hydraulic gradients exist between the macropores and the micropores and the latter will gain or loose water in consequence. The osmotic gradient contributes to the transfer of water out of the micropores. If the hydraulic gradient is higher micropores will gain water and the prevailing matric suction decreases (Figure 5.13.a and 5.13.c). Because it is assumed that the clay clusters are surrounded by a non ideal semi permeable membrane, solute concentration also increases into the micropores but this is a slow process given the low value of the diffusion coefficient micro and of the high value of the osmotic efficiency coefficient (σ_m=0.95) (Figures 5.13.b and 5.13.c). Hydration of the microstructure will continue until reaching a situation of a temporary equilibrium since there is almost as much gain as loss of water from the microstructure due to the combined effects of the osmotic and hydraulic gradient. When the concentration into the micropores increases the osmotic gradient reduces allowing further hydration of the microstructure (tertiary swelling) (Figures 5.13.a and 5.13.b).

Based on these observations, it is inferred that primary swelling develops relatively rapidly, as it is linked to the rate of matric suction dissipation in the two structural levels. The assumed macroscopic permeability is relatively high, as macroscopic matric suction completely dissipates, secondary swelling develops and it is induced by further dissipation of microstructural matric suction. Tertiary swelling develops more slowly, because it is controlled by the transfer of solute and water into the microstructure.

Figure 5.14.a shows the evolution of swelling with time together with the evolution of matric suction and solute mass fraction in the two structural levels for the case of c=4 M. As for the previous cases water and solute are driven into the material by diffusion and advection to dissipate the gradient of matric suction. However, in this case after a very low initial swelling, the material shows a small compression. In fact, the high increase of solute concentration into the macropores leads to higher osmotic gradient in comparison to the hydraulic gradient which induces desorption of water from the micropores, so that microstructural matric suction increases initially. Accordingly the microstructural mean stress increases (Equation (5.30)) inducing some compression of the microstructure. Simultaneously dissipation of macrostructural matric suction induces swelling of the macrostructure.

Figure 5.14: Case of c=4M anḍ σm =0.95. (a) Swelling and evolution of matric suction in the macro and micro structures. (b) Swelling and evolution of solute mass fraction in the macro and microstructures. (c) Evolution of matric suction together with the solute mass fraction in macro and microstructures.

A net compression is observed because for this material it was assumed that the microstructural mechanisms (a_m=-0.028, a_2=-0.014) dominate the overall behaviour of the material. This small compression is followed by a primary swelling induced essentially by a dissipation of macrostructural matric suction. This stage is followed by tertiary swelling associated to the transport of water and solute from the macrostructure of the microstructure (Figure 5.14.a, b). In fact, when the solute reaches the microstructure the prevailing osmotic gradient reduces, allowing the hydration of the microstructure thereby decreasing matric suction micro (Figure 5.14.c).
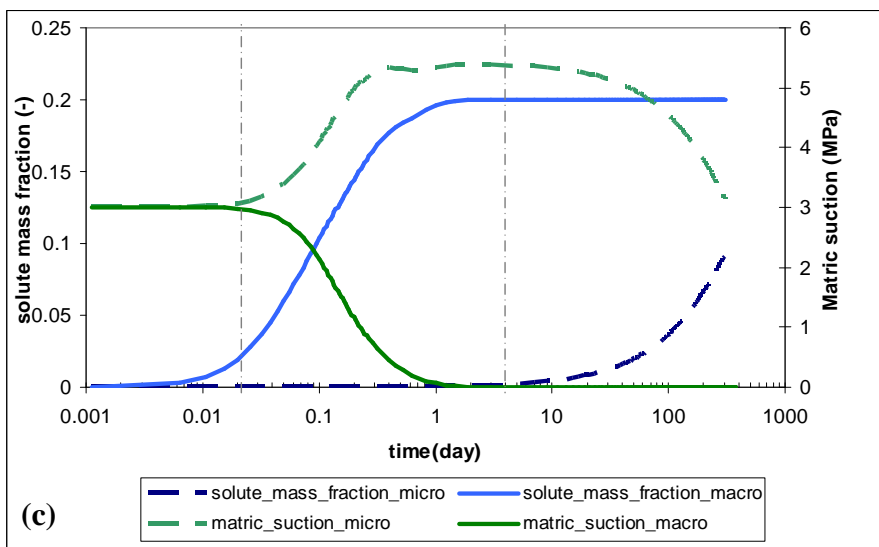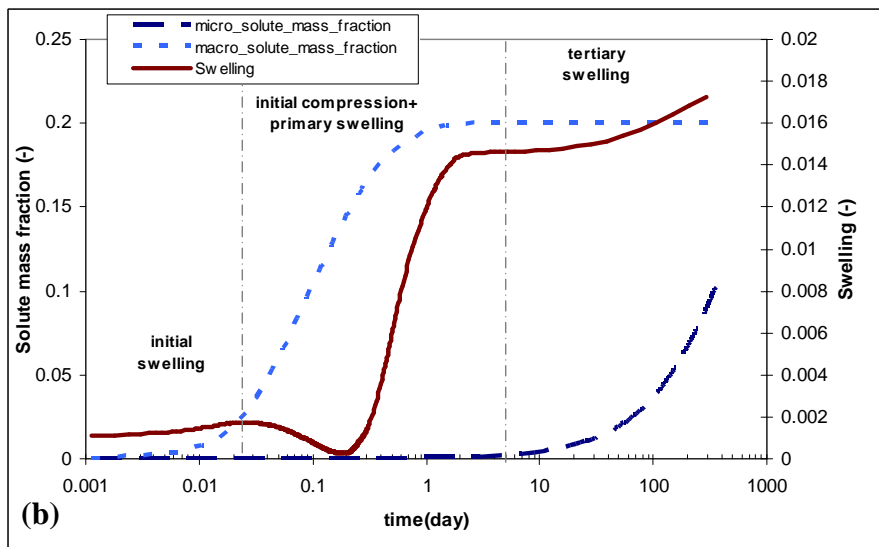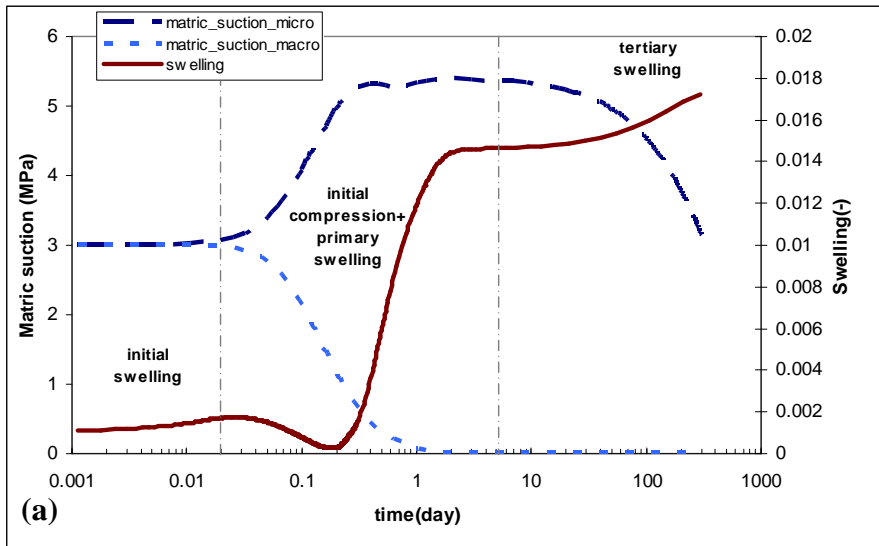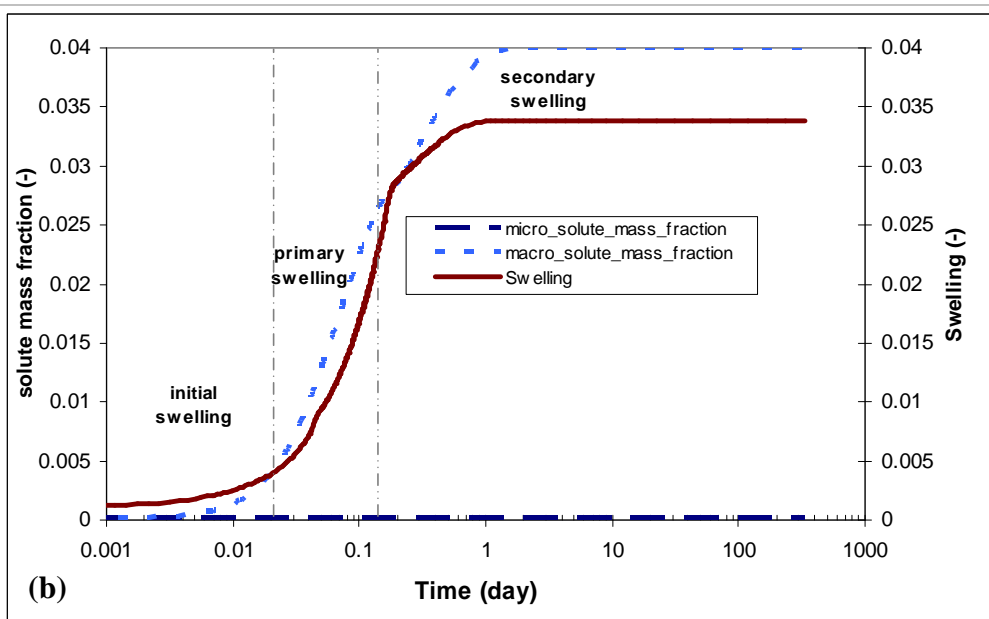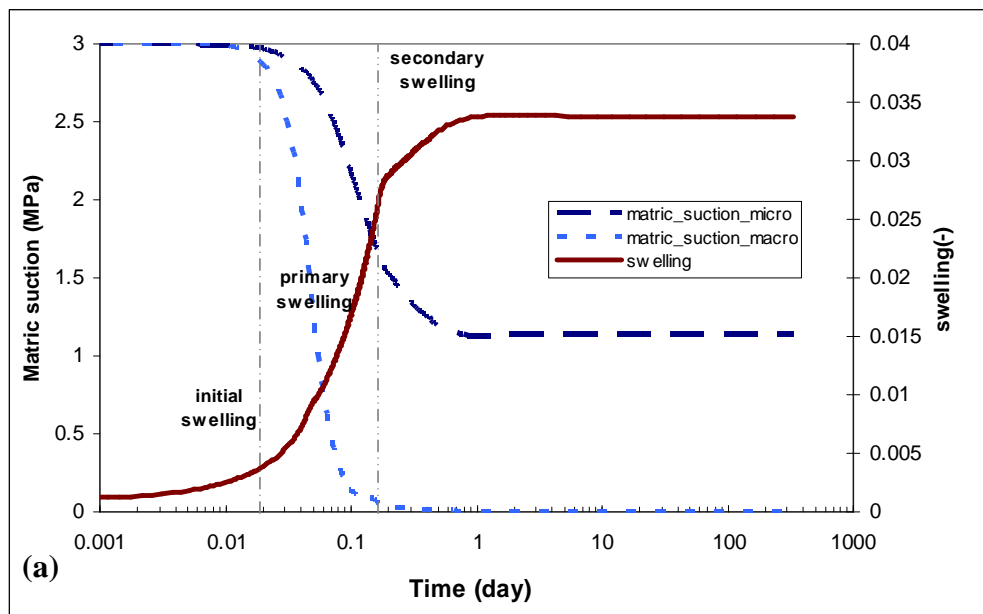

Figure 5.15. Case of c=0.8M and σ_m =1. (a) Swelling and evolution of matric suction in the macro and micro structures. (b) Swelling and evolution of solute mass fraction in macro and microstructures.

The effect of the microstructural efficiency coefficient on the swelling deformation is shown in detail for the case of c=0.8M and c=4M (Figures 5.15 and 5.16). It is interesting to observe that there is no tertiary swelling for the case of c=0.8M when σ_m=1 (ideal semi permeable membrane surrounding the clay clusters). In fact in this case, no transfer of solute is allowed into the microstructure (Figure 5.15.b). After the small secondary swelling there is stabilization of the deformations (Figure 5.15). The same trends are observed for the case of c=4 M, since the transfer of solute is totally prohibited (σ_m=1) the swelling associated to the osmotic gradient between the microstructure and the macrostructure is not observed (Figure 5.16).

5.6 Summary

A formulation has been proposed for the analysis of deformation induced by osmotic processes in double structure porous media. The balance equations for water, dissolved salts are written including the coupled flows, namely osmotic flow and ultrafiltration. For the mass balance of the solid phase, micro porosity is introduced. A relation is developed to describe the exchange of mass between the macro pores and the micro pores. The balance equations are coupled to the equilibrium of stresses. The formulation has been implemented in the finite element program CODE_BRIGHT. The formulation was combined to an adequate mechanical constitutive model. The microstructural deformation has been assumed to be purely elastic.

Results of numerical free swelling test tests offer an evidence of osmotic effects on the swelling of double structure porous media and the way they may develop. It has been observed that the matric suction of the compacted specimens was dissipated by inflow of water and solute. The diffusion of solutes into the macropores dissipates the osmotic suction difference between the material and the reservoir. However an osmotic gradient is created between the microstructure and the macrostructure. The time swelling curves have been divided into initial, primary swelling, secondary swelling and a small long term tertiary swelling. If the material is soaked with a solution with higher concentration, a small initial compression is observed and primary swelling is followed

by a long term tertiary swelling. In this case the osmotic gradient between the micro and the macrostructure is higher than the prevailing hydraulic gradient. Hydration of the microstructural is allowed when the osmotic gradient between the macro and microstructure reduces due to the intrusion of the solute into the micropores.
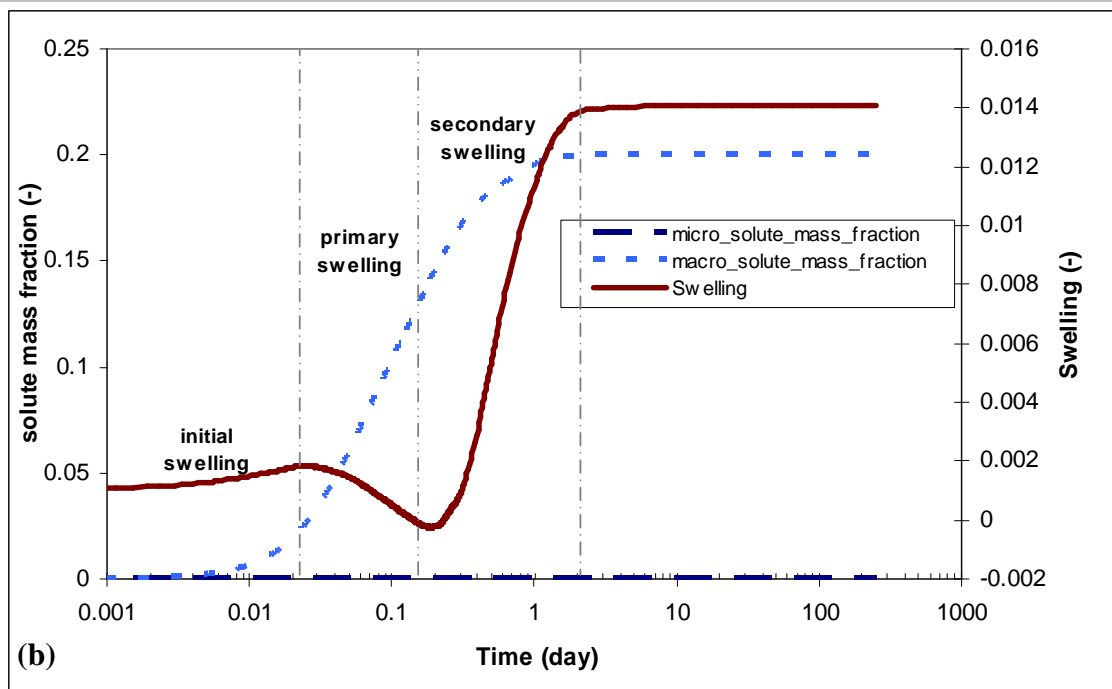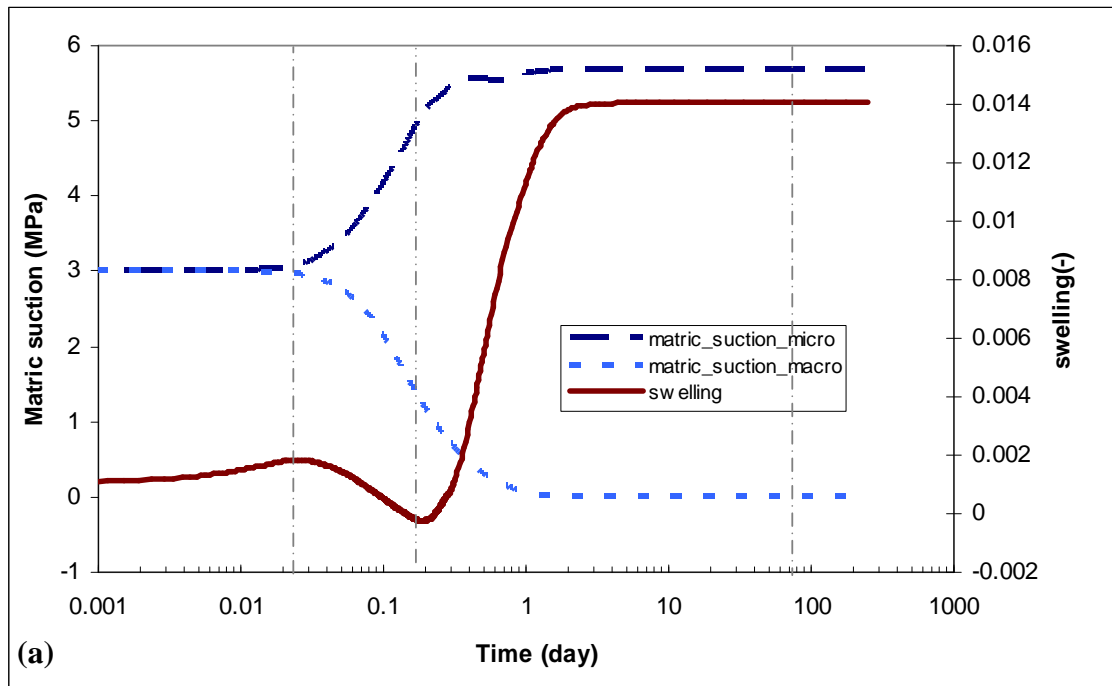

Figure 5.16. Case of c=4M and σ_m =1. (a) Swelling and evolution of matric suction in the macro and micro structures. (b) Swelling and evolution of solute mass fraction in macro and microstructures.

In general primary swelling is related to a simultaneous dissipation of matric suctions into both structural levels. In fact since the parameter B'_w is set to a relatively high value, there is an instantaneous hydration of the microstructure. Secondary swelling is linked to dissipation of microstructural matric suction. Tertiary swelling develops more slowly is linked to the microstructural osmotic efficiency. In fact, for the case of an ideal semi permeable membrane surrounding the microstructure, no transfer of solute is allowed, that is, tertiary swelling does not develop.

The powerful capability of this formulation can be exploited to model and understand the water-solute processes in clays involving deformations. As mentioned before these type of processes may appear in different isolation barrier engineering problems.

5.7 References

Alawaji, A.: Swell and compressibility characteristics of sand–bentonite mixtures inundated with liquids. Applied. Clay. Science., 15, 411–430, (1999)

Alonso, E.E.: Modeling expansive soil behavior. Proc. 2nd Int. Conf. Unsaturated soils, China, 37-70, (1998)

Barbour, S., and Fredlund, D.: Mechanisms of osmotic flow and volume change in clay soils. Can Geothec J., 26, 551-562, (1989)

Barbour, S.L., and Yang, N.: A review of the influence of clay-brine interactions on the geothecnical properties of Ca-montmorillonitic clayey soils from western Canada. Can. Geotech. J., 30, 920-934, (1993)

Bear, J., and Bachmat, Y.: Introduction to modeling of transport phenomena in porous media. Kluwer Acad. Publ., New York.(1990)

Castellanos, E., Gens, A., Lloret, A., and Romero, E.: Influence of water chemistry on the swelling capacity of a high density bentonite. Proc. 4nd Int. Conf. Unsaturated soils, Carefree, Arizona. April 2-6, 2006.ASCE, Reston, Virginia, 1: 963-972,

Castellanos, E., Villar, M.V., Romero, E., Lloret, A., and Gens, A.: Chemical impact f the hydro-mechanical behaviour of high-density Febex bentonite. Phys Chem Earth., 33, 516-526, (2008).

Di Maio, C.: Exposure of bentonite to salt solution: osmotic and mechanical effects. Géotechnique., 46(4), 695-707, (1996)

Fritz, S.J., and Marine, I.W.: Experimental support for a predictive osmotic model of clay membranes", Geochmica et Cosochimica Acta., 47,1515-1522, (1983)

Fritz, S.J.: Ideality of clay membranes in osmotic processes: a review", Clay and Clay minerals., 43 (2): 214-223, (1986)

Garavito, A.M.:Chemical osmosis in clayey sediments", PhD thesis, University of Utrecht, the Netherlands, (2005)

Garavito, A.M., De Cannière, P., and Kooi, H.: In situ chemical osmosis experiment in the Boom clay at the Mol underground research laboratory", J. Phys and Chem. Earth., (2006)

Gajo, A., Loret, B., Hueckel, T.: Electro-chemo-mechanical couplings in saturated porous media: elastic–plastic behaviour of heteroionic expansive clays. International Journal of Solids and Structures., 39, 4327–4362, (2002)

Gajo, A., and Loret, B.: Transient analysis of ionic replacements in elastic–plastic expansive clays. International Journal of Solids and Structures., 41, 7493–7531, (2004)

Gens, A., and Alonso, E.E.: A framework for the behavior of unsaturated expansive clays. Can Geotech. J., 29, 1013-1032, (1992)

Guimaraes, L.: Análisis multi-componente ni isotermi en medio poroso deformable no saturado. PhD Thesis, Dept. of Geotechnical Engineering and Geosciences, Technical University of Catalonia, Barcelona, Spain (2002)

Handbook of chemistry and physics, 63rd edn., edited by R.C. Weast, CRC Press, Cleveland, Ohio, p. D261, (1982)

Hassanizadeh, S.M.: Derivation of basic equations of mass transport in porous media, Part 2. Macroscopic balance laws. Transport in porous media., 9, 196-206. (1986a)

Hassanizadeh, S.M: Modelling species transport by concentrated brine in aggregated porous media. Transport in porous media ., 3: 299-318. (1988)

Hueckel, T.: On effective stress concepts and deformation in clays subjected to environmental loads: Discussion. Can. Geotech. J., 29, 1120-1125, (1992a)

Hueckel, T.: water–mineral interaction in hygromechanics of clays exposed to environmental loads: a mixture theory approach. Can. Geotech. J., 29, 1071-1085, (1992b)

Keijzer, T., Kleingeld, P.J., and Loch J.P.G.: Chemical osmosis in compacted clayey material and the prediction of water transport", Engineering Geology., 53:151-159. (1999)

Keijzer, T.: Chemical osmosis in natural clayey material", Ph.D. thesis, Universiteit Utrecht, The Netherlands, (2000)

Lever, D.A. and Jackson, C. P.: On the equation for flow of concentrated salt solution through a porous medium, U.K. DOE Report No. DOE/RW/85.100. (1985)

Loret, B., Hueckel, T., and Gajo, A.: Chemo-mechanical coupling in saturated porous media: elastic–plastic behaviour of homoionic expansive clays.Int. J. Solids and Structure., 39, 2773-2806, (2002)

Ma, C.M., Hueckel, T.: Effects of inter-phase mass transfer in heated clays: a mixture theory. Int. J. Eng. Sci., 30(11), 1567–1582, (1992).

Malusis, M.A., Shackelford, C.D., Olsen, H.W.:A laboratory apparatus to measure chemico-osmotic efficency coefficents for clay soils. Geotechnical testing journal, ASTM 24 (3), 229-242. (2001).

Malusis, M.A., Shackelford, C.D., Olsen, H.W.: Flow and transport through clay membrane barriers", Engineering Geology., 70, 235-248. (2003)

Marine, I.W., and Fritz, S. J.: Osmotic model to explain anomalous hydraulic heads", Water Resources Research., 17 (1), 73-82. (1981)

Mitchell, J.K.: Fundamentals of soil behaviour. 2nd Edition. John Wiley and sons. New York, (1993)

Murad, M.A.: Thermo-mechanical model for hydration swelling in smectitic clays. Int. J. Num. Anal. Meth. Geomech., 27 (7), Part I:673–696, Part II: 697–720. (1999)

Musso, G., Romero, E., Gens, A., Castellanos, E.: The role of structure in the chemically induced deformation of FEBEX bentonite", Applied Clay Science., 23, 229-237, (2003)

Musso, G., Romero, E.: chemo-mechanical behavior of high-density bentonites. Imbibitions and diffusion tests. Anvances in understanding engineered clay barriers. E.E Alonso and A. Ledesma (eds). Taylor and Francis Group, London. 283-291, (2005).

Neuzil, C.: Osmotic generation of"anomalous" fluid pressures in geological environments. Nature., 403, 182–184.(2000).

Olivella, S., Carrera, J., Gens, A., and Alonso, E.E.: Non isothermal multiphase flow of brine and gas through saline media. Transport in porous media., 15:271-293, (1994).

Pusch, R.: Experimental study of the effect of high pore water salinity in the physical properties of natural smectic clay. SKB, Technical Report, TR-01-07. Sweden (2001).

Romero, E.: Characterization and thermo-hydro-mechanical behavior if unsaturated Boom clay: an experimental study. PhD Thesis, Dept. of Geotechnical Engineering and Geosciences, Technical University of Catalonia, Barcelona, Spain (1999).

Rao, M. and Shivananda, P.: Role of osmotic suction in swelling of salt amended clays. Can. Beotech.J., 42, 307-315, (2005).

Rao, M., Thyagaraj, T., and Thomas, H.R.: Swelling of compacted clay under osmotic gradients. Geotechnique., 56 (10), 707–713, (2006).

Rao, M. and Thyagaraj, T.: Role of direction of salt migration on the swelling behaviour of compacted clays. Applied Clay Science., 38, 113–129 (2007).

Sanchez M., Gens, A., Guimaraes L., and Olivella, S.: A double structure generalized plasticity model for expansive materials. Int. J. Numer. Anal. Meth. Geomech., 29:751–787, (2005).

Schmitz, M.: Can the diffuse double layer theory describe changes in hydraulic conductivity of compacted clays?. Geotechnical and Geological Engineering., 24, 1835–1844, (2006).

Van Genuchten, M.T.: A closed form equation for prediction the hydraulic conductivity of unsaturated soils. Soil. Sci.Soc.Am., 44, 379-392, (1980).

Yang, N., and Barbour, S.L.: The impact of soil structure and confining stress on the hydraulic conductivity of clays in brine environments. Can.Geotech..J., 29, 730-739, (1992).

Yong, R.N., Mohamed, A.M.O and Warkentin, B.P: Principles of contaminant transport in soils. Development in Geotechnical Engineering, 73, Elsevier, Amsterdam. (1992).

Chapter 6

Effect of changes of pore fluid concentration on compressibility and shear strength of Boom Clay

6.1 Background

For nuclear waste disposal sites, the effects of salts on the hydro-mechanical properties of clay soils is very important because of the possible hydration with brine or leachant coming from the waste which can possibly affect the safety of the disposal site i.e. engineered barrier or/and host rock.

A great number of experimental studies dealing with the chemical effect on the hydro-mechanical properties of clays are available in the literature. Most of these studies focused on the chemical effect on the swelling behavior of clayey soils (Rao and Shivananda, 2005; Rao et *al.,* 2006, 2007: Alonso, 1998; Musso et *al.*, 2003; Alwaji, 1999; Yong et *al.*, 1992; Pusch, 1991). Others focused on the effect on chemical changes on compressibility, hydraulic conductivity, and on shear strength (Di Maio, 1996, Di Maio et *al.*, 2004; Barbour and Yang, 1993; Barbour and Fredlund, 1989; Mesri and Olson, 1970; Fernandez and Quigley, 1988; Kaya and Fang, 2000; Anandarajah, 2003; Park et *al.,* 2006; Yang, 1990; Abdullah, 1997; Studds et *al.*, 1998, Cey et *al.*, 2001, Castellanos et *al.*, 2006, Yilmaz et *al.,* 2008, Mishra et *al.,* 2008). Few analyses have focused on the behavior of compacted samples (Yang 1990; Musso et *al.*, 2003; Musso and Romero, 2005; Castellanos et *al.*, 2006 and 2008). Musso et *al.* (2003) have shown that the behavior of compacted bentonite samples with a complex structure incorporating several levels, differ form the one of samples reconstituted from slurries.

Most of the experimental analyses available in the literature focus only on the behavior of samples reconstituted form slurries and have been carried out under saturated conditions, at very high void ratio. Under these conditions, the influence of changes of

pore water concentration is very important and can be qualitatively explained by the concept of the Diffuse Double Layer (DDL). However, this theory fails in the description of compacted, high density clay materials like most of natural and engineered barriers. Schmitz et *al.* (2006), Ma and Hueckel (1992), Hueckel (1992a, b) and Guimaraes (2002) discussed the extent at which the DDL theory can describe chemically induced changes in compacted clays. They reported that in the case of highly compacted clays, (as used for radioactive waste repositories), the effect of the DDL is limited because the particles are compacted and are too close together for the DDL to form correctly. For this case, the influence of the DDL is smaller than at lower stress levels when the soil is more slurry like.

In what follows, available information on the influence of changes on soil pore water concentration on the hydraulic conductivity, compressibility and shear strength of clay soils are synthesized. Because the literature is extensive, the references that follow provide only a somewhat eclectic choice. Chemical effect on swelling rates and swelling potentials are discussed in Chapter 5.

6.1.1 Chemical effects on hydraulic conductivity of chemically sensitive clays

A great number of experimental studies dealing with the effects of chemicals on hydraulic conductivity of clays are available in the literature. Their consequences can be crucial on ensuring the safety of barriers and liners. Many studies have been conducted to evaluate the effects of organic liquids on the hydraulic conductivity of clay liners (Fernandez and Quigley, 1988; Kaya and Fang, 2000; Anandarajah, 2003; Park *et al*., 2006). Fernandez and Quigley (1988) have investigated the effect of permeation with dioxane and Ethanol of Sarnia clay on its hydraulic conductivity, with or without the presence of external effective stress. Measured differences of permeability at the same void ratio were up to 5 orders of magnitude. The authors concluded that the higher the dielectric constant of the fluid, the lower is the hydraulic conductivity. To investigate the causes behind the change of hydraulic conductivity of three types of soils (bentonite, kaolinite and a local clay soil) when exposed to organic fluids, Kaya and Fang (2000) determined some physical parameters of these soils as a function of dielectric constant,

among others, the cation exchange capacity, pore size distribution, and the Atterberg limits as a function of dielectric constant.

Other studies focused on inorganic liquids (Barbour and Yang, 1993; Yang and Barbour, 1992; Abdullah 1997; Studds et *al.*, 1998; Cey et *al.*, 2001; Castellanos et *al,*. 2006 and 2008; Yilmaz et *al.*, 2008; Mishra et *al.*, 2008). Yang (1990), Yang and Barbour (1992) and Barbour and Yang (1993) studied the impact of soil structure and confining stress on the hydraulic conductivities of Regina clay and glacial till during exposure to concentrated NaCl solutions. The samples were prepared with different methods of compaction in order to see the effect of the initial structure of the materials and were tested under various levels of confining stress and salt concentration. The authors observed that depending on the applied confining stress, osmotic consolidation may induce an increase or decrease of the hydraulic conductivity of both materials. Indeed, under low confining stress exposure to high concentration NaCl solution induces an increase of hydraulic conductivity. This increase can be prevented if high confining stresses are applied. However, for some cases a decrease in hydraulic conductivity is observed. Cey et *al.* (2001) performed constant head hydraulic conductivity tests and osmotic flow tests on undisturbed cretaceous samples from southern Sasktchewan over a range of pore fluid concentration. The authors observed that the hydraulic conductivity increased as the pore fluid concentration increased. Castellanos et *al.* (2006) presented the results of an experimental tests performed under oedometer conditions aimed at understanding the effect of the water chemistry on the swelling capacity of a statically compacted Ca- bentonite. Two electrolytes solutions were used NaCl and $CaCl_2$. Higher water permeability was observed at higher concentration. Mishra et *al.* (2008) investigated the effect of various concentrations of NaCl and $CaCl_2$ on the permeability of four different soil bentonite mixtures. The hydraulic conductivity of any mixture was found to be increasing with the increase of the salt concentration. Yilmaz et *al.* (2008) conducted laboratory hydraulic conductivity tests on low plasticity and high plasticity compacted clays. The samples were exposed to five different inorganic salt solutions NaCl, NH_4Cl, KCl, $CaCl_2$, and $FeCl_3$ at various concentrations. The hydraulic conductivity was found to increase for high plasticity clay when the salt concentrations increased whereas for the low plasticity clay, when the salt concentrations were increased, the hydraulic conductivity decreased.

6.1.2 Chemical effects on compressibility and shear strength of chemically sensitive clays

Some researchers investigated the role of change in pore water concentration on compressibility and shear strength of clay materials. Barbour and Yang, (1993) presented a summary of osmotic consolidation tests conducted by Yang, (1990), Ho (1985) and Barbour, (1986). Remolded and undisturbed samples of glacial till and glaciolacustrine clay under variety of solution concentrations were tested. The samples were loaded to specified stress level and were then equilibrated with NaCl solution by diffusion. They were then reloaded to higher stresses. Figure 6.1.a shows that when water saturated clay is exposed to NaCl brine they underwent a decrease in volume. In every case this volume change were accompanied by an apparent increase in the preconsolidation stress and decrease in the compressibility of the sample until this new preconsolidation stress has been exceeded. At this point the samples continue to consolidate along the same virgin compression line. Similar results have been reported by Barbour and Fredlund (1989). Ho, (1985) (After Barbour and Yang, 1993) have shown the results of samples remolded with brine and then tested in water. An interesting observation is that submersion of the samples with water caused the sample to decrease in volume under constant effective stress (Figure 6.1.b). Di Maio, (1996) investigated the effects of the exposure, of water-saturated specimens of Ponza bentonite, alternately to pure water and saturated NaCl, KCl, or $CaCl_2$ solutions. Exposure to the three electrolytes produced consolidation of the specimens, large volumetric deformations, and an increase in residual shear Strength. Effects of exposure to NaCl were reversible when the samples were re-exposed to pure water, whereas those for KCl and $CaCl_2$ were not, due to ion exchange reactions. Musso et *al.*, (2003) investigated the effect of a salinization-desalinization path on Febex bentonite samples prepared at approximately the same void ratio by means of either static compaction at hygroscopic humidity or stating from slurries consolidated under mechanical loads. In both cases the samples were exposed to NaCl solution and then to distilled water. As a consequence of the chemical cycle the samples experienced chemical consolidation and swelling. Interestingly, the authors observed that times for complete chemical swelling are significantly larger than consolidation ones, which reflect that one phenomenon does not seem to be the reversal of the other.
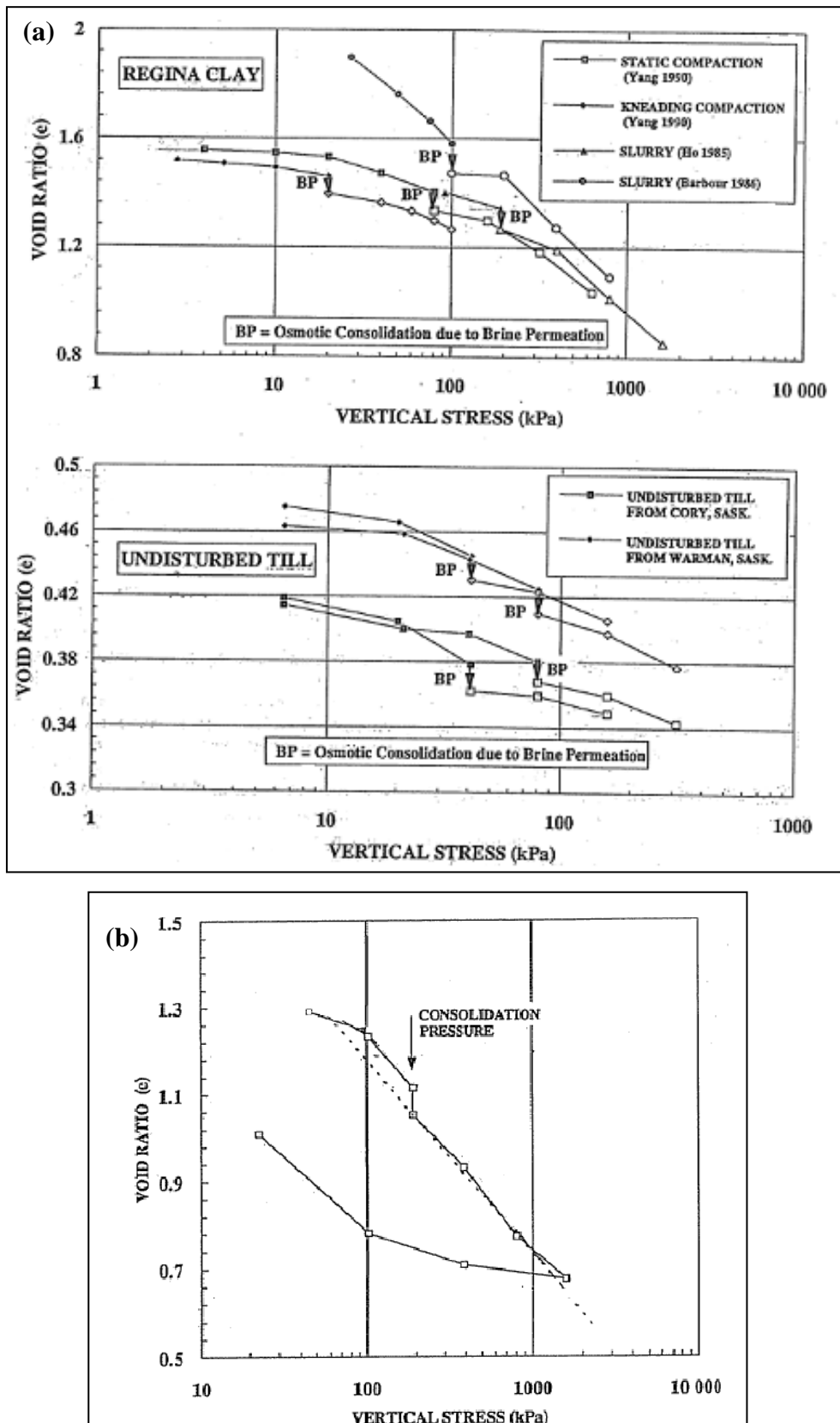
Figure 6.1: Mixed chemical-mechanical loading (a) for specimens initially prepared with distilled water then exposed to brine and (b) for a specimen initially prepared with brine then exposed to water. (Barbour and Yang 1993)

Figure 6.2 shows the results of a mixed chemo-mechanical cycle reported by Di Maio (1996). In both cases exposure to brine solution induces large volumetric deformation. It has to be noted that in this case, after chemical equilibration, when the samples are reloaded no chemical preconsolidation is observed. The slope of the stress–strain curve is the elastic–plastic slope right from the beginning of the stress increase. Loret et *al.*, (2002) attributed this result to the high initial void radio of the tested samples. Di Maio (2004) analyzed the influence of mineral composition and pore fluid composition on volume change behavior of four different clayey soils. Oedometer tests were conducted on the reconstituted material mixed with distilled water or concentrated NaCl solutions or with an organic fluid. The results showed that an increase in pore solution concentration causes a reduction in compressibility. The effect increases with the smectite content.
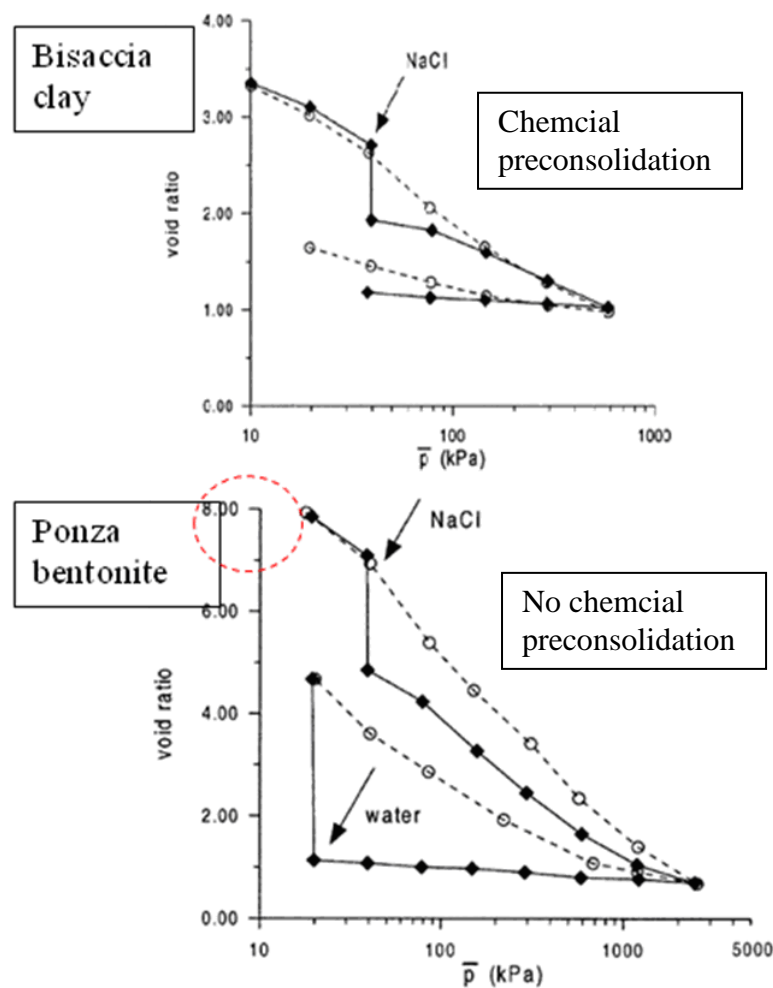

Figure 6.2: Mixed chemical-mechanical loading for a specimen initially prepared with distilled water (Di Maio, 1996)

Di Maio (1996) and Di Maio et *al.* (2004) tested specimens prepared at water content higher than the liquid limit. Void ratios for all tests ranged from 2 to 8. It is believed that one of the causes of the dramatic volume change obtained by Di Maio (1996) and Di Maio et *al.* (2004) is caused by the high void ratios of the tested samples which are not representative of clayey soils encountered under natural or compacted states.

Ho (1985) (After Barbour and Yang, 1993), tested samples of Regina clay and Indian head till prepared with distilled water and then permeated with 4 M NaCl solution. Triaxial undrained consolidated tests were run on fresh water samples and brine permeated samples. The results showed a significant increase in shear strength for both clays (Figure 6.3).
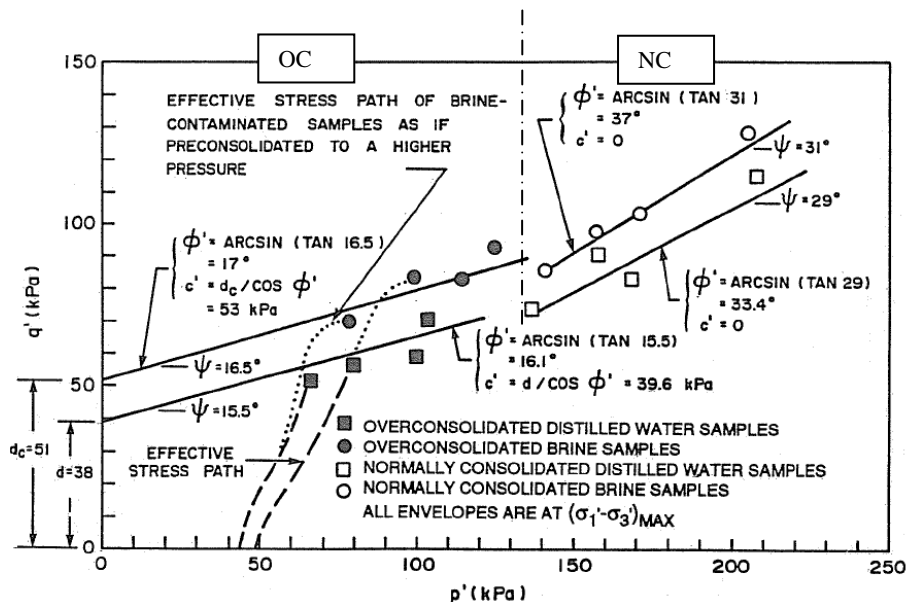
Figure 6.3: Undrained triaxial tests, samples prepared with distilled water then exposed to NaCl solution (Ho, 1985 after Barbour and Yang, 1993)

Di Maio (1996) and Di Maio et *al.* (2004) also reported results on the effect of pore water concentration on residual shear strength of two types of clay soil, Ponza bentonite and Bisaccia clay. The samples were reconstituted and immersed in saturated NaCl solutions. It was observed that the residual shear strength increases with respect to the values obtained with distilled water. The author observed that the largest variation occurred for concentration in the range of 0 to 0.5 M (Figure 6.4).

149
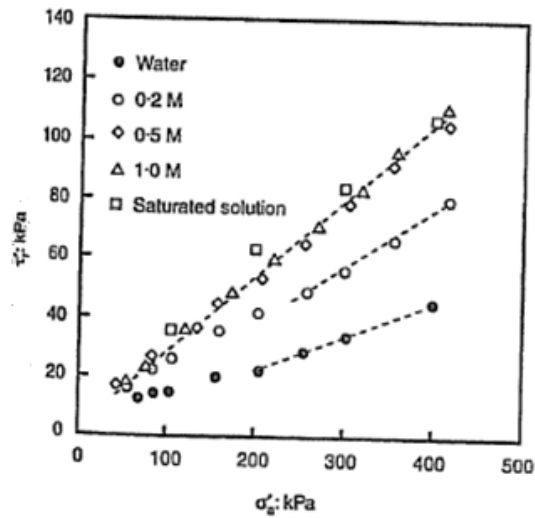
Figure 6.4: Direct shear test performed on Ponza bentonite prepared with various concentration of NaCl under residual conditions (Di Maio 1996)

6.1.3 Previous mechanical approaches

Several constitutive models have been suggested to describe the chemo-mechanical behaviour of clays. Ma and Hueckel (1992) and Hueckel (1992a,b) proposed to treat clays exposed to chemical change, or as called by these authors subjected to chemical loading, as a two phases mixture, with absorbed water being a part of solid phase. Adsorption and desorption of the adsorbed water is modeled by the use of an interphase transfer term. Hueckel (1992a, b) extended Terzaghi's principle of effective stress by assuming that the stress in solid porous skeleton is equal to the specific electrochemical forces (R-A). Therefore, the chemical strain induced by transfer of the adsorbed water is now, additive to the mechanical strain. Mesri and Olsen (1970), Barbour and Fredlund (1989), Barbour and Yang (1993), among others, have shown that chemical change under constant effective stress can produce plastic consolidation strain. Hueckel (1992) postulated that change in dielectric constant or concentration of pore water causes closure of the micropores by transfer of the absorbed water, which produces plastic or no recoverable compression. Another important result, pointed out by Hueckel (1992) is the shrinking of the elastic domain referred to as chemical softening (Figure 6.5).
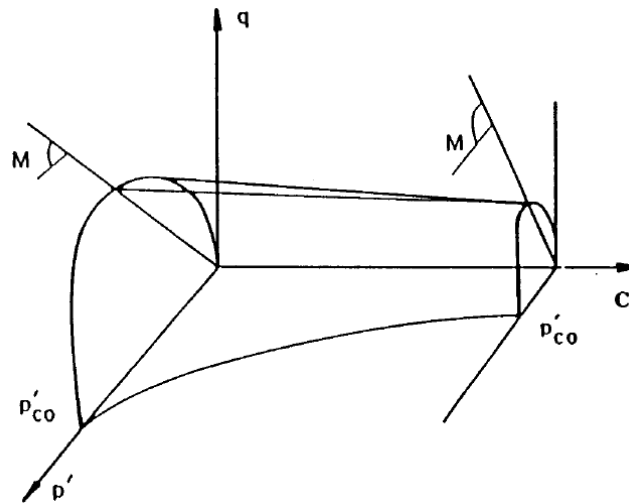
Figure 6.5: Representation of chemical softening of yield locus in q, p', and concentration space. (Hueckel , 1997)

Hueckel (1997) presented a chemo-elasto-plastic model to describe strain induced by permeation of a clay material with a low dielectric constant organic contaminant. Chemical softening is accounted for, introducing   a scalar multiplier referred to as the chemical softening function. Within the elastic domain, chemical effects induce chemo-elastic strain. At plastic yielding chemo-plastic compaction takes place. Loret et *al.* (2002) presented a chemo-elasto-plastic model to describe the chemo mechanical behavior of saturated homonoic clays following a thermodynamical development. The authors followed the same approach as Hueckel (1992, 1997), considering the medium as constituted of two overlapping phases, attributing the adsorbed water to the solid phase. The authors intended to reproduce the experimental results obtained by Di Maio (1996) and Di Maio and Finelli (1997). They assumed that chemical consolidation under constant effective stress has first an elastoplastic stage followed by an elastic stage. The size of the elastoplastic stage increases with the stress level. During this stage two competing processes takes place, chemical softening (i.e decrease of the preconsolidation stress due to chemical change) and hardening which increases the preconsolidation stress. Loret et *al.* (2002) stated that further mechanical loading during this stage leads to an elastoplastic behavior that is the stress strain curve is directly the elastoplastic one. If mechanical loading resumes during the elastic stage the behavior will be elastic. Gajo et *al.* (2002) extended the frame work proposed by Loret et *al.* (2002) to include the presence of several counter ions. Similarly, Guimaraes (2002) proposed a model for expansive clays, which describes the effects of changes in ionic

151

solutions on the microstructure and the macrostructure of the clay, as well as the interactions between the two scales.

Few investigations have been devoted to the study of chemo-hydro-mechanical behavior of partially saturated clays. Boukpeti et *al.* (2004) and Liu et *al.* (2005) investigated the effect of chemical changes on the behavior of partially saturated clays. The authors used the concept of chemical softening proposed by Hueckel et *al.* (1992, 1997) and modeled the influence of partial saturation on the constitutive behavior following the Barcelona Basic Model (Alonso et *al.*, 1990). The authors have shown only numerical simulation due to the lack of experimental results dealing with chemical effect on partially saturated clays.

6.2 Characterization of tested material. Experimental performed program

In Belgium, The Boom Clay, a slightly over-consolidated marine Oligocene deposit, is considered as a reference host formation for the geological disposal of high level and long lived radioactive waste because of its expected favorable characteristics. At Mol site in northeast Belgium, the tertiary Boom Clay formation is situated between 186 and 288 m depth. Intensive experimental investigations revealed that, this clay formation has physical and mechanical properties very favorable to the final disposal of radioactive waste. Among these are permeability, diffusion coefficient, coefficient of thermal expansion and thermal conductivity. The low permeability ($\sim 10^{-19}$ m^2) and high porosity (~ 0.39) of the clay formation gives it a good capacity to retain radionuclides (Weetjens, 2003). Another important property is its self healing capacity (Picard, 1994; Coll et *al.*, 2004; Bernier et *al.*, 2006).

Mineralogically, the Boom Clay soil consists of about 65 to 70% of clay minerals dominated by illite, with some interstratified smectite/ illite, kaolinite and traces of chlorite. The non clayey fraction is dominated by quartz (30 to 35%) with other components like pyrite; feldspars and calcite representing less than 5% of total solids weight (Romero, 1999). Detailed mineral composition is summarized in Table 6.1.

Tabla 6.1. Mineralogical composition of Boom Clay. ANDRA 1993;Rhattas (1994).

Clay minerals	65-70%
Kaolinite	6-17%
Illite+mica	11-12%
Interstrat. Illite/smectite	35-38%
Chlorite	3-4%
Non-clay minerals	30-35%
Quartz	15-20%
Micro-cline	5%
Plagio-clase	<5%
Pyrite	<5%
Siderite	<5%
Gyp-sum	5%

The soil used in the experiments was artificially prepared powder obtained from natural Boom Clay cores. Romero (1999) presented a complete characterization of the physical properties of the clay powder. The specific gravity of the soil grains is $G_s=2.7$, determined according to ASTM D854. The consistency limits were determined following ASTM D4318. The liquid limit and plasticity indices were determined to be W_l= (55.7±0.9) % and PI= (26.9±1.0) %, respectively, (Romero, 1999). Romero (1999) reported a value of the specific surface for Boom Clay of $S_s=40$ m^2/g which corresponds to an intermediate value between a kaolinite mineral (S_s=10 to 20 m^2/g) and illite mineral (S_s=80 to 100 m^2/g). The Cation Exchange Capacity is CEC= (30± 4) meq/100g (Volckaert et *al.*, 1996a, After Romero, 1999). The interstitial fluid of the Boom Clay, measured in situ, is composed of a slightly basic water (pH=8.2). The main cation present is Sodium ion Na+ at a concentration of about 10^{-2} mol/l. Traces of Potassium, Calcium and Magnesium are also detected but at 100 times lower concentrations (Romero, 1999). For the dry Boom Clay powder it is assumed that adsorbed cations are tightly held by the negatively charged clay particles in the strongly attracted adsorbed water corresponding to the hygroscopic humidity. Cations in excess of those needed to neutralize the electro- negativity of the clay surface and associated anions are present as salt precipitates (Mitchell, 1993). Upon wetting this precipitated salt goes into the free solution occupying the macropores. Romero (1999) analyzed this pore water, extracted by squeezing technique. An estimation of the concentration of the dissolved salts of the liquid based on the electrical conductivity-salinity apparatus calibration curve is approximately 5.8 ppt (g contained in 1 kg of water) at 20.3°C. The corresponding osmotic suction of this pore water is approximately 443 kPa.

The bituminized waste product described in the previous chapters contains a lot of salts, mainly $NaNO_3$. It has been shown in Chapter 4 that this salt can diffuse through the Boom Clay which could affect the properties of the clay hot rock in the nearby vicinity of the drift. This Chapter presents the results of a systematic experimental investigation aimed at understanding the influence of increase of pore water salt concentration and chemical paths (salinization/dilution) on compressibility and shear strength of prepared samples of Boom Clay. Different tests have been performed to characterize the tested material. Mercury Intrusion Porosimetry tests (MIP) (intrusion-extrusion cycle) have been carried out in order to find out the influence of pore fluid concentration on the micro and macrostructural levels. The influence of pore fluid salt concentration on the retention properties has been also investigated by means of WP4 dewpointmeter (Decagon Devices, Inc). Two types of hydro-mechanical experiments have been carried out. To characterize the effect of pore fluid concentration on compressibility, controlled-suction oedometer tests have been performed on samples initially mixed with $NaNO_3$ solution at a given concentration. Additional oedometric tests under saturated conditions have been performed on samples initially mixed with distilled water and then exposed to a $NaNO_3$ solution prepared at different concentrations. Finally, shear strength of prepared Boom Clay specimens initially mixed with $NaNO_3$ solution at different concentrations, has been studied by means of suction-controlled direct shear tests.

6.2.1 Mercury intrusion porosimetry test

It is has been pointed out in Chapter 5, that chemical effects on hydro-mechanical behavior of active clayey soils are due to changes at the different structural levels and the interactions between them. Up to three structural levels may be defined in active clays: microstructure, mesostructure and macrostructure (Romero, 1999). The microstructure is composed by the clay platelets arranged into clusters enveloped by external adsorbed water. The interlamellar pores are filled with internal absorbed water. This water has properties, such as density, or viscosity different form those of free water. The clusters can form aggregates. The intra-aggregate pores form the mesostructure. The macrostructure is composed by the global arrangements of clay clusters, with macro pores between them partially filled with free water.

Castellanos et *al.* (2006, 2008) studied the fabric of compacted bentonite after compaction and permeation with distilled water and 0.5 M NaCl saline solution. Some shrinkage of the microstructure was observed leading to a somewhat smaller pore size at the dominant microstructural mode.

Mata (2003) performed MIP tests on compacted mixture of sand-bentonite mixed with water of with a saturated NaCl solution. No microstructure differences were observed. However, the incremental intruded pore volume was higher for the case of the specimens saturated with brine solution. In this case, salt water effects were significant on the macropores and not important on the micropores.

In order to find out the influence of pore fluid salt concentration on the structural levels, MIP tests were performed on compacted specimens of Boom Clay. Soil samples were initially mixed with water or $NaNO_3$ solution (6.53 M $NaNO_3$, corresponding to an osmotic pressure π of 30.82 MPa), and then statically compacted at γ_d=12 kN/m^3 and w=20%. MIP technique requires dehydrated samples measuring approximately 1cm^3. To avoid excessive shrinkage, samples dehydration was obtained by means of a freeze drying process (Delage et *al.*, 1982). MIP tests results are depicted in Figure 6.6.

Figure 6.6.a represents the pore size distribution normalized by the total porosity n_0, which is defined as the porosity that can be intruded by pressured mercury (n_0=0.52). The n/n_0 value is equivalent to the degree of saturation for the non wetting mercury (Romero, 1999). The plot shows that both samples appear to have a bimodal distribution defining peaks at approximately 40 and 0.2 μm for the case of the sample prepared with distilled water and at approximately 30 and 0.07 μm for the sample prepared with the $NaNO_3$ solution. Two structural levels can be distinguished, the macroporosity (pore size grater than 1μm) and microporosity (pore size less than 1μm). According to Figure 6.6.a the micropores represent 60 % of the total porosity for the case of distilled water and 50% of the total porosity for the case of the sample prepared with $NaNO_3$ solution.
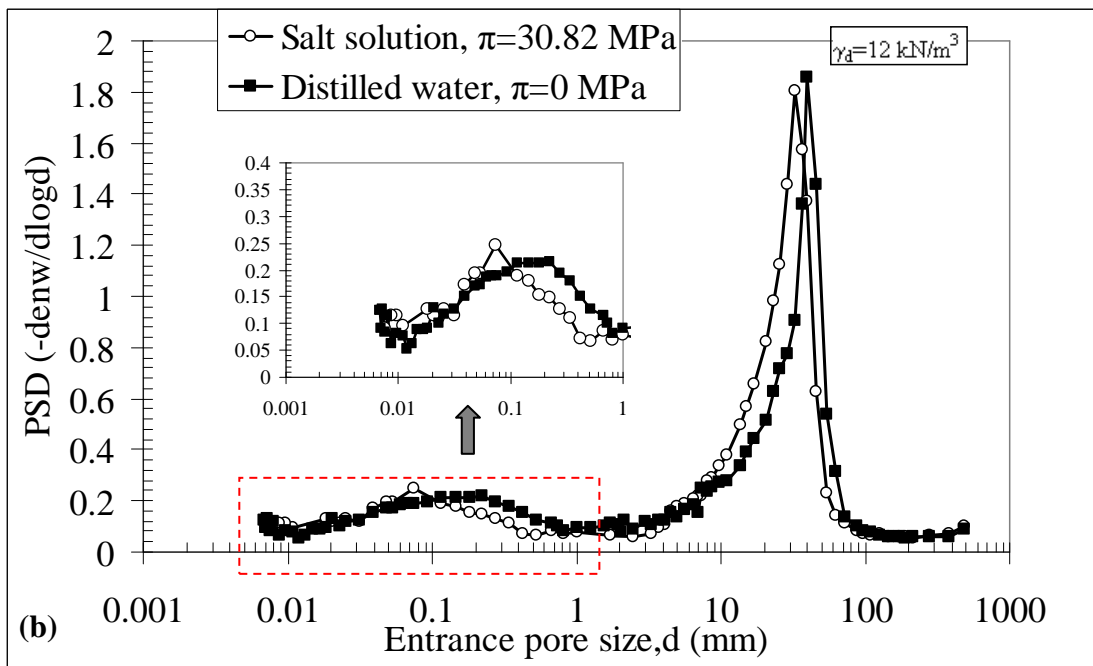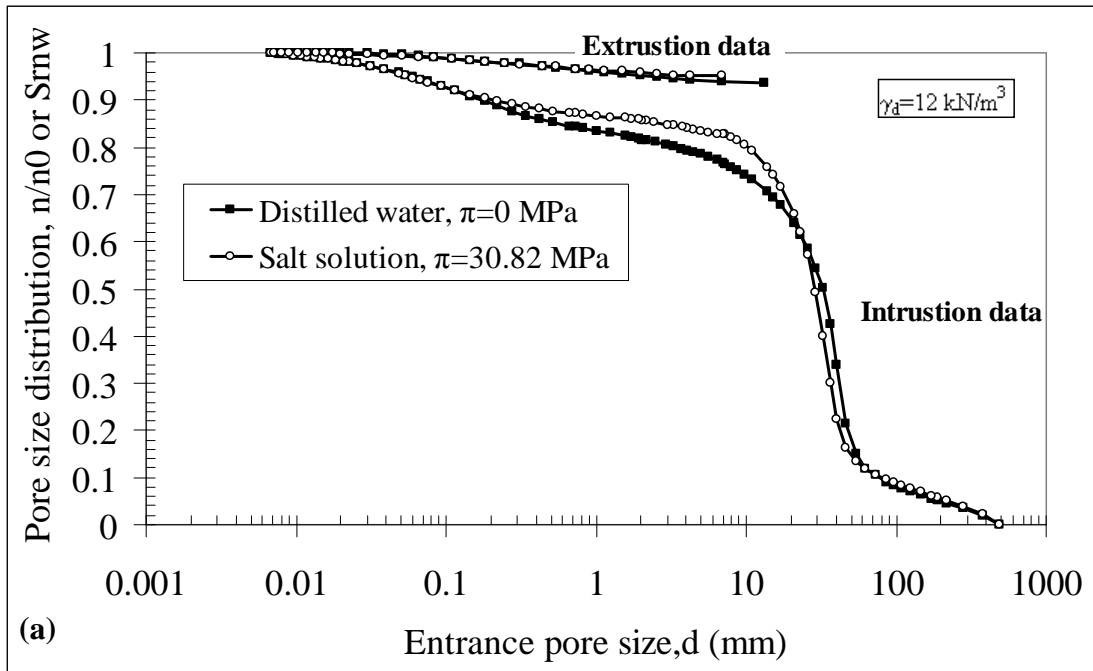
Figure 6.6: Mercury intrusion porosimetry tests for compacted Boom Clay samples compacted at γ_d=12 kN/m^3 and w=20%. The specimens were freeze dried. (a) Pore size distribution for different pore fluid solutions. The results of the MIP tests were normalized and translated to degree of saturation of the intruded mercury during the test $S_{r_{nw}}$. (b) The results of the MIP tests are expressed in terms of the pore size density function

Some differences were observed between the samples prepared with distilled water and NaNO$_3$ salt solution. There is a slight decrease of the predominant pore size in the macrostructure for the case of the sample prepared with salt solution. Thus, a higher content of the pores between 7 to 20 µm is observed. A similar result was obtained by

Castellanos et *al.* (2006). Some changes are also observed at the microstructural level. The sample prepared with $NaNO_3$ solution displays a lower content of pores between 0.1 and 0.8 μm. Therefore, mixing the clay soil with the salt solution seems to cause some contraction of the clay aggregates leading to development of new inter aggregate pores (pore size between 7 and 20 μm).

MIP tests offer an interesting preliminary evidence of the effect of pore fluid concentration on the structural distribution of Boom Clay samples. However, it fails into the complete characterization of the microstructure due to the limit accessibility of the apparatus to penetrate the smallest pores in the samples. More information about possible microstructural changes may be obtained using BET technique (Romero, 1999; Sing, 2001).

6.2.2 Water retention results

It is well known that retention curve depends on several factors like void ratio, soil type, or temperature. However, less information are available about the influence of pore fluid concentration on the retention properties of active clayey soils. Mata et *al.* (2002) and Mata (2003) checked out the influence of pore water concentration on retention properties of bentonite-sand mixtures. Different sand-bentonite mixtures were initially saturated with water or salt solution. Total suction was measured by means of transistor psychrometers following a drying path. The authors observed that measured total suction was higher for specimens saturated with salt solution that those saturated with distilled water while measured matric suction for specimens hydrated with salt water was smaller than matric suction of specimens hydrated with distilled water. Because in drying paths free water evaporates, an increase of osmotic suction while water content decreased was observed. A similar observation was reported by Sreedeep and Singh (2006) who determined osmotic suction of marine soil as the difference between total suction measured using WP4 dewpoint meter and matric suction measured using a pressure membrane extractor.

In order to find out the influence of pore fluid salt concentration on retention properties of Boom Clay soil, total suction of samples initially mixed with distilled water or $NaNO_3$ saline solution were measured using a chilled-mirror psychrometer (WP4

Dewpoint PotentiaMeter, Decagon Devices, Inc). Figure 6.7 shows a schematic representation and a picture of the WP4 Dewpoint PotentiaMeter device. The WP4 Dewpoint PotentiaMeter uses a sealed chamber to equilibrate the liquid-phase water of the sample with the vapor-phase water in the headspace above the sample. A mirror situated in the headspace above the sample is Peltier-cooled until the dew point is reached, which is detected as a sudden decrease in mirror reflectance because of condensation. The dew point and sample temperatures are then recorded and used to calculate the headspace water vapor pressure (p_v) and the saturated water vapor pressure (p_{v_0}), respectively. Total suction (ψ) in then calculated as following,

$$\psi = -\frac{RT\rho_w}{M_w} \ln\left(\frac{p_v}{p_{v_0}}\right)$$

(6.1)

where R is the universal gas constant [J/ (mol K)], T is the absolute temperature [K], ρ_w is the density of water [kg/m^3], and M_w is the molecular mass of water.

The operating range of the WP4 is about 1 MPa to 300 MPa.

Figure 6.7: WP4 Dewpoint Potential Meter.
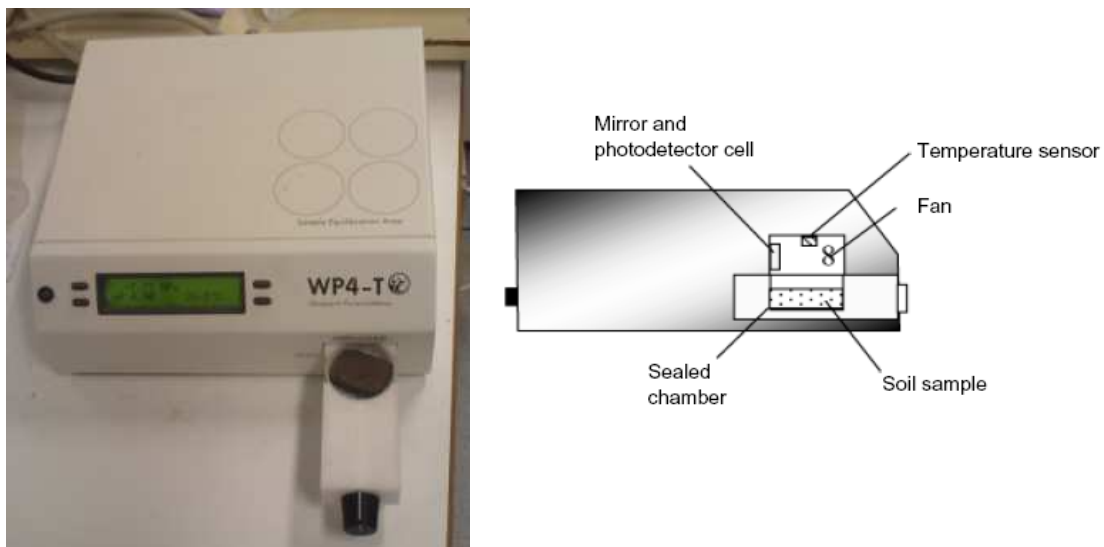**Schematic representation after (Cardoso et al., 2007)**

Boom Clay powder were mixed with distilled water then statically compacted in a strain controlled press at γ_d=12 kN/m^3 and w=20%. Once the samples had been compacted the initial total suction was measured by means of WP4. The sample was then progressively dried under controlled temperature and humidity conditions.

To determine the influence of pore fluid concentration on retention properties, Boom Clay powder was mixed with NaNO₃ solution (6.53 M NaNO₃) then statically compacted in a strain controlled press at γ_d=12 kN/m³. In order to prevent concentration increase that is osmotic suction increase, due to water evaporation if a drying path is followed, three distinct samples were prepared at different initial water contents. Once the samples had been compacted the initial total suction was measured by means of WP4.

Figure 6.8 shows that the measured total suctions were higher for specimens saturated with salt solution that those saturated with distilled water. In Chapter 4 Equation (4.3) has been proposed to calculate the osmotic suction corresponding to a given NaNO₃ salt concentration. The value obtained for 6.53 M NaNO₃ solution is π=30.82 MPa. Figure 6.9 shows the difference between the total suctions of the salt water cases and the distilled water case. Osmotic suctions values calculated as the difference between the total suction measured in the case of distilled water and the total suction measured in the case of NaNO₃ solution range between (~32 to ~33 MPa). The average osmotic suction over the three measured value is (~32 MPa) which is in the range of the theoretical osmotic suction π=30.82 MPa calculated using Equation 4.3.

MIP results can be used in order to determine the retention curve of the soil considering that the mercury intrusion process is similar to the air intrusion during the drying path of the retention curve. The injection of non wetting mercury is then equivalent to the injection of the wetting phase by the non wetting front advance of air, for the same diameter of pores being intruded (Romero, 1999).

The relationship between the equilibrium mercury intrusion pressure (p) and matric suction ($s=u_a-u_w$) can be obtained as (Romero, 1999),

$$u_a - u_w = -\frac{\sigma \cos \theta_w}{\sigma_{Hg} \cos \theta_{nw}} p \approx 0.196 p \tag{6.2}$$

where σ is the water surface tension, σ_{Hg} is the surface tension of mercury, θ_{nw} is the contact angle between the mercury and the pore wall, and θ_w the contact angle between the water and the pore wall. The same values are considered for the case of distilled water as well as for the case of salt solution.
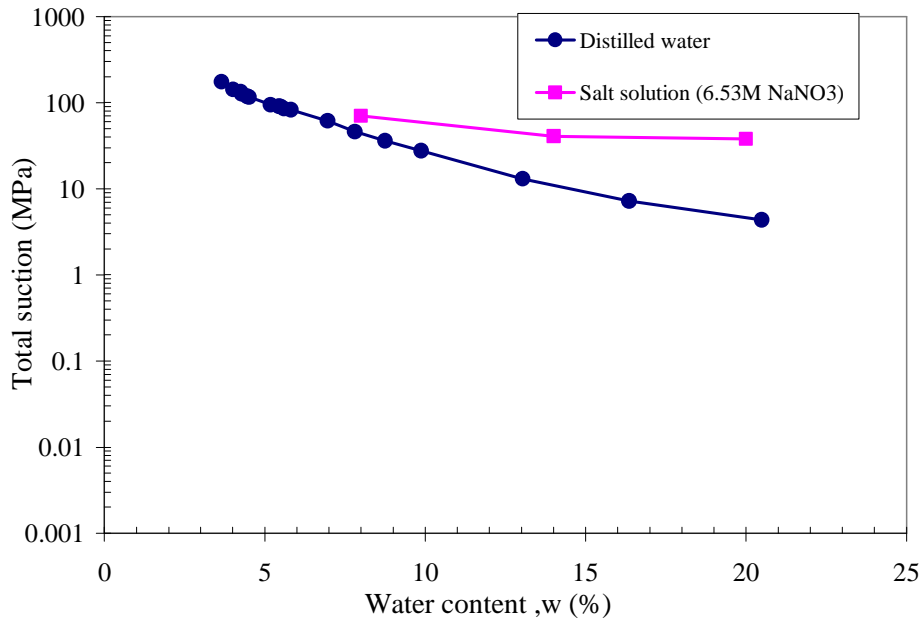
Figure 6.8: Retention curve for samples mixed with distilled water or NaNO3 solution (6.35 M) at γ_d=12 kg/m^3. Results obtained with WP4 Dewpoint PotentiaMeter. For the case of the salt solution the three points corresponds to three different samples.
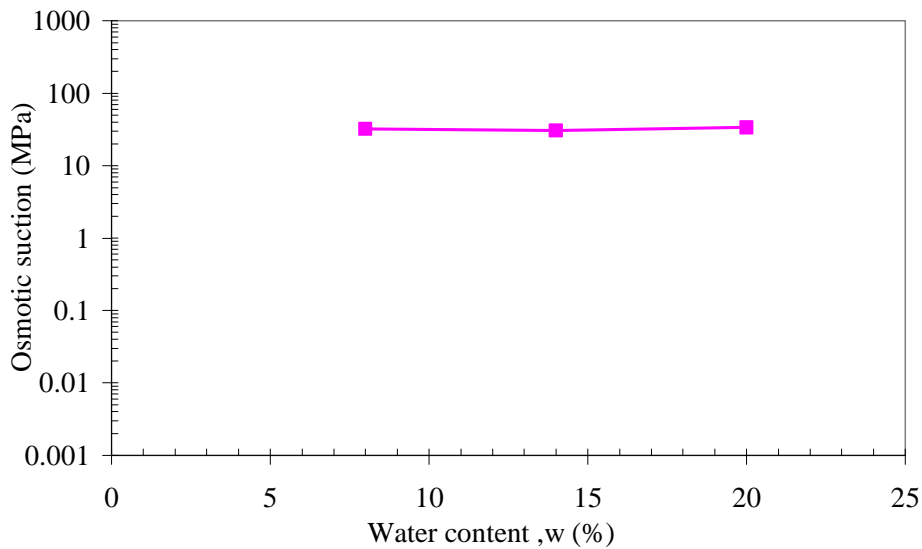
Figure 6.9: Difference between the total suction for the salt solution case and the distilled water case

The corresponding water content can be calculated as, (Romero, 1999)

$$w = \left(1 - S_{r_{nw}}\right)\left(w_{sat} - w_r\right) + w_r \qquad (6.3)$$

where $S_{r_{nw}}$ is the degree of saturation of the non wetting mercury, w_{sat} is the liquid content corresponding to complete saturation conditions. This equation takes into account the residual water content corresponding to the non intruded porosity (w_r). w_r is derived form WP4 measurements.

In most soils, water is generally held due to capillarity at low suctions (<2MPa) and by adsorption on particle surfaces and in clay interlayer at high suctions (Romero and Simms, 2008; Romero, 1999). Therefore, the derivation of the matric-suction relationship is limited to the low suction range (<2MPa) in which capillarity dominates the retentions properties of fluids (Romero, 1999; Romero and Simms, 2008). To complete the retention curve at high suction values, WP4 data are used.

The MIP data were processed and suction values corresponding to the applied mercury pressure were estimated using Equation (6.2). Water contents were calculated using Equation (6.3). To complete the retention curve at high suction values, WP4 data are used. A modified form of Van Genuchten Equation (Van Genuchten, 1980) is used to fit the bimodal retention curves (Alferi et al., 2010),

$$\frac{w-w_r}{w_{sat}-w_r}=\frac{e_m}{e_0}\left[\frac{1}{1+\left(\alpha_m s\right)^{\beta_m}}\right]^{1-\frac{1}{\beta_m}}+\frac{e_M}{e_0}\left[\frac{1}{1+\left(\alpha_M s\right)^{\beta_M}}\right]^{1-\frac{1}{\beta_M}} \qquad (6.4)$$

where w_{sat} is the saturated water content, w_r is the residual water content, s is the matric suction, e_0 is the initial void ratio of the soil, e_m is void ratio due to microporosity, e_M is void ratio due to macroporosity, and α_m, β_m, α_M and β_M are fitting parameters for the micropores and for the macropores respectively.

Equation 6.4 is obtained applying Van Genuchten (Van Genuchten, 1980) expression both for the micro and the macrostructure. The value of e_m and e_M can be estimated directly form the pore size density. The curve fitting parameters are reported in Table 6.2. The obtained retention curves for the case of distilled water and $NaNO_3$ solution are shown in Figure 6.10. Figure 6.10.a shows the retention curves represented in terms of total suction. For the case of $NaNO_3$ solution, the MIP data are added to the average osmotic suction and completed by the WP4 results. For the case of distilled water based on the assumption that solutes present in the soil are dilute enough, it is assumed that the pore fluid osmotic suction is negligible which implies that total suction is equal to matric suction in this case.

Table 6.2 Curve fitting parameter for retention curves.

		water		NaNO$_3$	
Micro-porosity	α_m		183		126
	β_m		1.95		3.33
	e_m		0.5		0.5
Macro-porosity	α_M		0.10		0.09
	β_M		1.38		1.1
	e_M		0.5		0.5
	R^2		0.99		0.99

Figure 6.10.b shows the retentions curves represented in terms of matric suction. It was observed that measured matric suction for the specimen hydrated with salt water (MIP results) was smaller that matric suction of the specimen hydrated with distilled water. A similar result has been reported by Thyagaraj and Rao (2010). In this study, the observed behavior is in agreement with the expected change in retention properties due to the change of structure of the soil as salt concentration in pore fluid is higher. In fact, according to the results in Figure 6.6, the sample prepared with NaNO$_3$ solution display a higher content of pores between 7 and 20 μm. Therefore, a possible explanation is that matric suction decreases because of the reduction of the capillary potential induced by the increase of the radius of the macropores.

6.3 Influence of pore fluid concentration on compressibility of Boom Clay prepared samples

In order to characterize the effect of pore fluid concentration on compressibility of clayey soils, oedometer tests have been carried out on samples of Boom Clay initially mixed with NaNO$_3$ solution at different concentrations or with distilled water and then exposed to sodium nitrate solution (that is, chemical loading). Two sets of tests have been performed, oedometer tests under controlled matric suction conditions and oedometer tests under saturated conditions.

6.3.1 Controlled –suction oedometer tests

6.3.1.1 Test equipment and procedure

Specimens were prepared by mixing the Boom Clay powder with NaNO$_3$ solution prepared at different salt concentrations. The mixtures were statically and one dimensionally compacted at a dry density of γ_d=12 kN/m^3 and at a constant water

content w=20% corresponding to an initial matric suction of 4.3 MPa for the case of samples prepared with distilled water and a slightly lower value for the case of samples prepared with sodium nitrate solutions (Figure 6.10.b). A constant vertical displacement rate of 0.2mm/min was selected for all the one dimensional compaction tests.
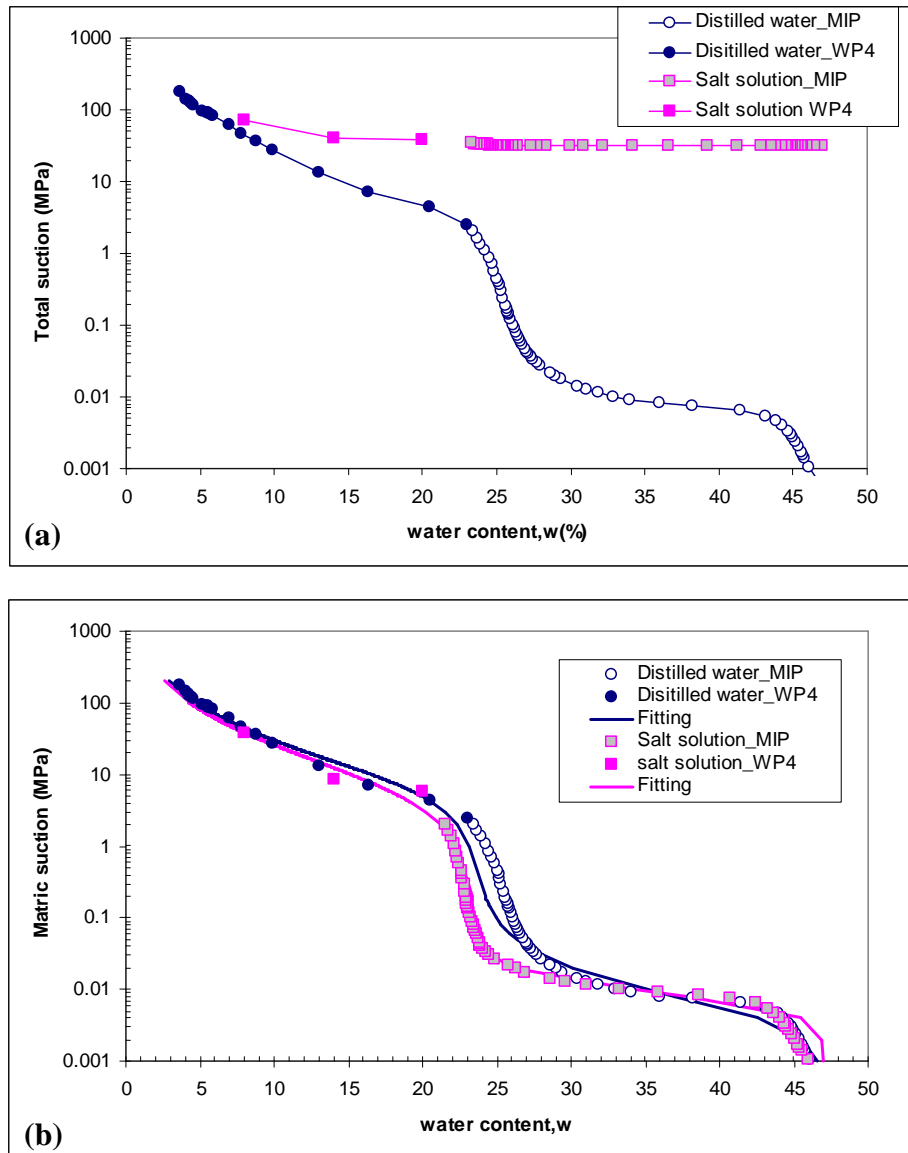

Figure 6.10: Retention curve for samples mixed with distilled water or NaNO$_3$ solution (6.35 M) at γ_d=12 kg/m^3. Results obtained with MIP and WP4 Dewpoint PotentiaMeter.

The specimens were 20 mm high and 50 mm in diameter. The maximum fabrication vertical net stress defines the pre-consolidation stress for the initial suction of the specimens. The maximum static compaction stress was around 200 kPa for the case of samples prepared with distilled water and slightly higher for the case of samples

prepared with $NaNO_3$ solution. Table 6.3 completes the information of the initial conditions.

Table 6.3 Initial properties of soil samples

$\gamma_d(kN/m^3)$	12
w (%)	20
$s_r(\%)$	43
e(-)	1.25
Initial matric suction, $\pi=0$ (MPa)	s=4.3
Initial matric suction, $\pi>0$ (MPa)	s< 4.3
Maximum fabric stress, $\pi=0$ (MPa)	$\sigma_0=0.2$
Maximum fabric stress, $\pi>0$ (MPa)	$\sigma_0>0.2$

The tests were performed in a controlled suction – oedometer cell. The cell which is shown in Figure 6.11, performs oedometer tests on unsaturated soils (maximum 20 mm height in a 50 mm diameter ring) controlling suction through the application of the axis translation technique. The soil specimen rests on a HAEV ceramic disc inside the cell where a controlled air pressure can be applied (Figures 6.11.a and 6.11.b). The HAEV ceramic is installed in a base plate with a 3-mm groove in the form of a spiral. The ceramic presents the following properties; air-entry value: 1.5 MPa, thickness: 7.40 mm, diameter: 50 mm, porosity: 0.32 and water permeability: 5.64×10^{-11} m/s. The upper coarse porous stone (Figure 6.11.a) is made up of metallic grains with sizes gradually varying between 600 and 90 μm (in contact with soil). Diaphragm pressure up to 2.0 MPa is pneumatically applied with compressed air (Figure 6.11.a), which is controlled by air regulators. The combination of regulators with pressure transducers allows the control of pressures within a resolution of 1kPa. A 1-mm thick rubber membrane separates the diaphragm pressure chamber from the pore-air pressure chamber (Figure 6.11a, b). Vertical displacements are measured with a dial gauge (Figure 6.11.c). The cell is connected to a standard pressure/volume controller which is a water pressure source and volume change gauge composed of a stepping motors and a screw-drive accurate piston which directly pressures water (Figure 6.11.c).
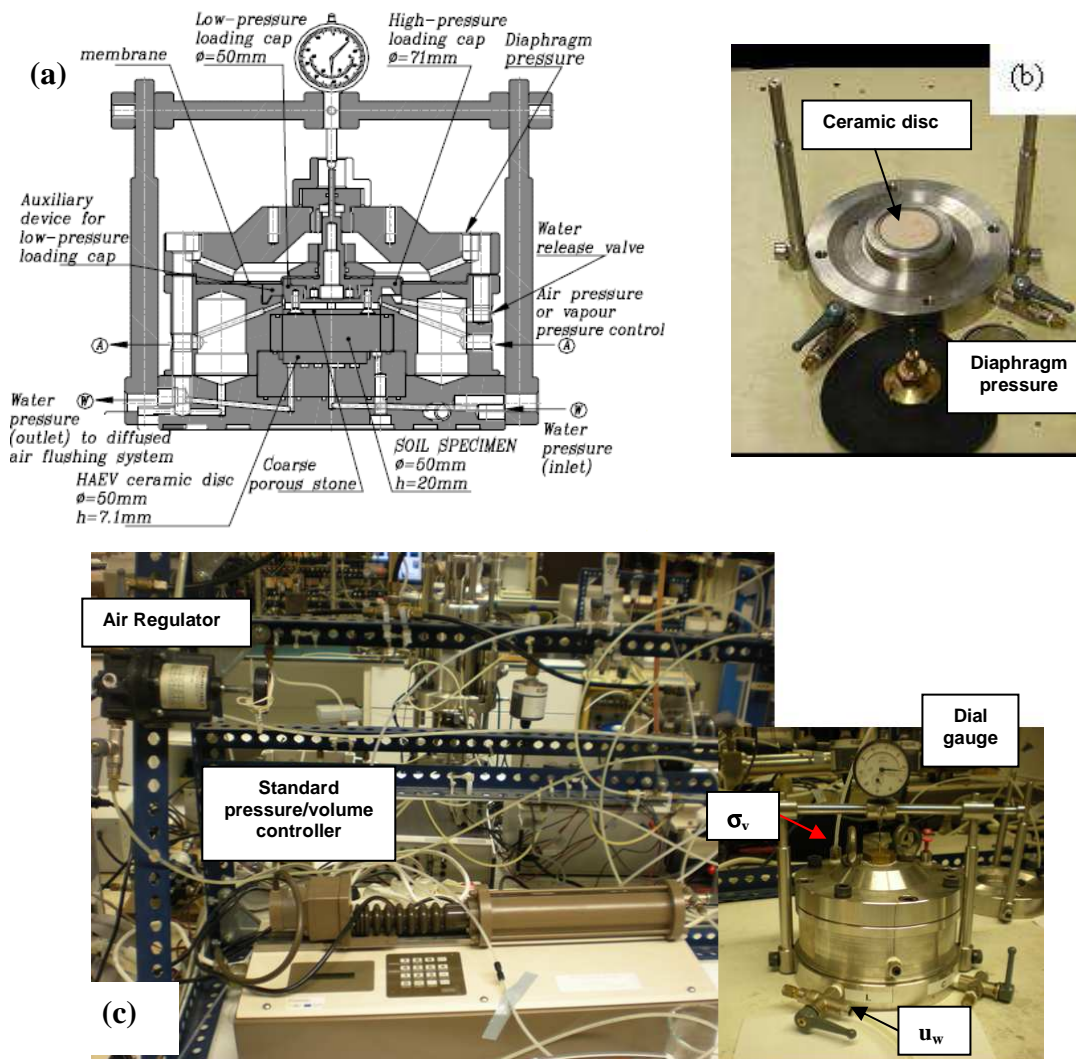
Figure 6.11: Controlled suction oedometer cell. (a) Schematic vertical section. (b) Ceramic disc and diaphragm membrane.(c) Pneumatic and Hydraulic conditions

Three different solutions were used to prepare the tested samples: 0 M $NaNO_3$ (distilled water) (sample1 and 4), 4 M $NaNO_3$ (sample 2) and 5.4 M $NaNO_3$ (sample 3). The tested samples have osmotic suctions of 0 MPa, 11.21 MPa and 20.4 MPa (Equation 4.3). Once compacted the samples were placed in the oedometer cell and the following steps were followed (Figure 6.12),

- Wetting path AB at a low vertical net stress (σ_v-u_a) the samples were allowed to equilibrate to reach the target matric suction 500 kPa (samples 1, 2 and 3). For each sample the osmotic suction was maintained constant. For the case of distilled water, one sample (sample 4) has been allowed to reach saturated condition, that is, zero matric suction.

- Loading-unloading path BCD at constant matric suction s=500kPa. The pre and post yield compressibility parameters for changes in vertical net stress, as well as the yield stress, were determined for each total suction level.
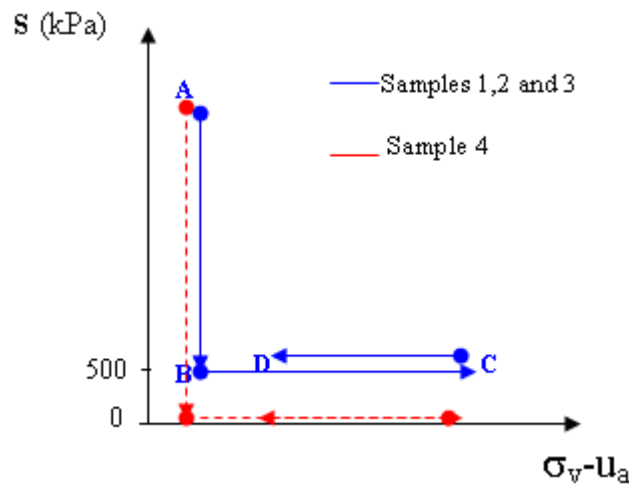

Figure 6.12: Stress path followed on tests under Controlled suction oedometer cell

6.3.1.2 Controlled –suction oedometer results

The influence of pore fluid concentration on clay compressibility has been studied by many authors (e.g. Mesri and Olsen, 1970; Di Maio, 1996; Di Maio et *al.*, 2004; Barbour and Yang, 1993; Barbour and Fredlund, 1989). However, most results refer to dilute solutions. Di Maio (1996) and Di Maio et *al.* (2004) investigated also the case of concentrated salt solutions but as mentioned in Section 1, the tests have been carried out under saturated conditions, and at very high void ratio which is not representative of natural clayey soils encountered under normal circumstances.

Figure 6.13 shows the measured vertical net stress-void ratio relationship for the case of samples 1 and 4 (prepared with distilled water at different matric suctions: s=500 kPa and s=0 kPa).A yield stress of approximately $(\sigma_v - u_a)_0^* \approx 80 \text{kPa}$ was identified. This value defines the pre-consolidation stress at saturated conditions. The post yield compressibility parameter calculated as $\lambda(s) = -\dfrac{\delta e}{\delta \ln(\sigma_v - u_a)}$ is equal to 0.33 for the case of s=0.5 MPa and 0.24 for the case of s=0 MPa. The slope $\lambda(s)$ of the normal compression line showed a significant drop when matric suction was reduced to zero. The normal compression line for zero matric suction (saturated conditions) fell considerably below the normal compression line for s=500 kPa. This variation of

166

$\lambda(s)$ is not consistent with the proposals of Alonso et *al.* (1990) who proposed a monotonic decrease of $\lambda(s)$ with increasing matric suction so that the normal compression line for different values of suction diverged with increasing the vertical net stress. The behavior shown in Figure 6.13 is however similar to the result obtained by Wheeler and Sivakumar (1995) and Sun et *al.* (2004).
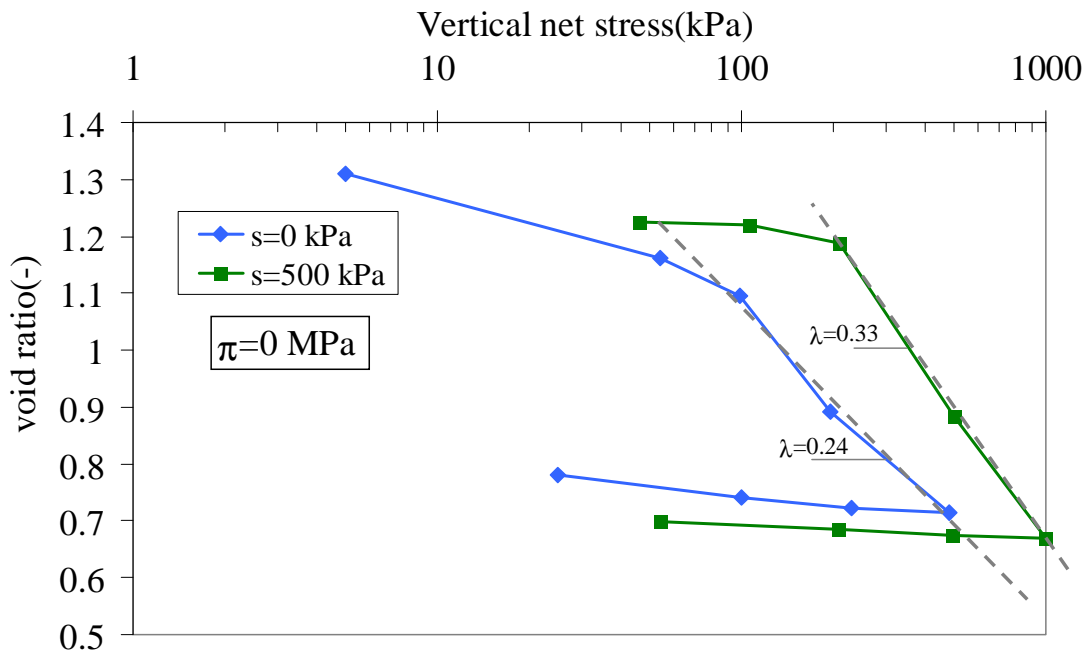

Figure 6.13: Vertical net stress-void ratio relationship for samples 1 and 4 prepared with distilled water.

Figure 6.14 shows the measured vertical net stress-void ratio relationship for the three tested specimens (samples 1, 2 and 3). The pre-consolidation stress $(\sigma_v - u_a)^*$ was around 200 kPa for the different osmotic pressures which is consistent with the fabrication stress. Nevertheless, some small increase of $(\sigma_v - u_a)^*$ is detected when π increases. Additionally a slight decrease of the compressibility of the material is observed as the osmotic pressure increases. It appears that the stiffer clusters induced on saline water addition originates a skeleton that requires higher $(\sigma_v - u_a)^*$ on fabrication. The post yield compressibility is not so affected by the large increase of the osmotic pressure.
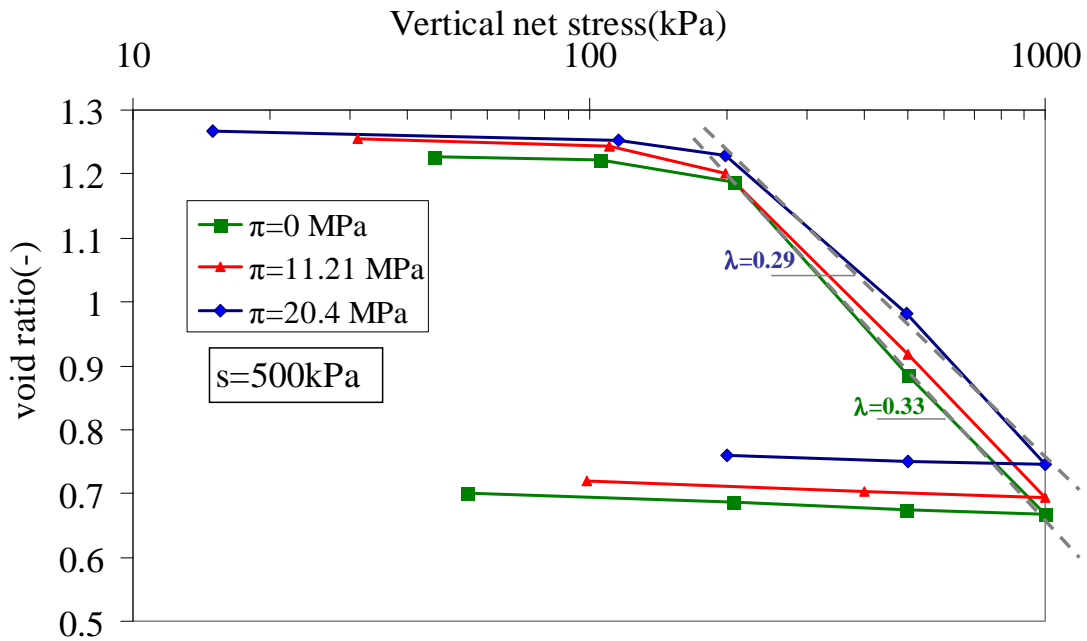
Figure 6.14: Vertical net stress-void ratio relationship for samples 1, 2 and 3 prepared with 0M, 4M and 5.4 M NaNO$_3$ solution respectively.

6.3.2 Oedometer tests under saturated condition

Specimens were prepared by mixing Boom Clay powder with distilled water to slurry at about the liquid limit. The tests were performed in conventional oedometer (Figure 6.15). The samples were loaded to specified stress levels and were then surrounded with NaNO$_3$ solution. Diffusion was allowed to bring the pore fluid in the sample to chemical equilibrium with the surrounding salt solution. The samples were then subjected to loading/unloading path doubling the pressure for successive loads.

Figure 6.16 shows the result obtained for a specimen that was initially loaded while in water up to 50 kPa, and then exposed to a NaNO$_3$ solution (6.53 M NaNO$_3$; π=30.82 MPa) and, once at equilibrium, loaded up to 1000 kPa. Subsequently, it was unloaded to 50 kPa and then re-exposed to distilled water (π=0 MPa).
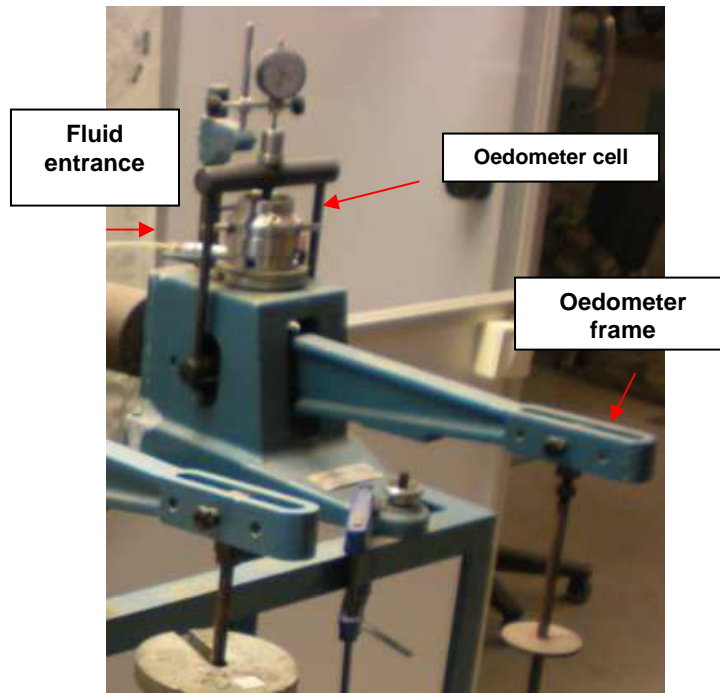
Figure 6.15: Conventional oedometer test´s device
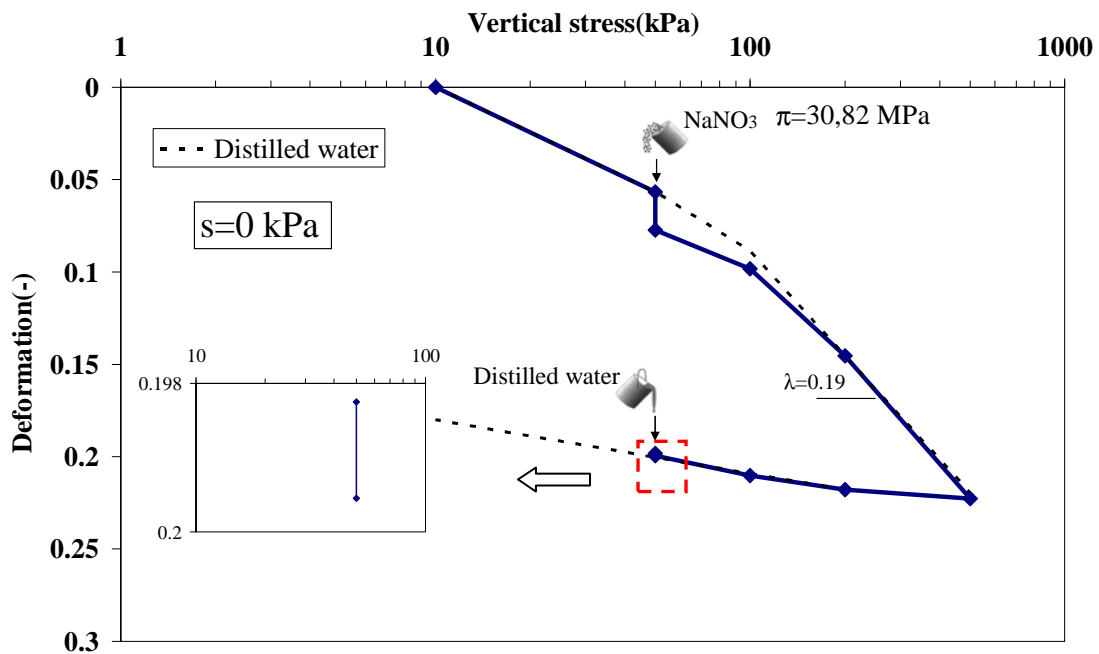
Figure 6.16: Mixed chemo-mechanical loading. Sample initially prepared with distilled water then exposed to high concentration NaNO₃ solution (6.53 M) under σ_v=50 kPa

Figure 6.16 illustrates that exposure to the salt solution produced a decrease in volume of the sample of about ~2%. This volume change was accompanied by an apparent increase in the pre-consolidation stress and a decrease in the compressibility of the sample until this new pre-consolidation stress has been exceeded. At this point, the

sample continues to consolidate along the same virgin branch consistent with the previous results in which no significant dependence of λ on π were observed. A similar result was reported by Barbour and Yang (1993). Upon Re-exposure to distilled water, the sample showed no significant swelling.

Figure 6.17 shows the result obtained for a specimen that was initially loaded while in water up to 200 kPa, and then exposed to a dilute $NaNO_3$ solution (1.72 M $NaNO_3$, osmotic suction π~2 MPa) and, once at equilibrium, loaded up to 1000 kPa. At this stress level the sample was exposed to a high concentration $NaNO_3$ solution (6.53 M $NaNO_3$, π=30.82 MPa). Subsequently, it was unloaded to 10 kPa and then re-exposed to distilled water. As for the previous case exposure to the salt solution produced a decrease in volume of the sample of about ~2.2%. Here the effect of exposure of the soil to a more a dilute solution is not clear as it is combined with an increase of the applied vertical stress in comparison to the case where a high concentrated $NaNO_3$ solution was put in contact to the sample.

No increase of the pre-consolidation stress was observed. In fact, when chemical loading is followed by mechanical loading the slope of the stress strain curve in directly the elasto-plastic one. No significant volume decrease was observed upon exposure of the sample to a higher concentration $NaNO_3$ solution (6.53 M $NaNO_3$, π=30.82 MPa) which suggests that the amount of volume reduction induced by an increase of pore fluid concentration, that is an increase of osmotic suction, depends on the applied stresses. Indeed, Di Maio (1996) and Di Maio et *al*. (2004) showed that the different compression curves of samples prepared with and immersed in NaCl solutions at various concentrations converge towards a narrow range of void ratio in the considered stress range. A similar behavior is observed for the case of partially saturated soil where the magnitude of collapse measured during sample saturation decreases until becoming quite small at high confining stresses (Josa et *al*. 1992, Wheeler and Sivakumar, 1995).

In order to test the reversibility of the effect, the sample was exposed after mechanical unloading to distilled water. As for the previous case, upon re-exposure to distilled water, the sample showed a small swelling. Di Maio (1996) showed that upon re-exposure to distilled water of specimens of Ponza bentonite (Na-Montmorillonite) that

had been previously exposed to KCl and CaCl$_2$, no significant swelling had been observed. The author attributed this result to the substitution of exchangeable Na$^+$ originally present in the bentonite by Ca^{2+} or K$^+$. However, this is probably not the case of the tested soil given that the main exchangeable cation present in Boom Clay is Sodium ion Na+ with the Exchangeable Sodium Percentage (ESP) around 32%, (Romero, 1999). An additional factor could be that the time required to dilute pore water concentration is much higher than during a salinization process. Nevertheless, this has been studied in this work and no significant swelling was observed when distilled water was put in contact with the soil for long period (around 1 year). Finally, further research needs to be done on swelling on dilution of sample with a mechanical stress history.
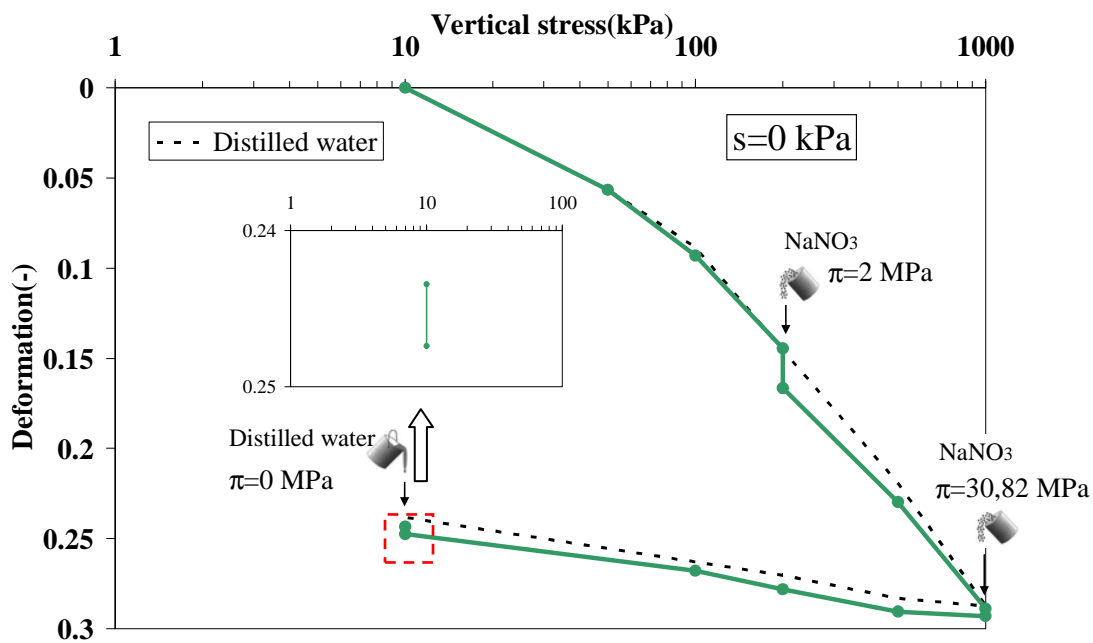

Figure 6.17: Mixed chemo-mechanical loading. Sample initially prepared with distilled water then exposed to a dilute NaNO$_3$ (1.72 M) solution under σ_v=200 kPa

The sample shown in Figure 6.18 was prepared by mixing Boom Clay powder with salt solution (4 M NaNO$_3$, π=11.21 MPa) to slurry at about the liquid limit and then loaded up to 500 kPa. At this stress level the sample was exposed to distilled water. Interestingly, this caused the sample to decrease in volume. A similar result has been shown by Barbour and Yang (1993) for samples prepared and remolded in brine and then exposed to distilled water at a fixed vertical stress of 200 kPa (Figure 6.1.b). At this stage, it is interesting to note that whether the clay soil sample was initially prepared with distilled water or salt solution, if the pore fluid of the samples is replaced

by different solution (salt solution or distilled water), the volume of the soil always decreases. Barbour and Yang (1993) explained this behavior on the basis of the double layer theory. The authors stated that an increase of the pore fluid concentration produces the contraction of the diffuse double layer and the increase of the true effective stress (Chapter 5, Equation 5.34) which causes the contraction of the aggregates and shrinkage of the sample. For the case of Figure 6.18, the stiff and salinized aggregates are expected to adsorb water and thus to become less rigid. Probably, at this elevated stress level (500 kPa) the soil skeleton with less rigid aggregates undergoes contraction. Finally further research needs to be done on dilution at lower stress levels.

The sample was subsequently unloaded to 10 kPa and then re-exposed to $NaNO_3$ solution at higher concentration (5.4 M $NaNO_3$, π=20.4 MPa). A small deformation of about 0.75 % is observed, consistent with compression opposite trend observed on dilution on Figures 6.16 and 6.17.

A similar test has been performed but in this case the sample has been loaded up to 2000 kPa and then exposed to distilled water (Figure 6.19). No significant deformation has been observed. At this elevated stress level and low porosity the change in pore fluid concentration has no important effects. Again it can be said that the amount of volume reduction induced by a change of pore fluid concentration depends upon the applied stress.

6.4 Influence of pore fluid concentration on shear strength of Boom Clay prepared samples

In order, to characterize the effect of pore fluid concentration on shear strength, shear tests have been carried out on compacted samples of Boom Clay initially mixed with $NaNO_3$ solution at different concentrations.

Two sets of tests have been performed in direct shear cells at different vertical stresses:

- A multistage stress tests under controlled matric suction conditions
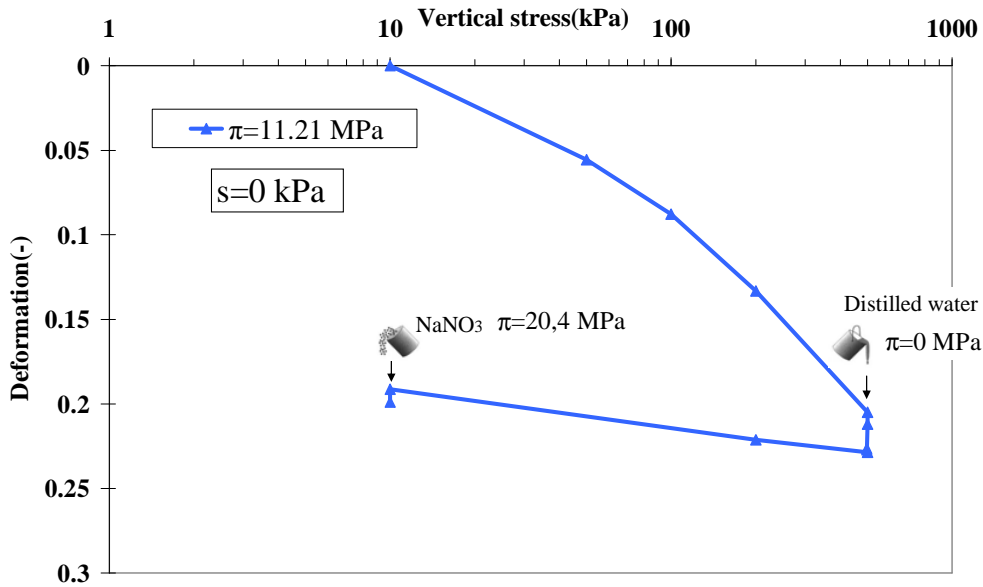- A simple stress stage test under saturated conditions

Figure 6.18: Mixed chemo-mechanical loading. Sample initially prepared with NaNO₃ solution (4M) then exposed to a distilled water under σ_v=500 kPa.
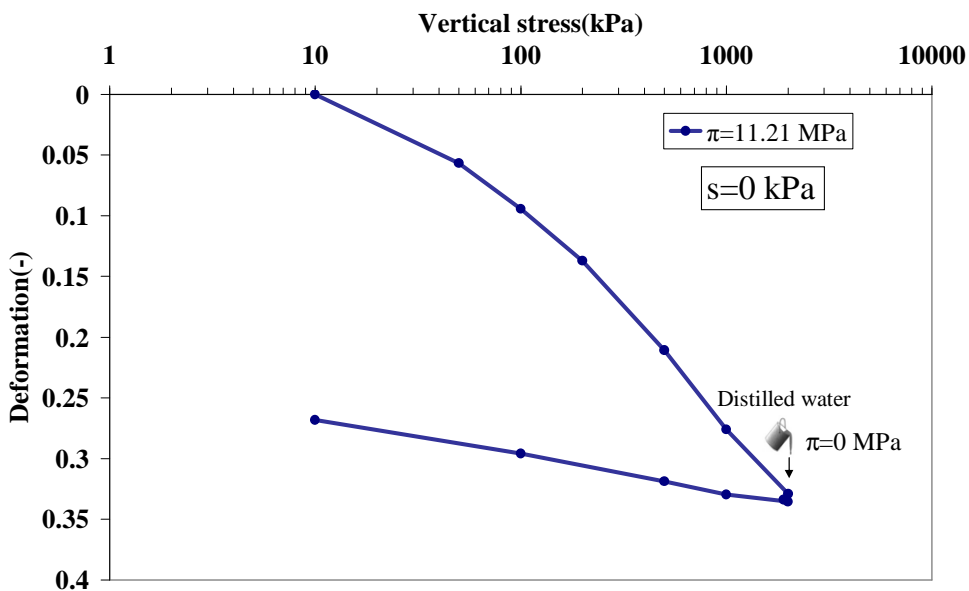
Figure 6.19: Mixed chemo-mechanical loading. Sample initially prepared with NaNO₃ solution (4M) then exposed to a distilled water under σ_v=2 MPa.

6.4.1 Direct shear test under saturated condition

Direct shear test under saturated condition (zero matric suction) was carried out using a conventional direct shear box. A series of 6 direct shear tests were carried out on compacted samples prepared with distilled water and $NaNO_3$ solution. The specimens (60 mm diameter and 25 mm high) initially mixed with distilled water or $NaNO_3$ solution (6.53 M, $\pi=30.82$ MPa) were prepared at a dry density of $\gamma_d=12$ kN/m³ and at a

constant water content w=20%. The samples were loaded up to (σ_v-u_a) =40 kPa and then inundated up to saturation. Distilled water was used as the cell fluid for the case of samples at null osmotic suction while a saline solution (6.53 M $NaNO_3$) were used for the case of samples at an osmotic suction of 30.82 MPa. The equalisation of the sample was assumed based on vertical displacement readings. Once the equilibrium is attained the samples were consolidated up to a fixed normal effective stress and then sheared. For both osmotic suctions (π=0 MPa and π=30.82 MPa), soil samples were consolidated at vertical effective stresses of 100, 200 and 300 kPa. The samples were consolidated in increments and then sheared with a displacement rate of 0.005mm/min.

Figure 6.20 shows the evolution of shear stress for the case of samples mixed with $NaNO_3$ solution and distilled water. The tests results showed that the shear strength increased with increase in osmotic suction. Figure 6.21 shows the data plotted in form of shear strength (value corresponding to 3 mm of horizontal displacement) against applied axial stress for particular salt concentrations. A slight variation in the internal friction angle is observed. Approximately a 1.3° increase in ϕ' has occurred for the samples prepared with and tested in $NaNO_3$ solution. Similar results have been reported by Di Maio (1996) and Barbour and Yang 1993 (Figures 6.3 and 6.4). Di Maio (1996) has shown that for Ponza bentonite samples (80% clay fraction, plasticity index ~320%) prepared with and tested in NaCl solutions at various concentrations, the largest variation occurred in the range 0-0.5 M, and only negligible variations occurred for concentrations higher than 0.5 M (Figure 6.4). However, this was not the case here for Boom Clay samples (65-70% clay fraction, plasticity index ~26.9%), since only a small variation occurred in the range 0 to 6.53 M (nearly saturated $NaNO_3$ solution).
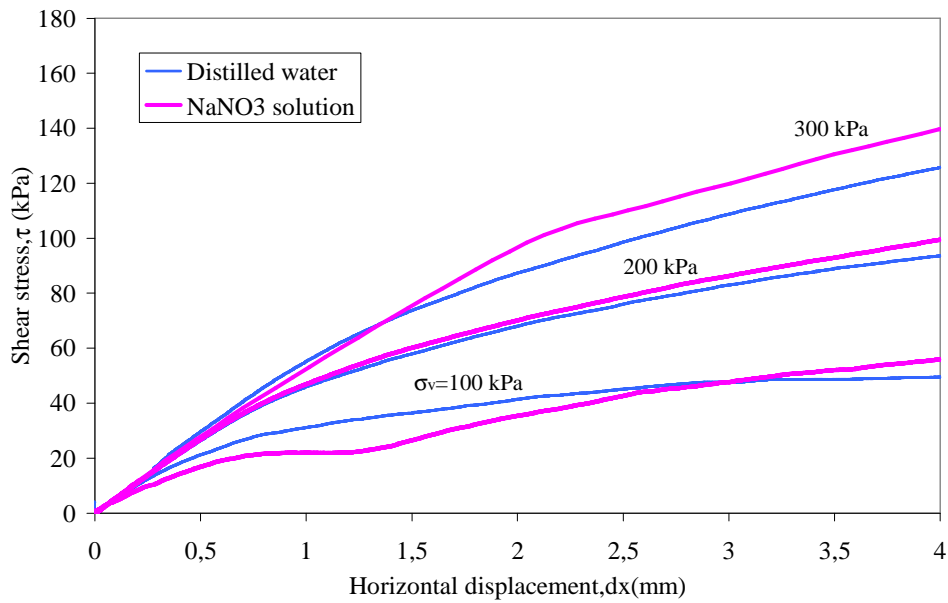
Figure 6.20: Direct shear test performed Boom Clay prepared with various concentration of NaNO$_3$. Shear stress versus horizontal displacement.
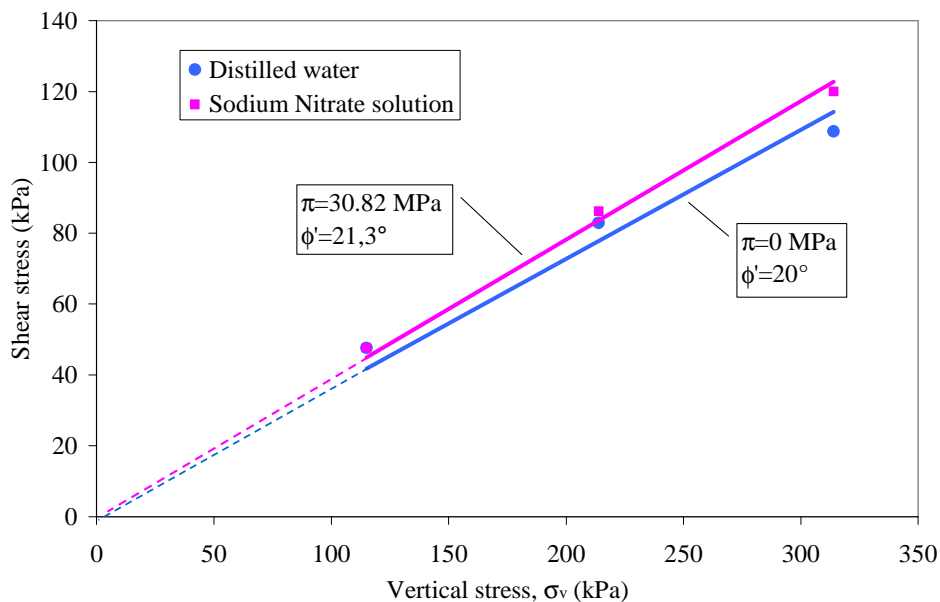
Figure 6.21: Direct shear test performed Boom Clay prepared with various concentration of NaNO$_3$. Failure envelopes.

6.4.2 Controlled suction multistage shear tests

6.4.2.1 Test equipment and procedure

The experimental layout and a schematic drawing of the controlled-suction direct shear cell are presented in Figure 6.22, which is the same cell described by Escario (1990). The shear box of standard design (50 mm diameter and 22 mm high) is enclosed in an air pressure chamber. The lower face of the sample is maintained in contact with the

HAEV ceramic, which is installed in a base plate with 3-mm grooves to facilitate the flushing of dissolved air. The ceramic presents an air-entry value of 1.52 MPa and a water permeability of 4.60×10^{-11} m/s. The vertical load is applied through a 10-mm diameter ram by means of air pressure acting on an airtight piston with a Bellofram seal (air pressure for σv in Figure 6.22). A horizontal extension of the loading ram supports the mobile core of the vertical LVDT (LVDT dy in Figure 6.22). A constant horizontal displacement rate is ensured by the push rod (push rod dx in Figure 6.22), which is transferred to the mobile upper part of the shear box through a 10-mm diameter horizontal ram connected to a load cell. The lower part of the box is fixed. A special bushing is provided to ensure a centred vertical load throughout the test (Figure 6.22.b). This mechanism divides the vertical load in two equal parts, each part acting on a horizontal lever. The levers rest on the centre of the loading cap and on sliding supports at each side of the chamber.

Specimens were prepared by mixing the Boom Clay powder with distilled water and $NaNO_3$ solution prepared at different concentrations. The mixtures were statically and one dimensionally compacted at a dry density of γ_d=12 kN/m^3 and at a constant water content w=20% corresponding to an initial matric suction around 4 MPa. The specimens were 22 mm high and 50 mm in diameter.

Multi-stage controlled-suction direct shear tests are performed on samples at different matric suctions and osmotic suctions. The idea is to investigate the combined effect of both suctions (matric and osmotic suctions) on the variation the shear strength. The samples were tested at two matric suctions (200 and 700 kPa) and three osmotic suctions (0 MPa, 0.75 MPa and 30.82 MPa) corresponding to (0 M, 1M and 6.53 M $NaNO_3$).
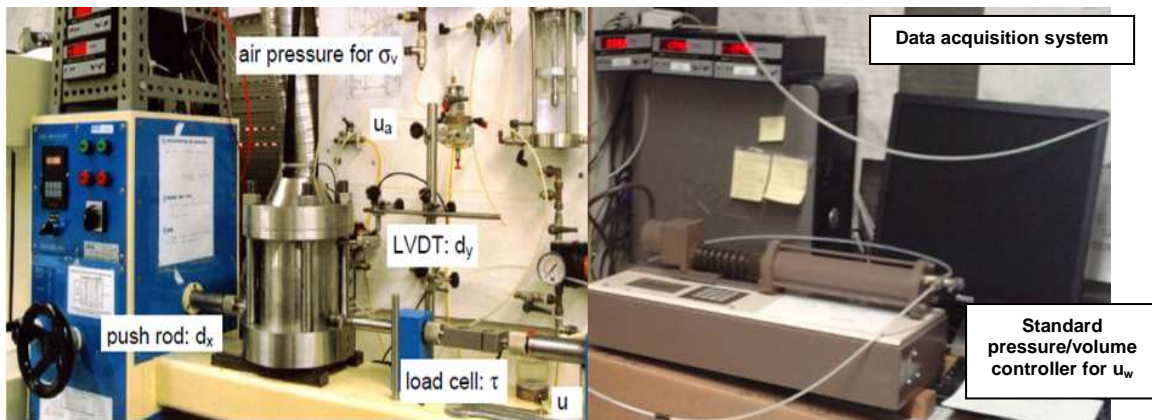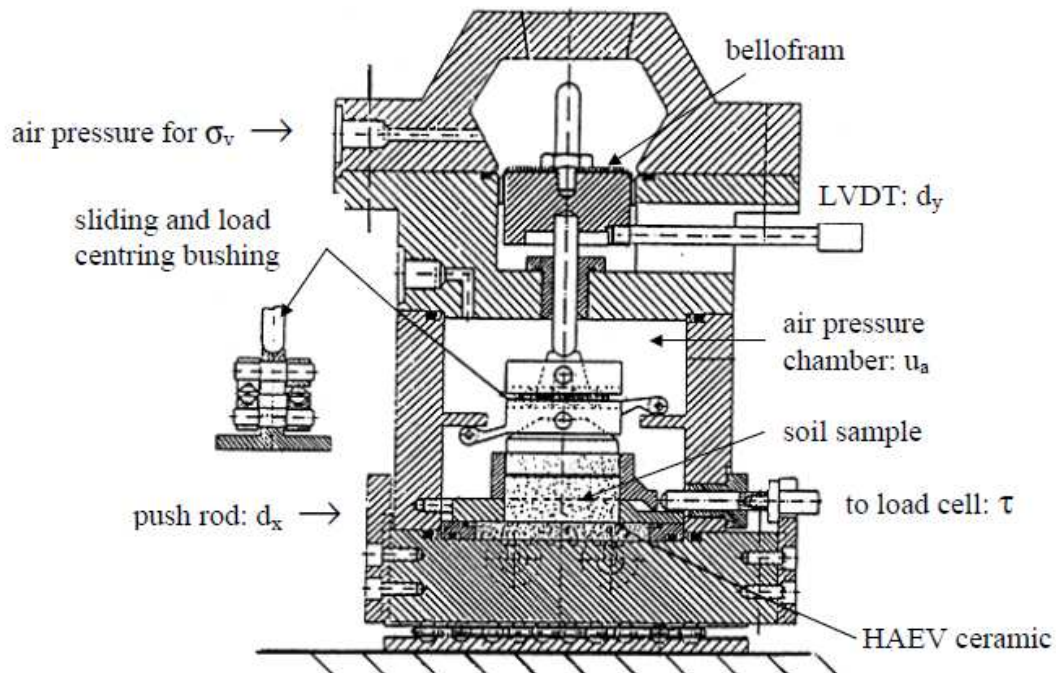
Figure 6.22: Controlled suction direct shear test. Experimental layout.

The multistage protocol involved the following steps (Figure 6.23):

- Wetting path, the samples initially prepared at a given osmotic suction (test A_i: 0MPa, test B_i: 0.75 MPa, test C_i: 30.82 MPa; i=1, 2) were loaded to $(\sigma_v - u_a) = 40$ kPa and then allowed to equilibrate at two target suctions (200 kPa and 700 kPa). Where i=1 denotes the tests performed at a matric suction s =200 kPa and i=2 denotes the tests performed at s=700 kPa.

- Vertical loading and shearing stages, normal net stresses were applied in three stages (100, 300 and 500 kPa) which were maintained for 24 hours before the shearing stages. The samples were then sheared under drained conditions (low

displacement rate of 0.005mm/min). In this way, one sample provided the failure envelope for a given suction.

Figure 6.23: Stress path followed in the controlled-suction direct shear tests

6.4.1.2 Controlled –suction multistage shear results

As described in the previous section, controlled-suction multi-stage shear tests were performed on compacted samples of Boom Clay prep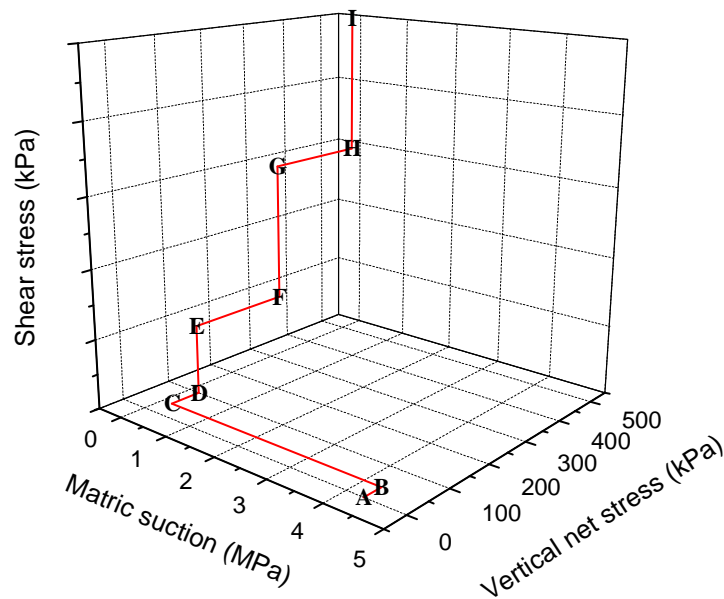ared at three different osmotic suctions 0MPa, 0.75 MPa and 30.82 MPa. In the multi-stage procedure a single specimen was subjected to increasing (σ_v-u_a) values after each shear strength determination. A single stage proving test was performed at (s=700 kPa, π=0.75 MPa and (σ_v-u_a) =500 kPa) and at (s=200 kPa, π=0.75 MPa and (σ_v-u_a) =500 kPa) to check the validity of the procedure for the particular soil under investigation.

Figure 6.24 shows the shear stress and vertical displacement evolutions for test B_2 and the single stage proving test. In test B_2, the sample was wetted to reach s=700 kPa under (σ_v-u_a) =40 kPa. Almost four days are needed for the equilibration stage. The sample were then loaded up to (σ_v-u_a) =100 kPa. After 24 hours the shearing was performed. The second and the third shearing stages were performed at (σ_v-u_a) = 300 and 500 kPa respectively. On the other hand in the proving test (test B'$_2$) after the equalization stage, the sample was loaded in steps up to (σ_v-u_a) =500 kPa and after 24 hours the shearing stage was performed. A slightly higher shearing strength and compression are observed in the case of the single stage shearing test. It is important to remark that the last

shearing stage of the multistage test was only maintained along 1 mm, leading possibly to a reduced value of the shear strength.

A monotonic decrease in volume was always observed on multistage shearing with no peak in shearing strength. This makes the multistage procedure adequate and representative of a normally consolidated state.

Figure 6.24: Shearing stages. Multi shear tests B$_2$ and B'$_2$. (a) Shear stress versus horizontal displacement. (b) Vertical displacement versus horizontal displacement.

Figure 6.25 shows the shear stress and vertical displacement evolutions for test B_1. The sample in this case wetted to reach s =200 kPa. The three shearing stages were performed at $(\sigma_v\text{-}u_a)$ =100, 300 and 500 kPa. A two stage complementary shearing test (test B'_1) were performed under the same hydraulic condition (s=200 kPa). In this case the sample were sheared at $(\sigma_v\text{-}u_a)$ =500 and 750 kPa. As for the previous case a slightly higher shearing strength is observed at $(\sigma_v\text{-}u_a)$ =500 kPa in the case of the two stage shearing test if compared to test B_1. A similar result was obtained by Romero et *al*. (2002) for specimens of sand/ bentonite mixture tested under different suctions.
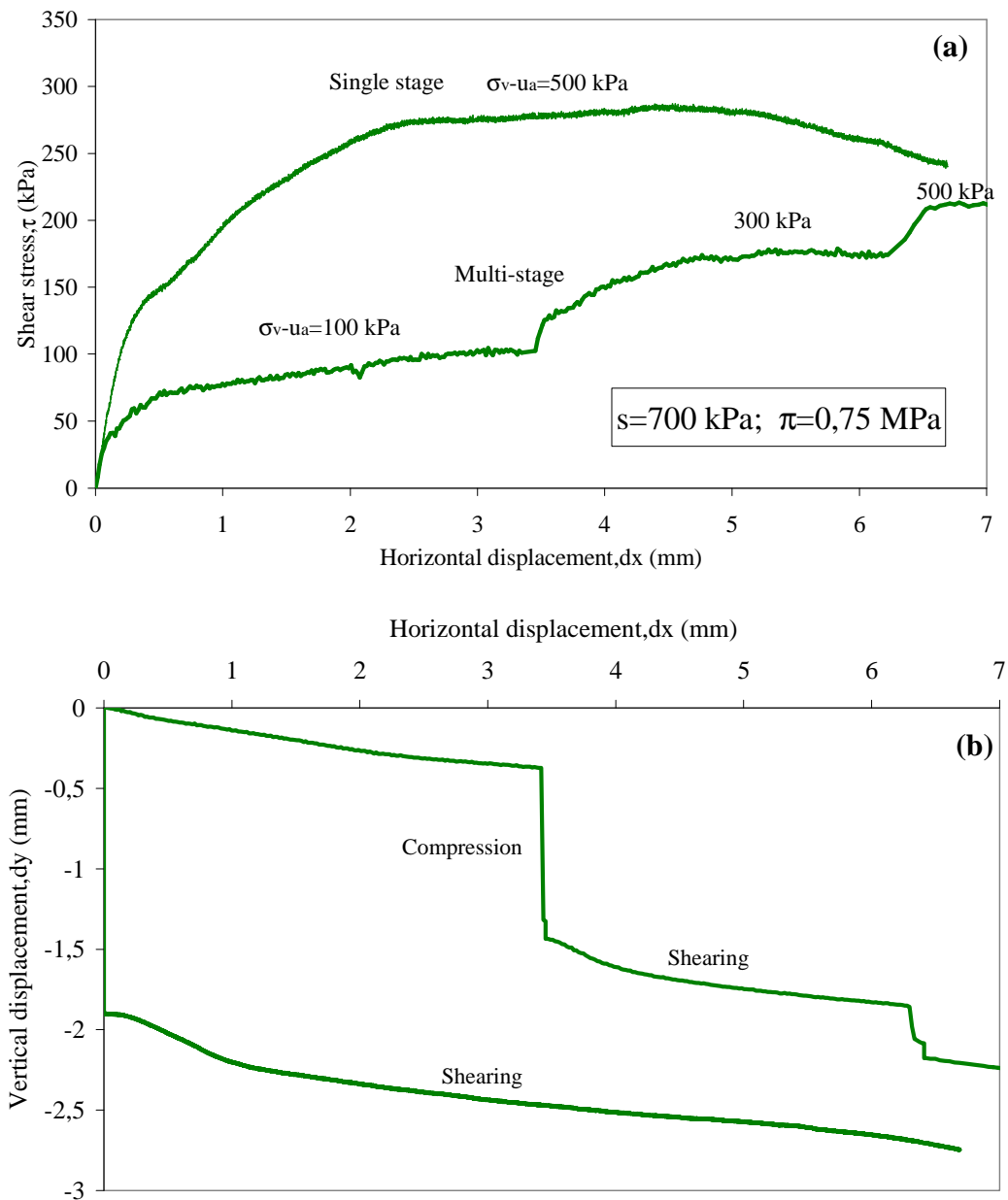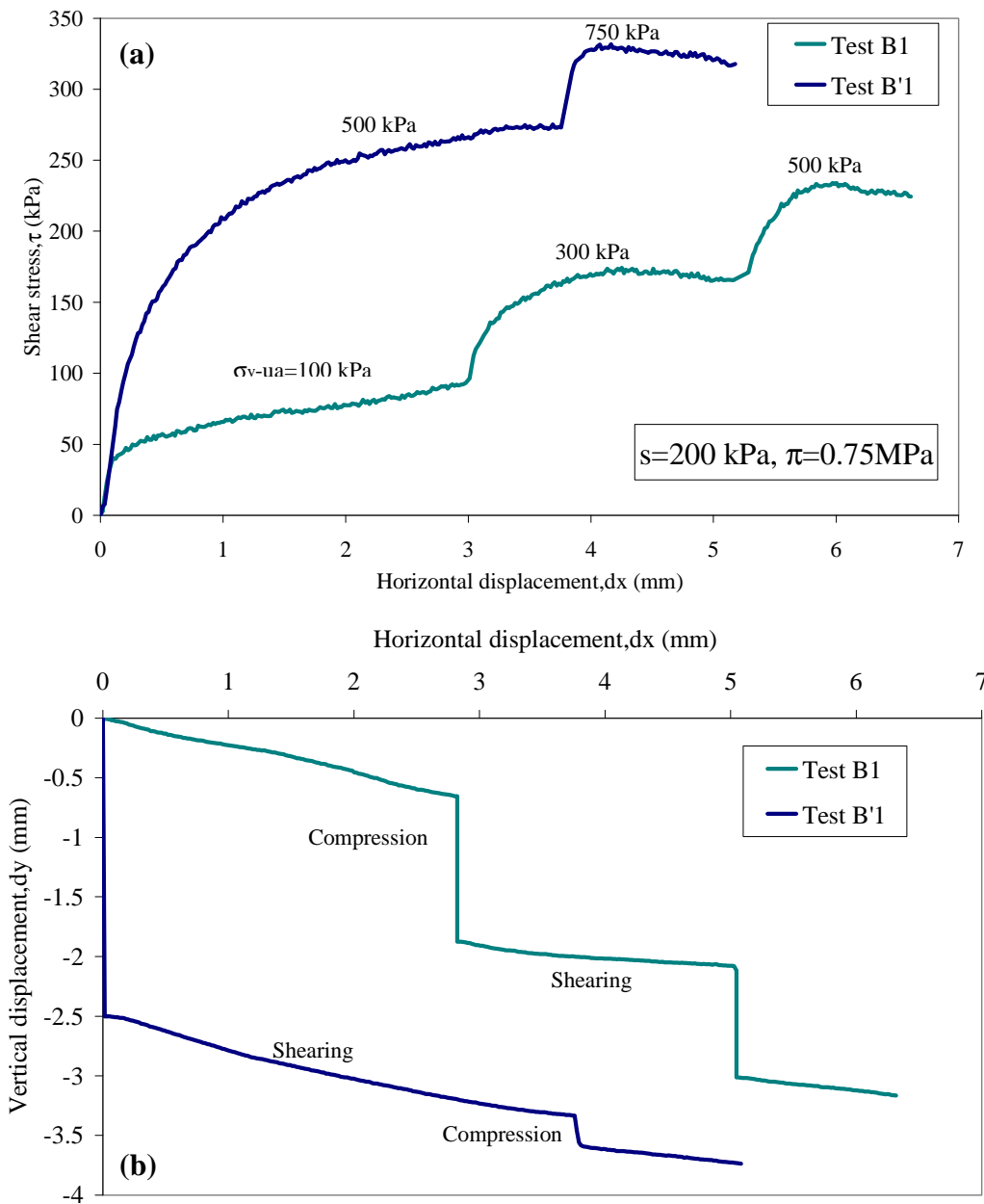

Figure 6.25: Shearing stages. Multi shear tests B_1 and B'_1. (a) Shear stress versus horizontal displacement. (b) Vertical displacement versus horizontal displacement.

Figure 6.26 shows the shear stress evolution of the two multistage tests B_1 and C_1 performed under controlled suction s =200 kPa. The tests results showed that the shear strength decreased with increases in pore fluid concentration that is in osmotic suction, contrary to what was observed in Figure 6.20.
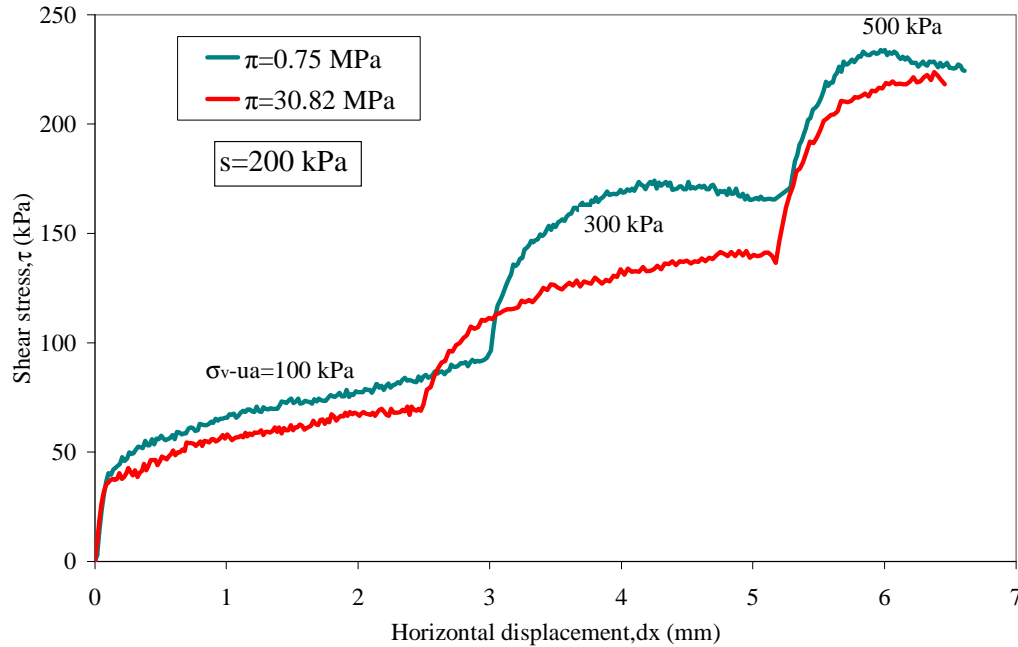
Figure 6.26: Shearing stages. Multi shear tests B_1 and C_1.

Figure 6.27 shows the shear stress evolution of the two multi-stage tests B_2 and C_2 performed under controlled suction s =700 kPa. Test C_2 consisted of two shearing stages. The sample was wetted to reach s=700 kPa under a low (σ_v-u_a) and then allowed to equilibrate for one week. The equalisation of the sample was assumed based on vertical displacement readings. The two shearing stages were performed under (σ_v-u_a) =100 kPa and 300 kPa respectively. The vertical stresses were maintained for 24 hours. In addition, a complementary single stage shearing test (test C'_2) was performed at (σ_v-u_a) =500 kPa (Figure 6.28). Test B_2 was performed at the same target suction. The shearing stages in this case were performed at (σ_v-u_a) =100 kPa, 300 kPa and 500 kPa. In addition as mentioned above, A single stage probing test (test B'_2) were carried out at (σ_v-u_a) =500 kPa. Figure 6.28 shows the shear stress evolution of the two single-stage tests B'_2 and C'_2.

As for the previous case (tests performed at s=200 kPa), the results of the tests performed at a higher matric suction (s= 700 kPa) showed that the shear strength slightly decreased with increase in pore fluid concentration that is in osmotic suction.
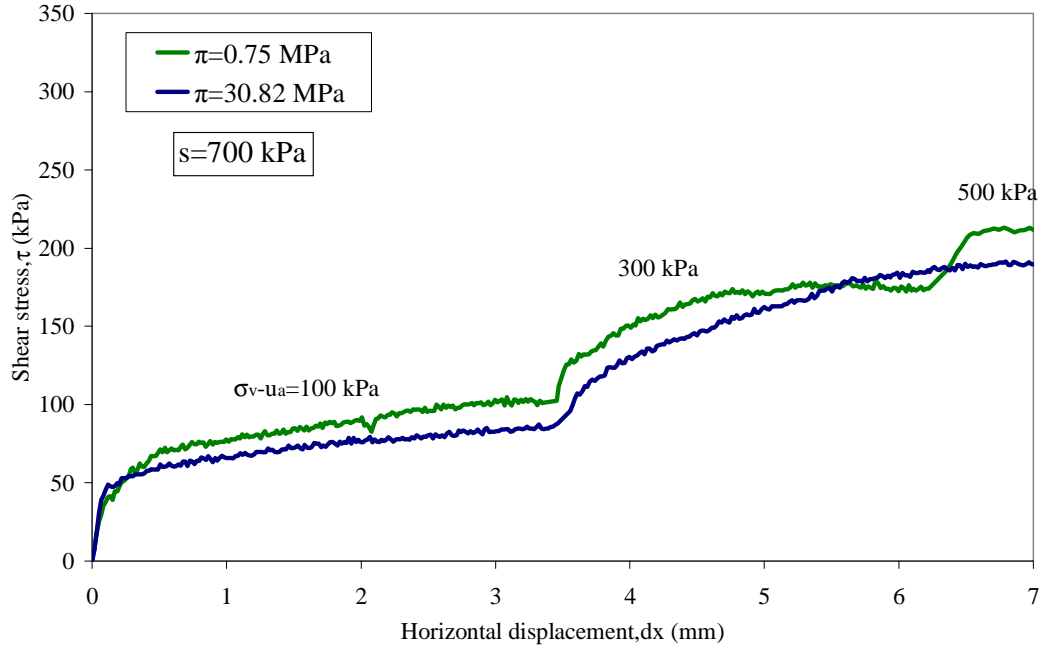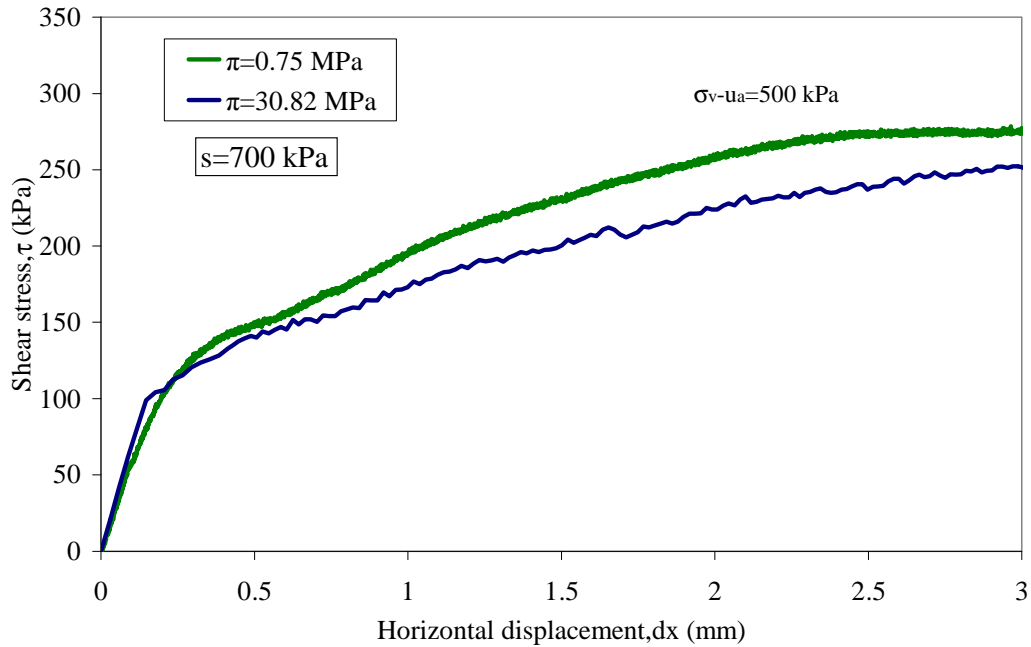

Figure 6.27: Shearing stages. Multi shear tests B$_2$ and C$_2$.

Figure 6.28: Shear stress evolution. Tests B'$_2$ and C'$_2$

In Figure 6.29 the shear strength (the value corresponding to 2 mm of horizontal displacement) is plotted against applied axial stress for the two matric suctions levels (s=200 and 700 kPa) and for π= 0.75 and 30.82 MPa. A decrease of the shear strength is clearly observed at higher osmotic sutions. In addition for both matric suction levels, it is observed that the largest variation occurred for the case of π= 0.75 MPa in comparison to the case of distilled water and only a negligible variation occurred when the osmotic suction was further increased to 30.82 MPa. Di Maio (1996) also showed that largest variation of shear strength of samples of Ponza bentonite prepared at various NaCl concentrations were observed in the range 0-0.5 M NaCl (low osmotic suction).

Figure 6.30 shows the evolution of the shear strength (the value corresponding to 2 mm of horizontal displacement) against the applied osmotic suction at three stress levels and for both matric suctions (s= 200 and 700 kPa). The results show that the variation of shear strength with respect to osmotic suction at a constant net stress is non linear. The rate of change of shear strength is strongly dependent upon the pore fluid concentration. It decreases with pore fluid concentration increase. It is also observed that the rate of change of shear strength with osmotic suction is also dependent upon the applied net stress. In fact no variation is observed for (σ_v-u_a) =100 kPa as the osmotic suction increases.

The variation of *tanϕ*' with osmotic suction at different matric suctions levels is shown in Figure 6.31. At null matric suction, no significant variation of the internal friction angle is observed. Under partially saturated conditions, a marked non linear behavior is observed. A higher influence is observed for dilute solutions. The observed variation seems to level off with a substantial increase of concentration that is of osmotic suction.
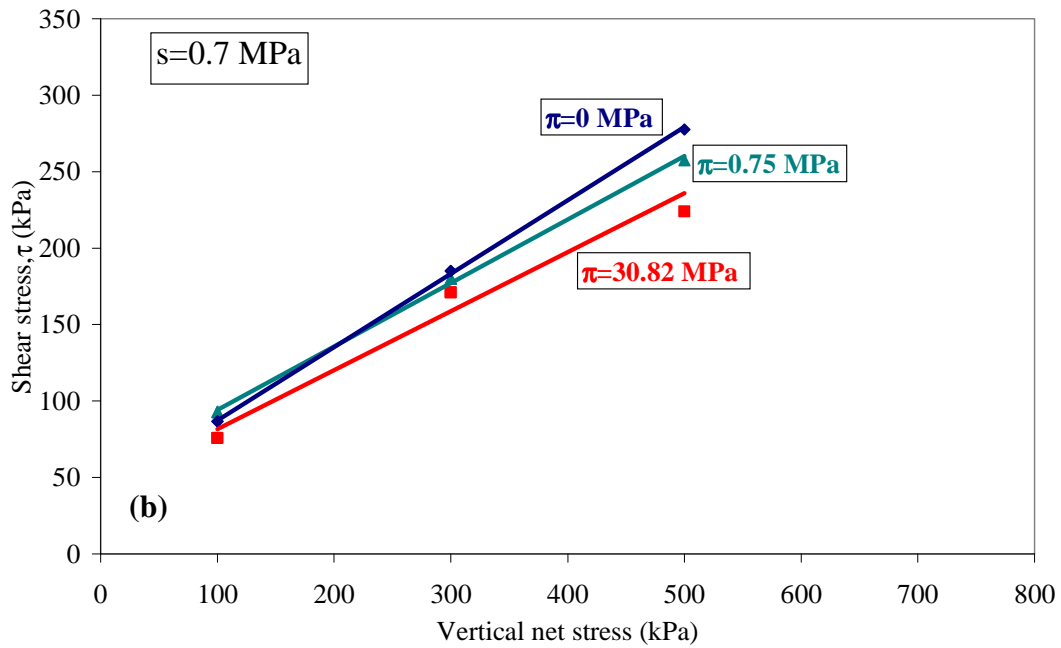
Figure 6.29: Controlled-suction multistage direct shear test performed Boom Clay prepared at various concentration of NaNO₃. (a) Shear strength envelope at s= 200 kPa.(b) Shear strength envelope at s= 700 kPa
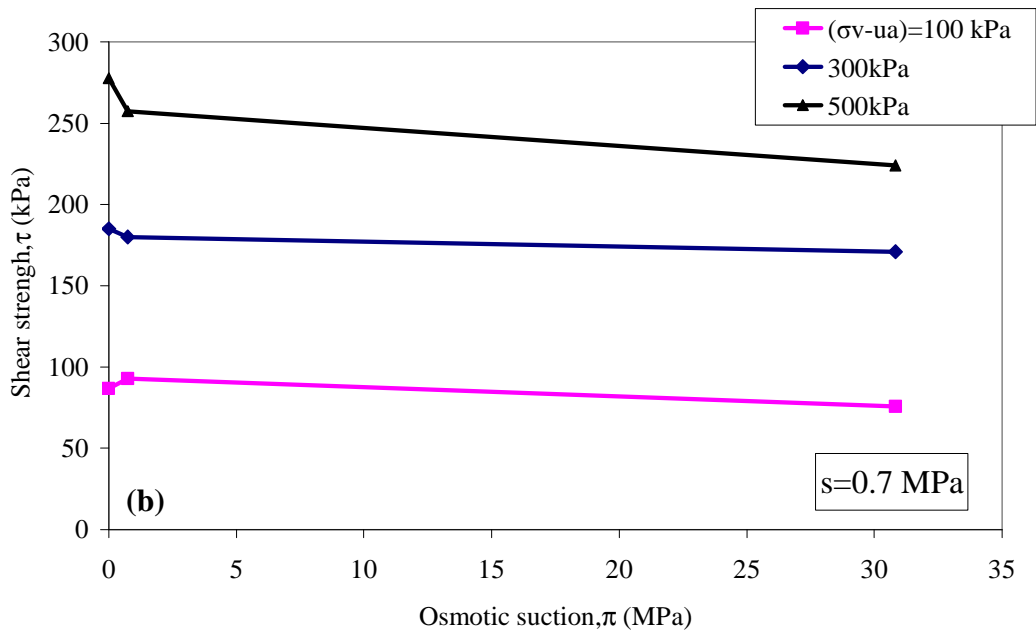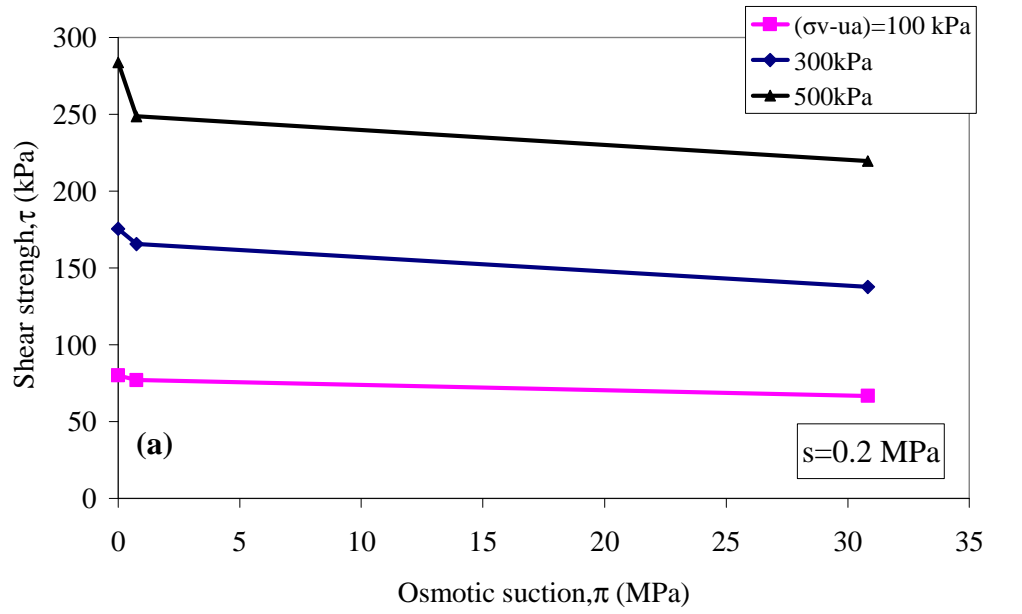
Figure 6.30: Evolution of shear strength with respect to osmotic suction at various net stresses. (a) Case of s = 200 kPa. (b) Case of s= 700kPa.
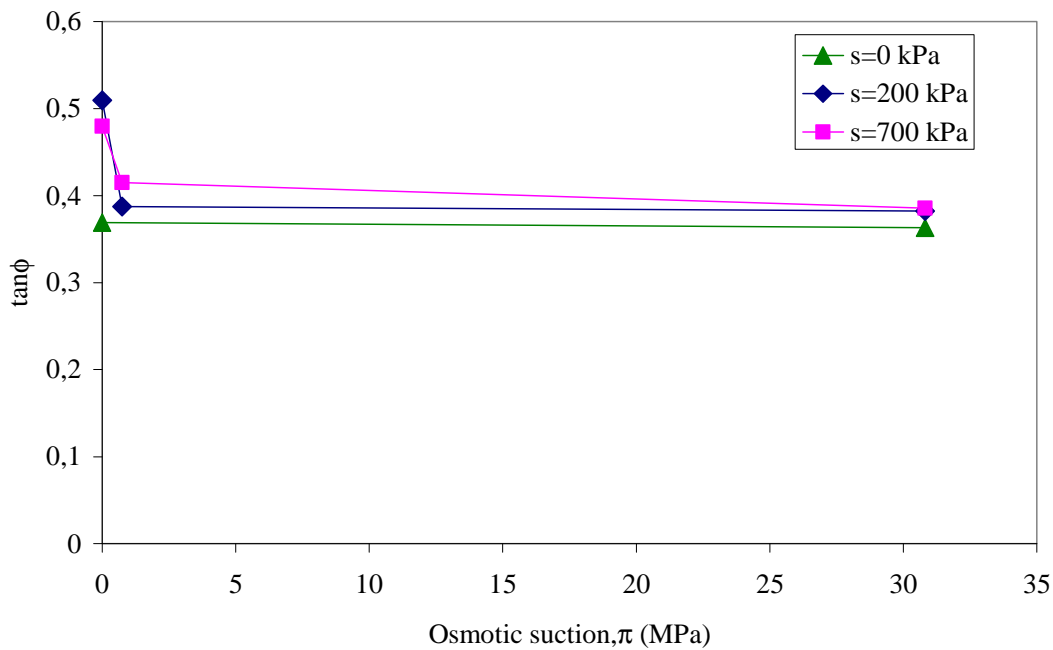
Figure 6.31: Variation of *tanφ* as a function of the osmotic suction for different matric suctions.

Figure 6.32 shows the data plotted in form of shear strength (value corresponding to 2 mm of horizontal displacement) against applied axial stress at different matric suction levels for $\pi = 0.75$ and 30.82 MPa. An increase of shear strength is observed at higher matric suction. For the case of $\pi = 30.82$ MPa, it appears that the gain in strength due to an increment in the vertical net stress at constant matric suction is independent of the suction level (internal friction angle of ~20°). The same behaviour was observed for the case of $\pi = 0.75$ MPa. For both suction levels the internal friction angle is ~22°. However, an increase of the apparent cohesion is observed when the matric suction increases (Figure 6.33).

Figure 6.34 shows the evolution of the shear strength (the value corresponding to 2 mm of horizontal displacement) against the applied matric suction for the case of $\pi=30.82$ MPa, at two stress levels. The results show that the variation of shear strength with respect to matric suction at a constant net stress is non linear, the non-linearity resulting of the diminishing contribution of the matric suction to the shear strength at increasing matric suctions values. Similar results have been reported by several authors (e.g. Fredlund et *al.*, 1996; Vanapalli et *al.*, 1996; Sivakumar et *al.*, 2006).
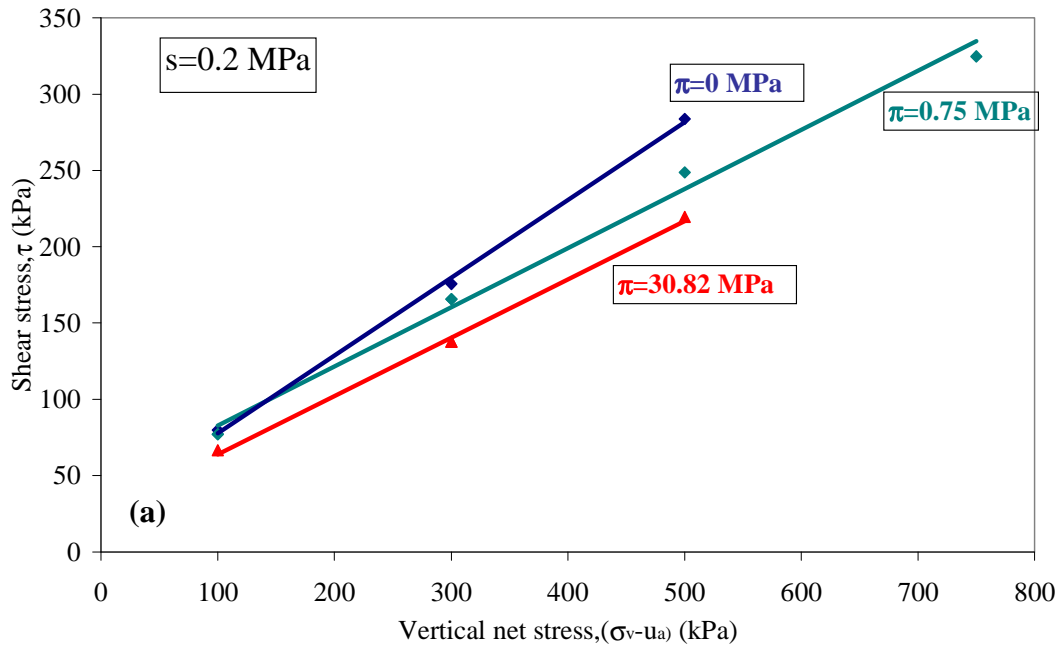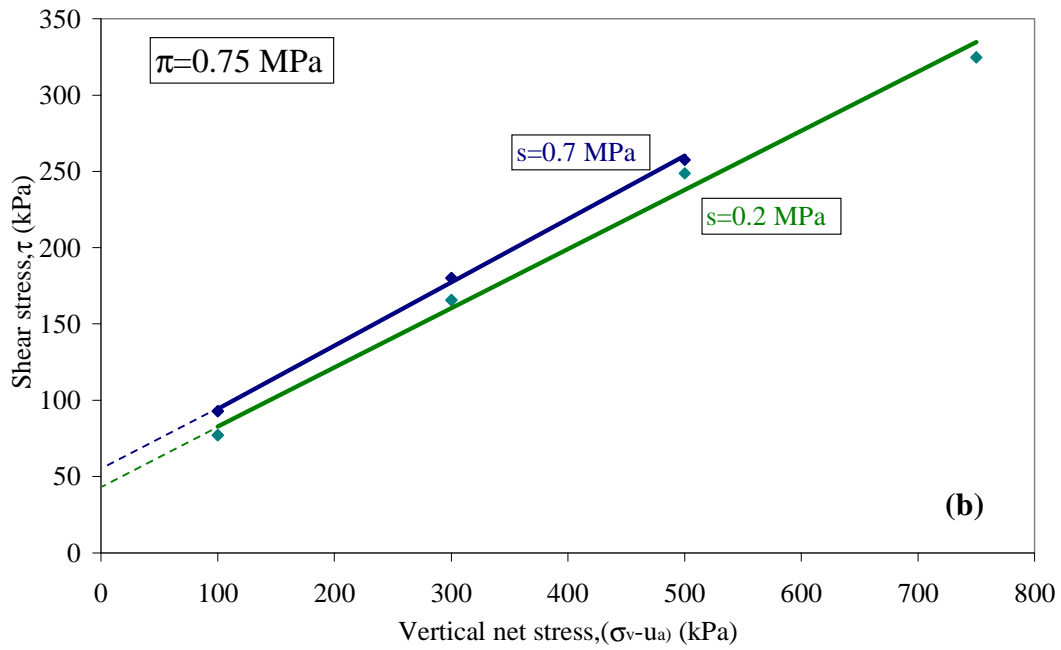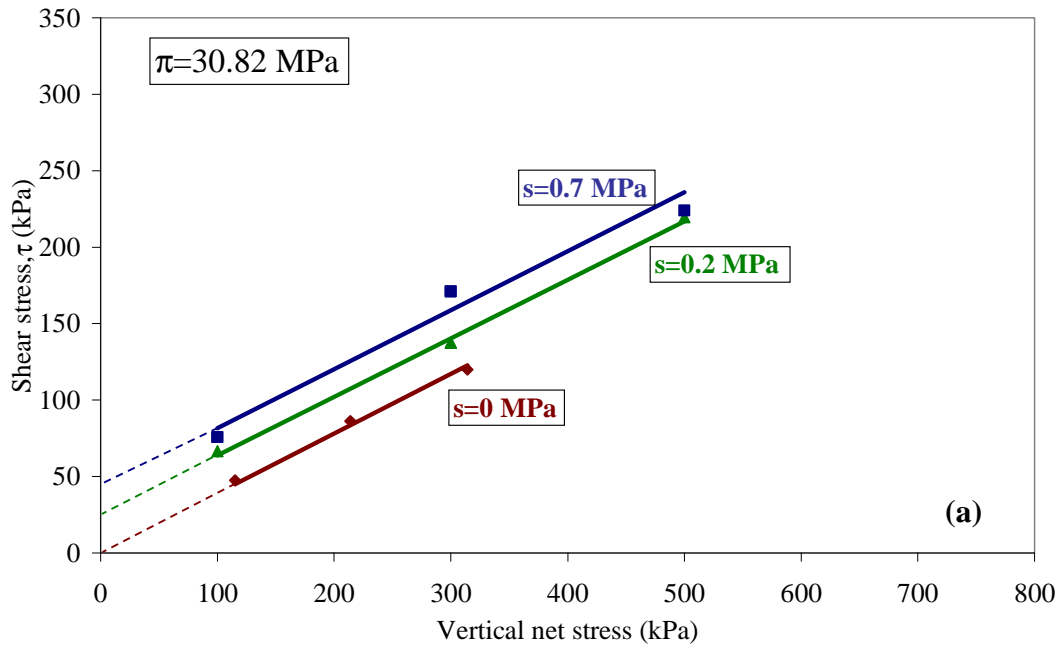
Figure 6.32: Controlled-suction multistage direct shear test performed Boom Clay prepared at various matric suctions. (a) Shear strength envelope at c= 6.53 M. (b) Shear strength envelope at c= 1M.
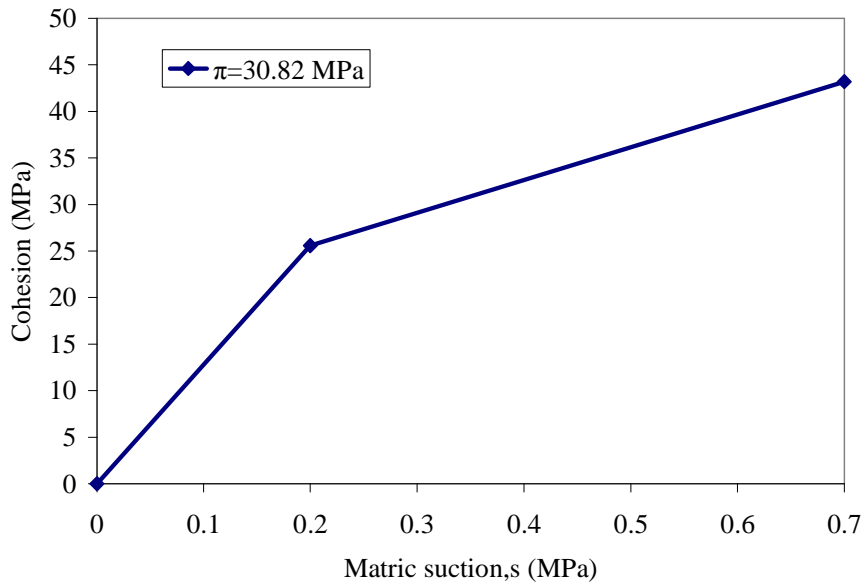
Figure 6.33: Variation of apparent cohesion with matric suction for the case of π=30.82 MPa.
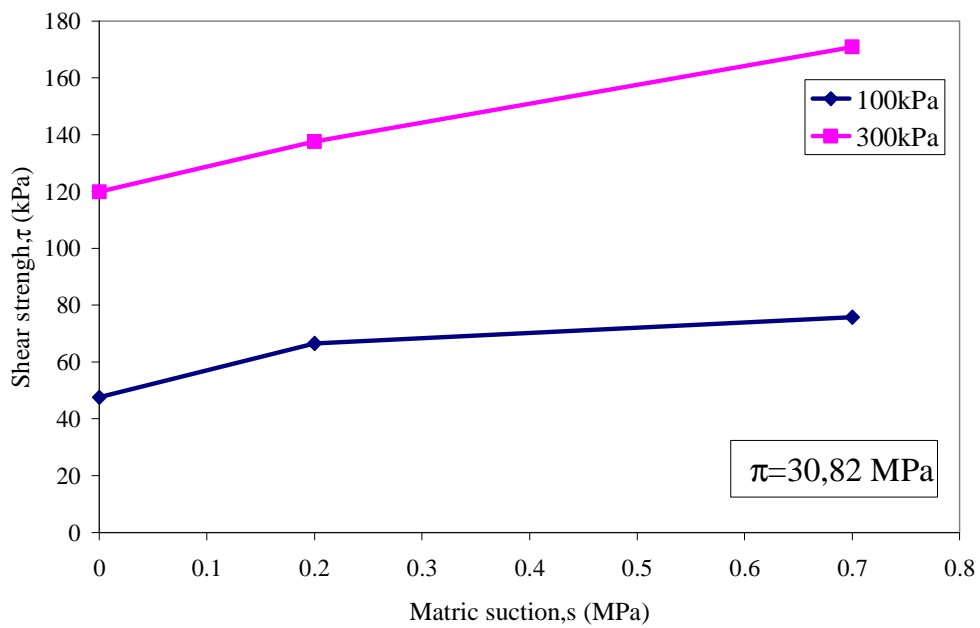
Figure 6.34: Evolution of shear strength with respect to matric suction at various net stresses for the case of π=30.82 MPa.

6.5 Summary and Discussion

In this chapter, the influence of pore fluid concentration and the chemical path (salinazation/dilution) on the geotechnical properties and behavior of Boom Clay prepared samples under partially saturated conditions is investigated (shear strength and

volume change behavior). The investigation illustrates that increase of pore fluid concentration has a significant influence on a number of soil properties.

It has been observed that under partially saturated conditions an increase in salinity causes a slight decrease in compressibility (Figure 6.14) and shear strength (Figures 6.26, 6.27 and 6.28). These trends, however, differ from those reported in the literature. Di Maio (1996), Di Maio et *al.* (2004), Barbour and Yang (1993) among others, have shown that when clay soils are permeated with a saline solution an increase of salt concentration decreases the soil compressibility and results in a higher strength. It is important to remark that these tests were performed under saturated conditions (s=0 MPa). In addition most of the tested specimens described in these researches were prepared by exposure of soil specimens initially mixed with distilled water and then permeated with brine. This method represents the situation where the original soil structure is partly intact while the pore fluid is being replaced, that is short term exposure to salt solution. Nevertheless, Di Maio (1996), Di Maio et *al.* (2004) also performed shear tests on samples initially reconstituted with brine and an increase of shear strength were also observed in this case. However, the material prepared with brine showed a lower void ratio which probably contributed to the increase in strength associated with the increase of pore solution concentration.

The specimens used in this study have been prepared by mixing the Boom Clay powder with $NaNO_3$ solution. The samples were compacted at $\gamma_d=12$ kN/m^3 and w=20%. Initial void ratio for all the tests was around e=1.25 and thus permitting a well defined initial state. This method simulates long-term exposure to salt solution wherein the pore solution is allowed to form a different soil structure. Indeed, MIP tests offered an interesting preliminary evidence of the effect of pore fluid concentration on the long term structural distribution of Boom Clay samples (Figure 6.6.b). In addition this change of structure is accompanied by a slight change in retention properties (Figure 6.10.b)

The suction controlled oedometer tests have shown that the samples display a slight increase of pre-consolidation stress and a decrease in compressibility when the pore fluid concentration increases. This implies that soil specimens prepared with solution at different concentrations and compacted to the same dry density (same void ratio) will

require a slightly higher static compaction stresses probably due to the somewhat stiffer aggregates induced by higher concentrations. Despite the stiffer behavior, these specimens, when tested under shear conditions show lower strength with the increase of pore fluid concentration. Similarly, Warkentin and Yong (1963) reported that for Na-saturated montmorrillonite, strength at constant void ratio decreased with increasing salt concentration.

It has to be noticed that samples prepared with $NaNO_3$ solution have shown a decrease in water content at a given matric suction (Figure 6.10). The observed reduction in shear strength may also be a consequence of the lower water content of the material equalized at given matric suction with the electrolyte. In fact the dependency of shear strength on saturation degree or water content has been widely investigated (e.g. Fredlund et *al.*, 1996; Vanapalli et *al.*, 1996; Sivakumar et *al.*, 2006). This fact shows the importance of determining the skeleton properties in term of matric suction at different concentration i.e. at different osmotic suctions.

Oedometer tests performed under saturated conditions have been also carried out on Boom Clay samples prepared with distilled water and then exposed to $NaNO_3$ solution at various concentrations. This short term permeation has produced a decrease in volume of the samples. Following saline permeation some samples also appeared to have undergone an increase of the pre-consolidation stress. If fact, when the pore fluid is changed from distilled water to salt solution there is transfer of water from the microstructure towards the macrostructure, this causes the contraction of the clay clusters inducing stiffer aggregates. Under constant vertical stress, there is shrinkage of the sample causing the decrease of the compressibility and an increase in the pre-consolidation stress. Once this pre-consolidation pressure is exceeded the soil consolidates along the distilled water compression line. It appears that short term exposure to salt solution does not significantly change the soil structure. A similar conclusion was reported by Barbour and Yang (1993) (Figure 6.1.a).

Finally, after loading/unloading cycle re-exposure of the sample to distilled water produced a negligible swelling deformation. This suggests that chemical effects are strongly affected by the mechanical loading history.

6.6 References

Abdullah, W.S., Al-Zou'bi, M.S., and Alshibli, K.A.: On the physicochemical aspects of compacted clay compressibility. Can. Geotech. J. 34, 551–559, (1997).

Alawaji, A.: Swell and compressibility characteristics of sand–bentonite mixtures inundated with liquids. Appl Clay Sci. 15, 411–430, (1999).

Alferi, M., Romero, E., and Manassero, A.D.: LNAPL retention in partially saturated silty sand. . Proc. 5rd Int.Conf. on Unsaturated Soils, UnSAT 2010, Alonso and Gens (EDS.), Barcelona, Spain Vol.2, p.1445-1450, (2010).

Alonso, E. E., Gens, A., and Josa, A.: A constitutive model for partially saturated soils. Géotechnique 40(3), 405-430, (1990).

Alonso, E.E.: Modeling expansive soil behaviour", Proc. 2nd Int. Conf. Unsaturated soils, China, 37-70, (1998).

Anandarajah, A.: Mechanism controlling permeability change in clays due to changes in pore fluid. J Geotech Geoenviron., 129, 163–172, (2003).

ASTM. Annual book of ASTM standards, Vol. 14.03, Philadelphia, (1993).

Barbour, S.L.: Osmotic flow and volume change in clay soils. Ph.D. Dissertation, Departement of Civil Engineering, University of Saskatchewan, Saskatoon, (1986).

Barbour, S., Fredlund D.: Mechanisms of osmotic flow and volume change in clay soils. Can. Geothec. J., 26, 551-562, (1989).

Barbour, S.L., and Yang, N.: A review of the influence of clay-brine interactions on the geothecnical properties of Ca-montmorillonitic clayey soils from western Canada. Can. Geotech. J., 30, 920-934, (1993).

Bernier F., Li X.L., Bastiaens W., Ortiz L., Van Geet M., Wouters L., Frieg B., Blümling P., Desrues J., Viaggiani G., Coll C., Chanchole S., De Greef V., Hamza R., Malinsky L., Vervoort A., Vanbrabant Y., Debecker B., Verstraelen J., Govaerts A., Wevers M., Labiouse V., Escoffier S., Mathier J.-F., Gastaldo L., Bühler Ch. SELFRAC: Fractures And Self-Healing Within The Excavation Disturbed Zone In Clays- Final report, European Commission, CORDIS Web Site, EUR 22585, (2006).

Boukpeti, N., Charlier, R., Hueckel, T., and Liu, Z.: A Constitutive Model for Chemically Sensitive Clays Robert Hack, Rafig Azzam, and Robert Charlier (Eds.): LNES 104, 255–264, (2004).

Castellanos, E., Gens A., Lloret A., and Romero E.: Influence of water chemistry on the swelling capacity of a high density bentonite. Unsaturated soils. Geotechnical Special Publication No. 147 (ISBN 0 7844 0802 5). Proc. 4nd Int. Conf. on Unsaturated soils, Carefree, Arizona. April 2-6, 2006. ASCE, Reston, Virginia, 1: 963-972.

Castellanos, E., Villar, M.V., Romero, E., Lloret, A., and Gens, A.: Chemical impact f the hydro-mechanical behaviour of high-density Febex bentonite. Phys Chem Earth., 33, 516-526, (2008).

Cardoso, R., Romero, E., Lima, A., and Ferrari, A.: a comparative study of soil suction measurement using two different high-range psychrometers. Experimental Unsaturated Soil Mechanics. Springer-Verglag, Berlin, 2007, 79-93.

Cey, B.D, Barbour, S.L., and Hendry, J.M.: Osmotic flow through Cretaceous clay in southern Saskatchewan, Canada. Can. Geotech. J., 38: 1025–1033, (2001).

Coll C., Escoffier S., Hamza R.W., Vervoort A., Blümling P., Frieg B., Bastiaens W., Berest P., Bazargan B., Desrues J., Viaggiani G., Labiouse V., Dehandschutter B., Wouters L., Vanbrabant Y., Mertens J., Li X.L., Bernier F. EC SELFRAC Project – FIKW-CT-2001- 00182, Deliverable 1: State of the art on Fracturation and Sealing-Healing Processes and Characterisation, EURIDICE, (2004).

Delage, P., and Lefebre, G.: study of the structure of a sensitive champlian clay and of its evolution during consolidation. Can. Geotech. J., 21:21-35, (1982).

Di Maio, C.: Exposure of bentonite to salt solution: osmotic and mechanical effects. Géotechnique., 46(4), 695-707, (1996).

Di Maio, C., Fenelli, G.: Influenza delle interazioni chimico-fisiche sulla deformabilita di alcuni terreni argillosi. Rivista Italiana di Geotecnica 1, 695–707, (1997).

Di Maio, C., Santoli, L., and Schiavone, P.: Volume change behaviour of clays: the influence of mineral composition, pore fluid composition and stress state. Mechanics of materials 36,435-451, (2004).

Escario, V.: Strength and deformation testing of soils under controlled suction. Colloque sur les sols non saturés. EPFL, Lausanne. (1990).

Fernandez, F., and Quigley, R.M.:Viscosity and dielectric constant controls on hydraulic conductivity of clayey soils permeated with water soluble organics. Can. Geotech J.25, 582-589, (1988).

Fredlund, D.G., Xing, A., and Fredlund M.D.: the relationship of the unsaturated soil. Shear strength function to the soil water characteristic curve. Cand. Geotech. J., 32, 40-448, (1996).

Gajo, A., Loret B., Hueckel T.: Electro-chemo-mechanical couplings in saturated porous media: elastic–plastic behaviour of heteroionic expansive clays. Int. J. Solids Struct., 39, 4327–4362, (2002).

Guimaraes L.: Análisis multi-componente no isotermo en medio poroso deformable no saturado. PhD Thesis, Dept. of Geotechnical Engineering and Geosciences, Technical University of Catalonia, Barcelona, Spain, (2002).

Ho, T.A.: the effects of brine contamination on the properties of soils. M.Sc.theis, Departement of Civil Engineering, University of Saskatchewan, Saskatoon. (1985)

Hueckel, T.: On effective stress concepts and deformation in clays subjected to environmental loads: Discussion. Can. Geotech. J., 29, 1120-1125, (1992).

Hueckel, T.: water–mineral interaction in hygromechanics of clays exposed to environmental loads: a mixture theory approach. Can. Geotech. J. 29, 1071-1085, (1992).

Hueckel, T.: Chemo-plasticity of clays subjected to stress and flow of a single contaminant. Int. J. Num. Ana. Methods in Geom., 21, 43-72, (1997).

Josa A., BAlmaceda., Gans., and Alonso E.E.: An elastoplastic model for partially saturated soils exhibiting a maximum of collapse. Proc. 3rd Int. Conf. Computational Plasticity, Barcelona, 815-826, (1992).

Kaya, A., and Fang, H.Y.: The effects of organic fluids on physicochemical parameters of fine-grained soils. Can. Geotech. J., 37, 943–950, (2000).

Liu, Z., Boukpeti, N., Li, X., Collin, F. Radu, J.-P, Hueckel, T., and Charlier, R.: Modelling chemo-hydro-mechanical behaviour of unsaturated clays: a feasibility study. Int. J. Num. Ana. Methods Geom., 29,919–940, (2005).

Loret, B., Hueckel, T., and Gajo, A.: Chemo-mechanical coupling in saturated porous media: elastic–plastic behaviour of homoionic expansive clays. Int. J. Solids Struct., 39, 2773-2806, (2002).

Ma, C.M., Hueckel, T., 1992. Effects of inter-phase mass transfer in heated clays: a mixture theory. Int. J. Eng. Sci. 30(11), 1567–1582, (1992).

Mata, C., Romero, E and Ldesma, A. Hydro-chemical effects on water retention in bentonite sand mixture. Proc. 3rd Int.Conf. on Unsaturated Soils, UnSAT 2002, Jucá, J.F.T., de Campos, T.M.P. and Marinho, F.A.M. (EDS.), Refife, Brazil, Vol.1,p.283-288 (2002).

Mata C.: Hysdraulic behaviour of bentonete based mixture in engineered barriers: the backfill and plug test at the ASPO HRL (Sweben) PhD Thesis, Dept. of Geotechnical Engineering and Geosciences, Technical University f Catalonia, Barcelona, Spain, (2003).

Mesri, G., and Olsen, R.E.: Shear strength of montmorillonite. Géotechnique., 20(3), 261-270, (1970).

Mishra, A.K., Dhawan, S., and Rao, M.: Analysis of Swelling and Shrinkage Behavior of Compacted Clays. Geotech. Geol. Eng., 26, 289–298, (2008).

Mitchell, J.K.: Fundamentals of soil behaviour. 2nd Edition. John Wiley and sons. New York, (1993)

Musso, G., Romero, E., Gens, A., Castellanos, E.: The role of structure in the chemically induced deformation of FEBEX bentonite. Appl Clay Sci., 23, 229-237, (2003).

Musso, G., Romero, E.: chemo-mechanical behavior of high-density bentonites. Imbibitions and diffusion tests. Anvances in understanding engineered clay barriers. E.E Alonso and A. Ledesma (eds). Taylor and Francis Group, London. 283-291, (2005).

Ninjgarav, E., Chung S., Jang W.Y., and Ryu C.: Pore Size Distribution of Pusan Clay Measured by Mercury Intrusion Porosimetry. J. Civil Eng.,11(3),133-139, (2007).

Park, J., Vipulanandan, C., Kim, J.W., and Oh, M.H.: Effects of surfactants and electrolyte solutions on the properties of soil. Environ.Geol, 49, 977–989, (2006).

Picard J.M.: Ecrouissage thermique des argiles saturées : application au stockage de déchets radioactifs. PhD Thesis, École Nationale des Ponts et Chaussées, Paris, p 283. (1994).

Pusch, R.: Experimental study of the effect of high pore water salinity in the physical properties of natural smectic clay. SKB, Technical Report, TR-01-07. Sweden (2001).

Rao, M. and Shivananda, P.: Role of osmotic suction in swelling of salt amended clays. Can. Geotech.J., 42, 307-315, (2005).

Rao, M., Thyagaraj, T., and Thomas, H.R.: Swelling of compacted clay under osmotic gradients. Geotechnique. 56 (10), 707–713, (2006).

Rao, M. and Thyagaraj, T.: Role of direction of salt migration on the swelling behaviour of compacted clays. Appl Clay Sci., 38, 113–129, (2007).

Rhattas, A.: Transfer de masse dans les matériaux argileux á faible porosité. Analyse théorique et résultats expérimentaux. PhD Thesis. Université D'Orleans, (1994).

Romero, E.: Characterization and thermo-hydro-mechanical behavior if unsaturated Boom Clay: an experimental study. PhD Thesis, Dept. of Geotechnical Engineering and Geosciences, Technical University of Catalonia, Barcelona, Spain, (1999).

Romero, E., Alonso, E.E. and Knobelsdorf, J.: Laboratory tests on compacted sand-bentonite buffer material for the GMT emplacement project. Ref.: 010102. January (2002).

Romero, E., and Simms, P.H.: Microstructure Investigation in Unsaturated Soils: A Review with Special Attention to Contribution of Mercury Intrusion Porosimetry and Environmental Scanning. Geotech Geol., 26 (6), 705-727, (2008).

Schmitz, M.: Can the diffuse double layer theory describe changes in hydraulic conductivity of compacted clays?. Geot Geol., 24, 1835–1844, (2006).

Sing, K.: The use of nitrogen adsorption for the characterisation of porous materials. Colloids and Surfaces A: Physicochem. Eng. Aspects., 187–188, (2001)

Sreedeep, S., and Singh, D. N.: Methodology for determination of osmotic suction of soils. Geotech Geol., 24, 1469–1479, (2006).

Sun, D. A., Matsuoka, H. and Xu, Y. F.: Collapse behaviour of compacted clays in suction-controlled triaxial tests, Geotech Test J, ASTM., 27(4): 362-370, (2004).

Studds, P. G., Stewart, D. I., and Cousesns, T. W.: The effects of salt solutions on the Properties of bentonite-sand mixtures. Clay Miner., 33, 651–660, (1998)

Thyagaraj, T. and Rao, M.: Influence of Osmotic Suction on the Soil-Water Characteristic Curves of Compacted Expansive Clay. Geoenviron Eng., 136(12), 1695-1702, (2010).

Van Genuchten, M.T.: A closed form equation for prediction the hydraulic conductivity of unsaturated soils. Soil. Sci.Soc.Am. 44, 379-392, (1980).

Vanapalli, K., FRedlund, G., Pufahl, E.: the relationship between the soil water characteristic curve and the unsaturated shear strength of a compacted glacial till. Geotech. Test. J. 259-268, (1996).

Volckaert, G., Bernier, F., and Darnaise, M.: Demonstration of the in situ application of an industrial clay-based backfill material (Bacchus 2). Publication of the European Communities, EUR 16860 EN, Luxembourg, (1996b).

Warkentin, B.P. and Yong, R.N.: Shear strength of montmorillonite and kaolinite related to interparticle forces. Proc 9th National Conf. on Clay and Minerals. 210-218, (1963).

Weetjens, E.: Characterisation and compatibility with the disposal medium of Eurochemic reprocessing waste forms. Restricted contract report. SCK•CEN-R-3767 03/EWe/P-46, (2003).

Wheeler, S.J., and Sivakumar, V.: An elasto-plastic critical state framework for unsaturated soil. Géotechnique., 45(1): 35-53, (1995).

Yang, N., and Barbour, S.L.: The impact of soil structure and confining stress on the hydraulic conductivity of clays in brine environments. Can.Geotech..J., 29, 730-739, (1992).

Yang, N.: Impact if soil structure and confining stress in the permeability of clayey soils in brine environments. M.Sc.theis, Departement of Civil Engineering, University of Saskatchewan, Saskatoon, (1990).

Yılmaz, G., Yetimoglu, T., and Arasan, S.: Hydraulic conductivity of compacted clay liners permeated with inorganic salt solutions. Waste Manag Res., 26, 464–473, (2008).

Yong, R.N., Mohamed, A.M.O and Warkentin, B.P: Principles of contaminant transport in soils. Development in Geotechnical Engineering, 73, Elsevier, Amsterdam. (1992).

Chapter 7

Summary, Conclusions and Future work

7.1 Summary and conclusions on scientific achievements

In the Belgian radioactive waste management program, the geological disposal of Eurobitum Bituminized radioactive Waste product (BW) is one of the considered options. The Boom Clay, a geologically stable clay formation, is currently investigated as a possible host for a repository that would be situated at a depth between 200 and 300 m. The interaction of a BW and the host formation is complex due to the presence of hygroscopic soluble salts (mainly $NaNO_3$ crystals) embedded in the low porous bitumen matrix. In contact with water, these hygroscopic soluble salts will take up water resulting in dissolution and subsequent leaching of these salts and in an osmosis-induced swelling of the waste. The swelling BW may induce a mechanical disturbance of the Boom Clay. In addition, the barrier function of the Boom Clay in the nearby vicinity of the disposal gallery could be affected by the release of large amounts of $NaNO_3$ in the clay formation.

This chapter summarizes of the main findings of this research. The main contributions of this thesis are:

1. An improvement of the understanding of processes controlling the water uptake and the subsequent swelling of bituminized waste containing soluble salts ($NaNO_3$) under conditions that are representative for geological disposal conditions. A better understanding of these processes allows a better prediction of the long-term behaviour of Eurobitum under disposal conditions.

2. Investigation of the possible effects of an increase in salt concentration in the pore fluid on swelling, compressibility and shear behaviour of the clay host rock.

As for the first contribution of this thesis, a formulation for the analysis of deformation induced by the dissolution of salts in porous media with semi-permeable membrane properties in contact with water is proposed. A multiphase transport approach is adopted and the balance equations for water, dissolved salts, crystals and solid phase are written including the coupled flows, namely osmotic flow and ultrafiltration, and the dissolution/precipitation of salts. The balance equations are coupled to the equilibrium of stresses. Although some formulations for coupled flow of water and solute in porous media can be found in the literature, the formulation presented in this work is original in the sense that it assumes the existence of high concentrations gradients maintained for a long time which influences the density and motion of the fluid.

An essential part of the approach to model the swelling of the BW is its mechanical response which should be interpreted with a constitutive equation. Laboratory and numerical research on the mechanical behavior of a BW are presented. The material is considered as a mixture of a porous bitumen matrix and salt crystals. A model that predicts the overall creep behavior of the BW, of which both constituents are viscoplastic, is developed. The influence of the crystals on deviatoric creep deformation is investigated. It is observed that there is a significant decrease of creep deformation when the crystal volume fraction increases. The creep model is compared with the experimental data of compression tests under oedometeric conditions. It is observed that by volumetric deformation the bituminized waste evolves from a porous material to an uncompressible material.

The combination of the elasto-viscoplastic constitutive model with the proposed formulation for the analysis of the deformation induced by the dissolution of salts provides a powerful tool to model the volumetric deformations of the bituminized radioactive waste induced by the uptake of water by the embedded crystals. It is shown how the swelling depends on the mechanical behavior of the material, and how it is moreover strongly coupled with the fluid fluxes.

From a mechanical point of view, it is observed that expansion of BW in contact with water is caused not only by reduction of the effective stress but also by effective stress values in tension. If this latter takes place, the expansive volumetric strain will be much

larger than during unloading. The results obtained from the model are consistent with those obtained from the water uptake experiments. Indeed, reasonably good estimates are obtained of the evolution of the swelling of small, inactive BW samples in constant stress water uptake tests and of the osmosis induced pressure in small, inactive BW samples in nearly constant volume water uptake tests. The results and observations reported in this work show that the uptake of water by, and the subsequent swelling of bituminized waste containing soluble salts (mainly $NaNO_3$), or the pressure increase in case that swelling is (partially) prevented, are largely controlled by osmosis.

The parametric study of the water uptake by the BW in restricted swelling conditions demonstrated that permeability, diffusivity and efficiency coefficient affect the magnitude and the duration of the overall process. These three parameters depend on the porosity and are coupled. Indeed, for low values of the intrinsic permeability, advection is negligible and water is transported only by diffusion. As the permeability increases water is transported by both advection and diffusion. In addition, the higher the membrane efficiency, the faster the swelling and the pressure increase.

The dissolution of salt crystals and the recompression of highly leached layers have been also identified as controlling process of swelling and osmosis-induced swelling pressure increase in constant stress conditions and in constant volume conditions, respectively. In fact, the reduction of the outer pores induces the decrease of permeability and of the diffusion coefficient and the increase of the osmotic efficiency in these compressed layers while deeper in the sample they are increasing. Therefore, the outer layers act as highly efficient semi permeable membrane surrounding the less efficient swollen material. This maintains very slow the inflow of water toward the sample and the out flow of the solute over a long time period.

The crystals ensure, for long time, high concentration inside the material which has a great influence on the time duration of the process. The constant volume experiment demonstrates that pressure can grow continuously as crystals still dissolve and reaches a maximum of 20 MPa after almost 5.5 years of hydration. For the case of the water uptake test under constant stress, the stationary state is reached after 8 years of hydration when all salts in the material are dissolved. The maximum swelling

deformation is of the order of 22%. The high osmosis induced pressures and swelling deformations in the water uptake tests, demonstrate the importance of developing an appropriate design for the disposal gallery for Eurobitum, and thus of the compatibility studies on Eurobitum to avoid unacceptable perturbations of the Boom Clay. In fact, under geological disposal condition, after a first free swelling phase, during which, an osmotically –induced swelling of Eurobitum will take place until all free volume is filled with swollen material, the water uptake will induce an increasing stress on the Boom Clay which may induce unacceptable mechanical perturbations of the clay.

With regard to the second contribution of this thesis, a formulation has been proposed first for the analysis of deformations induced by osmotic processes in double structure porous media. A macroscopic description of the system is provided. Then the basic equations describing coupled flows of water and solutes and the transport of these components through macropores are obtained, as well as the, mass balance equations for water and solute in macro and micro pores. A relation is developed to describe the exchange of mass between the macropores and micropores. The effect of water and salt mass exchange between micropores and macropores on the deformation of the material is also addressed. The proposed formulation is particularly applied to analyze qualitatively the effect of osmotic suction on swelling of clayey soils. Transient and long term effects are analyzed.

Firstly, the effect of an increased salinity of the pore fluid on the swelling and mechanical behaviour of double structure porous media, i.e. media that contain micro- and macropores, was investigated by means of model simulations. The results of numerical free swelling tests offered a preliminary evidence of osmotic effects on the swelling of double structure porous media. In the case where the clay soil is put in contact with a solution at higher concentration compared to the pore fluid solution, the time swelling curve is categorised into initial, primary swelling, secondary swelling and a small long term tertiary swelling. Primary swelling is related to a simultaneous dissipation of matric suctions into both structural levels. Secondary swelling is linked to dissipation of microstructural matric suction. Tertiary swelling develops more slowly and is linked to the microstructural osmotic efficiency. In fact, for the case of an ideal semi permeable membrane surrounding the microstructure, no transfer of solute is allowed, that is, tertiary swelling does not develop.

Secondly, a systematic experimental research program involving osmotic suction and matric suction controlled experiments is carried out to investigate the effect of the increase of pore fluid concentration and chemical paths (salinization/dilution) on shear behaviour and on the volume change behaviour under odometer stress state conditions. The tests are performed on compacted samples of Boom Clay under saturated and partially saturated conditions. Two procedures are followed for samples preparation. A first series of specimens are prepared by exposure of soil specimens, which were initially mixed with distilled water, to $NaNO_3$ solution. This method represents the situation where the original soil structure is partly intact while the pore fluid in being replaced, that is short term exposure to salt solution. A second series of samples are prepared by mixing the Boom Clay powder with $NaNO_3$ solution at different concentrations. This method simulates long-term exposure to salt solution wherein the pore solution is allowed to form a different soil structure. It is observed that this change of structure is accompanied by a change in retention properties.

The experimental results illustrate that an increase of pore fluid concentration has a significant influence on a number of soil properties:

- The results of the oedometer tests performed under saturated conditions show that under constant vertical stress, there is shrinkage of the sample causing the decrease of the compressibility and an increase in the pre-consolidation stress. This is attributed to the contraction of the clay clusters caused by transfer of water from the microstructure towards the macrostructure. Once this pre-consolidation pressure is exceeded the soil consolidates along the distilled water compression line. After loading/unloading cycle re-exposure of the sample to distilled water produced a negligible swelling deformation. This suggests that chemical effects are strongly affected by the mechanical loading history.

- For specimens prepared according to the second method, the suction controlled oedometer tests shows that the samples display a slight increase of pre-consolidation stress and a decrease in compressibility when the pore fluid concentration increases. This implies that soil specimens prepared with solution at different concentrations and compacted to the same dry density (same void

ratio) will require a slightly higher static compaction stresses probably due to the somewhat stiffer aggregates induced by higher concentrations.

- Direct shear tests under saturated and partially saturated conditions have been carried out on reconstituted specimen of Boom Clay initially mixed with $NaNO_3$ solution prepared at different concentrations. No significant effect of the increase of pore fluid concentration was observed on the shear behavior of Boom Clay samples under saturated conditions. These specimens, when tested under partially saturated conditions show lower strength with the increase of pore fluid concentration.

A general conclusion is that the influence of a high $NaNO_3$ concentration on the mechanical properties of Boom Clay is expected to be moderate. However, this statement does not exclude the possibility and even the need to include the chemo-hydraulic disturbance of the Boom Clay in future modeling calculations to study the hydro-chemical-mechanical interaction between Eurobitum and Boom Clay.

7.2 Perspectives on future Works

Further work on this subject may be developed along the following lines of research:

- Increase of the predictive capability of the formulation to simulate the swelling of BW by incorporating the dependence of the membrane efficiency coefficient on the crystal content, and by improving the shape of the variation of the membrane efficiency with porosity. Once the expression for the membrane efficiency has been improved, the formulation of the model can be (further) validated by modelling the results of:

  o The parametric study of the water uptake by Eurobitum, i.e. study of the effect (on the water uptake by Eurobitum) of the water activity in the leachant, the salt content in Eurobitum, the ageing degree of the bitumen membrane, and the effective stress on the samples.

- Large scale water uptake tests under constant total stress conditions with Eurobitum samples of ~33 cm diameter and 8 cm height.

- Investigation of the geo-mechanical compatibility of BW with the geological Disposal Environment at large scale. This consists in analyzing in a coupled way the chemo-hydro-mechanical behaviour of the in a disposal gallery and the induced long term deformation of the Boom Clay.

- Experimental investigation to analyse osmotic suction effects on the mechanical behaviour of natural Boom Clay specimens.

- Modelling of the experimental results on the effect of $NaNO_3$ concentration and suction on the mechanical properties of Boom Clay. The chemo-mechanical effects might be described within an elasto-plastic framework based on the idea that the chemical effects act on the plastic properties by increasing or decreasing the pre-consolidation stress. Following the approach presented in chapter 5, the model for Boom Clay might be based on the distinction within the material of a microstructural and a macrostructural levels. Chemical changes have a significant effect on the microstructure. Under partially saturated conditions, the negative pressure associated with the capillary water affects the interconnected macropores. The yield surface might be defined for each associated capillary suction and concentration of pore fluid, so that, the behaviour of clays under unsaturated conditions and the behaviour at full saturation under chemical loading represent two limiting cases in the model.

Appendix A

Mass and volume averaged weighted velocities

The Volume weighted velocity is defined as (for a saturated porous material):

$$\mathbf{V}^v = \frac{\phi_f \rho_l^w v_l^w \mathbf{v}^w + \phi_f \rho_l^s v_l^s \mathbf{v}^s}{\phi_f \rho_l^w v_l^w + \phi_f \rho_l^s v_l^s} \tag{A1}$$

where $\rho_l^\alpha = \rho_l w_l^\alpha$; $\alpha = w, s$ and $\overline{\rho}_l^\alpha = \dfrac{1}{v_l^\alpha} = \dfrac{m_\alpha}{v_\alpha}$ With $\rho_l^w v_l^w + \rho_l^s v_l^s = 1$

The Mass weighted velocity is defined as:

$$\mathbf{V}^m = \frac{(w_l^s \rho_l \phi_f)\mathbf{v}^s + (w_l^w \rho_l \phi_f)\mathbf{v}^w}{(w_l^s \rho_l \phi_f) + (w_l^w \rho_l \phi_f)} \tag{A2}$$

where w_l^i ; $i = w, s$ is the mass fraction of the i-component in the liquid phase, with $w_l^s + w_l^w = 1$.

The total fluxes of water and solutes in the liquid phase are expressed in the formulation as:

$$\mathbf{j}_l^w = \mathbf{J}_l^w + w_l^w \rho_l \mathbf{J}_l + w_l^w \rho_l \phi_f d\mathbf{u}/dt = \mathbf{j}_l^{'w} + w_l^w \rho_l \phi_f d\mathbf{u}/dt \tag{A5}$$

$$\mathbf{j}_l^s = \mathbf{J}_l^s + w_l^s \rho_l \mathbf{J}_l + w_l^s \rho_l \phi_f d\mathbf{u}/dt = \mathbf{j}_l^{'s} + w_l^s \rho_l \phi_f d\mathbf{u}/dt$$

i.e. as a sum of nonadvective and advective terms.

This mass flux can be substituted in (A1) to give:

$$\mathbf{V}^v = \frac{\rho_l^w v_l^w \phi_f \mathbf{v}^w + \rho_l^s v_l^s \phi_f \mathbf{v}^s}{\rho_l^w \phi_f v_l^w + \rho_l^s \phi_f v_l^s} = \frac{\rho_l^w v_l^w \left(\mathbf{j}_l^w / \rho_l^w\right) + \rho_l^s v_l^s \left(\mathbf{j}_l^s / \rho_l^s\right)}{\rho_l^w v_l^w \phi_f + \rho_l^s v_l^s \phi_f} = \tag{A6}$$

$$= \frac{v_l^w \left(\mathbf{J}_l^w + \rho_l^s \mathbf{J}_l + \rho_l^w \phi_f d\mathbf{u}/dt\right) + v_l^s \left(\mathbf{J}_l^s + \rho_l^s \mathbf{J}_l + \rho_l^s \phi_f d\mathbf{u}/dt\right)}{\rho_l^w v_l^w \phi_f + \rho_l^s v_l^s \phi_f} =$$

$$= \frac{v_l^w \mathbf{J}_l^w + v_l^s \mathbf{J}_l^s + \left(\rho_l^w v_l^w + \rho_l^s v_l^s\right)\left(\mathbf{J}_l + \phi_f d\mathbf{u}/dt\right)}{\left(\rho_l^w v_l^w + \rho_l^s v_l^s\right)\phi_f} =$$

$$= \left(v_l^w \mathbf{J}_l^w + v_l^s \mathbf{J}_l^s\right)/\phi_f + \left(\mathbf{J}_l/\phi_f + d\mathbf{u}/dt\right) =$$

$$= \left(\frac{\mathbf{J}_l^w}{\overline{\rho}_l^w} + \frac{\mathbf{J}_l^s}{\overline{\rho}_l^s}\right)/\phi_f + \left(\mathbf{J}_l/\phi_f + d\mathbf{u}/dt\right)$$

If the non-advective terms are assumed to cancel, it follows that:

$$\frac{\mathbf{J}_l^w}{\overline{\rho}_l^w} + \frac{\mathbf{J}_l^s}{\overline{\rho}_l^s} = 0 \Rightarrow \mathbf{V}^v = \left(\mathbf{J}_l / \phi_f + d\mathbf{u}/dt\right) \tag{A7}$$

This assumption permits to calculate the flux of water if the flux of solute is known. This implies a binary non-advective flux system. The fact that the volume averaged velocity has been considered implies that the advective fluxes represent the volume averaged velocity.

If a similar development is done for the mass averaged velocity:

$$\mathbf{V}^m = \frac{\rho_l w_l^w \phi_f \mathbf{v}^w + \rho_l w_l^s \phi_f \mathbf{v}^s}{\rho_l w_l^w \phi_f + \rho_l w_l^s \phi_f} = \frac{\rho_l w_l^w \left(\mathbf{j}_l^w / \rho_l^w\right) + \rho_l w_l^s \left(\mathbf{j}_l^s / \rho_l^s\right)}{\left(w_l^w + w_l^s\right)\rho_l \phi_f} = \tag{A8}$$

$$= \frac{\left(\mathbf{J}_l^w + w_l^w \rho_l \mathbf{J}_l + w_l^w \rho_l \phi_f d\mathbf{u}/dt\right) + \left(\mathbf{J}_l^s + w_l^s \rho_l \mathbf{J}_l + w_l^s \rho_l \phi_f d\mathbf{u}/dt\right)}{\rho_l \phi_f} =$$

$$= \left(\mathbf{J}_l^w + \mathbf{J}_l^s\right)/\left(\rho_l \phi_f\right) + \left(\mathbf{J}_l / \phi_f + d\mathbf{u}/dt\right) = \left(\mathbf{J}_l^w + \mathbf{J}_l^s\right)/\left(\rho_l \phi_f\right) + \mathbf{V}^v$$

But here the non-advective terms cannot cancel as the condition has already been imposed in (A7). Actually the sum of the nonadvective fluxes gives:

$$\mathbf{J}_l^s + \mathbf{J}_l^w = \rho_l \phi_f \left(\mathbf{V}^m - \mathbf{V}^v\right) \tag{A9}$$

Another interesting result can be obtained if (A6) and (A8) are re-written as:

$$\mathbf{V}^v = v_l^w \mathbf{j}_l^w / \phi_f + v_l^s \mathbf{j}_l^s / \phi_f = \frac{1}{\phi_f \overline{\rho}_l^w} \mathbf{j}_l^w + \frac{1}{\phi_f \overline{\rho}_l^s} \mathbf{j}_l^s \tag{A9}$$

$$\mathbf{V}^m = \frac{1}{\phi_f \rho_l} \mathbf{j}_l^w + \frac{1}{\phi_f \rho_l} \mathbf{j}_l^s$$

and substituted in (A9):

$$\mathbf{J}_l^s + \mathbf{J}_l^w = \rho_l \phi_f \left(\mathbf{V}^m - \mathbf{V}^v\right) = \mathbf{j}_l^w + \mathbf{j}_l^s - \frac{\rho_l}{\overline{\rho}_l^w} \mathbf{j}_l^w - \frac{\rho_l}{\overline{\rho}_l^s} \mathbf{j}_l^s = \mathbf{j}_l^w \left(1 - \frac{\rho_l}{\overline{\rho}_l^w}\right) + \mathbf{j}_l^s \left(1 - \frac{\rho_l}{\overline{\rho}_l^s}\right) \tag{A4}$$

The non-advective fluxes written with respect to the volume weighed velocity should satisfy the relation given by equation (A7). Note that from a mathematical point of view it is possible to choose between the volume and the mass weighted velocities as being

equal to the advective terms given by $\left(\mathbf{J}_l / \phi_f + d\mathbf{u} / dt \right)$ expressed as a velocity instead of a volumetric flux. The volume weighted velocity guarantees that there are not variations of volume by binary fluxes of mass as it has been imposed that the non-advective terms cancel by volume and not by mass.

APPENDIX B

Constitutive model for nonlinear creep of porous materials

In this appendix a derivation of the model for creep of porous materials obeying power law developed in Olivella and Gens (2002)is included.

The most common way to write the creep power law is:

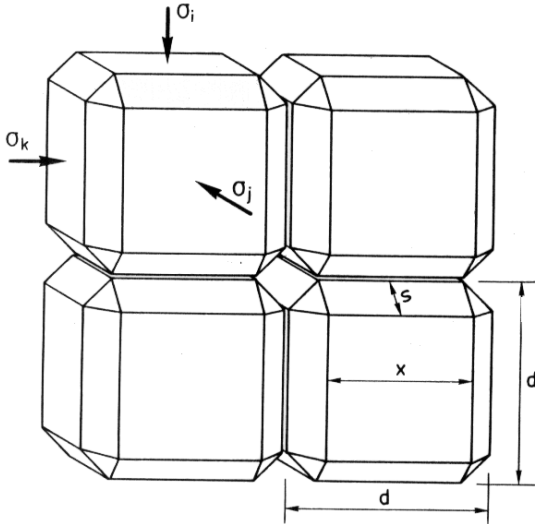$$\frac{d\varepsilon_{ij}}{dt} = Aq^n \frac{\partial q}{\partial \sigma_{ij}} \qquad \text{(B1)}$$

in the generalised case, $\left(q = \sqrt{3J_2}\right)$ refers to the deviatoric stress, $\left(J_2\right)$ is the second invariant of the deviatoric part of the stress tensor. $A(T)$ is a temperature dependent parameter, and n is the power of the creep law. It is important to notice that this law does not allow volumetric creep deformation. This power law is combined with an idealized geometry to obtain a law for porous materials.

Yet, another form of the power law can be obtained if the generalized one is particularised for the principal directions *(i)*:

$$\frac{d\varepsilon_i}{dt} = \frac{3}{2} Aq^{n-1} \left(\sigma_i - p\right) \qquad \text{(B2)}$$

where p refers to the mean stress. It does not matter if effective or total stress is used here because deviatoric stresses do not depend on pore pressure and this law does not contain volumetric contribution. Therefore, for porous materials, net stresses ($\sigma'_{ij} = \sigma'_{ij} - P_f \, \delta_{ij}$ in which P_f refers to the fluid pressure) will be considered in what follows. Assumptions are necessary to develop a macroscopic law, these are: simple stress distribution in the solid phase, the solid phase changes its shape without volume change, creep power law is valid to calculate the creep deformation of the solid phase. The macroscopic equations of the model will be built in three steps: 1) adoption of a stress distribution in a grain, 2) calculation of strain rates along the principal directions, and 3) generalization of the model to a tonsorial form.

A simplified geometry for solid phase and pores was considered with the following derived functions:

	Void volume:
	$$3s^2d - \frac{4}{3}\sqrt{2}s^3 = \lambda_v s^2 d$$ $$\lambda_v = 3 - \frac{4}{3}\sqrt{2}\frac{s}{d}$$ $$\lambda_v \approx 3(1 - e^{3/2})$$
	Solid volume: $$d_o^3$$
	Void ratio (void volume divided by solid volume): $$e = \frac{3s^2d - \frac{4}{3}\sqrt{2}s^3}{d_o^3} = \frac{\lambda_v s^2 d}{d_o^3}$$

Ratio of void size (s) to solid phase size (d):	Solid conservation (constant particle volume):	Ratio of contact size (x) to solid phase size (d):
$$\frac{s}{d} = \frac{\sqrt{e/\lambda_v}}{\sqrt{1+e}}$$	$$d^3 - ed_o^3 = d_o^3$$ $$d = d_o\sqrt[3]{1+e}$$	$$\frac{x}{d} = \frac{d - \sqrt{2}s}{d} = \frac{\sqrt{1+e} - \sqrt{2e/\lambda_v}}{\sqrt{1+e}}$$

Porosity (ϕ) and void ratio (e) are two different ways to measure the void volume in porous materials. While porosity is the void volume divided by the total volume, the void ratio is the void volume divided by the solid volume. They are related by: $e = \frac{\phi}{1-\phi}$ and $\phi = \frac{e}{1+e}$. Therefore the model can be written in terms of void ratio or porosity without loss of generality.

For the geometry of polyhedrons adopted, a simplified stress distribution inside the solid phase was considered: $(\sigma'_i)_c = (\sigma'_i)(d^2/x^2)$ which simply establishes that the stresses in the contact increase as the area of the contact decreases. Considering the

principal directions normal to the faces of the solid phase volumetric element, the strain rate for each principal direction can be calculated:

$$\frac{d\varepsilon_i}{dt} = \left(\frac{1}{d}\frac{dd}{dt}\right)_i \cong \frac{3}{2}Aq_i^{n-1}\left(\left(\sigma_i{}'\right)_c - p_i{}'\right)\frac{\sqrt{2}s}{d} + \frac{3}{2}Aq^{n-1}\left(\sigma_i{}' - p{}'\right)\frac{x}{d} \qquad (B3)$$

where p'_i and q_i are mean net stress and deviatoric stress in the zone of the solid phase near to the contact, i.e. computed with, $(\sigma'_i)_c$, $(\sigma'_j)_c$ and $(\sigma'_k)_c$; while, p' and q are mean net stress and deviatoric stress in the internal zone of the solid phase, i.e. computed with (σ'_i), (σ'_j) and (σ'_k). In this equation, the first term corresponds to the strain of the area near contacts and the second term corresponds to the strain in the core of the solid phase. As porosity tends to zero, the first term vanishes, and the original creep power law is obtained. A simple relationship is obtained if the stress state is considered isotropic, i.e. $(\sigma'_1) = (\sigma'_2) = (\sigma'_3)$:

$$\frac{d\varepsilon_v}{dt} = \frac{d\varepsilon_1}{dt} + \frac{d\varepsilon_2}{dt} + \frac{d\varepsilon_3}{dt} = 3A\left(\left(p{}'\right)_c - p{}'\right)^n \frac{\sqrt{2}s}{d} = \qquad (B4)$$

$$= 3A\left(\frac{(1+e)}{\left(\sqrt{1+e} - \sqrt{2e/\lambda_v}\right)^2} - 1\right)^n \frac{\sqrt{2e/\lambda_v}}{\sqrt{1+e}}\left(p{}'\right)^n = \frac{1}{\eta_v^{DC}(e,T)}\left(p{}'\right)^n$$

As an opposite state to isotropic, pure shear stress state is considered, i.e. $(\sigma'_3) = -(\sigma'_1)$ and $(\sigma'_2)=0$:

$$\frac{d\varepsilon_1}{dt} = \frac{3}{2}A(T)\left(\left(\sqrt{1+g+g^2}\right)^{n-1}\left(\frac{2g+1}{3}\right)f + \left(\sqrt{3}\right)^{n-1}\frac{1}{\sqrt{g}}\right)\sigma_1^{m} \qquad (B5)$$

The reason for these two particularizations (isotropic and pure shear) is to obtain simple relationships for volumetric strain rate and deviatoric strain rate. If a general stress state was assumed without any restrictions, these forms would be more complex due to the nonlinear (power) dependence of strain rate on stress for this mechanism. From (B4) and (B5) the following viscosities for volumetric and deviatoric creep can be obtained:

$$\frac{1}{\eta^v} = A(T)g^v(e) \qquad (B6)$$

$$\frac{1}{\eta^d} = A(T)g^d(e)$$

Where

$$g^v(e) = 3(g-1)^n f \tag{B7}$$

$$g^d(e) = \left(\sqrt{\frac{1+g+g^2}{3}}\right)^{n-1}\left(\frac{2g+1}{3}\right)f + \frac{1}{\sqrt{g}}$$

$$g = \frac{1}{(1-f)^2} = \frac{d^2}{x^2} \qquad f = \sqrt{\frac{2e}{3(1-e^{3/2})(1+e)}} = \frac{s\sqrt{2}}{d} \tag{B8}$$

$A(T)$ and n come directly from the creep power law, i.e. the nonporous material. The functions $g^v(e)$ and $g^d(e)$ depend on the idealized geometry and in turn on void ratio. However, because the creep law has a power, a dependence on n remains in these functions.

Equation (B3) has been developed on the basis of the idealized geometry adopted. However, it lacks generality because it has been written for strain rates along principal directions. One way to generalize (B3) is to use a flow rule. In this procedure, (B4) and (B5) are very useful to identify how this generalized form should be. The following general form, based on viscoplasticity theories for geological materials (Perzyna, 1966), was proposed:

$$\frac{d\varepsilon_{ij}}{dt} = \frac{1}{\eta}\Phi(F)\frac{\partial G}{\partial\sigma'_{ij}} \tag{B9}$$

In this equation, a viscosity parameter is included, G is a viscoplastic potential, F is a stress function and Φ is a scalar function of F.

In Equation (B9) the functions G and F should be taken as functions of stress invariants. The following form was proposed:

$$F = G = \sqrt{q^2 + \left(\frac{p}{\alpha_p}\right)^2} \tag{B10}$$

$$\Phi(F) = F^n$$

where n is the power of the creep law and α_p is a material function. Since $\Phi(F)$ is always positive, no threshold is considered in this law. This is consistent because creep materials develop viscous deformations under any stress level.

In order to exploit the theoretically derived equations (B4 to B8) this generalization of the model is complemented with definitions for η and α_p. By comparison of (B4) and (B5) with the results obtained using (B9) and (B10) under the same stress state (i.e. isotropic and pure shear) it is obtained that:

$$\eta = \eta^d \qquad \alpha_p = \left(\frac{\eta^v}{\eta^d} \right)^{\frac{1}{n+1}}$$

(B11)

When void ratio (or equivalently porosity) vanishes α_p tends to infinity and the volumetric term disappears.